GRAVEL TRANSPORT AND MORPHOLOGICAL MODELING FOR THE LOWER FRASER RIVER, BRITISH COLUMBIA

by

A. K. M. Shafiqul Islam

B.Sc. Eng., Bangladesh Agricultural University, 1994

M. Eng., Asian Institute of Technology, 1997

M. Sc., University of Stuttgart, 1999

A THESIS SUBMITTED IN PARTIAL FULFILLMENT OF

THE REQUIREMENTS FOR THE DEGREE OF

DOCTOR OF PHILOSOPHY

in

THE FACULTY OF GRADUATE STUDIES

(Civil Engineering)

THE UNIVERSITY OF BRITISH COLUMBIA

(Vancouver)

February 2009

ABSTRACT

This thesis investigates the potential application of a two-dimensional depth-averaged sediment transport and morphological model on a large braided river system and examines its capability to build a computational gravel budget and predict the morphological changes. The Lower Fraser River gravel reach is characterized by an irregularly sinuous single-thread channel split around large gravel bars and vegetated islands, and riverbed aggradation because of gradual gravel deposition over the years, bank hardening and channel confinement. Gravel removal from selected locations is considered as one of the viable management options to maintain the safety and integrity of the existing flood protection system along the reach. Therefore, any gravel removal plan in this reach requires a reliable sediment budget estimation and identification of deposition zones. It is also required to examine the possible future morphological changes with and without gravel removal and to assess its impact on design flood level.

The main objective of this study is to build a computational sediment (gravel) budget for the 33 km long gravel reach that extends from Agassiz-Rosedale Bridge to Sumas Mountain near Chilliwack. In this study, a two-dimensional depth-averaged curvilinear mathematical model MIKE 21C was modified and applied to predict the gravel bedload transport and detect the change of morphology for the next 10 years period. A gravel transport formula was coded and added into the MIKE 21C model. Sediment transport code modification and application has been done side by side in a trial and error fashion.

This is the first use of a conventional two-dimensional depth-averaged model for the entire gravel reach of the Lower Fraser River within affordable computational effort. The model application was successful in term of gravel budgeting, aggradation and degradation zones identification and long-term morphological change prediction, with some limitations and drawbacks. Further modification and model testing with recent bedload data is recommended.

TABLE OF CONTENTS

LIST OF TABLES

LIST OF FIGURES

LIST OF SYMBOLS

Roman Characters:

A	Area of a deposition or erosion zone
a	Empirical Co-efficient derived from curve fitting
b	Empirical exponent derived from curve fitting
C	Chezy's roughness coefficient
C_r	Courant Number
D	Diameter of the pipe
D_{50}	Particle size at which 50% of the bed material is finer than D_{50}
D_{84}	Particle size at which 84% of the bed material is finer than D_{84}
D_{90}	Particle size at which 90% of the bed material is finer than D_{90}
D_i	A individual sediment size class (or, range) of i
D_{sm}	Mean grain size
E	Eddy viscosity coefficient
F_i	Surface based size fraction in the ith size range
F_s	Percent sand content in surface bed materials
f	Friction factor
f'	Grain resistance
f''	Form resistance
G	Gravel transport rate
g	Acceleration due to gravity
g_{bi}	Bedload transport rate for a individual size class i
G_{bT}	Average annual gravel load
h	Water depth
H	Water level from a fixed datum
h_o	Channel water depth
I_g	Inflow volume at upstream boundary of an erosion/deposition zone
i_s	Helical flow intensity
k_s	Height of the bed roughness elements
K_n	a unit conversion factor
L	Pipe length
m	Total number of degradation cells
n	Total number of aggradation cells

N	Manning-Strickler number
n	Manning's coefficient
N_P	Total Number of Points
N_y	Difference between two survey periods in year
P	Flow flux density in the x-direction
p	Sediment porosity
p	Mass fluxes in the s-direction
q	Mass fluxes in the n-direction
Q	Flow flux density in the y-direction
Q_b	Bedload discharge
q_{bi}	Volumetric transport rate per unit width of size i
q_{bx}	Total sediment transport rate per unit length in the x direction
q_{by}	Total sediment transport rate per unit length in the y direction
q_i	Volume of bedload per unit width of bed surface
q_s	Sediment mass flux
R	Hydraulic radius,
R_s	Radius of curvature of s-line
R_n	Radius of curvature of n-line
s	Ratio of sediment to water density
S	Energy slope
S_n	Sediment transport rate in n-direction
S_s	Sediment transport rate in s-direction
S_{fx}	Chezy's friction slope in x direction
S_{fy}	Chezy's friction slope in y direction
t	Time
U	Velocity of flow in x-direction
U'	Fluctuating component of velocity
$\overline{U}$	Mean component of velocity
V	Velocity of flow in y-direction
V	Velocity of flow (in General)
V_{net}	Net aggradation or degradation volume per year in cubic meter
V*	Shear velocity
V_a	Aggradation volume in a cell
V_d	Degradation volume in a cell
V_i	Volumetric sediment input over specified period

V_t	Mean flow velocity in x or y direction
V_o	Volumetric sediment output over specified period
W^*	Dimensionless gravel transport rate
y	Distance
Y_0	Water depth from the channel bottom
Z_b	Bottom elevation of the channel

Greek Characters:

α	Coefficients
β	An exponent parameter
κ	Von Karman constant (usually 0.4)
λ	Porosity of the bed material
ΔC	Change in sediment concentration
Δn	Space in n-direction
Δq_e	Lateral sediment supply from bank erosion
Δs	Space in s- direction
Δt	Time step in a finite difference scheme
ΔV	Net difference between scour and fill
Δx	Horizontal distance in a finite difference scheme
Δy	Lateral distance in a finite difference scheme
Δz	Channel-bed elevation change in the vertical direction
ρ	Water density
τ	Fluid shear stress at the bed
τ_c	Critical fluid shear stress at the bed
τ_{ri}	Reference value of τ
τ_s	Shear stress in s-direction respectively
τ_n	Shear stress in n-direction respectively
τ_{rm}	Reference shear stress for the mean grain size
$\tau_{rm}{}^*$	Dimensionless Shield's parameter for the mean grain size
v_s	Kinematic Viscosity of a fluid
ϕ	Ratio of bed shear stress to reference shear stress
δ_s	Angle between flow direction and near bed shear stress
ρ_g	Bulk density of gravel

ACKNOWLEDGMENTS

First and foremost, I wish to express my sincere thanks to my supervisor, Professor Robert G. Millar, for his invaluable contributions and support during the completion of this thesis. His thoughtful suggestions, guidance and thorough review inspired me to continue this research. I should also like to express my gratitude to the other members of my committee: Professor Michael Church, Professor Greg Lawrence, Dr. Barnard Laval and Dr. Sheng Li for their input and review.

Thanks are extended to Mr. Ron Henry, senior hydraulic engineer responsible for Lower Fraser River (also with, Ministry of Environment B.C.) for his continued interest in the project and Vince Busto from Department of Fisheries and Oceans, Canada for his direct help and suggestions in gravel removal area selection in Lower Fraser River. I appreciate Dr. Sheng Li for his efforts in bedload formula coding and advices in numerical modeling task, Northwest Hydraulics and Hamish Weatherly for many air photos and plates, and Darren Ham for DEMs. I would be remiss if I did not thank Professor Michael Church for bedload data and discussion on bed materials formula selection and gravel sampling maps for Lower Fraser River.

Finally, I am grateful to my friends and family, especially my wife, who so strongly supported my decision to undertake a Ph. D.

To My Wife

1 INTRODUCTION

1.1 Introduction

The Fraser River is the fourth largest river in Canada and is British Columbia's largest river. The Fraser Basin covers some 240,000 square kilometers, roughly 25 percent of the province and equivalent in area to all of Great Britain or the State of California (FBC, 2003). From its source at Mount Robson, the highest peak in the Rocky Mountains, until it meets the Pacific Ocean at the Strait of Georgia, the Fraser River travels 1,370 km across British Columbia (Figure 1.1). It includes watersheds of dozens of tributaries, including the Nechako, Quesnel, Chilcotin, and Thompson and encompasses all but one of the 14 major eco-regions and climatic zones in British Columbia (FBC, 2003).

Fraser River remains a mountain river confined by the bedrock canyon and terraces through its 1,370 km long course, except the last 150 km downstream from Laidlaw (Figure 1.2). After Fraser River emerges from its steep bedrock canyon at Hope, it remains confined between Pleistocene terraces, landslide earth, or bedrock until Laidlaw. Beginning at Hope the Fraser River progressively reduces its gradient. The channel becomes unconfined at Laidlaw 40 km downstream from Hope, by which point it has reduced its gradient about one order of magnitude (Church, 2001a). Below Laidlaw, the Lower Fraser River is characterized by deposition, with the caliber (sediment size characteristics such as D_{50}, D_{90} or D_{10} etc.) of deposited sediment decreasing concomitantly with the slope. For example, D_{50} values at Hope (100 mm), Agassiz (42 mm) and Mission (0.38 mm) decrease with the slope towards the downstream. The coarsest fraction of river sediment load, mainly gravel, is deposited in the first 55 km reach between Laidlaw (km 150) and Sumas Mountain (km 95) (Figure 1.2). These deposited gravels forming irregular gravel bars and vegetated islands. This irregularly sinuous and divided channel pattern is known as "wandering gravel-bed" (Desloges and Church, 1989). There is a sharp transition from gravel to sand near Sumas Mountain (Figure 1.2), which is marked by an abrupt decrease in channel gradient.

1

British Columbia
(Canada)

Fraser River Basin

Prince
George

McBride

Quesnel   Valemount

Williams
Lake

Fraser River

Lillooet

Lytton

Hope

Chilliwack

Vancouver

100   0   100   200 Kilometers
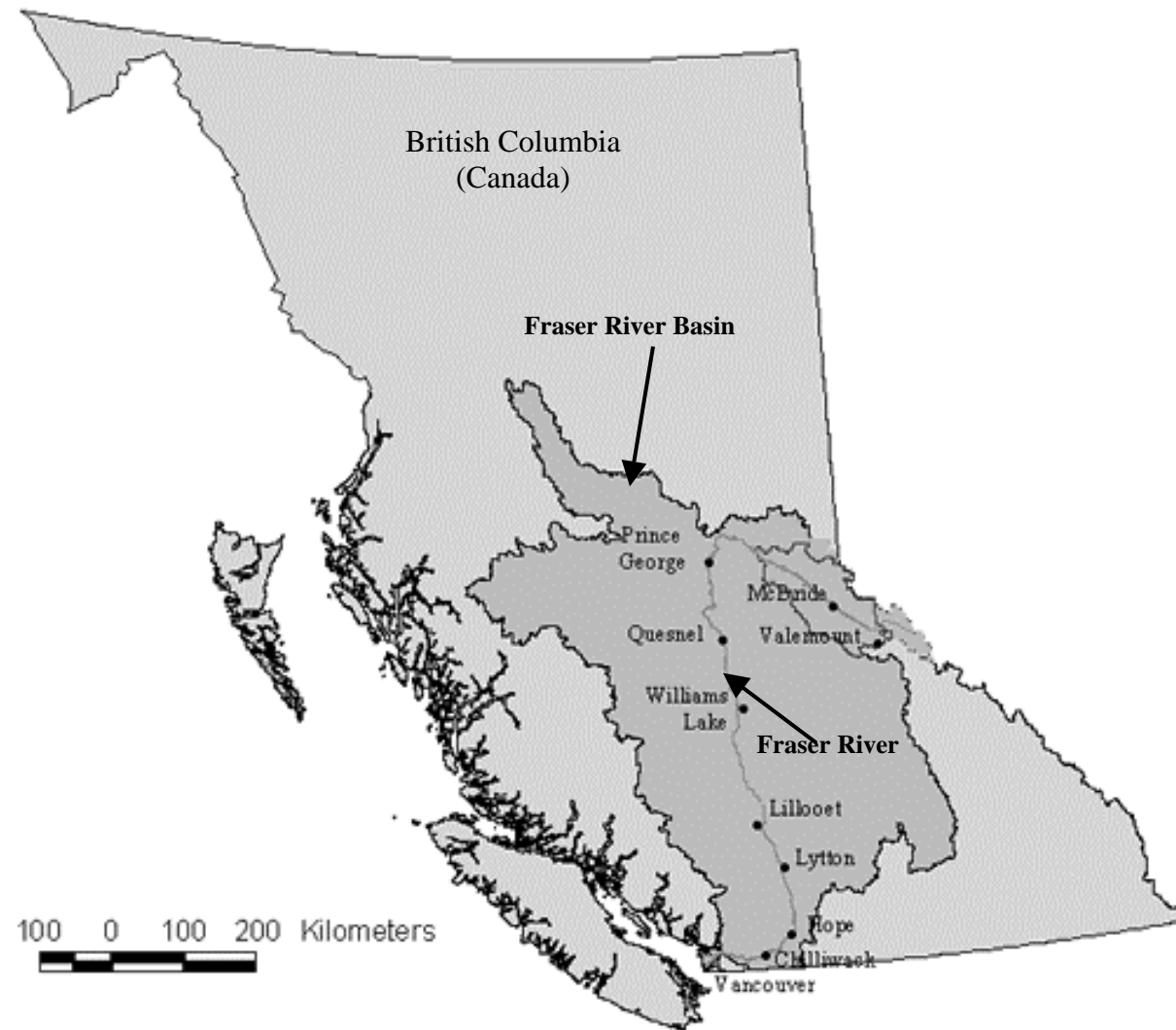
Figure 1.1: Location of the Fraser River drainage basin within British Columbia.
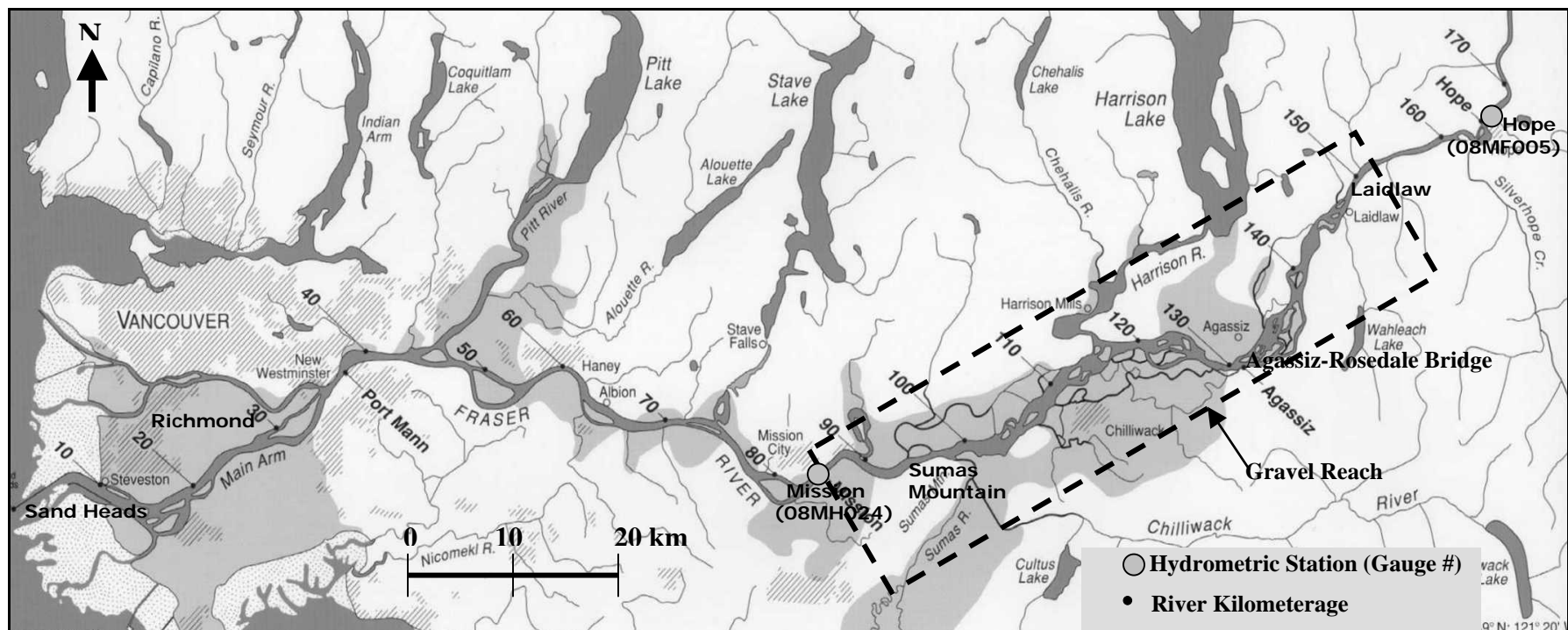
Figure 1.2: Fraser Valley from Hope to Georgia Strait (Source: Department of Geography, UBC).

The wandering gravel-bed reach between Laidlaw and Sumas Mountain (shown with the dashed rectangle in Figure 1.2), also referred as the "gravel reach", provides exceptionally rich and diverse aquatic habitat. The morphology of this reach is the consequence of gravel transport, erosion and deposition (Church et al., 2001). Surface materials of the channel consist of unimodal gravel but the sub-surface materials are strongly bimodal, and consist of gravel and sand (10-20%) mixture (Church et al., 2001). Significant gravel transport occurs during the annual freshets when the flow rate exceeds about 5,000 m^3/s (Church et al., 2001).

Two significant flood events occurred along the Fraser Valley in 1894 and 1948. The largest Fraser River flood on record occurred in 1894, which damaged an unknown number of homes, roads, railways and farms along the Fraser Valley. The second largest Fraser flood occurred in 1948. Although the flood level was slightly lower than the flood level in 1894, impacts were greater due to increased levels of development and a larger population (FBC, 2003). There were four recent moderately high flood levels in 1972, 1997, 1999 and 2007 respectively. It is estimated that there is a one-in-three chance of experiencing a Fraser River flood of record in the next 60 years (FBC, 2003).

The first dykes on Lower Fraser River were constructed in about 1892 to dam Hope and Camp sloughs near the City of Chilliwack. A century-long program of flood protection dyke construction was initiated after June, 1894 flood however, dykes were not continuous and systematically designed or constructed. After the 1948 flood, a series of Federal-Provincial program was initiated for systematic and continuous flood dykes reconstruction. Dyke crest elevations through the Lower Fraser Valley are based on the 1894 flood of record, with an estimated peak flow of 17,000 m^3/s at Hope plus 0.6 m of freeboard. However, recent revisions to the design flood profile have shown that the existing dykes do not provide adequate protection for the design flood along a significant section of the gravel reach (UMA, 2001a), as well as downstream in the sand-bed reach (nhc, 2006). The increase in the design flood profile is due to several factors including change in the channel geometry and alignment, gravel and sand deposition, confinement by the dykes, as well as changes the hydrologic and hydraulic assumptions and computational procedures (UMA, 2001a; nhc, 2006). Gravel extraction was

recommended as one of the viable management options to maintain the safety and integrity of the flood protection system (Church, Ham and Weatherly, 2000), however, gravel removal may impact the ecological integrity of the river system. Gravel removal should be based on a gravel budget that includes mean annual gravel influx and the longitudinal variation in gravel transport rates, and locations of aggrading and degrading zones along the channel. It is also important to determine the effectiveness of gravel removal and its impact on the design flood profile.

1.2 Estimates of Gravel Transport and Deposition

The first comprehensive gravel bedload transport measurements were conducted by Water Survey of Canada (WSC) at Agassiz-Rosedale Bridge and Mission Railway Bridge (Figure 1.2) over 20 years between 1966 and 1986. Estimates of annual gravel influx based on the 20 years field data have been completed and reported in 1999 (Ham, 2005a; Church et al., 2001; McLean et al., 1999a). An alternative approach called "morphological method" is based on comparisons of repeat bathymetric and topographic surveys to determine the change in volume of gravel in storage over time (Ham, 2005a; Church et al., 2001; McLean et al., 1999). Surveys of the gravel reach were undertaken in 1952, 1984, 1999 and 2003 (Ham and Church, 2003). The average annual gravel influx is estimated from the changes in volume between the repeat surveys. A significant difference was found between the estimates based on sampling, versus repeated surveys. The recent morphological estimate shows three times more gravel deposition in this reach than the previous WSC field sampling based estimation (Ham, 2005a). Both field measurement and morphological methods are direct measurement methods. However, reliability depends on data quality and both methods involve considerable and costly effort.

There are some cost effective and scientifically based alternative methods available to estimate gravel transport rate and gravel budget including hydraulic model studies (Lane et al., 1999). Application of a physical scale model is generally limited to local problems (e.g. hydraulic behavior near the intake of a pump station, tributary inflow into a large river etc.). When sediment transport and long-term consequences of morphological changes are of concern in a large river system then the only reasonable possibility is a mathematical model study.

The morphological change of a river channel is the result of the transport and deposition or erosion of the sediment over time and a large numbers of variables are interrelated in the morphological process. The channel geometry, bars, bed roughness, thalweg locations, grain size distribution, sinuosity and bed slopes can change over time with changes in water and sediment discharge. Therefore, to predict this complex process requires realistic simulation of bed resistance, hydrodynamics and sediment transport and information about sediment size distribution.

Existing one-dimensional (1-D) movable bed mathematical models can simulate longitudinal bed level change along the thalweg over 10 to 30 years of time (Enggrob, 1998). One-dimensional models use the St. Venant equation for liquid phase, which assumes hydrostatic pressure distribution and uniform velocity across a section. In reality, both the velocity and bed erosion and deposition are three-dimensional in nature and can vary substantially across a section, particularly in a wandering river. Importantly, one-dimensional cross-sectional averaged models fail to represent the spatial variability of bottom shear stress. Recent research showed that when the cross-sectional mean bed shear stress predicts zero transport, local high bed shear stress values are actually entraining sediment (Wilcock, 2001). Furthermore, one-dimensional models cannot capture the three-dimensional features of helical flow at bends in braided and meandered rivers. Therefore, one-dimensional models have limited applicability to simulate bedload transport.

Application of three-dimensional models in computational fluid dynamics (CFD) is becoming more common with the increase of computing power. Three-dimensional (3-D) CFD models can simulate the spatial variability of both the flow field and sediment transport encountered in nature (Morvan et al., 2002; Gessler et al., 1999; Shimizu et al., 1989). However, the computational effort and data requirement involved in a 3-D model development restricts its practical application in large reach scale river hydraulics problems. Most of the known 3-D models have been used either in very short reach simulations, for example a meander bend, flood flow and vortex effects behind bridge piers, or laboratory flume experiments. The practical use of 3-D models in large-scale river hydraulics problems has yet to be demonstrated.

At present two-dimensional (2-D) depth-averaged models represent realistic tools for river flow and sediment transport modeling. A quasi-three-dimensional or two-dimensional depth-averaged sediment transport and morphological model can simulate the flow patterns, process of sediment transport, and morphological changes over longer periods of time. However, these two-dimensional flow models provide only depth-averaged velocity in the water column (grid cell in a finite difference based model) from where bed shear stress must be derived, which is strictly applicable only to uniform flow (Steffler and Jin, 1993). In addition, the direction of the bed shear stress may be different from the mean flow direction. Therefore, while a two-dimensional depth-averaged model requires a secondary flow correction algorithm, it remains far more computationally efficient than a full 3D model (Kassem and Chaudhry 2002; Duan et al., 2001; McArdell and Faeh 2000). There are no two-dimensional depth-average models commercially available that are capable of simulating flow, gravel transport and morphological changes in a gravel-bed river. However, some of them can be used with modest modification at the code level, including the MIKE 21C model.

MIKE 21C is a fully two-dimensional depth-averaged hydrodynamic and morphological model developed by DHI Water and Environment (formerly The Danish Hydraulic Institute). MIKE 21C incorporates fully unsteady flow, bedload transport formulation and dynamic bed level changes through a simple sediment continuity equation (Exner equation). It also includes an analytical model for computing the secondary currents, and thus provides the three-dimensional effects in a two-dimensional model. MIKE 21C was mainly developed for sand-bed rivers and the existing inbuilt transport formulations do not adequately describe the important features of gravel transport such as sorting and armoring effect, hiding and exposure. As a result, addition of gravel transport functions was necessary. The Wilcock and Crowe (2003) surface-based gravel transport equations were coded and added in the MIKE 21C model by Dr. Sheng Li, a Research Associate in the Department of Civil Engineering, UBC, to enhance its capacity. A technical research collaboration was established between DHI Water and Environment and Civil Engineering, UBC to carry out this study over a five-year time frame. Financial support was provided by the Natural Science and Engineering Research Council of Canada (NSERC) as a research grant to Professor Robert Millar and Professor Michael Church. The level of precision

that can be achieved by the use of MIKE 21C and its wide acceptability in the scientific community were the main reasons to use this model as a research tool. The sediment transport code modification was done step-by-step in a trial and error fashion over the five-year period. This modified model has applied to carry out the gravel transport and morphological studies in Lower Fraser River gravel reach.

1.3 Research Objectives:

The main objectives of the study are –

- To build, calibrate and verify a two-dimensional hydrodynamic model for the Lower Fraser River gravel reach.

- To modify the sediment transport code of the two-dimensional model for application to gravel-bed river.

- To determine the annual gravel influx and prepare a distributed gravel budget for the Lower Fraser River gravel reach by using the two-dimensional mathematical model.

- To compare the computational sediment budget with the sediment budget based on repeat bathymetric and aerial surveys (Ham, 2005a) and identify the gravel deposition zones.

- To incorporate various gravel-extraction plans into the model and simulate morphological changes over a 10-year period and to investigate the effect of gravel removal on channel morphology of the Lower Fraser River gravel reach.

- To assess the application of a two-dimensional hydrodynamic model to gravel management along the Fraser River gravel reach.

This thesis is organized as follows: Chapter 2 is a literature review describing sediment budgeting methods and mathematical modeling techniques and governing equations, available mathematical models and their practical application. Chapter 3 describes the morphology and hydrology of the study reach and important gravel bars and islands from where gravel removals have been proposed in detail. In, Chapter 4 methodology is given in detail to describe how the model was implemented and result were analyzed. Chapter 5 presents the results and relevant discussion. Chapter 6 presents the conclusions and the recommendations.

2 LITERATURE REVIEW

2.1 Sediment and Sediment Transport

Clastic sediment is defined as fragmented material formed by physical and chemical weathering of rocks and their transport includes movement of boulders in steep mountainous rivers to colloid-sized material in estuaries (Wilcock, 2001). Transport is driven by gravity and fluid forces between the sediment and surrounding fluid (usually water). There are two common classifications of the load in a stream: the first divides the load into bedload and suspended load and the second separates the load into wash load and bed-material load (Chang, 1988). Bedload transport can be defined as a transport process wherein grains move along or near the bed by sliding, rolling, or hopping (Graf, 1971). Suspended load, by definition, moves in suspension. The bed material load is composed of grains found in the streambed, and wash load is composed of the finest portion of the sediment grains, generally silt and clay (Chang, 1988). Usually wash load transport is neglected because it has no relation to the transport capacity of the stream.

2.2 Sediment Budget

A sediment budget is the difference between the quantity of sediment entering and leaving a selected segment of river or estuary (USACE, 1992). It is based on the sediment transport, erosion and deposition within a given control volume. This control volume may be a section of a channel or even a portion of a wide estuary. A sediment budget may consist of either suspended load or bedload, or both. The behavior of suspended load transport capacity is fundamentally different from that of bedload transport and is in general not responsible for morphological changes in gravel-bed rivers. One of the most important processes in gravel-bed rivers is the bedload sediment transport. Bedload transport volume is usually 1-5%, or even less, out of total sediment volume transported per year in a gravel-bed river (Parker, 1990, Schumm, 1963). Nevertheless, it is responsible for the changes of channel configuration or river morphology. Therefore, to develop a reasonable sediment budget for a gravel-bed river,

estimation of bedload transport is important.

2.3 Estimation of Bedload Transport and Morphological Change

There are several methods available to estimate bedload transport. These methods can be divided into two main categories, direct and indirect estimation (McLean and Church, 1999b).

1) Direct estimation method: Sampling of gravel bedload using a variety of sampling devices to construct a bedload vs. discharge rating curve at any cross-section of a channel.

2) Indirect estimation methods are:

    a) Repeated Survey Method: Comparison of repeated hydrographic surveys to produce a long-term sediment budget (McLean and Church, 1999b).
    b) Morphological Method: Analysis of historical planimetric data (Aerial photographs) to estimate rates of morphological change and associated sediment transport rates (McLean and Church, 1999b).
    c) Bedload Predictors Method: Estimation of bedload transport with semi-theoretical bedload transport formulas.

The selection of a suitable method depends on purpose, time scale, stream size, data availability and financial capability of the party involved in the estimation process.

2.3.1 Direct Estimation Method: Bedload Transport Estimation Based on Discharge

In the direct estimation method, bedload estimation typically is developed from a sampling campaign, sometime done over several years. A bed-load discharge versus river discharge rating curve at a station is the main output from the direct estimation method. Eventually, bedload transport rate Q_b has to be estimated as a function of water discharge Q, and relation giving Q_b as a function of Q is called the bedload-rating curve. A bedload rating curve typically takes the form of a power function (Colby, 1957):

$Q_b = \alpha Q^\beta$ ……………………………………………………………………………… (2.1)

where,

Q_b is bedload transport rate (in tonnes/day or kg/hr)

Q is water discharge (in ft^3/s or m^3/s) and

α and β are coefficients to be determined from curve fitting.

Unfortunately, such a rating curve is site-specific. Differences in channel size, shape, slope, roughness, and bed material composition and supply limitation would produce very different Q_b for the same Q at different sites. This means that very different values of the coefficient α and the exponent β would be required in the power function [equation (2.1)] to estimate Q_b in different rivers or different reaches of the same river. It may not always be the case that the transport is actually well described by a power function. It can be very expensive and time consuming to develop rating curves for large and wide rivers. Even if a rating curve is developed, somehow it may not be valid over a longer period due to river bathymetry changes. However, a rating curve is useful in order to calibrate a bedload transport model, at least over some sections of the river. Importantly for this study, a gravel-bedload rating curve was developed at Agassiz-Rosedale Bridge with 20 years (1965-1986) of field samples collected by Water Survey Canada in Fraser River, British Columbia (McLean and Church, 1999b). A recent study showed that annual gravel transport rate at this station would be much higher than the values calculated from this rating curve (Ham, 2005a). Sometime measurement may produce inconsistent results or high variability with the same discharge. For example, the large scatter of the observed data in the Fraser River bedload rating curve plot indicates that there was variability in the measurements (Figure 2.1).
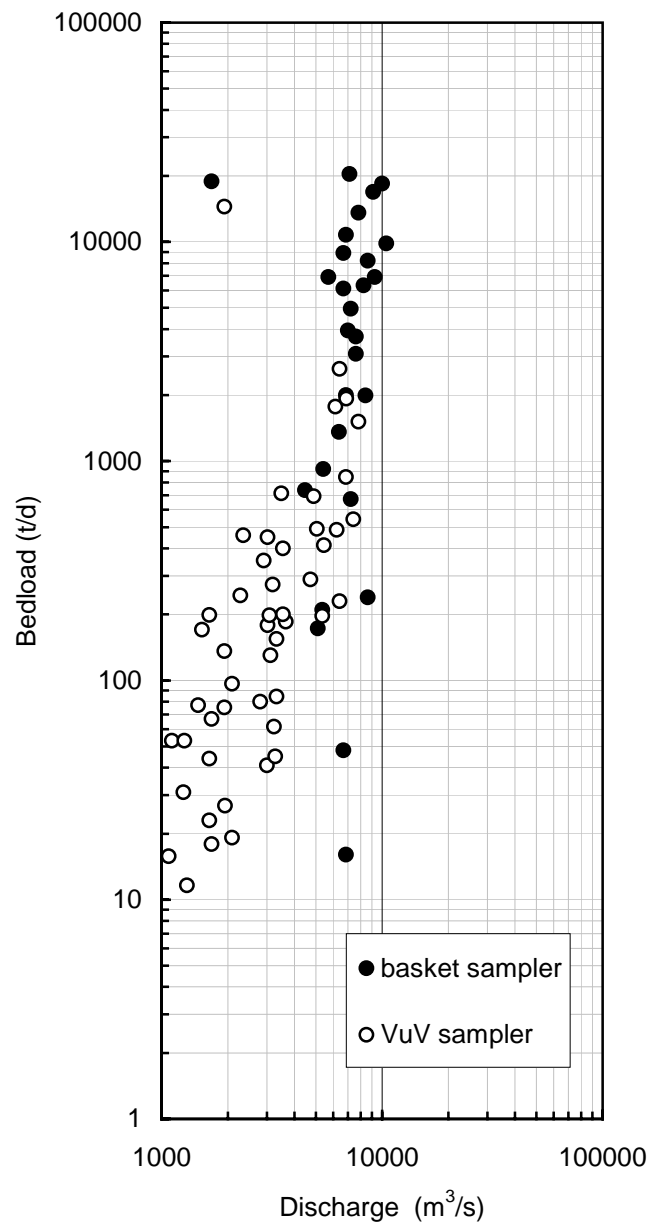
Figure 2.1: Bedload data at Agassiz-Rosedale Bridge showing variability in the measurements [bedload data (1965-1986) plotted from Environment Canada HYDAT CD-ROM].

2.3.2 Indirect Estimation Methods

(a) Repeated Survey Method:

In this method, the sediment budget is based upon repeated hydrographic surveys of the channel bed (bathymetry) to determine changes associated with sediment erosion and deposition. The survey interval depends on the river morphological characteristics. On the Lower Fraser River, changes occur over years to decades, with erosion and deposition occurring largely in distinct zones (McLean and Church, 1999b). Therefore, repeated bathymetric surveys can be used to describe these changes, provided the temporal and spatial resolution of the surveys is sufficiently high. For Lower Fraser River gravel reach, hydrographic surveys are available for 1952 and 1999 with partial surveys from 1984 (Mission to Agassiz), 1991 (Mission to Harrison River) and 2003 (Mission to Herrling Island). Figure 2.2 shows the historic channel surveys in 1952 and 1984 near Greyell Island on 1949 Base Map (Ham, 2005a).
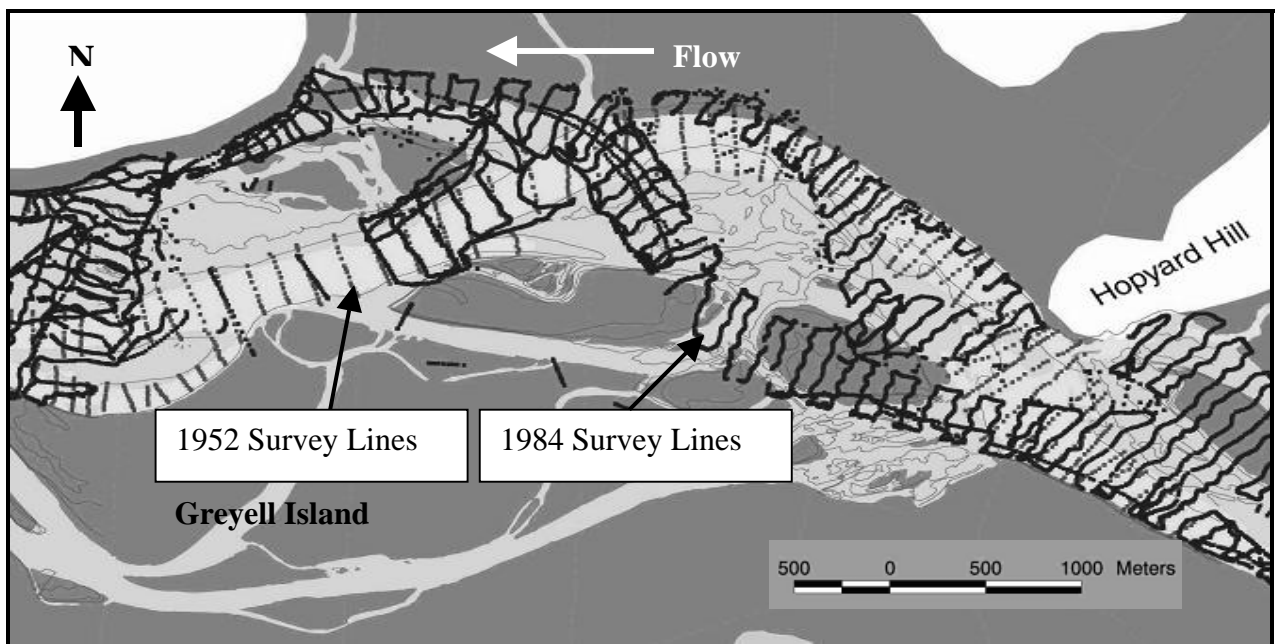
Figure 2.2: Historic Channel Surveys in 1952 (dotted line) and 1984 (solid line) near Greyell Island, Lower Fraser River (after Ham, 2005b).

McLean (1990) analyzed the surveys from 1952 to 1984 for gravel transport estimation for Lower Fraser River. Surveys from 1952 and 1984 have been re-analyzed (Ham, 2005a) to validate the methodological approach adopted in this study by comparing results with those given in McLean (1990) using the same data. In addition, the recent 1999 and 2003 resurveys of the channel have been used to provide an updated transport rate estimate at Agassiz, with an extension to Laidlaw. The additional surveys allow the spatial and temporal variability of storage and transport zones along the river to be determined more reliably than was possible using a single 32 years inter-survey period. The main drawback of this method is a series of survey data over a long period must be available. It also depends on the accuracy of the interpolation schemes used to generate the riverbed bathymetry. This method is particularly useful to determine the gravel budget for the Lower Fraser River, because all gravel passing the Agassiz-Rosedale Bridge is deposited before Sumas Mountain (Figure 1.2).

(b) Morphological Methods:

The basis for relating changes in channel morphology to sediment transport is the morphologic sediment budget, which can be expressed for a defined channel reach as (Church, Ham and Weatherly, 2001):

$$V_o = V_i - (1 - \mathrm{p})dV \quad \text{………………………………………………………..…… (2.2)}$$

where,
V_o is volumetric sediment output,
V_i is volumetric sediment input to the reach over some specified time,
dV is net difference between scour and fill of the channel between two surveys
p is sediment porosity.

The above equation can be converted to a mean transport rate equation by dividing the time between successive channel surveys. The complete budget may also take into account removals of sediment through dredging or artificial means and changes in storage associated

with erosion and deposition of island and floodplain deposits. Conventionally all terms are expressed as mineral volume (e.g. t/d or t/y). Virtually, there is not much difference between the morphological method and the repeated survey method. In the morphological method planimetric data, aerial photograph and satellite images are examined in detail and a geographic information system (GIS) is use as a major tool for all types of data processing and analysis. Data acquired from several sources such as hydrographic survey data, Light Detection and Ranging (LIDAR) survey data, Global Positioning System (GPS) and total stationing field survey data are accumulated together to create a representative bathymetry of the river and flood plain. The drawbacks of this method are that data acquisition may be expensive, and that it requires accurate estimation of any artificial gravel extraction or any other local sediment intrusion such as landslide debris intrusion.

(c) Bedload Estimation with Transport Equation:

Bedload transport equations provide an indirect estimate of bedload transport based on flow hydraulics and sediment characteristics. Researchers have been developing methods for estimating bedload flux for over a century. There are many non-cohesive bedload transport formulas available in relevant literature (Yang 1996; Chang, 1988; Vanoni, 1975; Graf, 1971). Four prime approaches have been used to design these formulas: the shear stress based approach (e.g. du Boys, 1879), physically and stochastically based approach (e.g. Einstein, 1950), stream-discharge based approach (e.g. Schoklich, 1934), and stream power based approach (e.g. Bagnold, 1980). In the above approaches bedload discharge is usually described either as a function of water discharge, $q_b = f(q - q_c)$ or velocity, $q_b = f(U - U_c)$ or shear stress, $q_b = f(\tau - \tau_c)$ or, stream power, $q_b = f(\omega - \omega_c)$ where, q_c, U_c, τ_c ω_c describe the critical or threshold values of the discharge (q), velocity (U), shear stress (τ), and stream power respectively.

A realistic measure of flow strength that has been found to provide a general description of transport rate is the bed velocity or bed shear stress (Wilcock et al., 2001). Most of the popular formulas use velocity or shear stress rather than direct use of discharge. Estimation of

bed velocity is generally more complicated than the estimation of bed shear stress (Wilcock et al., 2001). Again, the total bed shear stress is not responsible for bedload transport. Total bed shear stress can be divided into two components, grain shear stress and bed form shear stress (Einstein and Barbarossa, 1952). Only grain shear stress is responsible for bedload transport in gravel-bed river. Therefore, a useful sediment transport function must have a reduction factor or component to separate grain shear stress from total shear stress. A good example of this type of shear stress separation can be found in the Meyer-Peter and Müller (1948) bedload transport equation.

Many bedload transport formulas have been developed but all depend upon basic assumptions such as steady flow, equilibrium transport and negligible wash load transport, which might not be the reality (Cunge et al., 1980). Most of them are empirical or semi-empirical in nature and results obtained from different formulas may vary by one to two orders of magnitude with the same input data. The reasons might be that most of the formulas were developed from laboratory flume experiments or, using a particular data set. It is difficult to select one single formula that will best apply to a given river. No one formula can describe the complete physics of the bed material transport process (Gomez and Church, 1989), but computational sediment transport models are nonetheless dependent on these types of equations. However, a calibrated model may provide reasonably good results for scientific or engineering purposes. In the Lower Fraser River gravel reach it is important that the sediment transport equation specifically address bed armoring.

2.4 Mathematical Modeling for Flow Sediment Transport Simulation and Morphological Change Prediction

A mathematical model is by nature a simplified description of an actual system or process. Mathematical modeling is a quantitative way to understand complex systems and phenomena. Simulation is complementary to the traditional approaches of theory and experiment. Together, modeling and simulation make up an approach that can address a wide range of physical problems, and at the same time exploit the power of the fastest growing

computing facilities. A hypothetical morphodynamic model has three basic component hydrodynamics, sediment transport and morphology (Figure 2.3).

Hydrodynamics (water flow)	→	Sediment Transport (bedload discharge)	→	Morphology (bed elevation change)

Figure 2.3: A hypothetical morphological model.

The principles of mass, momentum, and energy conservation are used to describe the physics of fluid motion. Typically, the fundamental equations governing unsteady flow in open channels are premised on conservation of mass and momentum in a bounded system. The Navier-Stokes equations describe three-dimensional fluid motion. In river hydraulics, it is assumed that fluid is incompressible and mean effects of turbulence can be handled by some sort of averaging. These equations are known as Reynolds-averaged Navier-Stokes equations or RANS. Occasionally other terms must be added to the more fundamental equation forms in order to produce a widely useful numerical simulation model. There are three types of models available in river hydraulics based on the number of spatial dimensions: three-dimensional model, two-dimensional depth-averaged model, and one-dimensional section-averaged model. The number of equations required to develop a flow, sediment transport and morphological model depend on the spatial dimensions adopted. For example, in a one-dimensional model one continuity and one momentum equation (Saint Venant equations) for water flow, one continuity equation for bed level change (Exner equation) together with a sediment transport formula are required. In a two-dimensional model, two momentum equations (Reynolds-averaged Navier-Stokes equations) are required for water flow and another dimension will be added for both flow and sediment continuity equations.

Flow equations could be either in conservative or non-conservative forms. In conservative form flow derivatives are expressed in terms of discharge or flux and cross-sectional area, whereas in non-conservative form flow derivatives are expressed in terms of velocity and water depth. Comparing the conservative and nonconservative form of the momentum equation, the nonconservative form is simpler and appears to be more attractive. However, one clear prerequisite for using the nonconservative form of the momentum equation

is a continuous velocity field. For a discontinuous velocity field, related to the presence of shock waves, the conservative form must be used. Conservative form is suitable to handle both supercritical and sub-critical flow and non-conservative form is suitable to handle sub-critical flow such as alluvial stream flow in a wide downstream river reach. Some authors report increased numerical stability when the conservative form is used, although a rigorous analysis has not been performed (Luettich, et al., 1991). Note that the preservation of conservative property depends on the equation to be solved as well as the numerical method applied. Use of conservation form itself doesn't guarantee that the numerical solution is more stable and accurate

In practice, when all governing equations are solved simultaneously then it is called coupled solution. Alternatively, liquid phase and solid phase can be solved separately, which is called uncoupled solution. In an uncoupled model, the continuity and momentum equations for water are uncoupled from the sediment continuity equation. Sediment transport rate will be calculated when flow simulation has completed in response to updated bed level changes at previous time step. Then, the sediment continuity equation will be solved to obtain a new bed elevation. In a coupled model flow, sediment transport and morphological changes are calculated within the same time step.

All the governing equations are non-linear partial differential equations so a closed analytical solution is not possible, but a complete numerical solution may be possible. The common solution methods are finite difference, finite volume and finite element. Most of the existing models are based on the finite difference method. Use of finite element based models is increasing in river hydraulics with the development of faster computers and graphical user interface tool. In all methods, the flow domain is divided into discrete spatial increments and direct or iterative approximation techniques are used to approach a convergent solution. Therefore, the accuracy of the model results is influenced by the spatial descritization and solution techniques chosen. The details of governing equation for a depth-averaged two-dimensional hydrodynamic, sediment transport and morphological model are described in the next sub-section.

2.5 Governing Equations

For a depth-averaged two-dimensional hydrodynamic, sediment transport and morphological model the main governing equations are continuity and momentum equations for water mass (flow), sediment discharge equation and sediment continuity equation. In addition to these governing equations, a helical flow-equation for bend correction is required in standard two-dimensional depth-averaged modeling.

2.5.1 Continuity and Momentum Equations for Water Flow

The shallow water equations are frequently used in mathematical models to describe the water flow in wide rivers, coastal areas, lakes and estuaries. Natural stream flow is three dimensional in nature but the third dimension is supposed to be so restricted by the magnitude that the flow can be sufficiently described with two horizontal space variables. Thus, three-dimensional natural flow can be simplified to two-dimensional flow by using vertical averaging techniques (Vreugdenhill, 1994). The two-dimensional shallow water equations are based on the depth-averaged flow velocity (depth integration of the Navier-Stokes equations). These equations can be obtained by integrating the horizontal momentum equations and the continuity equation over the flow depth, h $(x, y) = H (x, y) - Z_b (x, y)$. The result of the integration over depth is as follows (Vreugdenhill, 1994 and DHI, 2002b):

Continuity equation-

$$\frac{\partial H}{\partial t} + \frac{\partial P}{\partial x} + \frac{\partial Q}{\partial y} = 0 \ \dots\dots\dots\dots\dots\dots\dots\dots\dots\dots\dots\dots\dots\dots\dots\dots\dots\dots\dots\dots\dots\dots \ (2.4)$$

x- momentum equation-

$$\frac{\partial P}{\partial t} + \frac{\partial}{\partial x}\left(\frac{P^2}{h}\right) + \frac{\partial}{\partial y}\left(\frac{PQ}{h}\right) + gh\frac{\partial H}{\partial x} + \frac{gP\sqrt{P^2+Q^2}}{C^2h^2} - \frac{\partial}{\partial x}\left(E\frac{\partial P}{\partial x}\right) - \frac{\partial}{\partial y}\left(E\frac{\partial P}{\partial y}\right) = 0 \ldots\ldots\ldots\ldots\ldots (2.5)$$

Local	Convective	Pressure	Friction	Turbulence
acceleration	acceleration	force	force	force
term	terms	term	term	term

y- momentum equation-

$$\frac{\partial Q}{\partial t} + \frac{\partial}{\partial y}\left(\frac{Q^2}{h}\right) + \frac{\partial}{\partial x}\left(\frac{PQ}{h}\right) + gh\frac{\partial H}{\partial y} + \frac{gQ\sqrt{P^2+Q^2}}{C^2h^2} - \frac{\partial}{\partial x}\left(E\frac{\partial Q}{\partial x}\right) - \frac{\partial}{\partial y}\left(E\frac{\partial Q}{\partial y}\right) = 0 \ldots\ldots\ldots\ldots (2.6)$$

where,

t - time,

x, y – Cartesian coordinate system,

H (x, y) - position of water level related to a fixed reference level (m),

P - the flux density in the x-direction given by $P = Uh$ (m^3/s/m),

Q - flux density in the y-direction given by $Q = Vh$ (m^3/s/m),

U and V - depth-averaged velocity components in x- and y-directions (m/s),

h - depth of the flow (m),

g - acceleration due to gravity (m/s^2),

C – Chezy's resistance coefficient (m$^{1/2}$ /s),

E - eddy viscosity coefficient and

Z_b (x,y) - bottom level of the channel (m).

      The two-dimensional shallow water equations used in a mathematical model are based on various underlying assumption that may include (1) single-layer flow (vertically homogeneous fluids), (2) incompressible fluid (constant density), (3) hydrostatic pressure distribution (vertical acceleration is neglected), (4) Fluid drag along the river banks is neglected, and (5) Coriolis forces, wind forces and barometric forces are neglected (DHI, 2002b). Therefore, the above hydrodynamic equations are generally valid for shallow, gently varying

topography and mildly curved and wide river channel with small Froude number.

2.5.2 Flow Resistance Equations

To calculate discharge or flow depth in a natural or artificial channel, it is necessary to adequately parameterize the flow resistance. The main sources of flow resistance may be categorized as follows (Bathurst, 1985; Leopold et al., 1960): (1) boundary resistance resulting from (a) friction or drag of the bed grains, (b) bed forms presents in the channel and (c) vegetation or wood, (2) flow resistance due to channel cross-sectional shape and longitudinal variability of bed slope and water surface slope and channel plan forms (meander bends, alternate bars, etc.) and resistance due to the presence of any artificial structure, (3) resistance to flow due to distortion of free surface of the channel such as hydraulic jumps, wave or bore, etc.

The first empirical approach to flow resistance was published by Antoine Chezy in 1700's and his relationship is widely known as Chezy's equation,

$$V = C\sqrt{RS} \qquad \text{... (2.7)}$$

where, V is the mean velocity of flow, R is the hydraulic radius, S is the energy slope and C is the Chezy's coefficient for resistance. Chezy's equation is not a rational equation, and Chezy's C has different values depending upon the system of units used (Henderson, 1966). However, a non-dimensional form of Chezy's equation $(C/\sqrt{g} = V/V_*, \text{ where}, V_* = \sqrt{gRS} =$ Friction Velocity) is also available in Fluid Mechanics literature (Becchi, 1979). Chezy's work was followed by Wiesbach. In 1845, Wiesbach published his empirical equation for head loss and flow resistance for pipe flow as

$$h_f = f\frac{L}{D}\frac{V^2}{2g} \qquad \text{... (2.8)}$$

where, D is diameter of the pipe, f is friction factor, V is flow velocity, L is the pipe length and g

is acceleration due to gravity. Later, this relationship was adapted for open channel flow considering $D = 4R$ (R is hydraulic radius of the channel), and $S = h_f/L$ (S is the energy slope),

$$f = \frac{8gRS}{V^2}$$ …………………………………………..…………………………………….……… (2.9)

Manning's equation followed Weisbach and was first published in 1891 in Ireland:

$$V = \frac{K_n}{n} R^{2/3} S^{1/2}$$ …………………………………………………………………….… (2.10)

where, n is known as Manning's coefficient and K_n is a unit conversion factor ($K_n = 1$ for Metric and $K_n = 1.49$ for English system, respectively).

Manning's equation is the most used and referenced relationship for flow resistance in open channels. The Manning's equation is not dimensionally correct. Conventionally, Manning's roughness coefficient "n" is considered to be a constant that is independent of either flow or depth. However, data presented in channel roughness catalogues such as Hicks and Mason (1991), clearly demonstrate that this is rarely true. Manning's n typically varies significantly with discharge and depth. Manning's and Chezy's equations can be readily inverted to define the friction slope in two-dimensional and three-dimensional moment equations (Vereugdenhill, 1974; Kuipers and Vereugdenhill, 1973). For example, Manning's friction slopes S_{fx} and S_{fy} in x and y directions of a two-dimensional model can be given as:

$$S_{fx} = \frac{n^2 U \sqrt{U^2 + V^2}}{h^{4/3}}$$ ……………………………………………………………………… (2.11)

$$S_{fy} = \frac{n^2 V \sqrt{U^2 + V^2}}{h^{4/3}}$$ …..………………………………………………………..…… (2.12)

and Chezy's friction slopes S_{fx} and S_{fy} in x and y directions of a two-dimensional model can be given as:

$$S_{fx} = \frac{U\sqrt{U^2 + V^2}}{hC^2}$$ .... (2.13)

$$S_{fy} = \frac{V\sqrt{U^2 + V^2}}{hC^2}$$ .... (2.14)

where, U, V are the mean velocities of flow in the x and y directions, respectively, and h is the flow depth.

An alternative approach to measure the flow resistance is based on turbulent boundary layer theory. A boundary layer is that part of an infinitely deep flow past a surface which is retarded by the friction at the surface (Bathurst, 1993). The velocity distribution law for a rough boundary layer flow can be written as

$$\frac{V}{V^*} = \frac{1}{\kappa}\left[\ln\left(\frac{y}{y'}\right)\right]$$ .... (2.15)

where, V is the velocity at a distance y from the boundary, κ is Von Karman constant (usually 0.4), V^* is the shear velocity and y' is the distance such that $V = 0$ at $y = y'$. This approach was adapted by Prandtl for smooth boundaries and Nikuradse for rough boundaries from a relationship of shear and velocity profile into a relationship of flow resistance as,

for smooth boundaries, $\dfrac{V}{V^*} = 5.75\log\left(\dfrac{V^* y}{v_s}\right) + 5.5$ .... (2.16)

for rough boundaries, $\dfrac{V}{V^*} = 5.75\log\left(\dfrac{h_0}{k_s}\right) + 8.5$ .... (2.17)

24

where, $V*$ is the shear velocity ($V* = \sqrt{gRS}$) defined by von Karman in 1930, h_o = channel water depth, ν_s is Kinematic Viscosity and k_s is the height of the bed roughness elements. Of all of the turbulent equations, the von Karman-Prandtl equations are the most fundamentally sound, but this equation assumes that the resistance is due solely to grain shear stress. It was developed primarily for sand where k_s = D$_{65}$, but the value of k_s for larger material and steeper channels was not discussed.

By integrating the Karman-Prandtl equation Keulegan (1938) obtained a relationship,

for smooth boundaries, $\dfrac{V}{V^*} = 5.75 \log\left(\dfrac{V^* R}{\nu_s}\right) + 3.25$ …..……..………….………… (2.18)

for rough boundaries, $\dfrac{V}{V^*} = 5.75 \log\left(\dfrac{R}{k_s}\right) + 6.25$ ………………………………..….…… (2.19)

Meyer-Peter-Muller (1948) was the first to point out that total channel resistance (f) can be divided into a grain resistance (f') and a form resistance (f''). Then, various researchers (Griffiths, 1981; Millar, 1999) tried to developed flow resistance formulas to fit it to the particular type of channel bed, such as sand-bed or gravel-bed or boulder-bed. A typical example of a gravel-bed resistance formula is Millar's (1999) formula,

$$f' = \left[2.03 \log\left(\dfrac{12.2 h_0}{k_s}\right)\right]^2 \text{……………………………………………………………… (2.20)}$$

In 1923, a particle size approach was proposed by Strickler. He showed that the resistance coefficient was independent of depth, but varied with the size of the bed material. Bed material characteristic size can be represented by a diameter with D_{50}, D_{16}, D_{84} etc. (D_s in meters).

$n = D_{50}^{1/6} / 6.7\sqrt{g}$ (Strickler, 1923) ……………………………………………………….… (2.21)

Several Strickler type formulas (in SI Unit and D_s in meter) have been developed over the years.

$$n = D_{50}^{1/6} / 25.2 \text{ (Kuelegan, 1938)} \dots\dots\dots\dots\dots\dots\dots\dots\dots\dots\dots\dots\dots\dots\dots\dots\dots\dots (2.22)$$

$$n = D_{90}^{1/6} / 26 \text{ (Meyer-Peter Mueller, 1948)} \dots\dots\dots\dots\dots\dots\dots\dots\dots\dots\dots\dots\dots (2.23)$$

$$n = D_{75}^{1/6} / 21.14 \text{ (Lane and Carlson, 1953)} \dots\dots\dots\dots\dots\dots\dots\dots\dots\dots\dots\dots\dots\dots (2.24)$$

All equations (2.21 – 2.24) were originally developed for sand bed application. However, few researchers have tried to apply Strickler type equation in gravel bed river such as Kellerhals (1967) used a Strickler type equation with a higher exponent value (1/4) of D_{90}. Several other researchers have pointed out that Manning's *n* is not solely based on bed material size, either D_{50} or D_{90}. Several equations have been published for gravel channels that recognize the effect of flow depth as well as size of bed material (Millar and Quick, 1993; Hey, 1979):

$$n = \frac{K_n R^{1/6}}{\sqrt{g}\, 5.75 \log\left(12.5 \dfrac{R}{3.5 D_{84}}\right)} \text{ Hey (1979)}\dots\dots\dots\dots\dots\dots\dots\dots\dots\dots\dots\dots\dots\dots\dots (2.25)$$

$$n = \frac{K_n R^{1/6}}{\sqrt{g}\, 5.75 \log\left(12.2 \dfrac{Y_0}{3.5 D_{90}}\right)} \text{ Millar and Quick (1993)}\dots\dots\dots\dots\dots\dots\dots\dots\dots\dots . (2.26)$$

In conclusion, some remarks can be made on flow resistance formulas and their formulation as follows:

i. Due to the complexity and variability of components of the friction loss in alluvial streams, and to the changeable property of resistance for flow carrying sediment, a unified and complete understanding of resistance in alluvial streams does not exist at

present. However, the resistance coefficient is the most significant variable in computational hydraulics.

ii. Presently available open channel resistance formulas are based on an assumption of steady, uniform flow which in reality, does not persist in natural river flow. The mostly adopted Manning's coefficient, "*n*" or Chezy's coefficient, "*C*" are not global constants. Often the coefficient varies spatially with flow depths and discharges in a mobile-bed river, and this variation needs to be considered.

iii. In the case of channels with large floodplains, determination of flow resistance for floodplains must be considered separately from the resistance of the main channel.

iv. None of the available formulas can guarantee the accurate calculation of this friction resistance co-efficient. As a result, flow resistance factor should be determined in the model calibration process and using observed discharges, water levels and flow velocity.

2.5.3 Turbulence Closure Equations

In natural rivers flow is always turbulent. A turbulent force term is an essential part of a momentum equation (for example, Equations 2.5 and 2.6). It can be incorporated into the momentum equation in many ways. Some discussion and review is necessary about this term. When the flow is turbulent it is preferable to decompose the instantaneous variables such as velocity components and pressure into a mean component and a fluctuating component, i.e. $U_i = \overline{U} + U'$. There are two reasons for decomposing the variables, the first one is when we measure flow quantities we are usually interested in the mean values rather than the instantaneous time histories. The second reason is that when we want to solve the Navier-Stokes equation numerically it would require a very fine grid to resolve all turbulent scales and it would also require a fine resolution in time (turbulent flow is always unsteady). We can write the generalized Navier-Stokes equations as

$$\frac{\partial U_i}{\partial t} + U_j \frac{\partial U_i}{\partial x_j} = -\frac{1}{\rho}\frac{\partial P}{\partial x_i} + \nu\nabla^2 U_i \;\ldots\ldots\ldots\ldots\ldots\ldots\ldots\ldots\ldots\ldots\ldots\ldots\ldots\ldots\ldots\ldots\ldots..\ldots\ldots\ldots\ldots \text{(2.27)}$$

where, ρ is fluid density, ν is the kinematic viscosity, U is the velocity vector of the fluid parcel and P is the pressure terms.

After incorporating the above decomposition terms into Navier-Stokes Equation, we can obtained Reynolds-averaged Navier-Stokes Equation (so-called RANS) as Reynolds appears to have been the first person who proposed this technique (Lane et al., 1999):

$$\frac{\partial U_i}{\partial t} + U_j \frac{\partial U_i}{\partial x_j} = -\frac{1}{\rho}\frac{\partial P}{\partial x_i} + \nu\nabla^2 U_i - \frac{\partial \overline{U_i' U_j'}}{\partial x_j} \;\ldots\ldots\ldots\ldots\ldots\ldots\ldots\ldots\ldots\ldots\ldots\ldots\ldots\ldots\ldots.\ldots\ldots\ldots\ldots \text{(2.28)}$$

This averaging adds one more term in the RANS that is called Reynolds stress tensor. It represents correlations between fluctuating velocities. In addition, it is an additional stress term due to turbulence (fluctuating velocities) and it is unknown. This term adds six more unknowns in the three-dimensional turbulence problem and causes it to have more unknowns than number of equations. This situation is called the closure problem: the number of unknowns (ten: three velocity components, one pressure and six stresses) is larger than the number of equations (four: one continuity equation and three components of the Navier-Stokes equations). Thus, we need a model for $\overline{U_i' U_j'}$ to close the system.

For decades, many different methods have been proposed to solve the closure problem. Turbulence models are typically called turbulence closure schemes since they allow the governing equations for shallow open-channel flow to become closed when considering the effects of turbulence. A short summary of different type of turbulence models is given in Table 2.1.

Table 2.1: Summary of turbulence models.

Name of the Models	Examples
Zero (0) equation models	Eddy viscosity model, Prandtl Mixing Length model, Cebeci-Smith and Baldwin-Lomax Models
1- Equation models	k-equation model, Wolfshtein, Baldwin-Barth and Spallart-Allmaras models
2-equation models	k-ε model, k-ω model

Zero- equation models or algebraic models consist of algebraic relations to define the local eddy viscosity. One- and two-equation models attempt to model the time history of turbulence. One-equation models consist of a single partial differential equation that attempts to capture some of the history of the eddy viscosity. Two-equation Models consist of two partial differential equations that attempt to capture some of the history of the eddy viscosity. As the number of equations increases, the computational effort increases and one has to balance improvements in modeling with the capture of important turbulence information.

Zero-equation models specify a constant eddy viscosity or determine the eddy viscosity based on a mixing length hypothesis. The turbulent transfer of momentum by eddies gives rise to an internal fluid friction, in a manner analogous to the action of molecular viscosity in laminar flow, but taking place on a much larger scale. The value of the coefficient of eddy viscosity (an exchange coefficient) is of the order of 1 m^2 s^{-1}, or one hundred thousand times the molecular kinematic viscosity depending on the spatial grid resolution. Eddy viscosity is often represented by the symbol v_t. The eddy flux in kinematic units is related to the mean vertical velocity gradient, such as in the following example for vertical flux of horizontal momentum:

$$\overline{u'w'} = -v_t \frac{\delta U}{\delta z}$$ ………………………………………………………………………………… (2.29)

where, w is vertical velocity, U is horizontal mean flow velocity in the x direction, the over bar represents an average and the prime denotes the deviation or perturbation from an average.

Eddy viscosity is a function of the flow, not of fluid properties. It is greater for flows with more turbulence. The eddy viscosity approach is a parameterization for the eddy momentum flux (Reynolds stress) that works reasonably well when only small eddies are present in the flow, but behaves poorly when large-eddy coherent structures. The eddy-viscosity assumption is valid under certain conditions such as equilibrium channel flow condition. Although eddy-viscosity models are not conceptually correct, they are extensively used and have achieved significant success in solving engineering problems.

In a two-dimensional depth-average hydrodynamic model, the turbulent fluctuations (Reynolds stresses) may be modeled employing the Boussinesq eddy viscosity concept (DHI, 2002a). Many efforts have been made to expand the applications of eddy-viscosity models in hydrodynamic models. For example, in the MIKE 21C model a total of three different turbulent closures can be used, these are: velocity based constant eddy viscosity, flux based constant eddy viscosity and Smagorinsky sub-grid scale eddy viscosity. Some others hydrodynamic models use more sophisticated turbulence closure schemes. For example, TELEMAC-2D provides the choice among the k-ε, Smagorinsky or Elder turbulence models (TELEMAC-2D, 1995). A description of a two-equation turbulence model is given in Lane and Richards (1998) who have been tested and applied a two-dimensional hydrodynamic model to a multi-thread reach of a proglacial stream.

Generally, the overall solution of the two-dimensional depth-averaged open channel flow equations is not highly sensitive to the selection of the eddy viscosity coefficient (SWMC/DHI, 2001a). However, the turbulence stress terms usually have a stabilizing effect on the numerical solution process (SWMC/DHI, 2000a). The velocity-based eddy viscosity formulation is more accurate than the other two formulations. Unfortunately, it is more difficult to implement in the numerical algorithms because the equation system uses the fluxes as the unknown parameters instead of velocities. To resolve this problem the velocity-based formulation is implemented by using the velocities from the previous time steps. This can create a stability problem when the eddy viscosity coefficient becomes large (DHI, 2002b). To avoid

this problem the Courant criterion (C$_r$): $\dfrac{V_t \Delta t}{\Delta x^2} \le \dfrac{1}{2}$ has to be fulfilled in all grids in any case in the depth-averaged two-dimensional model (for example MIKE 21C model). There is no straightforward rule to select the eddy viscosity in a hydrodynamic flow simulation model. The best way to select an eddy viscosity coefficient is trial and error or calibration based on the model user guidelines (if any). In river hydraulics literature, commonly used eddy viscosity values range from 0.1 m^2/s to 2 m^2/s in practical application for sand bed river (DHI, 2000a). For gravel bed rivers, a higher value is expected.

2.5.4 Sediment Continuity Equation (Exner Equation)

A sediment continuity equation is necessary to compute the riverbed level change due to sediment transport. Sediment continuity is derived from the conservation of mass or volume of the riverbed. It is important to know how a sediment continuity equation is derived for two-dimensional model application. Consider a reference area "A" of the sediment bed with unit width normal to the flow and with length Δx above a distance z from a datum plane (Figure 2.4).
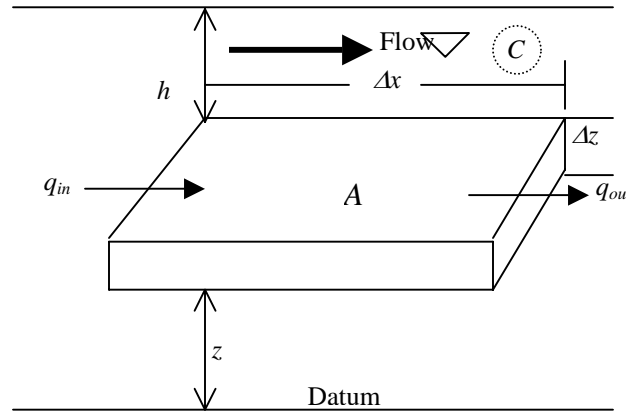
Figure 2.4: Schematic diagram to derive the sediment continuity equation.

If the flow is transporting sediment, then unit sediment transport (sediment transport rate /unit width) can be denoted by q_s. This may include sediment moving near the bottom or in suspension. Considering the volume of concentration of suspended sediment is C. The

31

difference between the sediment inflow $[q_s]_{in}$ and outflow $[q_s]_{out}$ can be describe by Δq_s

$$\left. q_s \right|_{in} - \left. q_s \right|_{out} = -\Delta q_s \dots\dots\dots\dots\dots\dots\dots\dots\dots\dots\dots\dots\dots\dots\dots\dots\dots\dots\dots\dots \quad (2.30)$$

Change in sediment storage (Δq_s) per unit time, Δt, in the reference area can be effected two ways: (i) by the deposition or erosion of the river bed which alters the bed elevation by an amount of Δz, and (ii) by the change of average concentration C of the sediment in suspension. Assume that the deposition or scouring occurs uniformly over the whole reference area for a unit time. Equating the difference between the sediment inflow and outflow over a unit width per unit time, Δt, and the total storage change we get (mass balance)

$$-\Delta q_s \Delta t = (1-\lambda)\Delta z\Delta x + h\Delta C\Delta x \dots\dots\dots\dots\dots\dots\dots\dots\dots\dots\dots\dots..\dots\dots\dots... \quad (2.31)$$

where, λ is the porosity of the bed and h is the depth of flow.

$$\text{or,} \quad -\frac{\Delta q_s}{\Delta x} = (1-\lambda)\frac{\Delta z}{\Delta t} + h\frac{\Delta C}{\Delta t} \dots\dots\dots\dots\dots\dots\dots\dots\dots.\dots.\dots\dots\dots...\dots..\dots \quad (2.32)$$

In the limit, as Δx and $\Delta t \to 0$,

$$-\frac{\partial q_s}{\partial x} = (1-\lambda)\frac{\partial z}{\partial t} + h\frac{\partial C}{\partial t} \dots\dots\dots\dots\dots\dots\dots\dots\dots\dots\dots\dots\dots\dots\dots..\dots\dots.. \quad (2.33)$$

This equation is the sediment continuity equation that relates the time rate of change of bed elevation at a point, $\dfrac{\partial z}{\partial t}$, to the downstream rate of change of sediment transport at that point, $\dfrac{\partial q_s}{\partial x}$, and the time rate of change of total suspended-sediment concentration in the flow, $\dfrac{\partial C}{\partial t}$. If there is no suspended sediment in the flow or if concentration does not change with time (i.e., sediment transport equal to the bedload transport, $q_s = q_b$) above mass balance equation

becomes,

$$(1-\lambda)\frac{\partial z}{\partial t} + \frac{\partial q_b}{\partial x} = 0 \dots\dots\dots\dots\dots\dots\dots\dots\dots\dots\dots\dots\dots\dots\dots\dots\dots\dots\dots\dots\dots (2.34)$$

If we consider unit lateral sediment inflow Δq_e from bank erosion and sediment transport in two-dimensional case then the above equation can be re-written as,

$$(1-\lambda)\frac{\partial z_b}{\partial t} + \frac{\partial q_{bx}}{\partial x} + \frac{\partial q_{by}}{\partial y} + \Delta q_e = 0 \dots\dots\dots\dots\dots\dots\dots\dots\dots\dots\dots\dots\dots\dots\dots.. (2.35)$$

where,

z_b is bed elevation,

q_{bx} and q_{by} are the total sediment transport rate/unit length in the x and y direction, respectively,

Δq_e is lateral sediment supply from bank erosion,

λ is the porosity of the bed material, and

t is time.

2.6 Sediment Transport Functions

Sediment transport equations suitable for gravel-bed rivers were reviewed and surface based sediment transport equations were found to be most suitable. A surface based relation can be applied for both equilibrium and non-equilibrium transport conditions. Two prominent formulations are the Parker (1990) and Wilcock and Crowe (2003) equations.

Parker, Klingeman and McLean (1982) developed an empirical formula for an armored gravel-bed river based on the concept of equal mobility. A consequence of the equal mobility hypothesis is that the bedload size distribution is approximated by that of the sub-surface. Two parameters, namely a dimensionless bedload transport function W_i^*, and dimensionless shear stress ϕ_i, were defined for different grain size classes. Then, they applied the concept of

similarity transformation to collapse different curves representing different size fractions into a single universal curve. Because of equal mobility of all size ranges, only one grain size, D_{50} of the sub-surface layer was used to characterize the bedload discharge as a function of dimensionless shear stress $[W^* = f(\phi)]$. Subsequently, Parker (1990) transformed the substrate-based Parker-Klingeman-McLean (1982) gravel transport relations to surface-based relations. The surface-based relation incorporates a hiding function which accounts for smaller particles sheltering amongst coarser grains. The hiding function allows for differential or selective transport of grains of varying sizes, and at the same time allows for the formation of a mobile armor.

Following Parker (1990), Wilcock and Crowe (2003) developed their surface based bedload transport equation using a similarity collapse over fractional transport rate, as used by others (Ashida and Michue 1971; Parker et al., 1982) successfully for substrate-based empirical models. It is essentially a modified form of the Parker (1990) surface based relation. This sediment transport equation is described in detail in the next sub-section.

2.6.1 Wilcock and Crowe surface based gravel bedload transport equation (2003)

Wilcock and Crowe (2003) equation is a recently developed surface based transport relation. This equation accounts for bed surface armoring, hiding of small particles amongst larger grains and allow for computation by individual grain sizes. The form of the similarity collapse is,

$$W_i^* = f(\tau / \tau_{ri}) \quad \text{..} \quad (2.36)$$

where, $\tau =$ bed shear stress, $\tau_{ri} =$ reference value of τ, and W_i^* is defined by

$$W_i^* = \frac{(s-1)g q_{bi}}{F_i \left(\dfrac{\tau}{\rho} \right)^{\frac{3}{2}}} \quad \text{..} \quad (2.37)$$

34

where, s = ratio of sediment to water density, g = acceleration of gravity, q_{bi} = volumetric transport rate per unit width of size i, F_i = proportion of size i on the bed surface, and ρ = density of water.

To find the q_{bi} from equation (2.37) one must calculate W_i^* for the size i. Wilcock and Crowe plotted W_i* as a function of (τ / τ_{ri}) for all size fractions for all their experimental runs (Fig. 6, Wilcock and Crowe, 2003) and established relation as follows:

$$W_i^* = \begin{cases} 0.002\phi^{7.5} & \phi < 1.35 \\ 14\left(1 - \dfrac{0.894}{\phi^{0.5}}\right)^{4.5} & \phi \geq 1.35 \end{cases} \quad\text{..}(2.38)$$

where, $\phi = \dfrac{\tau}{\tau_{ri}}$.

It is essential to know the reference shear stress, τ_{ri} for a size i and total bed shear stress, τ, to calculate W_i^* through ϕ. So, a general model for hiding function was introduced to find the relation between τ_{ri} of size D_i and a mean grain size D_{sm}. In this relation the partial shear stress for each individual size D_i present in a size distribution was scaled by the shear stress for the mean grain size, D_{sm}. The authors found a dimensionless relationship between these two non-dimensional parameters are as follows,

$$\frac{\tau_{ri}}{\tau_{rm}} = \left(\frac{D_i}{D_{sm}}\right)^b \quad\text{..}(2.39)$$

where, b is an exponent and can be written as

$$b = \frac{0.67}{1 + \exp(1.5 - D_i / D_{sm})} \quad\text{..}(2.40)$$

35

and *b* was estimated from a curve fitting through their experimental data. However, still a complete basis is required to predict the τ_{rm}. The reference shear stress (τ_{rm}) for the mean grain size can be written as dimensionless Shield's number,

$$\tau_{rm}^* = \frac{\tau_{rm}}{(s-1)\rho g D_{sm}} \quad \text{………………………..………………………………..………………… (2.41)}$$

where, τ_{rm}^* is the dimensionless Shield's parameter for the mean grain size. Typically this value was chosen for surface based gravel transport as 0.0368 (Parker, 1990).

Wilcock and Crowe (2003) showed that this value could be reduced further based on percent sand content in the channel bed-surface or from a bulk sample of the sub-surface. A general relation to calculate the τ_{rm}^* based on surface sand content F_s was given as

$$\tau_{rm}^* = 0.021 + 0.015 \exp[-20 F_s] \quad \text{…………………………………………………………… (2.42)}$$
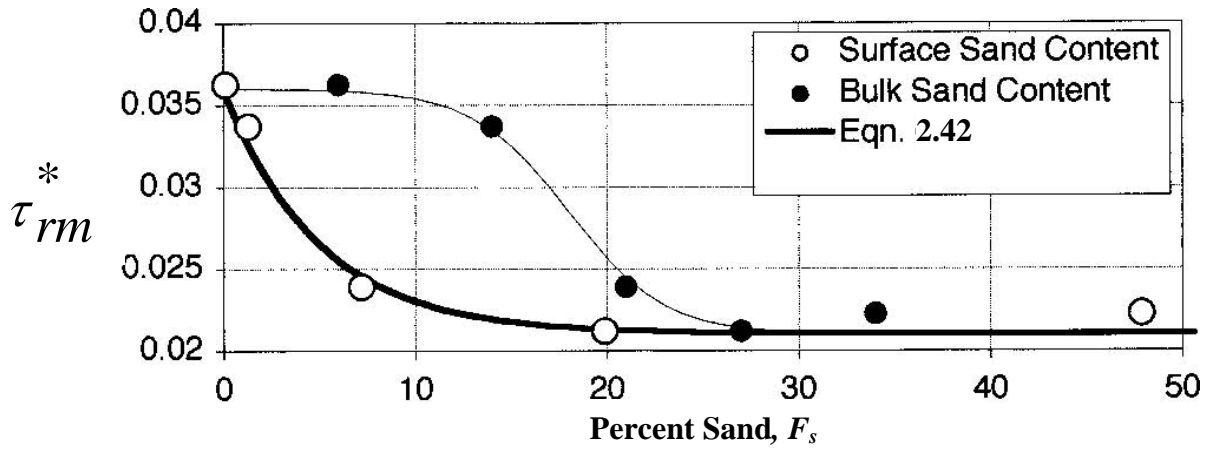
Figure 2.5: Variation of Shield's number, τ_{rm}^* as a function of percent sand content in the channel bed (after Wilcock and Crowe, 2003).

It can be seen from the Figure 2.5 that the Shield's parameter decreases from 0.036 to 0.021 with increasing sand content, F_s. The main reason for decreasing τ_{rm}^* with increasing percent sand content is the transformation the gravel-framework bed to a sand-matrix bed

(Wilcock, 1998). When there is a negligible amount of sand in the bed, the riverbed is composed of an interlocked framework of gravel grains. For, $F_s \geq 0.2$, individual framework grains begin to lose contact. At $F_s > 0.4$, the gravel framework is replaced by the sand matrix with interbedded gravel clasts. In matrix-supported beds, abundant sand is exposed on the bed surface at all possible flows and sand transport rates should approach those of a purely sand bed. Gravel entrainment is no longer influenced by adjacent gravel clasts and depends primarily on local exposure by sand scour.

When there is a very small amount of sand content in the bed then it will settle between the gravel grains, leaving little or no sand exposed to the flow so, it may be expected that τ_{rm}^* for sand is equal to τ_{rm}^* for gravel (Wilcock, 1998). This trace amount has no influence on τ_{rm}^* of gravel. As a result, for a minor amount of sand content ($F_s \rightarrow 0$), τ_{rm}^* is close to 0.036, which, was developed from purely gravel-bed river data from Oak Creek, Oregon (Parker, 1990).

2.7 Secondary Currents and Helical Flow at Bends

A circulatory motion is superimposed on the main flow in both straight and curved channels, which is commonly known as secondary current or secondary circulation (Grade & Raju, 1977). Many river channel features such as meander migration, bar formation, bend scouring, and sediment transport are influenced by this circulation. The magnitude of the helical flow (i.e. the transverse flow velocity component) is generally about one order less than that of the stream-wise flow and rarely exceeds 5-10 % of the main flow velocity in natural rivers (Chang, 1988). Detailed discussion and criticism on secondary flow at meander river bends were presented many authors (Dietrich et al., 1989; Thorne et al., 1985, Thorne and Hey, 1979).

Secondary currents associated with channel bends are studied extensively than those found in straight channels (Raudkivi, 1998). Most probably the reason is that secondary currents in straight channels are balanced from the centerline of the channel and have lesser effects on bed topography, sediment transport and morphology. For a straight channel, the mechanism of

secondary current development is caused by the non-uniform distribution of shear stress over the periphery of the cross section (Raudkivi, 1998).

Helical flow is a principal secondary flow phenomenon in meandered rivers. Whilst it does not have any strong influence on the general flow pattern in rivers with large width-depth ratios, it has a significant influence on the sediment transport direction and hence the morphological changes in the river channel (Olesen, 1987). The mainstream velocities in the upper part of the flow are greater than velocities in the lower part of the flow. Therefore, water particles in the upper part of the water column must follow a path with a larger radius of curvature than water particles in the lower part to maintain nearly constant centripetal force over the depth. Consequently, the normal acceleration is larger near the free surface than the bottom. The transverse pressure gradient is almost constant over a vertical section because of hydrostatic pressure distribution. As a result the transverse pressure gradient near the bottom is obviously greater than the transverse inertia term, and this imbalance sets up an inward flow near the bed (Jain, 2001). To satisfy flow continuity an outward flow near the free water surface will commence. This inward flow near the bottom and outward flow near the free surface will generate a secondary flow circulation at the bend. The secondary current is toward the concave bank (outer bank) of a meander bend in the upper portion of the flow and toward the convex bank (inner bank) in the lower portion of the flow. Therefore, it contributes to move the sediment in the transverse direction from one side of the channel to the other side. An interaction between the longitudinal channel flow and secondary flow will generate a spiral or helical flow at the bend that is three-dimensional in nature [Figure 2.6 (b)].
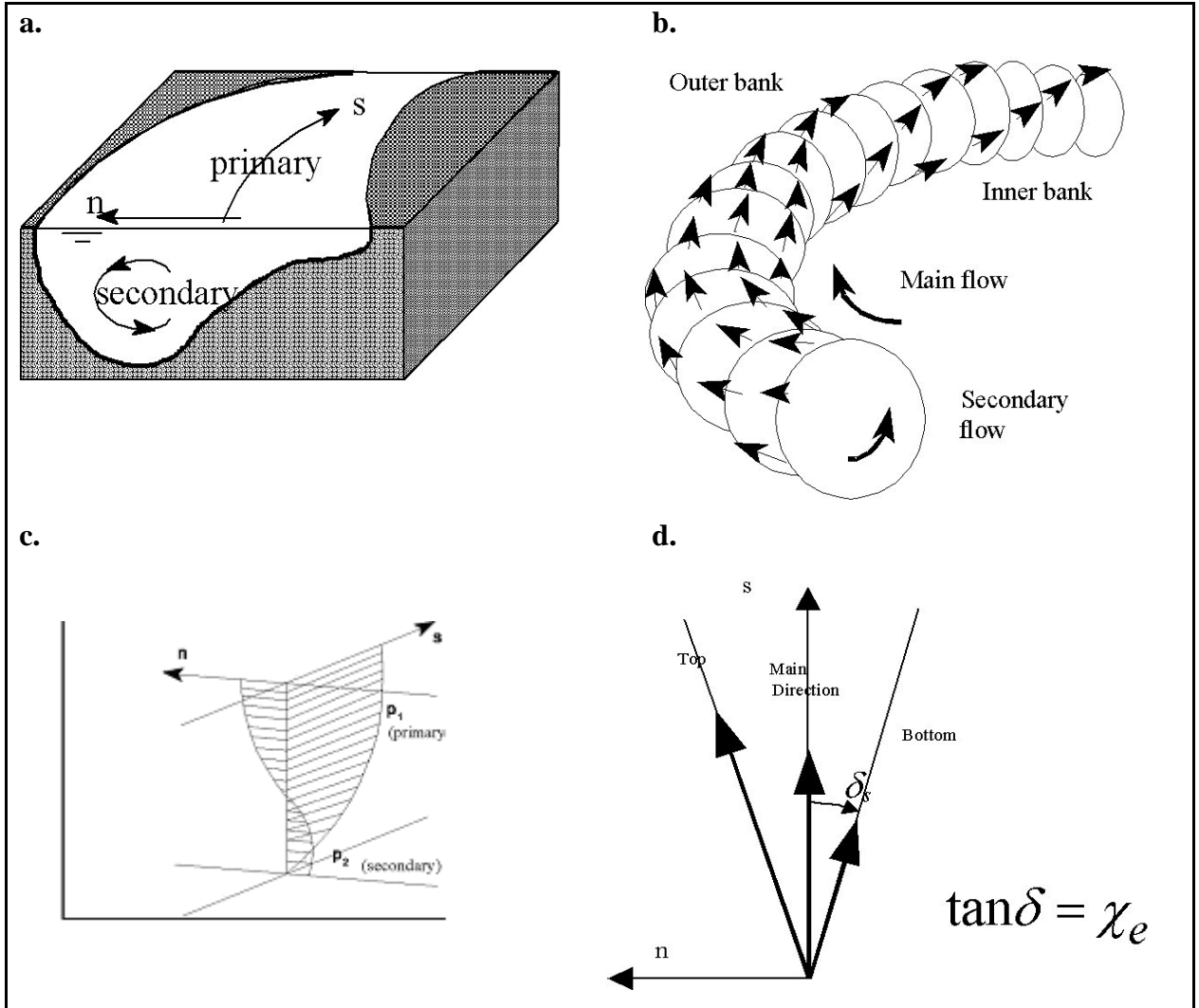
Figure 2.6: Showing primary and secondary currents magnitudes and resulting three-dimensional helical flow directions (DHI, 2002a).

The strength of the helical flow is used to determine the direction of both bedload and suspended load.Secondary current is an important component in the development of bend scour and in formation of point bars as well as alternate bars. Therefore, estimation of the helical flow strength is required with sediment transport simulations when river morphological changes are modeled. A three-dimensional model is necessary to capture the complete helical flow effect at bends. However, a depth-averaged two-dimensional model can be used if the sediment transport due to secondary flow effect can be taken into account. Analytical approaches have been demonstrated by many researchers (Engelund, 1974; Ikeda, Parker and Sawai, 1981; Struiksma

et al., 1985). Assuming a logarithmic main flow velocity distribution over the vertical and a parabolic eddy viscosity distribution, the magnitude of the secondary flow can be shown to be proportional to the main flow velocity, the depth of flow and the curvature of the main flow streamlines. The streamline curvature may be calculated explicitly from the depth integrated flow field. With streamlines radius of curvature R_s, depth H, main flow speed U and Chezy's number C the helical flow intensity can be expressed as:

$$i_s = U \cdot \chi_e$$ …………………………………………………………………….. (2.43)

where, $\chi_e = \dfrac{2}{\kappa^2}\left(1 - \dfrac{\sqrt{g}}{\kappa C}\right)\dfrac{H}{R_s}$ was first derived by Rozowsky, 1957,

κ = Von Karman constant, 0.4,

U = Flow velocity along the channel

g = Acceleration due to gravity.

Most analytical models of flow and bed topography in sinuous channels include the assumption that the secondary flow is locally adapted to channel curvature. Ikeda and Nishimura (1986) have, however, established the existence of a phase lag between the two, induced by inertia, i.e., downstream convective acceleration of the secondary flow. The analysis of Ikeda and Nishimura (1986), nevertheless, includes an unverified assumption.

In a depth-averaged two-dimensional model, the effective shear stress terms are replaced by Reynolds averaged stress terms. Three different terms associated with effective stresses are viscous stress, turbulence stress and dispersion stress. Only turbulence stress terms are modeled by a semi-empirical eddy viscosity approach; the other two types of stresses are ignored. In turbulent flow, viscous stress is not very important but the dispersion stress term can play a key role for secondary circulation. Therefore, many researchers try to incorporate this dispersion stress term in a two-dimensional depth-averaged model.

Three-dimensional numerical models do not require secondary flow correction as they predict vertical velocities directly with net downstream and cross-stream and vertical mass transfers that can be greater than zero. Thus, they allow a more complete representation of the three-dimensional velocity field in which coherent helical circulation does not occur in a cell like manner. If the main flow direction is not parallel to the centerline of the channel, it also can be visualized from the three-dimensional model. Unfortunately, their input data demand is so high that they have seen little application in regional scale river hydraulics applications. The best way to use three-dimensional models is in laboratory scale to improve understanding of secondary circulation effects; then those results can be used to investigate the way in which such three-dimensional effects may be parameterized in two-dimensional models. This type of approach was used by Shimizu et al. (1990) for meanders in which the result was a velocity profile treatment of the effects of secondary circulation.

2.8 Numerical Sediment Transport Models

Natural River flow is often considered as a three-dimensional open channel flow phenomenon. Computational modeling is one of the most cost-effective means of studying open channel flow problems, including sediment transport and morphological processes. The governing equations solved in the models are the Reynolds-averaged momentum equations and the continuity equation for the hydrodynamic flow field, the advection equation for mass transport, and finally the bedload equation compute the sediment transport and Exner equation determine the bed level change. Numerical solution techniques vary from the simple one-dimensional finite-difference method to the complex two-dimensional and 3D finite-difference, finite element or finite-volume schemes (ASCE, 2004).

Many numerical sediment transport models have been developed and used for the prediction of sediment transport and bed level changes. All numerical models developed so far can be divided into three categories according to their dimensions; i.e., one-dimensional, two-dimensional and three-dimensional models. Most commonly used models are one-dimensional and two-dimensional models. A channel network is most efficiently treated with a one-

dimensional model while the floodplain and adjacent areas are best simulated with a two-dimensional model. Although the morphological changes occurring in a river are three-dimensional in nature, due to the high computational cost and the lack of data, full three-dimensional models for this purpose have rarely been used until recently (Lane et al., 1999).

Because of the complex channel geometry, the numerical simulation of flow and sediment transport in a large and wide braided river is extremely difficult with a one-dimensional network model. It requires at least a multi-dimensional hydrodynamic and sediment transport model. Thus, hydraulic engineers in practice often adopt two-dimensional depth-averaged models because of their relative simplicity and less computation time (Fang, 2003). The conventional two-dimensional depth-averaged models corrected for secondary-current effect in the momentum equations and sediment transport equation may be a good alternative of a fully three-dimensional model.

2.8.1 Two-Dimensional Sediment Transport Models

In a two-dimensional sediment transport model, the determining variables (e.g. velocity, sediment concentration) are averaged in one direction, normally in the vertical direction depending upon the flow characteristics and field requirements. Based on this integration two-dimensional models can be classified as depth integrated or laterally integrated two-dimensional models. In depth integrated models all the model parameters and variables are assumed to be the same throughout a water column. In a two-dimensional depth-averaged model, bedload discharges are calculated based on a depth-averaged velocity. Application of two-dimensional models is more complicated as compared to one-dimensional models as this approach needs more resources in all aspects.

There are many advantages in using a depth-averaged two-dimensional- morphological model relative to the conventional branched or non-branched one-dimensional model. The most important model features areas follows:

1) A two-dimensional model can incorporate a full representation of the actual terrain of the area to be modeled (i.e., the model does not have to be schematized as a series of

interconnected cross-sections). This actual terrain representation is achieved through developing a digital elevation model (DEM) of the area from detailed survey data, and interpolating it onto the model grid.

2) A two-dimensional model will determine the actual flow paths to be used as a function of the terrain, as specified on the model grid, and by the applied boundary conditions. Thus, the flow paths of breakouts and complex floodplain flows do not need to be determined a priori as in a one-dimensional model. Further, the flow paths can vary with stage.

3) In a two-dimensional model sub-grid scale turbulence and dispersion of lateral momentum are taken into account by an eddy viscosity term. This allows accurate representation of two-dimensional flow effects such as flow separations, eddy formation, expansions and contractions, and their associated losses.

4) The bed-friction term needs only to incorporate the effects of the actual bed-roughness. Consequently, assigning appropriate bed-friction coefficients becomes more straightforward than in the one-dimensional modeling case. Further, the bed-friction coefficients can be specified in a detailed spatial roughness map, with individual values depending upon the local bed type such as gravel bar, vegetated island, main channel.

5) A two-dimensional model can handle the flooding and drying condition of a grid cell realistically by an incorporated sub-routine mentioning particular values for dry and flood conditions before simulation.

6) A two-dimensional model has vastly superior input and output capabilities. It can take time series of different variables (water level, flow rate or bedload discharge rate) and set flow tilting angles at boundaries as input variables. Water surface elevation, flow flux, sediment flux, depth of inundation, flow velocity, shear velocity and exact velocity directions are all available at every grid point as output variables. Thus, all these out-put parameters can be incorporated directly into mapping routines and/or GIS systems without the need for further interpretation.

2.8.2 Depth-averaged Two-Dimensional Sediment Transport Models

De Vriend (1977, 1987) worked on the theoretical basis of the behavior of two-dimensional sediment transport and morphological models. Struiksma et al. (1985) developed a two-dimensional sediment transport model to simulate large-scale bed change at Delft Hydraulics. Van Rijn (1987) developed a two-dimensional vertical model for predicting morphological changes in laboratory channels. Shimizu and Itakura (1989) developed a two-dimensional bed load transport model for alluvial channels. Kassem (1996) developed a two-dimensional bed load sediment transport model for straight and meandering channels. After the two-dimensional depth-averaged model, van Rijn (1993) used a two-dimensional depth integrated model and assumed a logarithmic velocity profile in the vertical direction to provide a quasi three-dimensional morphological model. He applied his model to steady state flows in a straight channel. Other two-dimensional, depth-averaged models identified in the literature (Kalkwijk and de Vriend, 1980; Shimizu and Itakura, 1989; Odgaard, 1989; Yen and Ho, 1990; Molls and Chaudhry, 1995; Ye and McCorquodale, 1997; Lien et al., 1999; Duan et al., 2001; Duan, 2004; Duan and Julien, 2005; Ghanem, Steffler, Hicks and Katopodis, 1996; Vasquez, Millar, and Steffler, 2007) simulated flow hydrodynamics, mass dispersion, and morphological bed processes. Some of the widely used two-dimensional sediment transport models are CCHE2D (Wu, 2001), RMA2-SED2 (a combination of RMA2 and SED2, USACE 2000), TWODSR, MIKE 21 (DHI, 2003) and MIKE 21C (DHI 2002a).

CCHE2D: CCHE2D is a depth-averaged two-dimensional hydrodynamic, sediment transport and morphological model developed by the Center for Computational Hydroscience and Engineering (CCHE), University of Mississippi. CCHE2D can simulate steady or unsteady free surface flows, sediment transport and morphological processes, including bed aggradation/degradation, bank erosion, channel widening and migration with and without stream structures. This model is numerically stable and computationally efficient (Wu, 2001). A special finite-element method called efficient element method (EEM) was used in this model. Hence, CCHE2D can work with a model domain of any irregular shape. The fourth-order Runge-Kutta time marching scheme is applied to solve the governing equations. Sediment transport modeling is based on equilibrium bedload transport of uniform materials. The bedload

(sand) transport formula developed by van Rijn (1993) has been used and the influence of secondary currents was taken into account by applying the semi-empirical function of Engelund (1974).

CCHE2D model was applied and verified both in laboratory (U-shaped flume study) and natural stream with spur dikes in Hotophia Creek, Mississippi (Duan, Wang and Jia, 2001). EnCCHE2D model, an enhanced version of CCHE2D, was developed by incorporating some additional empirical formulation based on 3-D model experiments (Duan, Wang and Jia, 2001). CCHE2D can simulate the morphological processes of a curved alluvial channel, including bank erosion, bar/pool formation and shifting, bank migration (advance or retreat), channel widening and meander evolution. The EnCCHE2D model was applied to simulate a selected laboratory experiment of the widening of a sine-generated channel (Nagata et al., 1997) and good quantitative agreement with physical model data was obtained.

RMA2-SED2D*:* The RMA2-SED2D model actually consists of two uncoupled models RMA2 and SED2D. RMA2 is a two-dimensional depth-averaged finite element hydrodynamic numerical model. It computes water surface elevations and horizontal velocity components for sub-critical, free-surface flow in two-dimensional flow fields. RMA2 uses a finite element solution of the Reynolds form of the Navier-Stokes equations for turbulent flows. Friction is calculated with the Manning or Chezy equation, and eddy viscosity coefficients are used to define turbulence characteristics. Both steady and unsteady state (dynamic) problems can be analyzed with RMA2. The models are run sequentially, with output information from RMA2 being passed to SED2D as input information. SED2D is a two-dimensional finite element model that solves the convection-diffusion equation with bed source-sink terms (USACE, 2000). These terms are structured for either sand or cohesive sediments. Cohesive deposited material forms layers, and bookkeeping allows layers of separate material types, deposit thickness, and age. SED2D uses the hydrodynamic solution generated by the RMA2 model. Since RMA2 and SED2D are uncoupled, a new geometry must be cycled back to RMA2 when the bed deposition and erosion patterns begin to significantly affect hydrodynamics.

The SED2D model can be applied in areas where flow velocities can be considered two-dimensional in the horizontal plane (i.e., the speed and direction can be satisfactorily represented as a depth-averaged velocity). It is useful for both deposition and erosion studies and, to a limited extent, for stream width studies. The program treats two categories of sediment: (a) non-cohesive, which is referred to as sand; and (b) cohesive, which is referred to as clay. Either steady state or transient problems can be analyzed. The exchange of material with the bed can be calculated or suppressed. Default values can be used for many sediment characteristics or these values may be prescribed by input data. Either the smooth wall velocity profile or the Manning equation may be used to calculate bed shear stress due to currents. The model supports both clay and sand beds individually, but the two bed types cannot be contained within the same model. Therefore, a separate model run is required for each effective grain size. Fall velocity must be prescribed along with the water-surface elevation, x-velocity, y-velocity, diffusion coefficients, bed density, critical shear stresses for erosion, and erosion rate constants (USACE, 2000).

RMA2-SED2D can be used in sediment scour, transport, and deposition studies near major obstructions to river flow, such as navigation dams and bridge crossings. The RMA2-SED2D numerical hydrodynamic and sedimentation models were used to address the navigation problem in the downstream approach channel in the Red River at Jho Lock and Dam (Raphelt, and Alexander, 2001).

River2D: The River2D is a two-dimensional depth-averaged finite element hydrodynamic model, which was designed for use in natural streams and rivers. It has been developed in the University of Alberta by Steffler and Blackburn (2001) and it is freely available at web site (http://www.river2d.ualberta.ca/index.htm). It has special features for supercritical and sub-critical flow transitions, ice covers, and has the capability to change the wet-dry perimeter. River2D is based on the 2D depth averaged St. Venant Equations expressed in conservative form; which form a system of three equations representing the conservation of water mass and the two components of the momentum vector. The dependent variables solved for are the water depth and discharge intensities in the two respective coordinate directions

(Steffler and Blackburn, 2002).

The Finite Element Method used in River2D's hydrodynamic model is based on the Upwind Petrov-Galerkin weighted residual formulation (Hicks and Steffler 1992). In this technique, upstream biased test functions are used to ensure solution stability under the full range of flow conditions, including subcritical, supercritical, and transcritical flow. A fully conservative discretization is implemented which ensures that no fluid mass is lost or gained over the modeled domain. This also allows implementation of boundary conditions as natural flow or forced conditions (Steffler and Blackburn, 2002). River2D do not have any sediment transport capacity however, some primitive type bedload transport capacity have been developed and added into the existing hydrodynamic model to simulate morphological changes in alluvial rivers. This trial version of the model is not available in the web however; application of the sediment transport and morphological model to straight and curve alluvial channels with a single-size sediment were reported by the developer in the technical paper (Vasquez et al. 2005).

TWODSR: TWODSR is an uncoupled, unsteady two-dimensional finite difference based water and sediment routing model. For hydrodynamics, it uses the continuity equation and Reynolds averaged Navier-stokes equations and for sediment transport it uses a two-dimensional expression of the Exner equation with a sediment transport function (a power function of discharge). To account for the bottom shear stress and the friction it uses the Manning or Chezy friction factor. This model was applied and tested for the U.S. Fish and Wildlife Service, Minnesota by Simon D. B. and Chen Y. H. in 1959.This would make it so early as to be obsolete.

Although the depth-averaged, two-dimensional model promises to be a cost-effective tool, determining if a depth-averaged, two-dimensional model can simulate flow hydrodynamics and sediment transport for a large braided gravel-bed river is still an unsolved question. Therefore, validation and verification of sediment transport models are essential for engineers to choose appropriate models for the desired accuracy of engineering applications.

2.9. MIKE 21C: Two-dimensional Hydrodynamic, Sediment Transport and Morphological Model

MIKE 21C is a curvilinear modeling system for two-dimensional free-surface flows developed by the Danish Hydraulic Institute (DHI), with a specific emphasis on river morphology. The standard MIKE 21 hydrodynamic model has been under continuous development at the Danish Hydraulic Institute since 1970, whereas the curvilinear version of MIKE 21 known as "MIKE 21C", using the same solution methods, was developed after 1990. MIKE 21C has been extensively used in many countries for various river applications, particularly where an accurate description of flow along the banks as well as helical quasi-three-dimensional flow is important.

MIKE 21C incorporates fully unsteady flow, bedload as well as suspended load, via a non-equilibrium transport formulation taking into account both phase and time lag effects in the adaptation of suspended load. It includes dynamic bed level changes through the sediment continuity equation (Exner equation), updates the alluvial resistance through a simple power function model on depth for Chezy's C and updates the planform through a bank erosion model and vertical erosion model of the islands. It includes an analytical model for computing the secondary currents, and thus provides the three-dimensional effects for a two-dimensional model. It was mainly developed for sand bed river application and there is no built in transport formulation which can simulate sediment transport in gravel-bed river. As a result, a modification of its sediment transport and morphological code is necessary to apply MIKE 21C in any gravel-bed river. The sequential steps of MIKE 21C hydrodynamic, sediment transport and morphological simulation mechanism are shown by a flowchart in Figure 2.7.
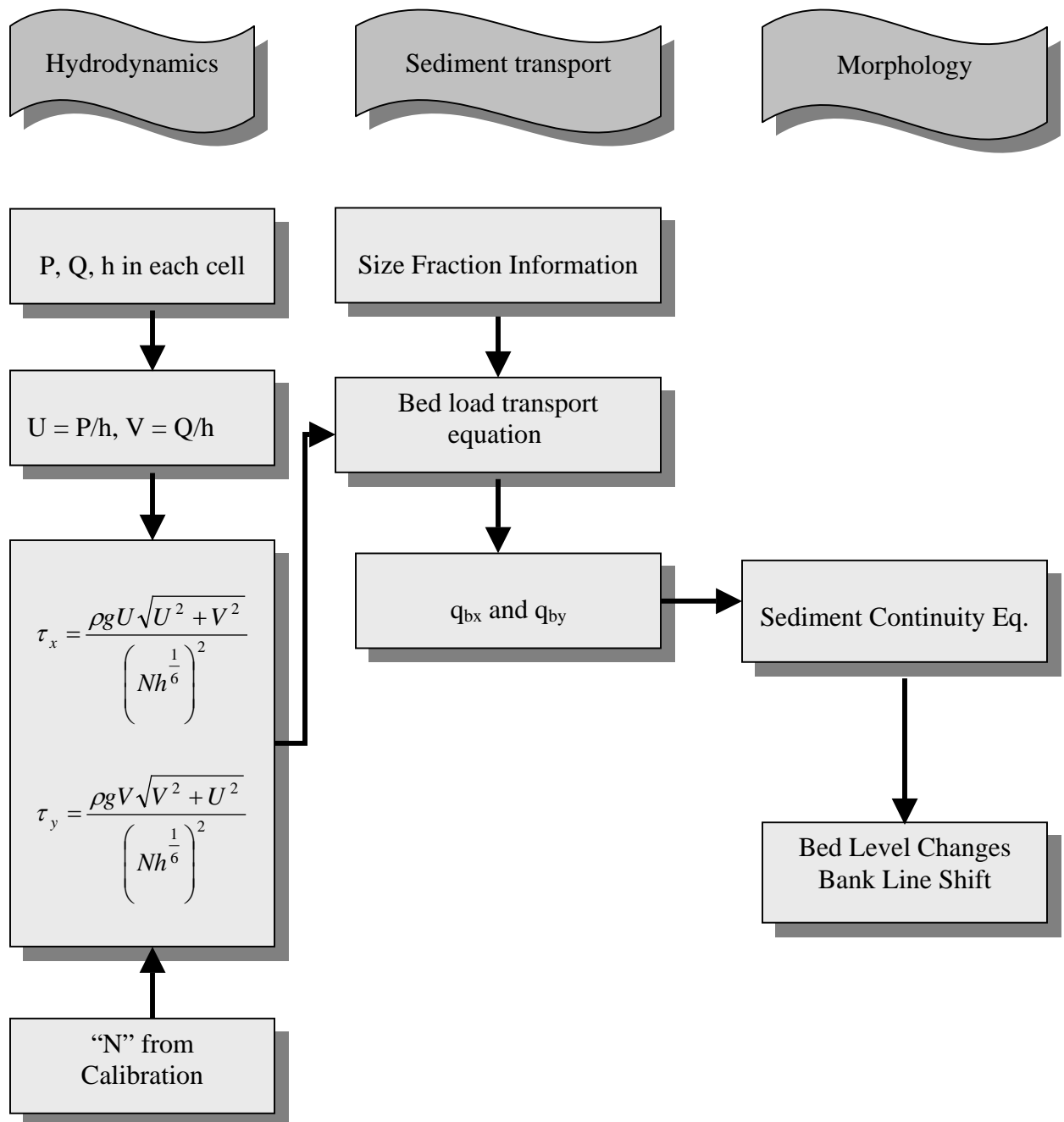
Figure 2.7: Flowchart of MIKE 21C Hydrodynamic, Sediment Transport and Morphological model simulation.

2.9.1 Curvilinear Grid

MIKE 21 C is based on an orthogonal curvilinear grid. An orthogonal curvilinear grid system preserves right angles between the two coordinates at every point of interest in the grid. Two horizontal axes denoted by s-axis and n-axis in a curvilinear orthogonal coordinate system are shown in Figure 2.8. The origin of the rectilinear (global) axes is denoted by "O" and also has shown in Figure 2.8.
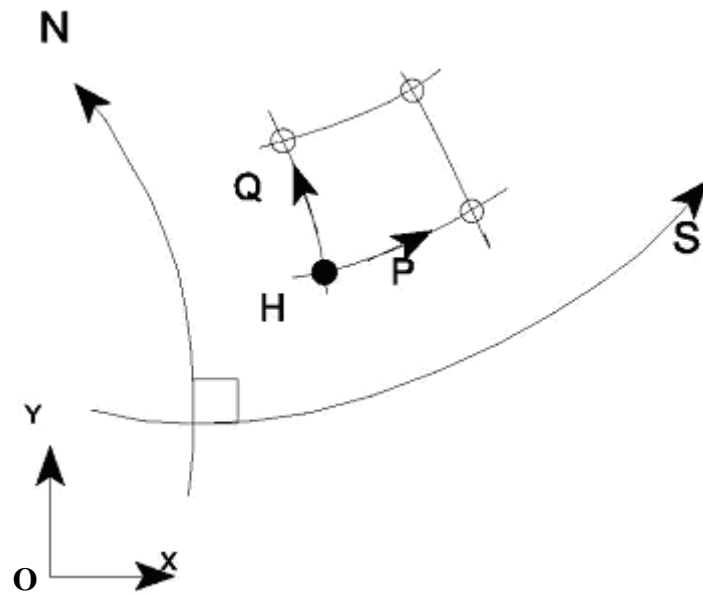
Figure 2.8: Curvilinear coordinate system (s, n) of MIKE 21C model shows a typical orthogonal grid with flow fluxes P and Q and flow depth H.

The main reason of using an orthogonal grid in River Hydraulics problem is that one horizontal axis can follow the bank lines of the river. Use of an orthogonal curvilinear grid makes the finite difference equations describing the two-dimensional flow become substantially simpler than if a rectilinear grid was used. This implies that the numerical scheme becomes more accurate with an orthogonal grid and that the computational speed of the engine improves. In MIKE 21C model, two files are required to define the curvilinear grid (Figure 2.9):

1. A grid (2D matrix) describing the coordinates (x, y) of the four corner points in each

computational grid cell.

2. A grid (2D matrix) describing the depths (and other features) at the center of each computational grid cell
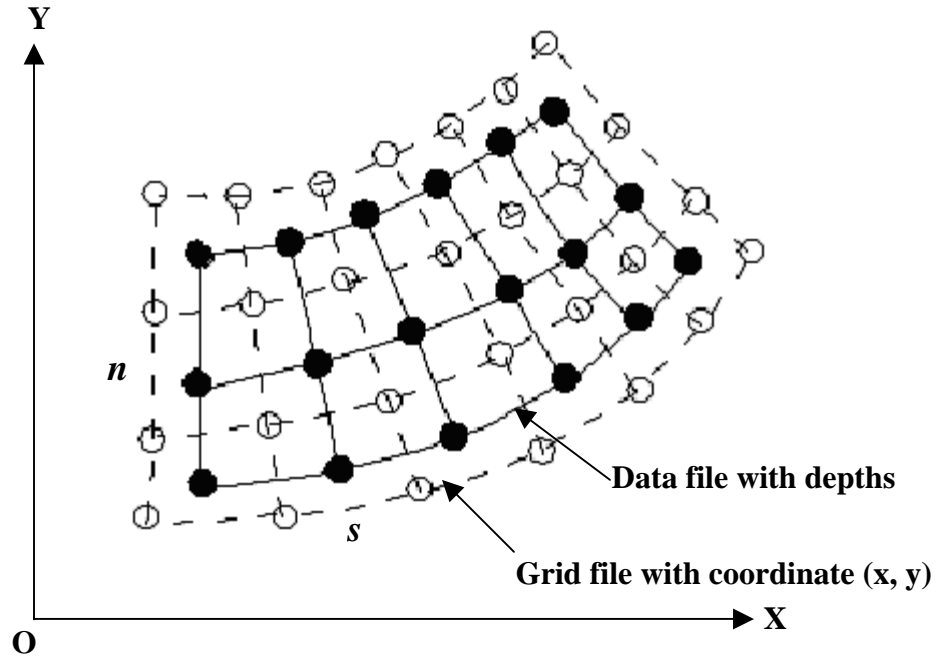
Figure 2.9: Two types of grid files used in MIKE21C Model.

To solve the difference equations in the curvilinear grid, coordinate system orientation is chosen to be parallel with one of the grid lines joining the centers of the grid cells (solid lines in Figure 2.9). The grid lines in this direction are defined as the s-lines. The grid has to be orthogonal, so the direction of the other axis will always be parallel (defined as the n-lines). The radius of curvature between two points (solid circle) can be calculated from the grid file (2D matrix) containing all coordinate (x, y) points. Scalar functions such as depth (h), denoted H in the curvilinear coordinate system ($h = H$), and vector functions such as the velocity components (u,v), denoted (U,V) in the curvilinear coordinate system ($u = U$ and $v = V$), are transformed differently between the two coordinate systems. R_s and R_n denotes the radius of curvature of the s-lines and n-lines respectively at the considered grid point. Transformations between Cartesian and curvilinear co-ordinate systems are shown below.

51

$$\frac{\partial h}{\partial x} = \frac{\partial H}{\partial s} \quad \text{.. (2.44)}$$

$$\frac{\partial h}{\partial y} = \frac{\partial H}{\partial n} \quad \text{.. (2.45)}$$

$$\frac{\partial u}{\partial x} = \frac{\partial U}{\partial s} - \frac{V}{R_s} \quad \text{.. (2.46)}$$

$$\frac{\partial u}{\partial y} = \frac{\partial U}{\partial n} - \frac{V}{R_n} \quad \text{.. (2.47)}$$

$$\frac{\partial v}{\partial x} = \frac{\partial V}{\partial s} + \frac{U}{R_s} \quad \text{.. (2.48)}$$

$$\frac{\partial v}{\partial y} = \frac{\partial V}{\partial n} + \frac{U}{R_n} \quad \text{.. (2.49)}$$

2.9.2 Governing Equations

In MIKE 21C, governing equations express the physical laws and process of the system or phenomenon like any other mathematical model. MIKE 21C model uses conservation forms of unsteady flow equations. Use of the conservation form of the mass equation improves global mass conservation for all of the model domains and decreases the error in numerical computation. Specially, conservation form of mass equation greatly improves local mass conservation in areas with steep bathymetry gradients (Lai et. al, 2002). However, stability, temporal and spatial accuracy results did not change significantly between the two formulations of the momentum equation.

The hydrodynamic model simulates the water level variation (depths) and flows (mass fluxes) in rivers and estuaries. The hydrodynamic model solves the full dynamic and vertically integrated equations of continuity and conservation of momentum in two directions. The

following effects can be included in the equations when used for river applications:

- flow acceleration (local acceleration)
- convective and cross-momentum
- pressure gradients (water surface slopes)
- bed shear stress
- momentum dispersion
- flow curvature and helical flow

The governing equations are very similar to the general flow equations described in section 2.4.1. The only difference is that MIKE 21C model simulations are based on a curvilinear computational grid rather than the conventional rectilinear grid covering the area of interest. The curvature of the grid lines results in some additional terms in the partial differential equations for the flow.

The equations solved in MIKE 21C are:

Continuity equation -

$$\frac{\partial H}{\partial t} + \frac{\partial p}{\partial s} + \frac{\partial q}{\partial n} - \frac{q}{R_s} + \frac{p}{R_n} = 0 \dots\dots\dots\dots\dots\dots\dots\dots\dots\dots\dots\dots\dots\dots\dots\dots\dots\dots\dots\dots\dots(2.50)$$

x- momentum equation-

$$\frac{\partial p}{\partial t} + \frac{\partial}{\partial s}\left(\frac{p^2}{h}\right) + \frac{\partial}{\partial n}\left(\frac{pq}{h}\right) + 2\frac{pq}{hR_n} + \frac{p^2 - q^2}{hR_s}gh\frac{\partial H}{\partial s} + \frac{gp\sqrt{p^2 + q^2}}{C^2 h^2} - \frac{\partial}{\partial s}\left(E\frac{\partial p}{\partial s}\right) - \frac{\partial}{\partial n}\left(E\frac{\partial p}{\partial n}\right)$$

$$+ \frac{2E}{R_s}\frac{\partial q}{\partial s} + \frac{\partial E}{\partial s}\frac{q}{R_s} + \frac{2E}{R_n}\frac{\partial q}{\partial n} + \frac{\partial E}{\partial n}\frac{q}{R_n} = 0 \dots\dots\dots\dots\dots\dots\dots\dots\dots\dots\dots\dots\dots\dots\dots\dots\dots\dots\dots(2.51)$$

y- momentum equation-

$$\frac{\partial q}{\partial t} + \frac{\partial}{\partial n}\left(\frac{q^2}{h}\right) + \frac{\partial}{\partial s}\left(\frac{pq}{h}\right) + 2\frac{pq}{hR_s} - \frac{q^2 - p^2}{hR_n} + gh\frac{\partial H}{\partial n} + \frac{gq\sqrt{p^2 + q^2}}{C^2 h^2} - \frac{\partial}{\partial s}\left(E\frac{\partial q}{\partial s}\right) - \frac{\partial}{\partial n}\left(E\frac{\partial q}{\partial n}\right)$$

$$-\frac{2E}{R_s}\frac{\partial p}{\partial s} - \frac{\partial E}{\partial s}\frac{p}{R_s} - \frac{2E}{R_n}\frac{\partial p}{\partial n} - \frac{\partial E}{\partial n}\frac{p}{R_n} = 0 \dots\dots\dots\dots\dots\dots\dots\dots\dots\dots\dots\dots\dots\dots\dots\dots \text{(2.52)}$$

where,

p, q = mass fluxes in the s- and n-direction, respectively

H = water surface elevation

h = water depth

g = gravitational acceleration

C = Chezy's roughness coefficient

E = Eddy viscosity coefficient

s, n = co-ordinates in the curvilinear co-ordinate system

R_s, R_n = radius of curvature of s- and n-lines, respectively.

Bed shear stress equations-

$$\tau_s = \frac{\rho g U \sqrt{U^2 + V^2}}{N^2 h^{\frac{1}{3}}} \dots\dots\dots\dots\dots\dots\dots\dots\dots\dots\dots\dots\dots\dots\dots\dots\dots\dots\dots\dots \text{(2.53)}$$

$$\tau_n = \frac{\rho g V \sqrt{V^2 + U^2}}{N^2 h^{\frac{1}{3}}} \dots\dots\dots\dots\dots\dots\dots\dots\dots\dots\dots\dots\dots\dots\dots\dots\dots\dots\dots\dots \text{(2.54)}$$

$$\tau = \sqrt{(\tau_s)^2 + (\tau_n)^2} \dots\dots\dots\dots\dots\dots\dots\dots\dots\dots\dots\dots\dots\dots\dots\dots\dots\dots\dots\dots \text{(2.55)}$$

where, τ_s, τ_n and U, V are shear stress and velocity in the s- and n-directions, respectively, ρ is water density, N is the Manning-Strickler number ($N = 1/n$), τ is the total bed shear stress. Bed shear stress is calculated at each time step for each model cell in the hydrodynamic simulation. Then, it is used in the sediment transport calculation. Hence, sediment transport is coupled with the hydrodynamic simulation.

2.9.3 Solution Schemes -The Finite Difference Method (FDM)

Finite difference methods (FDM) are an extensively used numerical solution technique for partial differential equations. FDM can be used for both conservative and non-conservative forms of the governing equations. The basic finite-difference form of the equations can be derived from Taylor series expansions. To express a partial derivative by the Taylor series expansion some higher order terms are neglected. Due to these neglected terms, a truncation error is always associated with the solution so, the finite-difference method becomes an approximate solution method. Based on the discarded terms a finite-difference equation could be of first order, second order, or higher order.

Difference schemes can be said to explicit or implicit based on the time discretization and forward, backward or center based on spatial discretization. The fully explicit schemes are the most popular scheme because they provide faster solution and convenience in comprehension and programming. The fully explicit scheme is faster than the fully implicit scheme however, it can be unstable or only conditionally stable which may put more restriction on the size of the time step. As a result, most of these useful fully explicit schemes are slow in their convergence because of the limitation imposed to the time step in order to ensure the stability of the scheme. From the computational time point of view, implicit techniques are the most efficient. The basic feature of these techniques is that the calculation of a variable at the unknown time level uses unknown values of the same variable at the same time level. Thus a system of equations is required to be solved. The great advantage of these techniques is that they are unconditionally stable, allowing the use of relatively large time steps, which are not strictly associated with the density of the computational grid. Many complex implicit schemes have been developed so far by modifying the basic schemes to increase the accuracy and stability of the numerical solutions (Chaudhry, 1993). When two-dimensional equations (e.g. shallow water wave equation or, heat diffusion equation) represented by the fully-implicit numerical scheme results a penta-diagonal system of equations which is difficult to solve, so a semi-implicit ADI method is applied to solve them by making two tri-diagonal system of equations in two directions or alternating the directions.

(a) First half-step　　　　　**(b) Second half-step**

● Explicit
○ Implicit
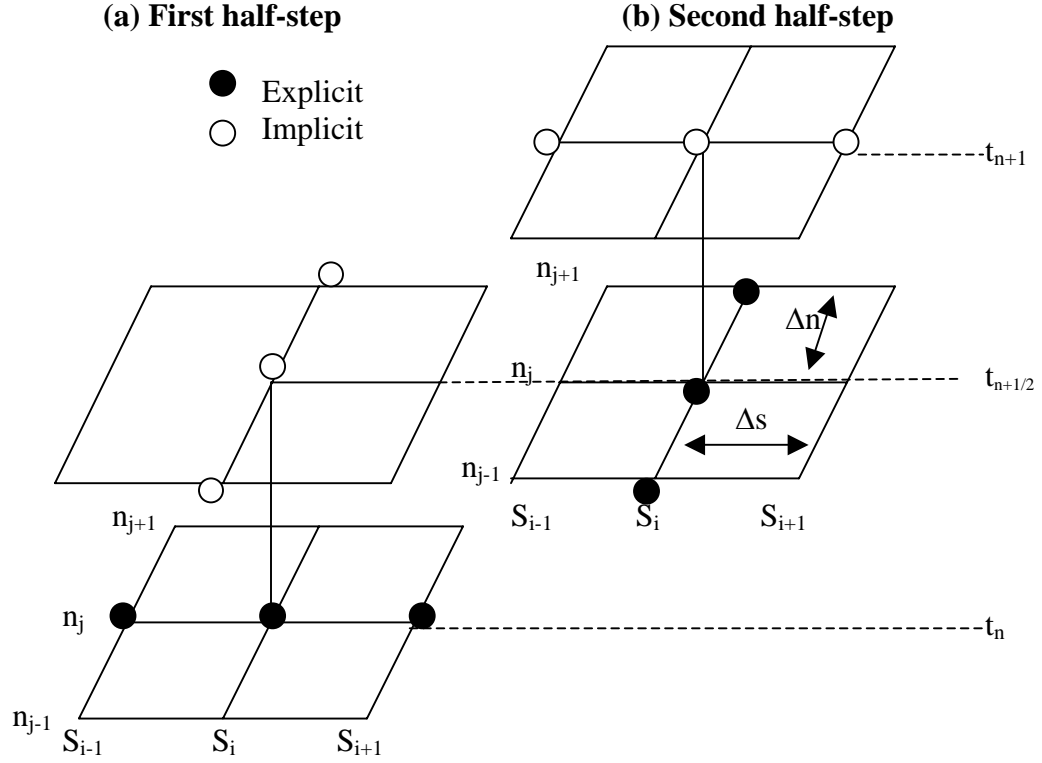
Figure 2.10: Schematic representation of the ADI scheme (showing the typical Cartesian coordinates).
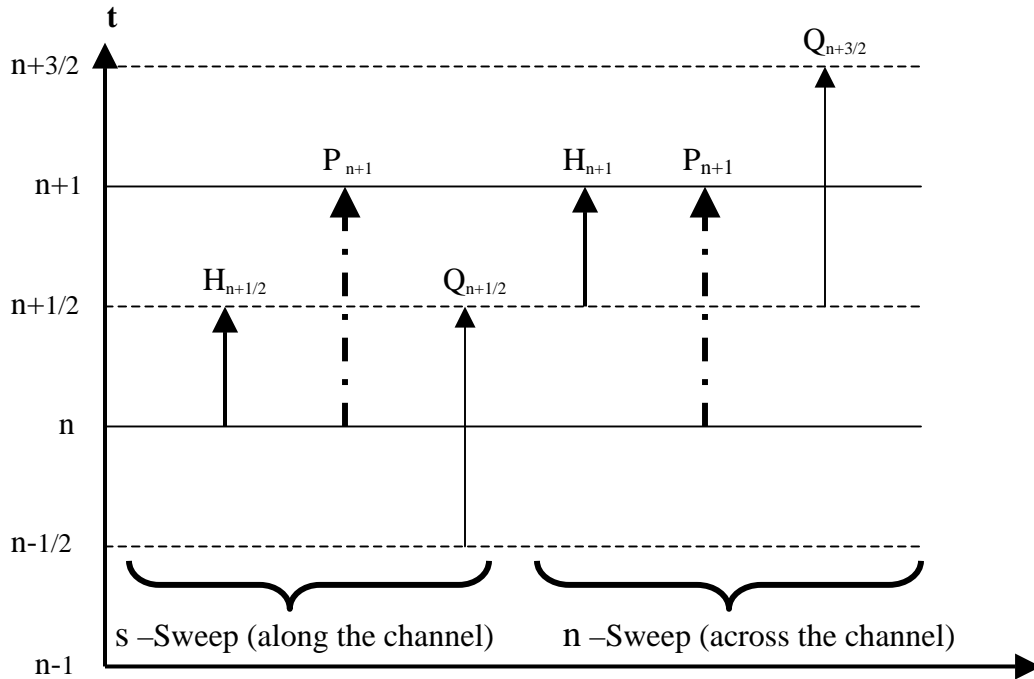
Figure 2.11: Time centering of a typical ADI scheme.

MIKE 21C is a decoupled model. Hydrodynamic simulation and morphological simulation use two different types of numerical schemes. The hydrodynamic model uses an alternating direction implicit (ADI) finite difference scheme (see Figure 2.10 and 2.11) and the morphological model uses an explicit finite-difference scheme. The ADI scheme is second order accurate and explicit scheme is a first order accurate scheme. It is note that explicit schemes can be formulated to have second order accuracy. In the ADI scheme, spatial difference terms are expressed on a staggered orthogonal grid in s and n directions. Staggered (fractioned) means that each time increment is executed in two steps (i.e. two half time steps). In the first half-time step, dependent variables in the s-direction are computed explicitly and in the n-direction implicitly. As a result, some error could be associated with this explicit approximation. In the second half-time step, the dependent variables in the n direction are computed explicitly and in the dependent variables in the s direction are computed implicitly (see Figure 2.10). This way, the error in first half time step is minimized in the later half time step and the scheme becomes very efficient and fast by avoiding the necessity for iteration.

Second order accuracy is ensured through the centering in time and space of all derivatives and coefficients. Time centering of the three unknown variables H, P and Q in three equations (Eq. 2.50 to 2.52) are shown in Figure 2.11. In the s-sweep the continuity and x-momentum equations are solved taking H from n to n+1/2 and P from n to n+1, and Q from two levels of known values from two old time step n-1/2 and n+1/2. In the n-sweep the continuity and y-momentum equations are solved taking H from n+1/2 to n+1 and Q from n+1/2 to n+3/2, and P from the values just calculated in the s-sweep at n and n+1. Adding the two sweeps together gives perfect time centering at n+1/2. It will be worthwhile to mention here, $\Delta s = \Delta n$ has shown in the ADI scheme in Figure 2.10 for the simplicity. Actually, every Δs and Δn may different from each other in the curvilinear grid representation. The application of the semi-implicit finite difference scheme (ADI Scheme) results in a tri-diagonal system of equations for each grid cell in the model. The solution is obtained by inverting the tri-diagonal matrix using the 'Double Sweep algorithm', a very fast and accurate form of Gaussian elimination technique (DHI, 2002b).

A spaced centered - time forward explicit scheme is used in MIKE 21C to solve the sediment continuity equation in the morphological simulation. The time step is limited by the Courant criterion and the Courant number should be less than one to maintain the stability of the scheme. The total sediment transport (S) at each computational grid cell can be divided into two components, S_s and S_n, toward the s and n orthogonal directions in the curvilinear grid (S_s and S_n are analogues to q_{bx} and q_{by} on subsection 2.5.4). The spatial distance between two computational nodes is not constant in the curvilinear grid. This problem is handled by using different Δs and Δn at inflow and outflow boundaries to each grid cell (see Figure 2.12).

Based on the notation shown on the Figure 2.13 (D indicates Δ) the continuity equation for the sediment in a curvilinear grid can be expressed as follows:

$$(1-\lambda)\frac{z_{j,k}^{n+1} - z_{j,k}^{n}}{\Delta t} + \frac{Ss_{j,k}\Delta n_{j,k} - Ss_{j-1,k}\Delta n_{j-1,k}}{\left(\dfrac{\Delta s_{j,k} + \Delta s_{j,k-1}}{2}\right)\left(\dfrac{\Delta n_{j,k} + \Delta n_{j-1,k}}{2}\right)} + \frac{Sn_{j,k}\Delta s_{j,k} - Sn_{j,k-1}\Delta s_{j,k-1}}{\left(\dfrac{\Delta s_{j,k} + \Delta s_{j,k-1}}{2}\right)\left(\dfrac{\Delta n_{j,k} + \Delta n_{j-1,k}}{2}\right)} = 0$$

………………………………………….... (2.56)

Where,

Ss = sediment transport rate in s-direction (longitudinal)

Sn = sediment transport rate in n-direction (lateral)

λ = bed porosity

Δt = time step

Δs = space in s-direction

Δn = space in n-direction

s, n curvilinear co-ordinates

(j, k) grid co-ordinates
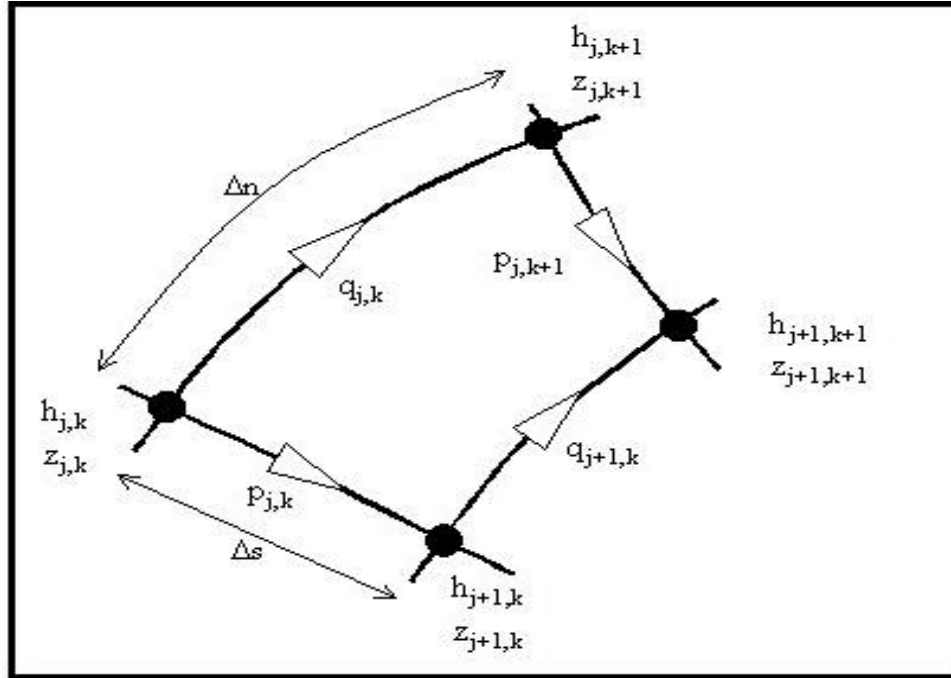
Figure 2.12: Water flow continuity equation descritized on curvilinear grid.
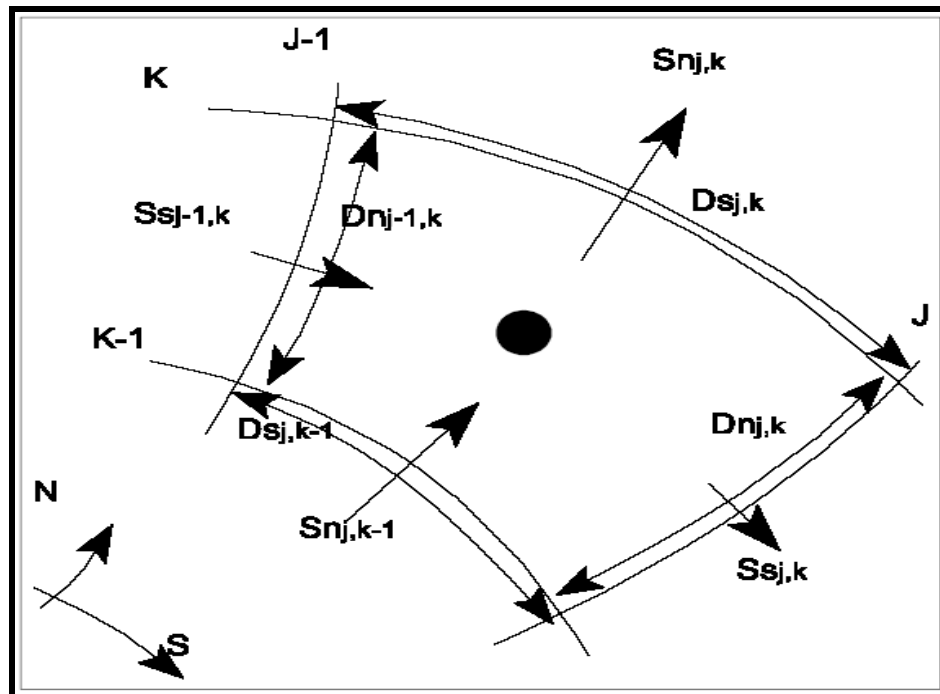
Figure 2.13: Sediment continuity equation descritized on curvilinear grid.

When bedload is dominant in the transport process an uncoupled model is preferable. The argument is that there is an order of magnitude time difference between bed-perturbation waves and water waves. Normally, the morphological simulation time step is much larger than the hydrodynamic time step. It may be as much as 10^4 times larger than the hydrodynamic time step (Jansen et al., 1979). For small hydrodynamic time step, bed variations are neglected. An explicit scheme is chosen to reduce the computational time and increase the ability to simulate longer periods (10 - 50 years). In a coupled formulation the same time step is used for both flow and sediment transport simulation. To increase the efficiency a sediment time step factor (2 to 5) is used in the explicit solution. Therefore, bed level changes are not computed in each hydrodynamic time step. For example, if the hydrodynamic time step is 5 sec and the sediment time-step factor is 3, then bedlevel change will be computed in each 15 sec.

2.9.4 Important Model Outputs

Several outputs can be obtained from the MIKE 21C hydrodynamic and morphological model. Results can be obtained from all grid cells at all time steps or from a specific area (area of interest) by specifying the horizontal (row s) and vertical (columns) grid numbers. The specific simulation period can be fixed by entering the start time end time and time-step increment. The important outputs are as follows:

- Water surface elevation - the water surface elevation, including bed level changes due to morphological change. The water surface elevations saved in the HD Result file are relative to the original bathymetry. The results stored here are updated at each time step to account for bed level change.

- Helical flow intensity - results of the computed deviation of bed shear stress direction compared to depth-averaged flow direction.

- Bedload - computed bedload transport (excluding porosity). Units are m^3/m/s.

- Net sedimentation - computed net sedimentation, with deposition positive and erosion negative. Units are g/m^2, however the results can be converted to a depth by dividing by the bulk sediment density (including porosity, which for gravel is typically 1.7 x 10^6 g/m^3).

- Bed level - computed bed level. Units are m.

- Bed level change - change in bed level from initial bed level, with deposition positive and erosion negative. Units are m.

- Mean grain size - if using a graded sediment model, the mean grain size is saved. Units are mm.

- Single fraction number - if selected result from, only the specified sediment component will be saved. If not, the sum of all components is saved.

- Single-layer number - if selected, only the specified bed layer will be saved. If not, the results of all bed layers are saved.

- Layer thickness - computed depth of each bed layers. Units in m.

3 FRASER RIVER GRAVEL REACH

3.1 Lower Fraser River Gravel Reach

Fraser River is the major river draining south-central British Columbia, Canada. Within its 1,200 km long course, the lower 70 km long reach between Laidlaw and Sumas Mountain near Vedder River at Chilliwack displays a "wandering" gravel-bed morphology (Desloges and Church, 1989). The gravel reach consists of frequent mid-channel islands and low-order braiding. Prominent mid-channel gravel bars are displayed during low flows. Different types of bars such as lateral bars that are attached to the shore or to islands, point bars at bends, and mid-channel bars in areas of flow expansion are available in this reach. The growth of the bars creates flow diversions that may produce a strong flow impingement on the adjacent banks, which initiates new episodes of erosion and channel instability along the river (McLean and Church, 1990). Figure 3.1 and Figure 3.2 shows the limit of study area and a satellite image of Lower Fraser River gravel reach, respectively.

The morphology of Lower Fraser River has been described in several publications and technical reports (Ham, 2005a; Church et al., 2003, 2001; Church 2001; McLean and Church, 1999, 1994). The Lower Fraser River runs in a more-or-less straight path, mainly confined by terraces and landslide deposits upstream of Hope, where it picks up rocks, gravel, sand, silt and clay from the banks and tributaries. Downstream of Hope at Laidlaw, the river emerges into a wider valley and becomes an anastomosing cobble/gravel-bedded river until its confluence with the Sumas River (Figure 3.1). Downstream of Hope, the gradient of the Lower Fraser River decreases progressively as it approaches sea level (McLean and Church, 1990). As a result, the larger fractions of the sediment load are selectively deposited as the gradient is reduced. The largest material (mainly gravel and cobbles) is deposited first so that the river between Hope and Sumas Mountain flows through its own gravel deposits (McLean and Church, 1990). These deposits form a confined alluvial fan upstream of Sumas Mountain. Essentially, all of the river's gravel-bedload is deposited upstream of Sumas Mountain, where there is an abrupt transition from gravel to sand.
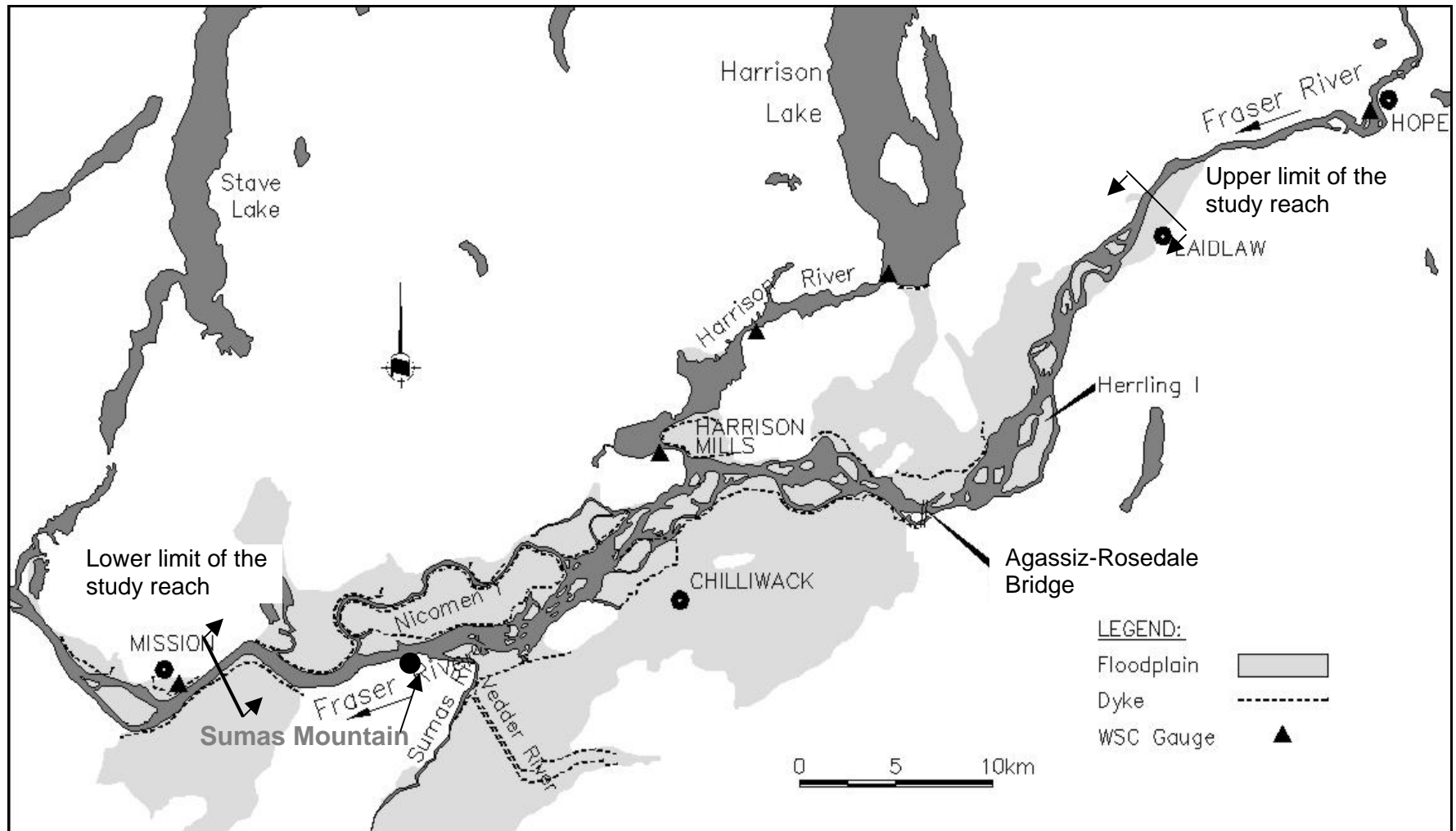
Figure 3.1: Map of the Study Reach between Laidlaw and Mission (Source: Ham 2005b).
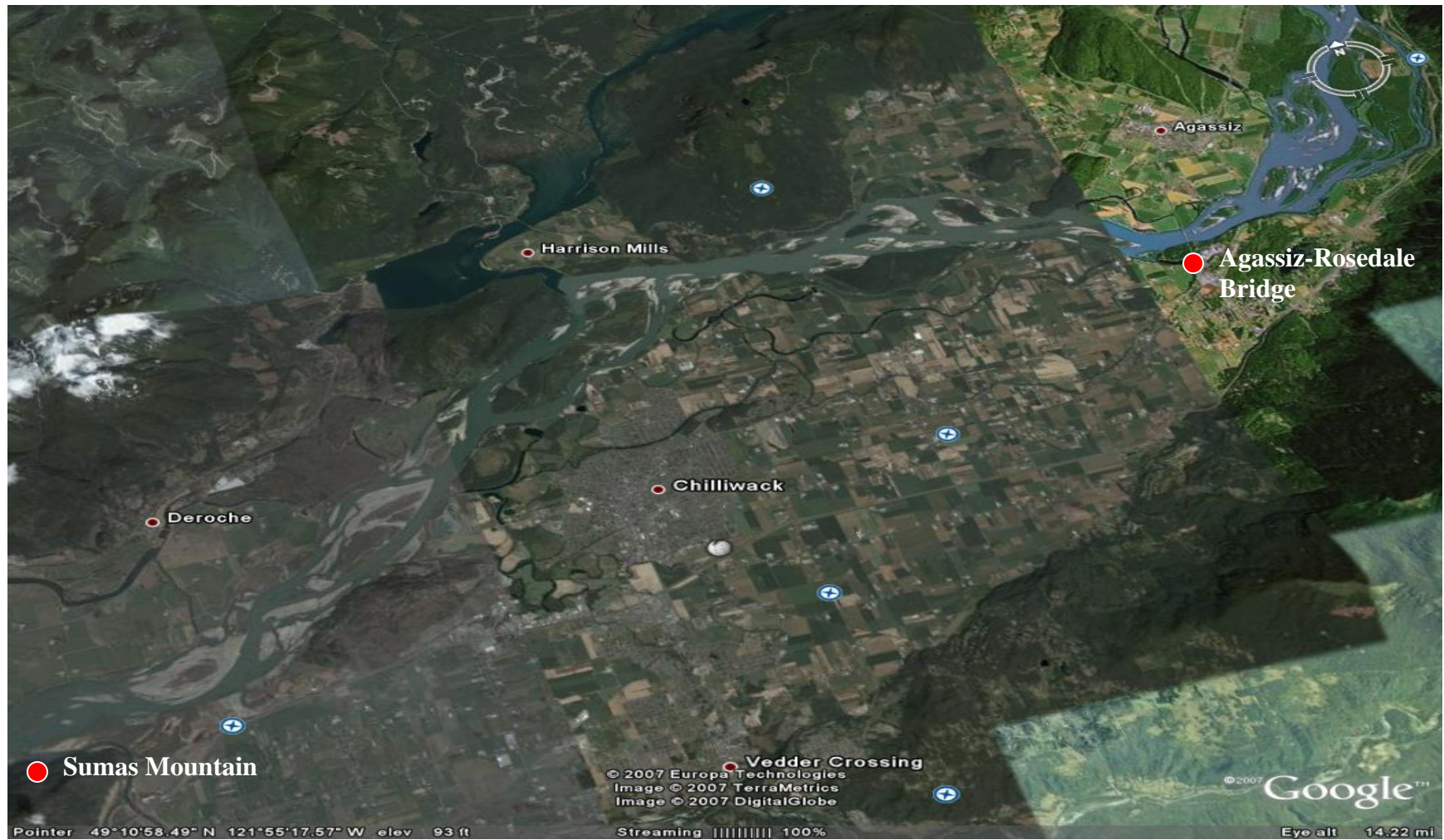
Figure 3.2: A bird's eye view of the gravel reach from Agassiz to Sumas Mountain (Source: Goggle Earth Image, © 2007).

The Lower Fraser River at Mission is tidally influenced and the magnitude of the tidal range is controlled by the seasonal fluvial flow. Tidal effect is negligible during the summer freshet at Mission (McLean and Church, 1990). Thus, in the Lower Fraser River, the gravel reach (Laidlaw-Sumas) and sand reach (Downstream of Sumas Mountain-Sandheads) represents two different types of channel morphology.

Morphological change and channel stability are closely related to the type of material that forms the bed and lower banks of the channel (McLean and Church, 1990). This material is transported as bedload during high flows. Measurements in the gravel reach indicate that significant gravel transport in the gravel reach commences at flows near 5,000 m^3/s, which represents the threshold condition at which the armored surface of the channel becomes mobilized (McLean and Church, 1999a). McLean and Church reported that when flows increase above 10,000 m^3/s, the armored surface is removed and the flow picks up the subsurface material from the bed (McLean and Church, 1999a). The subsurface channel deposits are strongly bimodal with a coarse fraction consisting of gravel (median diameter typically 20-25 mm), and a fine fraction consisting of medium sand (McLean and Church, 1990). The sand fraction occupies the voids between the gravel clasts. Surface material exposed on bars is typically unimodal gravel, similar in composition to the subsurface material except that the sand sizes are absent, i.e. the bar shows an armored surface. Surface deposits of sand are found on the downstream side of the bars and along some of the secondary channels. However, over the course of individual freshet events the sand is usually removed (McLean and Church, 1999a).

One of the most important sediment transport characteristics of the gravel reach is that the river bed shear stress is generally only slightly above the threshold condition for bed material (gravel) transport during flood, which is a typical feature of "wandering" gravel-bed rivers. This lack of strength of the flow precludes the formation of a well-defined channel in the gravel reach and is one of the essential causes of the reach instability. The river continuously re-works and re-distributes the bed material in finding its path through the gravel-bed. The term wandering river is used to describe multiple channel systems that split and flow around vegetated and relatively stable islands that remain emergent at or near bankfull flow (Desloges

and Church, 1989). Some basic hydraulic characteristics at mean annual flow were presented in the Table 3.1.

Table 3.1: Hydraulic characteristics at the mean annual flood (Q_{MAF}) of Lower Fraser River (after Church and McLean, 1999a).

Station	Q_{MAF} (m^3/s)	Depth (m)	Width (m)	Velocity (m/s)	Froude Number	Mean Bed Slope (m/m)	Bed Surface Material D_{50} (mm)
Hope	8,550	10.1	268	3.2	0.32	0.006	100
Agassiz	8,560	6.6	512	2.6	0.32	0.0048	42
Mission	9,590	12.6	540	1.5	0.13	0.0005	0.38

3.2 Hydrology of Lower Fraser River Gravel Reach

Fraser River drains about 250,000 km^2 of British Columbia, Canada (Figure 1.1). Since much of its basin area is located above an elevation of 1,000 m, a high proportion of the Fraser River runoff is snowmelt induced. The main freshet usually commences in April/May and lasts until mid-August with peak flows occurring in June. The long-term (30 years) mean annual flow is approximately 3,500 m^3/s at Hope, while mean annual peak discharges are approximately 8,550 m^3/s at Hope and Agassiz and 9,590 m^3/s at Mission (Church and McLean, 1994). The discharge remains virtually constant between Hope and Agassiz (Millar and Barua, 1999), while increased discharge at Mission reflects the addition of inflows from Harrison and Chilliwack rivers. In the Agassiz to Mission reach, the Harrison and the Chilliwack Rivers add about 4.6% to the drainage area, increasing the mean annual flow by about 18% and typically increasing flood flows by 10-15% (Church and McLean, 1994). Some largest annual maximum flood events according to magnitude are summarized from Environment Canada HYDAT-CD-ROM and presented in Table 3.2.

Table 3.2: Largest recorded mean daily flood peaks for the Lower Fraser River.

Date	Discharge at Hope (m^3/s)	Water Level at Mission (m Geodetic)
05 June, 1894	17,000 (estimated)	7.92
31 May, 1948	15,200	7.60
16 June, 1972	12,900	7.17
20 June, 1950	12,500	7.44
21 June, 1964	11,600	6.99
29 June, 1955	11,300	6.81
05 June, 1997	11,300	6.39
10 June, 2007	11,200	6.33
23 June, 1999	11,100	6.30
21 June, 1974	10,800	6.21

The flood of record occurred in 1894, before flow gauging was established. The peak discharge at Hope is estimated to have been 17,000 m^3/s (UMA, 2001a). This flood plus 0.6 m free board has been adopted as the design flood for major infrastructure development work along the Lower Fraser River floodplain, including the extensive network of dykes to protect many communities and infrastructures.

3.3 Lower Fraser River Sediment (Gravel) Budget

The sediment budget is of particular importance as gravel accumulation in the reach could substantially reduce the margin of flood protection provided by local dykes. Estimation of a sediment budget in Lower Fraser River gravel reach has been started long ago. Detailed bathymetric surveys of Lower Fraser River gravel reach were completed in 1952, 1984, 1999 and 2003. The 1952 and 1999 surveys were extended from Mission (at km 86) to Laidlaw (at km 150). The 1984 and 2003 surveys were extended between the Mission and Agassiz-Rosedale Bridge and Mission and Herrling Island respectively. Water Survey of Canada also has been undertaken direct measurements of sediment transport along the Lower Fraser River between

67

1965 and 1986. Suspended load and bedload sediment samples were collected at Hope (suspended only), Agassiz and Mission.

McLean and Church (1994) and McLean (1990) analyzed the river survey data and Water Survey of Canada sediment samples (1966-1986) to construct a sediment budget. A sediment budget was established in 1990 for this reach by comparing the survey data and computing volumes of net channel change (McLean, 1990). This produced an estimated average gravel influx at Agassiz of 150,000 t/y between 1952 and 1984 (no estimate of the sand fraction was given). Review of their procedures suggests that not all significant changes along the channel were captured. Later re-analysis by McLean et al. (1999a) reported an annual gravel bedload estimate of 225,000 t/y in the gravel reach. The authors concluded that the best estimate of the annual gravel transport past the Agassiz-Rosedale Bridge was in the of order 200,000 t/y, and that deposition downstream produced localized changes in bed elevation of as much as ±1 m over four decades. Gravel removals from the channel during that period reduced the overall aggradation by 38% below what it otherwise would have been (McLean et al., 1999b).

The original McLean and Church (1986) analysis was undertaken before Geographic Information System (GIS) programs became widely available. Their method included setting up a primitive GIS to do the survey comparison (Ham and Church, 2003). McLean's work represents an average of changes over a period of thirty years, but longer and shorter-term fluctuations in gravel transport are still poorly understood, including the potential long-term effects of gravel removal. However, their study improved the understanding of gravel recruitment and deposition in this reach.

The 1999 channel survey included a stretch of the Lower Fraser River upstream of the Agassiz-Rosedale Bridge that was not surveyed in 1984. The most recent channel survey was conducted in 2003 with additional cross-sections between Mission and Herrling Island. These surveys allowed updates to the sediment budget for the gravel-bed reach (Ham, 2005a; Church, Ham and Weatherly, 2000, 2001). In 2000, a sediment budget study was completed by Church, Ham and Weatherly for Lower Fraser River gravel reach. Digital maps of the river at several

dates in the past and historic aerial photographs (1928 to present) were used to map bar, island, and bank position changes through time. Morphological changes such as erosion and deposition patterns and rates were calculated more precisely than previous gravel budgets because the data analysis has been automated by an Arc/Info GIS software. Detailed sediment budgets have been calculated for three periods: 1952 to 1984, 1984 to 1999, and 1952 to 1999 (Church, Ham and Weatherly, 2000, 2001). The results from the sediment budget (2000) are presented in Table 3.3.

Table 3.3: Summary of sediment budget (Church, Ham and Weatherly, 2000).

Period	Average Inflow at Agassiz-Rosedale Bridge $\times 10^3$ (tonnes/year)		Average Outflow at Mission $\times 10^3$ (tonnes/year)	
	Gravel	Sand	Gravel	Sand
Agassiz-Mission				
1952-1984	265	3,656	0	3,544
1984-1999	556	2,486	0	2,640
1952-1999	409	3,290	0	3,255
Laidlaw -Mission				
1952-1999	416	3,293	0	3,255

The first two budgets extend up to the Agassiz-Rosedale Bridge (at km 130) only, which was the limit of the 1984 survey. The 1984 survey was undertaken in a year with only a moderate freshet and boat access to back channel areas was more restricted in comparison with the 1952 and 1999 surveys. The 1952-1984 budget was systemically underestimated because most of these excluded areas were zones of recent deposition (Ham, 2005a). To rectify this problem, additional elevations were derived photogrammetrically for the 1984 survey. As a result, three surveys encompass a common area (Church, Ham and Weatherly, 2000; 2001). The latest models of the channel bed and banks were interpolated for the 1952, 1984 and 1999 surveys after the procedures developed for improving model accuracy. Other than the incorporation of the bankline contours, the only data added were the 1100 photogrammetrically derived points for the 1984 survey. These points were collected on bar surfaces where the

density of available survey data was insufficient to capture the topographic complexity. The sediment budget has been calculated on a cell-by-cell basis for the three periods. Each computing cell was approximately 1 km in length with a total of 65 cells between Mission and Laidlaw. Cell-by-cell computation has allowed identifying sites of erosion and deposition.

Over the full study period, the average annual gravel deposition in the Agassiz-Mission and Laidlaw-Mission reaches were 409,000 t/y and 416,000 t/y respectively. However, gravel influx increased in the period 1984–1999, in comparison with the earlier period, by 2.5 times. This substantial fluctuation is possible, considering the low average annual flux. Over the entire 45-year record, the average aggradation in the Mission-Agassiz reach is +28.4 cm. Considering gravel mining; the actual average bed elevation change was +20.6 cm (Ham, 2005a). Over the entire Laidlaw-Mission reach, the corresponding figures are +19.3 cm and +12.9 cm. In the entire Laidlaw-Mission reach, gravel mining over 45 years reduced the net aggradation by 33% (Ham and Church, 2003). Aggradation is concentrated in the region between Lower Herrling Island and mid-Nicomen Island. At either end of the reach, there are zones of significant degradation. The gravel budget estimates has been updated and include the additional 2003 survey coverage. The revised estimate of gravel influx indicates that on average, approximately 243,000 ± 15,000 m^3/y or, 425,000 t/yr of gravel (Table 3.4) is transported past the Agassiz-Rosedale Bridge each year (Ham, 2005a). For perspective, this is equivalent to about 1 cm of aggradation per decade when averaged over the entire active floodplain area.

Table 3.4: Average annual sediment transport rate at Agassiz-Rosedale Bridge (Ham, 2005a).

Period	Average Inflow past Agassiz-Rosedale Bridge (m^3/y)		
	Gravel	Sand	Total bed material
1952-1984	180,000	-27,000	153,000 ± 16,000
1984-1999	378,000	116,000	494,000 ± 33,000
1999-2003	494,000	203,000	697,000 ± 41,000
1952-1999 (direct)	212,000	25,000	237,000 ± 11,000
1952-1999 (sum)	243,000	19,000	262,000 ± 15,000

3.4 Lower Fraser River Gravel Removal

The Fraser River Technical Committee recommended gravel removal as one option to control long-term aggradation and maintain the existing flood profile (FBC, 2001). However, this reach has an exceptionally diverse aquatic ecosystem with high economic value. In alternate years, up to two million pink salmon use the gravel-bed reach for spawning (Church, Ham and Weatherly, 2000). Therefore, any strategy to manage flood hazard must recognize and attempt to maintain this value. However, there is an increasing demand for this resource with rapid urbanization and increasing construction works in the Fraser valley. Currently, there are some active gravel removal operations on the Lower Fraser River. Indeed, there may be more significant gravel removal operations in the coming years in some critical locations.

Two engineering studies (UMA, 2001b; nhc, 2006) have concluded that even very substantial gravel removals would have little or insignificant effect on reducing the design flood profile. Currently, the main thalweg impinges directly on Harrison Knob at the confluence with the Harrison River, forcing the flow to make an abrupt, sharp turn to the left. This is a very inefficient alignment, which acts as a hydraulic control, causing a backwater upstream. This backwater has raised the level of the design flood profile locally by roughly 1.5 m or so, and has caused significant gravel deposition at Harrison Bar and further upstream.

As part of the study, some knowledge of previous gravel extraction in this reach is essential. Before 1954 the gravel removal from the riverbed was not regulated and unregulated gravel removal was undertaken. Kellerhals Engineering Services Ltd. (KESL) completed an inventory of gravel removal for the period 1953-1986 (Kellerhals Engineering Services Ltd., 1987). Much of the information for this inventory was gathered by discussions with local gravel operators and representatives of the Department of Fisheries and Oceans (DFO), Provincial Ministry of Forests and Lands (the Lands function of which is now administered by British Columbia Assets and Land Corporation), and British Columbia Ministry of Transportation (MoT). The inventory compiled by KESL appears to be a fairly accurate record because British Columbia Assets and Land Corporation (BCAL) has regulated gravel extraction from Lower

Fraser River since 1954. The regulatory agency requires that a provincial royalty must be paid for every cubic meter of gravel removed from Crown land. This policy was initially requested to the province by DFO as a means of controlling the location and volume of gravel extraction.

DFO has required permits for gravel extraction since 1980 and additional records of gravel removal, particularly from private land, are available. The effect of this policy was to restrict permits for instream gravel extraction to few of established operations. For some cases since the late 1980s, DFO has requested pre- and post-excavation surveys to verify removal volumes. However, these records alone do not represent a complete record of gravel removal because provincial records of gravel removal are based on volumes reported by gravel operators. Pre- and post-excavation survey information is generally not available and therefore the actual amount of gravel removed cannot be verified (Church, Ham and Weatherly, 2000). In addition to that, the British Columbia Ministry of Transportation has a few established gravel reserves along the Lower Fraser River and these reserves are not subject to the regulations imposed by BCAL and MoT has no internal records of gravel removal (Church et al., 1999). Gravel removal operations on private land are also not controlled by BCAL.

3.5 Recent Gravel Removal Sites

There are several gravel removal sites under consideration. Most of the sites were developed from a multi-year gravel removal study conducted by Kerr Wood Leidal Associates (KWL 2001, 2002, 2003). Of these, six locations Queens Island, Harrison Bar, Gill Island, Hamilton Island, Big Bar and Powerline Bar were selected for this study. The main reason for selecting these sites is that all of them were developed based on 2003 survey data. Each location may contain one or more than one extraction site (Figure 3.3). Figure 3.3 shows all extraction sites between Agassiz to Minto Island. Queens removal site was developed earlier and does not appear in this figure.

Figure 3.3: Showing gravel extraction areas except Queens Bar (after nhc, 2004).

3.5.1 Queens Bar Gravel Removal Site

Queens Bar forms a major depositional zone of bars and islands that extends upstream from Island #22 to Harrison Knob, immediately downstream of Minto Island (Figure 3.4).

Figure 3.4: Location of Queens Bar (B.C. Ministry of Environment, Lands and Parks, 1999).

A detail review of morphological developments in the Queens Bar area was undertaken by Northwest Hydraulic Consultants in 2002 (nhc, 2002). The current morphologic configuration was established by early 1980's and has generally become increasingly stable (nhc, 2002). This stabilization is strongly related to consistently below (long-term) average flood flows which slowed the rate of bank erosion and bed material transport allowing vegetation to establish and mature on elevated bar surfaces (nhc, 2002). Apart from minor localized bank erosion, the major change has been toward increased vegetation growth on the bars.

During the past few years, several small but important changes in local channel configuration have occurred such as erosion along the upstream and midsections of Harrison Island. This has resulted in deposition of gravel along a series of point bars that has contributed to an increased upstream sinuosity and directed attack to Island #22. The most significant was growth of a large bar along the left bank directly across from upper Queens Bar, developed as the thalweg shifted toward Island # 22 (Figure 3.5).
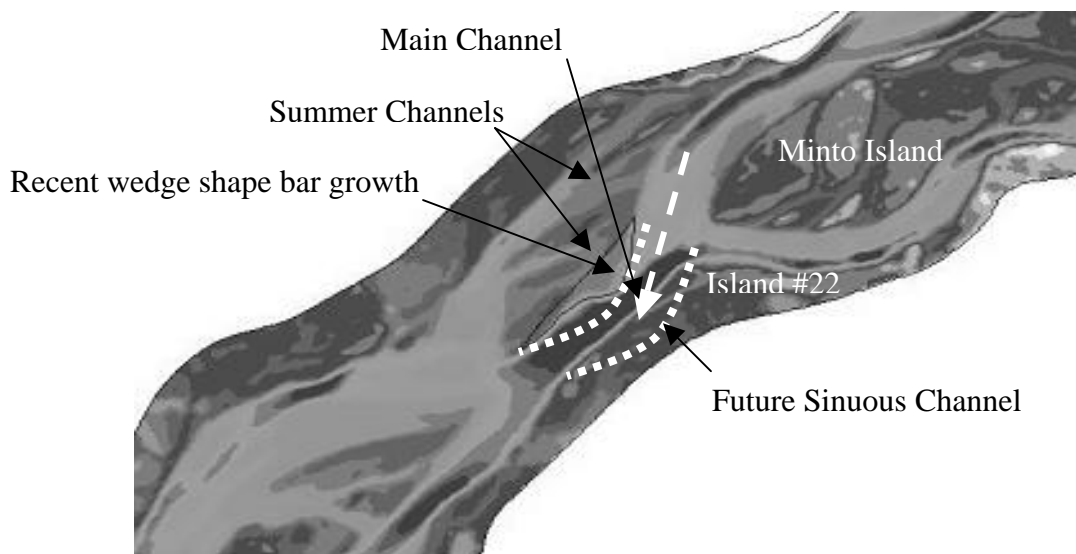
Figure 3.5: Showing recent Queens bar growth towards Island 22 (figure produced from 1999 Model Bathymetry).

As a result, a prominent wedge-shaped bar has formed which extends into the main channel, deflecting currents toward Island #22 (Figure 3.5). This wedge extends roughly 300 meters downstream, and 100 meters laterally towards Island #22. Field investigation showed that erosion of unprotected bank and slumping of rip-rapped sections of right bank of Island #22 was initiated (nhc, 2000).

No additional vertical aerial photographs are available since 2001, but 35 mm oblique taken by nhc on July 31, 2003 shows new lateral growth of Queens Bar (Figure 3.5). If this growth and bank erosion continues without any preventive measure, then the future channel shape may likely be sinuous, as suggested by the white dotted lines in Figure 3.5. Based on the current pattern of morphologic development within this reach of Lower Fraser River, it has been suggested that excavation of sediment along the margin of the wedge to alter channel alignment is the only practical means of addressing this continuing problem (nhc, 2004). DFO has approved 500,000 cubic meters of gravel removal from this site (Busto, 2005).

3.5.2 Harrison Bar

Harrison Bar is a site of recent major sediment deposition. Harrison Bar is situated on the left side of the main channel opposite the Harrison River confluence (Figure 3.6). At this location the main branch of Lower Fraser River makes a 90° turn as flow impinges against the bedrock of Harrison Knob. The backwater effect induced by the addition of Harrison River flow and the sharp bend has resulted in significant gravel deposition on Harrison Bar and further upstream over the last twenty-five years. Until the late 1960's, the main flow of Lower Fraser River channel was on the south side of the main channel with most of the flow directed through upper Minto Channel. The area around Harrison Bar consisted of a side channel flowing through the two substantial islands near the mouth of Harrison River (Figure 3.6). The realignment of the river was partially forced by the bar growth and accretion of material to Foster Bar beginning in the 1960's which blocked the entrance of main channel flow into Minto Channel (KWL, 2003).

Figure 3.6: Gravel removal sites Site1, Site 2, Site 3 and Site 4 near Harrison bend (nhc, 2004).

The present configuration of the Lower Fraser River will continue to promote gravel deposition at Harrison Bar, which will be more apparent after an above-average freshet. In addition, there is also a need to increase the channel capacity at the mouth of Harrison River (WMC, 2001). Harrison Bar has been given a high priority rating for gravel removal due to the combination of significant gravel aggradation and low dykes upstream (by 0.4 to 0.8 m lower than the standard dyke).

Several sites on Harrison Bar were identified for the removal. The sites are geomorphologically safe; bedrock protects neighboring banks and will limit morphological change. The geometry of these bars makes it a relatively low use site for recreational fishing and a less productive rearing habitat compared with more complex areas (KWL, 2001, 2002). With continued erosion upstream of this site, it is expected that gravel will be recruited to the excavation site relatively quickly. There are four sites at Harrison Bar, which have been selected for gravel removal: Harrison Site 1 (Known as Harrison inside channel), Harrison Site 2, Harrison Site 3 and Harrison Site 4 (Figure 3.6).

3.5.3 Gill Island Complex

Gill Island is a complex of wooded islands and gravel bars located about 5 km downstream from the Agassiz-Rosedale Bridge (Figure 3.7). At present, the main channel of Lower Fraser River makes a northward meander bend to flow around the Gill Island complex. A major side channel divides Gill Island along an east-west orientation, separating the complex into an outer (north) and inner (south) area. The outer bar consists of three vegetated islands that are connected to one another at low flow by extensive gravel bar deposits. The inner portion of the complex consists of a series of gravel bars that are diagonally dissected by some summer channels and smaller side channels. Greyell Island is situated to the immediate south of Gill Island.

Since 1991, the meander curvature around Gill Island has increased and erosion has occurred on the left bank of Gill Island, prompting the development of a small reverse eddy bar off the Gill Island point bar (KWL, 2003). The eddy bar is perhaps indicative of imminent meander cutoff and increased flows through Gill Island. In the last several years, increased boat traffic has used the side channel due to higher flows and improved navigation (KWL, 2003). While the meander bend still captures most of the flow, the side channel has abstracted increased flows.

Several sites have been considered for gravel excavation in the Gill Island complex. Gravel extractions have already commenced in some areas, others are coming up in the near future and some areas are still under consideration for DFO approval. Only three areas, Gill West, Gill East and Gill North are shown in Figure 3.7. The excavation plan was based on survey data provided by Tunbridge & Tunbridge on December 5, 2004, and recent air photographs of the gravel reach dated December 18, 2003 (nhc, 2004). Gravel extraction at the downstream end of the Gill Island complex was proposed for 2005. Historical evidence suggested that morphological changes would continue around the Gill Island complex until a stable configuration is reached (Weatherly and Church, 1999).
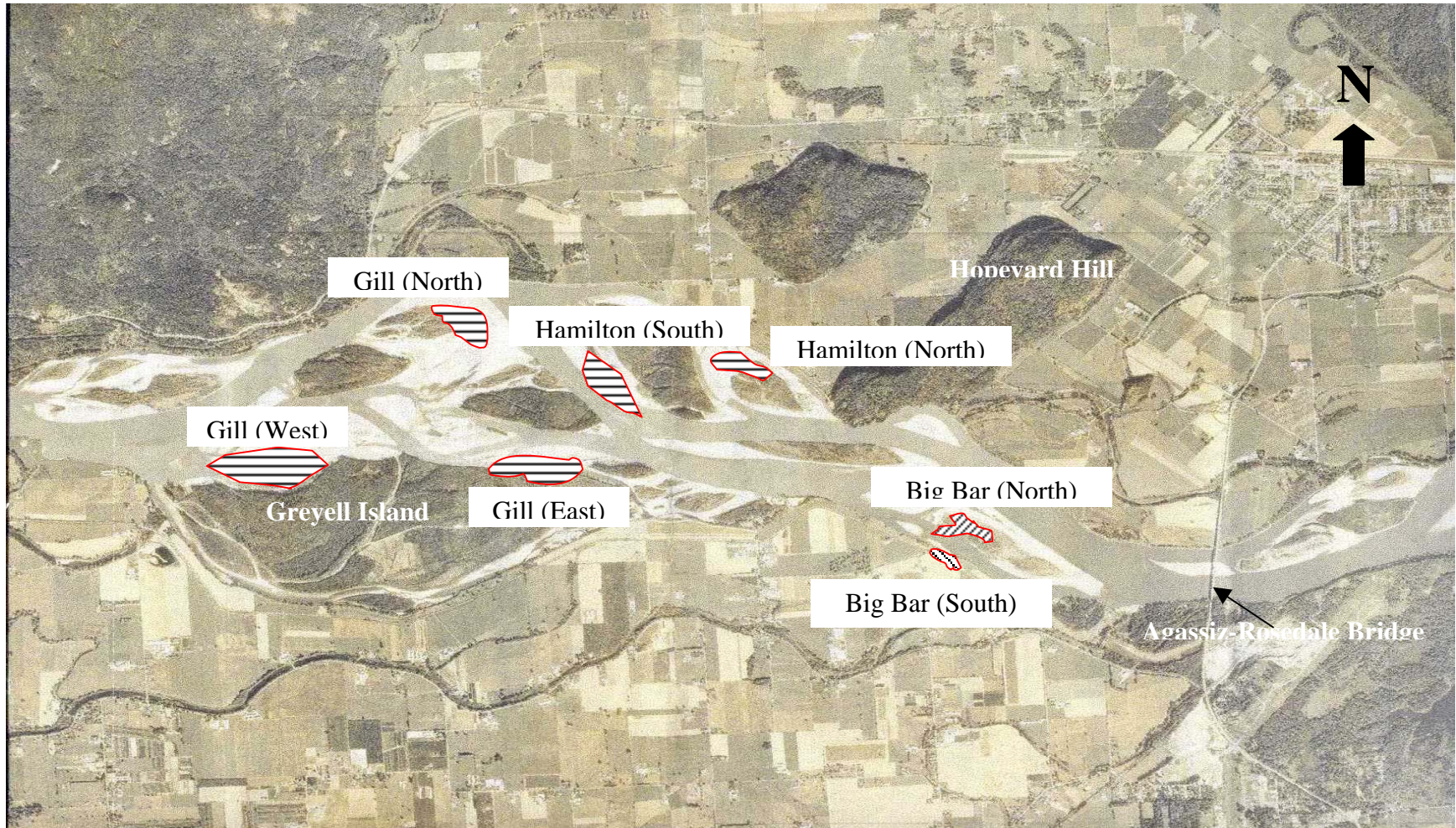
Figure 3.7: Gravel removal sites in Gill Island, Hamilton Bar, Big Bar and Power Line Bar. (Sketched on Ministry of Environment, Lands and Parks, B. C, 1999 Ortho Photo Image).

The proposed removal area of Gill West is located near the confluence of the side channel and the main channel, on a gravel bar located at the west edge of the Gill Island complex (Figure 3.7). Another smaller channel joins the major Gill Island side channel just upstream (East) of the bar. At higher flows, the outer part of the bar is dissected by some summer-channels. The proposed removal is aligned along the dominant East-West oriented summer channel. The proposed removal area is bounded to the south by a large expanse of sandy material. The proposed removal design anticipates that approximately 52,000 m^3 of gravel will be excavated from the bar. The removal area is about 600 m long with a maximum width of approximately 50 m. The removal has been designed as a bar-edge excavation (KWL, 2003). There is presently minimal habitat complexity within the proposed removal area, which consists of simple bar edge. KWL's 2003 removal plan contains habitat features designed to create complexity, including a 0.3 m step, a large upstream channel nook feature, and two smaller nook features (KWL, 2003).

Gravel removal from Gill East site was initiated in March 2003. Approximately 50,000 m^3 of gravel was removed from this site. During March 2003, gravel was removed from two locations near the side channel that divides the complex. Approximately 45,000 m^3 of gravel were removed from the more downstream site and 10,000 m^3 from the upper site (Figure 3.7). The removal area is about 300 m long with a maximum width of 50 m. The removal area ties into an existing low level bar surface at the downstream end to prevent fish stranding. The removal is concentrated on the lower 2/3 of the bar to avoid destabilizing the bar head, which is composed of a coarser and more stable surface armour.

The Gill North gravel removal site is located at the east side of the Gill North Bar near the left side of the main channel. At the site, the gravel bar edge slopes relatively gradually to the main channel. The proposed removal design anticipates that approximately 20,000 m^3 of gravel will be excavated from the bar (Busto, 2005). The removal area is about 400 m long with a maximum width of approximately 65 m. The removal has been designed as a bar-edge excavation. There is presently minimal habitat complexity within the proposed removal area, which consists of simple bar edge.

3.5.4 Hamilton Bar

Hamilton Island is a complex of wooded islands and gravel bars located on Lower Fraser River about 4 km downstream from the Agassiz-Rosedale Bridge (Figure 3.7). The Bar complex consists of two stable vegetated islands and bare gravel bars surrounding them. Two side channels surround the two vegetated islands. The side channel north of the North Hamilton bar is usually dry in the winter. Another side channel also has very low flow during winter months.

Gravel deposition in the side channels was observed over the last two decades (KWL, 2003). Significant aggradation has occurred and the dykes on both sides of the river are 0.4 m below from the design standard (UMA, 2001a). The side channel has been a considerable gravel removal site since the 1990's. In 2001 and 2002 about 10,000 cubic meters of gravel were extracted from this site (KWL, 2003). Presently two sites, one inside the north side channel and the other in the middle side channel, are proposed for gravel removal (Figure 3.7). Approximately on the order of 15,000 m^3 and 50,000 m^3 of gravel will be removed from the north and south sites of the Hamilton Bar complex, respectively.

3.5.5 Big Bar

Big Bar consists of a tail shaped vegetated bar surrounded by several small bare gravel bars. It is located about 1 km downstream of Agassiz-Rosedale Bridge. A small side channel separates it from the south bank of the Lower Fraser River (Figure 3.7). Another small side channel divides the Big Bar at the middle into Upper Bar and Lower Bar along the east-west direction. The sub-surface D_{50} values are 54 mm and 30 mm at Upper Bar and Lower Bar respectively (Church, 2003). A GIS cell based morphological study showed that an overall gravel deposition along the Upper Bar and erosion near the Lower Bar (Church, Ham and Weatherly, 2000). Gravel has been deposited on the north side of the Big Bar and inside the south side channel at upper bar over the decades and it became a potential gravel removal site.

From a flood control perspective Big Bar high priority for gravel removal. Two sites were recommended for gravel removal on Big Bar. One is located on the south side and the

other is near the north side of the Upper Bar. The proposed amount of gravel removals from the south site and the north site are 50,000 m^3 and 20,000 m^3, respectively. The depth of the removal is 1.5 m and 1.2 m, respectively from the south site and the north site.

3.5.6 Powerline Bar

Powerline Bar is located on the right bank of the Lower Fraser River at the Agassiz-Rosedale Bridge. Powerline Bar consists of a vegetated bar in the core surrounded by other small bars and summer channels. The upstream side of the bar is wider and gradually become thinner toward the downstream side. Due to the bend near the Agassiz-Rosedale Bridge, the main flow is gradually shifting southward and increasing the erosion risk on the south bank of Lower Fraser River. On the other hand, flow and velocity both have been reduced inside the side channel between Powerline Bar and the North Bank of Lower Fraser River. As a result, gravel has been deposited in this area for several years.

About 200,000 m^3 of gravel was removed from inside the side channel in 1996. This removal was recommend by Northwest Hydraulics Consultants after an erosion control study for the Cheam Indian Band in 1996 (nhc, 1996). The Cheam First Nation has indicated that the gravel deposition inside the side channel between Powerline Bar and the north bank of Lower Fraser River continues (KWL, 2003). Approximately 200,000 m^3 of gravel removal was recommended by the KWL and approved by DFO in 2005.

3.5.7 Summary of Gravel Extraction Plan

Any gravel removal plan requires approval by the DFO before implementing. There are several proposed gravel removal sites between the Agassiz-Rosedale Bridge and Sumas Mountain recommended by the local consultants in their technical study reports (nhc, 2002, 2004; KWL, 2001, 2002, 2003). DFO can either approve or deny any removal plan after the screening process. If any removal plan may adversely affect the aquatic habitat, then it will not be approved by the DFO. After discussion with Mr. Vince Busto, P. Eng., a Habitat Engineer of DFO in October, 2005 the following sites have been selected for model application (Table 3.5).

All of the selected sites were recommended by the local consultants (nhc, 2004, KWL, 2003). These thirteen sites are under implementation after 2003 or will be implemented in the coming years. All sites between the Agassiz-Rosedale Bridge and Sumas Mountain were selected solely to test the MIKE 21C sediment transport and morphological model performance as well as effectiveness of the gravel removal plan.

Table 3.5: Summary of gravel removal site (Busto, DFO, Personal Communication, October, 2005)

Removal Site Number	Extraction Locations (from Sumas to Agassiz)	Field Extraction Volume (m³)	Field Extraction Bottom EL. (m Geodetic)	Source
1	Queens Bar	500,000	4.5	Busto, DFO (2005)
2	Harrison Site 1	161,000	7.5	NHC (2004)
3	Harrison Site 2	122,000	6.5	NHC (2004)
4	Harrison Site 3	53,000	6.5	NHC (2004)
5	Harrison Site 4	156,000	6.5	NHC (2004)
6	Gill West	52,000	9.1 to 9.5	Busto, DFO (2005)
7	Gill North	20,000	10.5	Busto, DFO (2005)
8	Gill East	50,000	10.5 to 11	Busto, DFO (2005)
9	Hamilton South	44,000	11	NHC (2004)
10	Hamilton North	4,200	12	NHC (2004)
11	Big Bar South	50,000	12.1- 12.8	Busto, DFO (2005)
12	Big Bar North	20,000	12.5	NHC (2004)
13	Powerline Bar	61,000	13.5	NHC (2004)

4 METHODOLOGY

4.1 Mathematical Model Selection and Modification

Two depth-averaged two-dimensional mathematical models, MIKE 21C and River2D, were initially selected for the study. MIKE 21C is commercially available software and one must register and pay an annual license fee to use it. River2D is free-of-cost, public domain software. The MIKE 21C curvilinear grid model was selected as the main tool for the study since River2D does not have any sediment transport and morphological change simulation capability. Recently, sediment transport capabilities are being developed in River2D for a single size fraction (D_{50}) and the model remains experimental in nature (Vasquez, 2006). As a result, River2D was selected to compare and verify the hydrodynamic output of the MIKE 21C simulation. Sediment transport and morphological evolution in this thesis is solely based on MIKE 21C model simulations.

Pre-existing sediment transport theories in the MIKE 21C model were applicable to sand transport simulation in sand-bed rivers only. As a result, two gravel transport formula, Parker's (1990) and Wilcock and Crowe's (2003) surface based gravel transport equations, were programmed into the MIKE 21C model. Both formulas have been coded and incorporated into the MIKE 21C model jointly by the Department of Civil Engineering, UBC and DHI Water and Environment, Denmark. This has enhanced the capacity of MIKE 21C to simulate bedload transport for gravel-bed rivers with a wide range of sediment size fractions. Except for this change to the bedload transport algorithms all other MIKE 21C model features and input/output utilities were unchanged.

River2D is a finite element based hydrodynamic model, but is limited by the total number of nodes and simulation time. For example, it takes about 30 minutes in MIKE 21C and approximately 2 hours in River2D to perform a hydrodynamic simulation with 30,000 computational nodes over 2 days practical time. Due to these limitations, River2D can cover an approximately 30 km long river reach out of 70 km total reach length (Mission-Laidlaw) to

perform the hydrodynamic simulation. Therefore, River2D was selected to perform hydrodynamic simulations only from Agassiz-Rosedale Bridge to Sumas Mountain reach.

4.2 Model Input Data

Channel bathymetric, hydrometric and sedimentologic data were required for model development, calibration, verification, hydrodynamic simulation, sediment budget estimation and morphological change prediction. Table 4.1 has shown the summary of basic data types used for model development and simulation.

Table 4.1: Summary of basic data types used in model development and simulation.

Basic Data Type	Data	Use
Geometric data	Digital Elevation Model (DEM)	Bathymetry Preparation
Hydrometric data	Discharge	Inflow boundary
	Water Level Stage	Downstream boundary
	Rating Curve	Downstream boundary
	Staff-Gauge Water Level	Model Calibration
	ADCP Velocity Data	Model Calibration
Sediment data	Grain Size Distribution	Sediment transport simulation
	Bedload Data	Sediment transport simulation

4.2.1 Geometric Data

The digital elevation model (DEM), a database of points in space referenced to a common elevation datum, is the basis for mathematical representation of riverbed bathymetry. Channel cross-sections and terrestrial survey data were collected by Public Works and Government Services Canada (PWGSC) and Terra Surveys, respectively in 1999 and 2003. The PWGSC cross-sections were sounded at high river stages, and Terra Survey's airborne laser profiling (known as Light Detection and Ranging [LIDAR] survey) was done at low river stages. These two data sets overlapped each other substantially throughout the surveyed reach.

A 25 m × 25 m DEM was developed from the LIDAR data points and cross sections survey data by Mr. Ham in the Department of Geography, UBC. This DEM provides an approximate coverage over the entire gravel reach and is used in the model for river bathymetry preparation. In 2003, a new DEM was developed using new LIDAR and cross-sectional survey data (from Mission to Herrling Island). This part was merged with the upper part of the 1999 DEM (from Laidlaw to Herrling islands) to obtain a new 2003 DEM for the entire gravel reach. The 2003 DEM is used in this thesis for gravel removal case studies (Chapter 5).

4.2.2 Hydrometric Data

Hydrometric data for Fraser River at Hope and Mission gauging stations (Figure 1.2) are well documented in digital format and available in Environment Canada's HYDAT CD-ROM. Hydrometric data for major tributaries such as Harrison River and Chilliwack River were also available in the HYDAT CD-ROM. A list of the hydrometric stations used in this study is summarized in Table 4.2.

Table 4.2: List of Hydrometric Stations used in the Study.

WSC Gauging Station	Station ID	Data Type	Start year	End Year	Active/ Discontinued
Fraser River at Hope	08MF005	Flow	1912	2007	Active
Harrison River at Harrison Hot Springs	08MG012	Flow	1933	2007	Active
Chilliwack River at Vedder Crossing	08MH001	Flow	1911	2007	Active
Fraser River at Mission	08MH024	Water Level	1936	2007	Active

Mean daily values were recorded for discharges and water levels. All water level data at Mission were depth data calculated from an arbitrary gauge reference value. All Mission water level data were converted to match the Geodetic Survey of Canada (G.S.C) datum similar to the

DEM data. A gauge reference value +0.04 m was added to all the Mission water level data for correction.

There is no discharge measuring station adjacent to the Harrison and Lower Fraser River confluence. The Harrison Hot Springs gauging station is located at Harrison Lake, a few kilometers upstream from the Lower Fraser River confluence. Harrison River peak discharge into the Lower Fraser River is affected by both Harrison Lake water level and Lower Fraser River peak discharge. Therefore, Harrison River discharge data at Harrison Hot Springs must be corrected before application in the model calibration. Water Survey of Canada formulated a peak discharge correction equation based on the water level data at Harrison Lake and Lower Fraser River discharge at Hope. This equation was used to correct all the Harrison Hot Springs discharge data before applying those in the model calibration. Harrison River discharge is approximately 10 % to 20 % of Lower Fraser River discharge during peak flows (UMA, 2001b). Chilliwack River discharge data are available at Vedder Crossing but there is no significant increase of flow downstream of that gauge station so this discharge may be used directly in the model as Chilliwack River discharge.

Daily water levels data are available from several gauges that are operated by various local agencies, including the B.C. Ministry of Land, Water and Air Protection, City of Chilliwack, and District of Kent, primarily during the annual freshet (Figure 4.1). Water levels are recorded manually once a day from each of the gauges during the freshet period, however the collection time is not the same for all gauges. Due to the lack of continuous water level gauge data a constant mean daily discharge value will be appropriate for the hydrodynamic model calibration and verification. Accurate water level gauge locations are important in a two-dimensional river flow model calibration. Water level gauge locations (latitude, longitude) were determined through a hand held GPS survey. These data were verified with existing records where available. Approximate locations of water level gauge locations in Lower Fraser River are shown in Figure 4.1 and a location summary with UTM coordinates is presented in Table 4.3. Johnson Slough gauge is above the Gauge # 45 and does (Gauge # 43) not shown in Figure 4.1.
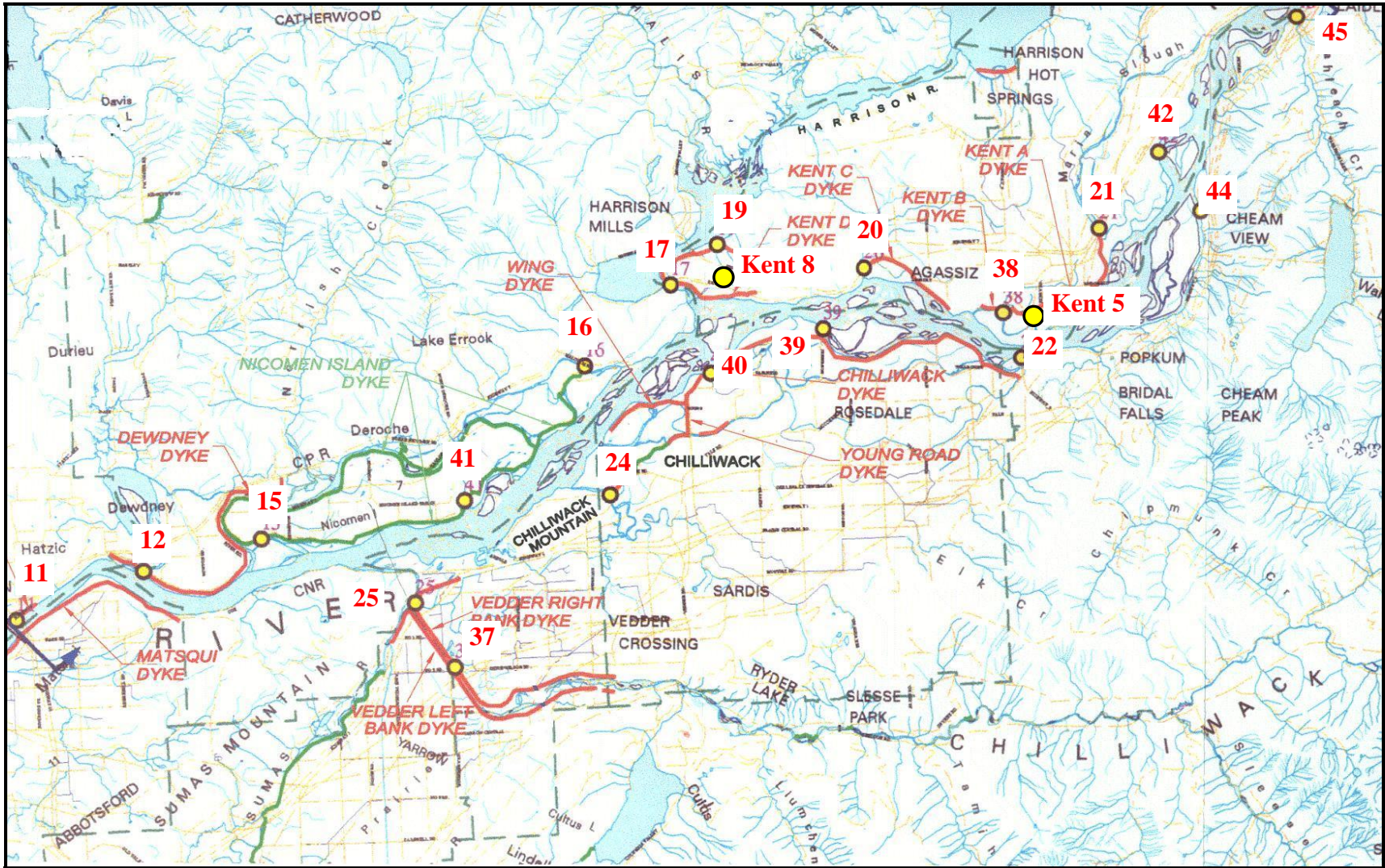
Figure 4.1: water level gauge locations in the gravel reach of Lower Fraser River

Table 4.3: Water level gauges and their locations in UTM coordinate in gravel reach of Lower Fraser River (from downstream to upstream).

Gauge No.	Gauge name	UTM (NAD-83) Easting	UTM (NAD-83) Northing
Mission	At Mission Railway Bridge	550850.90	5441885.49
12	Dewdney Pump Station	555515.14	5443361.58
41	Quaamitch Slough	565815.10	5446038.81
16	Bell Dam (Out side)	552655.98	5450950.95
40	Minto Landing Area	555356.65	5450551.91
Kent # 8	Scowlitz	558085.96	5453444.41
39	Carey Point	581543.88	5452039.58
20	Hammersley PS	583390.31	5454396.88
22	Agassiz Rosedale Bridge	589212.55	5450812.53
Kent # 5	Agassiz Rosedale Bridge	589160.56	5451288.60
44	Herrling	596094.00	5455526.00
42	Seabird Island	594160.00	5458600.00
43*	Johnson Slough	599239.59	5463803.04
45	Wahleach (Jones) Creek	599940.00	5463600.00

* Gauge #43 is not shown in Figure 4.1.

4.2.3 Sediment Data

No direct measurement of gravel bedload transport rates has been undertaken since 1986 in Lower Fraser River gravel reach. Only bedload data from the period 1965 to 1986 at Agassiz-Rosedale Bridge are available from the Environment Canada HYDAT CD-ROM. It was not a continuous daily record over the 20-year period. Rather, periodic sampling was carried out at different time of the year, mostly during high flow season. Between 1968 and 1986, 110 sets of bedload measurements were made at the Agassiz-Rosedale Bridge, of which 62 were made during the freshet. Two types of sampler were used for bedload measurement. A half size VuV sampler was used when flow was lower than 5000 m^3/s, otherwise a basket sampler was used for sampling (McLean and Church, 1999a). All bedload data sets at Agassiz-Rosedale Bridge were plotted against the corresponding discharge at Hope and a rating curve was prepared from these data (McLean and Church, 1999a). The bedload data were not used directly as input into

the model but a modified rating curve prepared from the McLean and Church (1999) rating curve, eliminating the bedload discharges < 5000 m^3/s, was used for bedload model calibration.

Data of bed material sediment size distribution were collected from Department of Geography, UBC. Sediment size fraction information along the Lower Fraser River gravel reach was available in spreadsheet format from Professor Michael Church, Department of Geography, UBC (Church, 2003). There were two sets of data available and the first set was based on 1983-1984 sample collection and the second set was based on 1999-2001 sample collection. A complete surface and sub-surface (bulk sampling) sampling was done in year 1983 for the entire Lower Fraser River. In 1999-2001 some surface and sub-surface samples were collected. The entire gravel reach was divided into several gravel size zones starting from downstream toward the upstream (for example Zone 1, Zone 4, Zone 25 etc) during data collection. The 1999-2001 data set did not cover the whole gravel reach but it covers almost the whole study area. The 1983-1984 data record was used for only one missing zone in the 1999-2001 data record.

All samples were collected on the exposed bar tops and no underwater samples were collected. There was more than one format within the supplied data files since they were constructed at different times by different operators. However, they all contain the basic weights or stone counts, which have been extracted and reassembled for averaging in the appropriate way. Surface data were based on pebble counts and sieve sampling, which is generally known as "Wolman count data" and includes 11 size fractions (2, 4, 8, 11.3, 16, 22.6, 32, 45.2, 64, 90.5, and 128 mm) based on the standard phi-scale (the phi-scale is expressed as $\phi = - \log_2 D$, where D is sediment size in mm). A total of nine different size fractions with geometric means 2.28, 8, 11.3, 16, 22.6, 32, 45.2, 64 and 105.62 mm were used in the model. The percent content of each individual size fraction varies along the gravel reach. A total of 12 different gravel size distribution zones between Agassiz-Rosedale Bridge and Sumas Mountain were selected based on the sediment size distribution data (Figure 4.2). Figure 4.3 and Table 4.4 give the gravel grain size distribution for each zone.
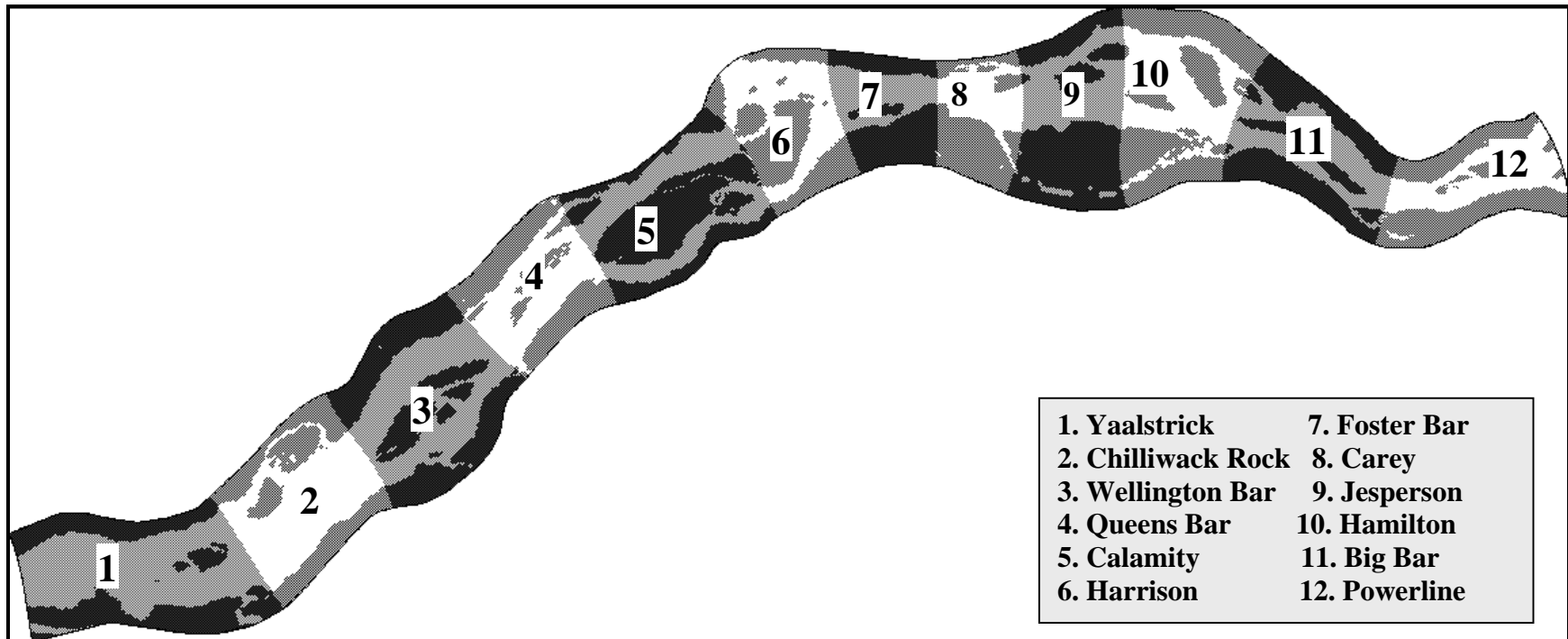
Figure 4.2: Gravel size distribution zones along the Lower Fraser River gravel reach (Source: Church, 1999-2001 and Church, 1983-1984, Department of Geography, UBC).
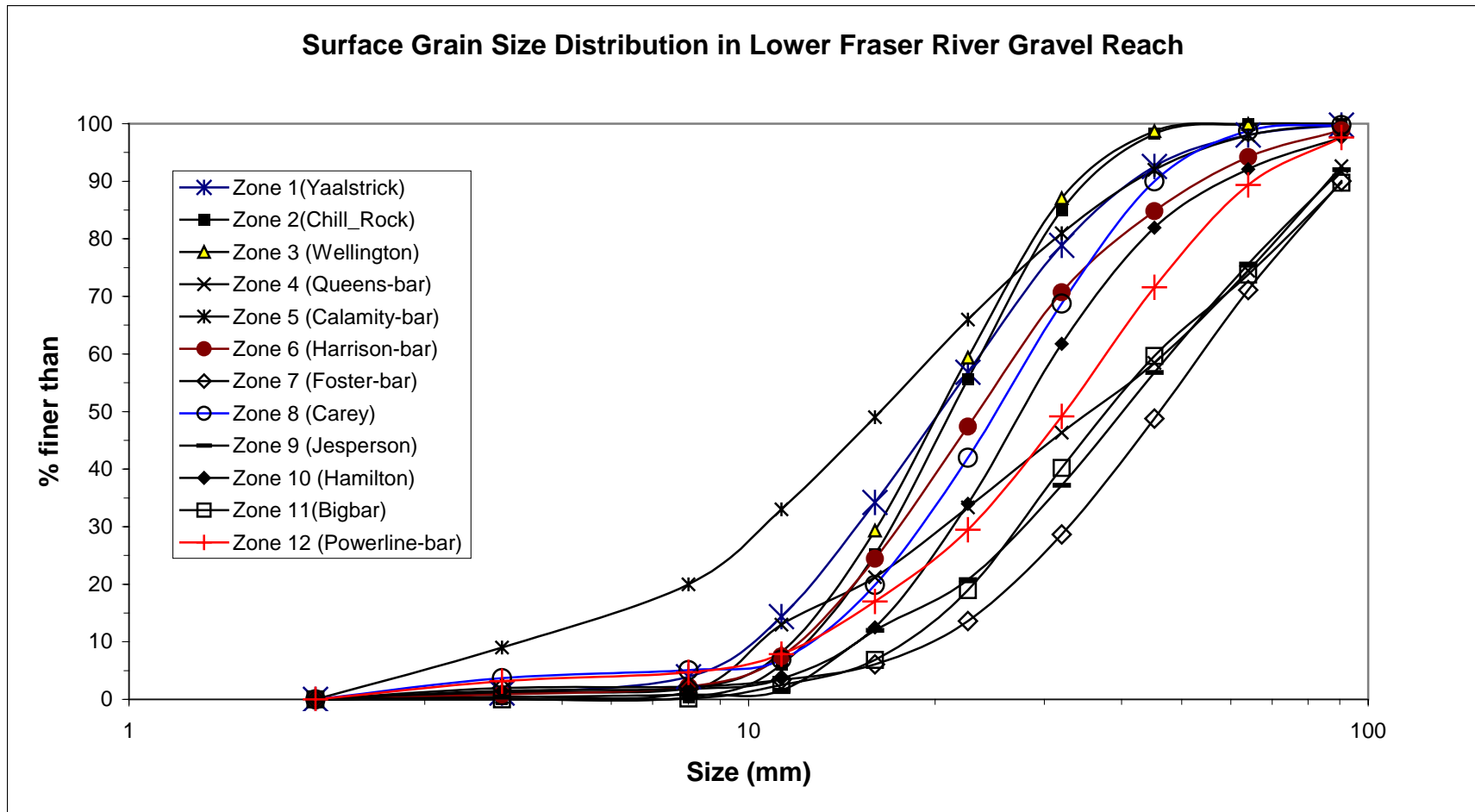
Figure 4.3: Surface grain size distribution in 12 sampling zones of Lower Fraser River gravel reach (Source: Church, 1999-2001 and Church, 1983-1984, Department of Geography, UBC).

Table 4.4: Showing the values of percent (%) content of different size fractions in different zones (Source: Church, 1999-2001 and Church, 1983-1984, Department of Geography, UBC.

Fraction No.	Size (mm)	Zone 1 (Yaalstrick)	Zone 2 (Chilliwack Rock)	Zone 3 (Wellington Bar)	Zone 4 (Queens)	Zone 5 (Calamity)	Zone 6 (Harrison)
9	105.62	0.99	0.98	0.98	5.36	0.99	1.15
8	64	1.53	0.98	0.98	18.18	1.98	4.65
5	45.2	5.41	1.61	1.24	16.02	5.94	9.41
6	32	13.61	12.89	11.42	12.12	10.89	14.09
5	22.6	21.86	28.65	25.15	12.99	14.85	23.33
4	16	22.44	29.64	29.49	12.12	16.83	22.95
3	11.3	19.69	18.68	20.50	8.23	15.84	16.93
2	8	10.38	5.58	6.20	11.69	12.85	5.31
1	2.82	3.90	0.98	1.84	1.30	19.80	2.19

Fraction No.	Size (mm)	Zone 7 (Foster Bar)	Zone 8 (Carey)	Zone 9 (Jesperson)	Zone 10 (Hamilton)	Zone 11 (Big Bar)	Zone 12 (Powerline Bar)
9	105.62	9.95	0.99	5.95	2.39	10.15	2.38
8	64	18.93	0.99	16.33	5.52	15.84	8.26
5	45.2	22.33	8.50	18.53	10.15	13.98	15.59
6	32	20.15	21.05	19.52	20.15	19.31	22.40
5	22.6	15.05	26.59	16.33	25.81	21.04	19.50
4	16	5.52	21.93	8.56	21.45	12.00	12.45
3	11.3	2.65	12.86	10.36	8.91	4.33	9.13
2	8	1.21	1.84	1.00	1.56	2.35	3.18
1	2.82	2.18	5.02	1.00	1.82	0.99	4.69

4.3 Model Setup for the Lower Fraser River Gravel Reach

4.3.1 Model Extent

The extent of the main study area is approximately 30 km long between the Agassiz-Rosedale Bridge and Sumas Mountain (Figure 3.1). Unfortunately, there were no hydrometric data available at the downstream boundary near Sumas Mountain and the operation of the Agassiz-Rosedale Bridge hydrometric station (08MF035) near the upstream limit of the study area was also discontinued since 1986. Nearly 90 years of hydraulic data records were available at two hydrometric stations at Hope and Mission on Lower Fraser River (see Figure 1.2). As a result, the upper limit of the study reach was set at Laidlaw, 10 km downstream from Hope and the downstream limit at Mission. This extended gravel reach length was about ~70 km. It may be too long for morphological simulation with reasonable grid spacing (20-30 m). This entire 70 km long reach was selected for hydrodynamic model development and to generate enough downstream hydraulic boundary conditions at Sumas Mountain for various flows.

A 35 km short reach from Agassiz-Rosedale Bridge to Sumas Mountain was extracted from the extended model reach to simulate the sediment transport. This short reach remained unaffected by any boundary effects during hydrodynamic model calibration. The MIKE 21C model can simulate the hydrodynamics for the entire 70 km long reach with desirable grid resolution between two selected models. Since total number of nodes is limited by the computer capacity in River2D, only a 30 km long reach from Agassiz-Rosedale Bridge to Sumas Mountain was used for hydrodynamic simulation. The downstream boundary of River2D was extracted from the MIKE 21C full extent hydrodynamic model.

4.3.2 Curvilinear Grid Generation

Orthogonal curvilinear grids (mesh) with variable mesh size were generated for the entire 70 km long gravel reach by MIKE 21C grid generator utility called 'Gridgen'. There were a total of 64,310 (1090 × 59) cells in the grid. Coarser and finer grid was generated according to the area of interest in the model domain. A coarser grid was set for the relatively stable areas such as thickly vegetated islands or permanent islands and flood plains while a finer grid was set

for main and side channels, including riverbank and unstable gravel bars. If the horizontal grid spacing exceeds 5 times the lateral grid spacing in the water flowing area, then it may create a numerical instability problem during hydrodynamic simulation (DHI, 2002a). On the contrary, very small size grid can produce a large Courant number (C_r = U. $\Delta t/\Delta x$) during hydrodynamic simulation that may cause numerical instability problems. Therefore, the grid could not be overly fine. Grid spacing was checked visually and refined until it satisfied the above criteria.

The grid generation process with MIKE 21C requires a significant amount of time and was done step by step. First of all, small sub-grids for islands, main channels and flood plains were generated separately for a portion of the river then merged laterally (Figure 4.4) to make a larger sub-grid that covers the entire width of the river and floodplain. These larger sub-grids were refined to maintain the same number of lateral rows for each of them (Figure 4.5). Joining all river-wide larger sub-grids generated the final grid. After final grid generation, grid refinement and an overall smoothening were done again to satisfy the grid generation criteria. Smoothing makes grid shape as orthogonal as possible. The model boundary lines along the channel were kept unchanged during the smoothing process. As a result, internal cells between the two lines were adjusted to be as orthogonal as possible. The curvilinear grid for the 70 km gravel reach is shown in Figure 4.6. The variable mesh sizes are shown in Frame A through H in detail in Appendix E.

River2D uses a finite element mesh. The mesh generator of River2D "River2D mesh" was used to perform the grid generation for the selected portion of the study reach. In this case, maximum element length did not exceed 25-35 m. In River2D the total number of nodes was 9,654 and the mesh quality index was 0.25 which satisfies the minimum quality index criterion greater than > 0.2 (Steffler et al., 2000). The unstructured finite element mesh for the 35 km gravel reach (Agassiz to Sumas Mountain) is shown in Figure 4.7.
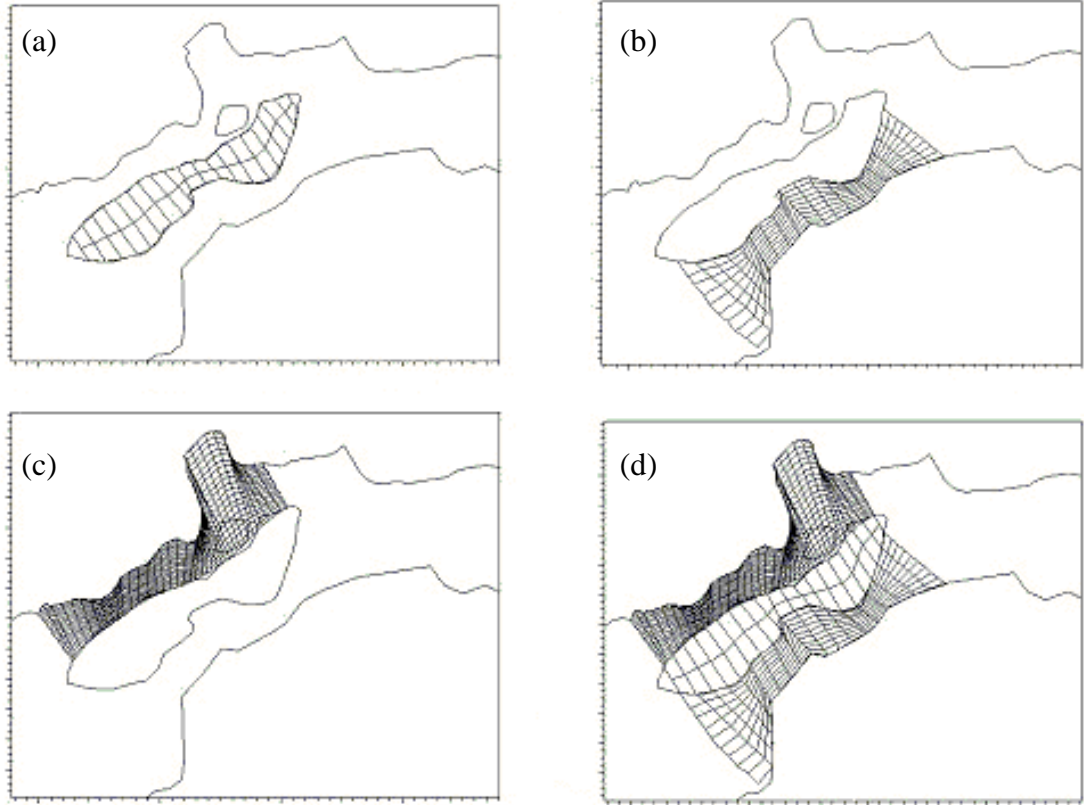
Figure 4.4: Showing small sub-grid generation near Harrison bend. (a) Minto Island (b), Minto channel (c) Fraser Main channel and Harrison bend and (d) larger sub-grid generation by lateral merging.
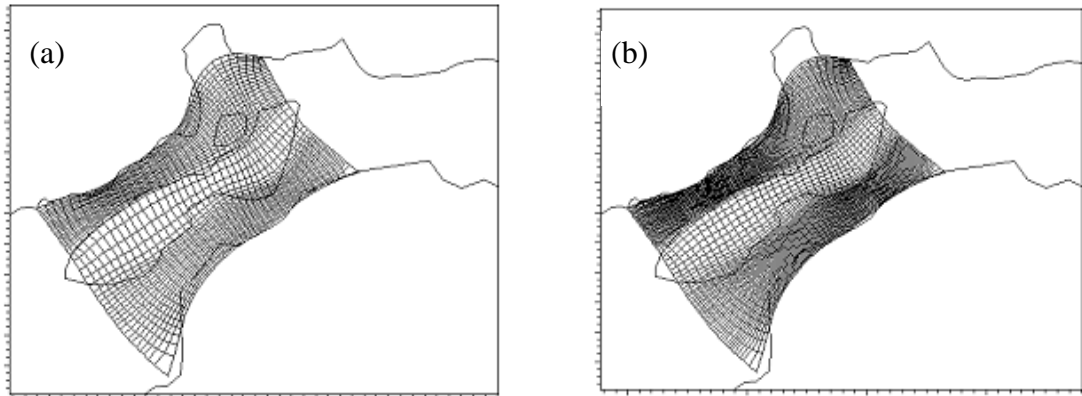
Figure 4.5: Showing (a) larger Sub-grids refinement (b) and fine-tuning near Harrison bend.
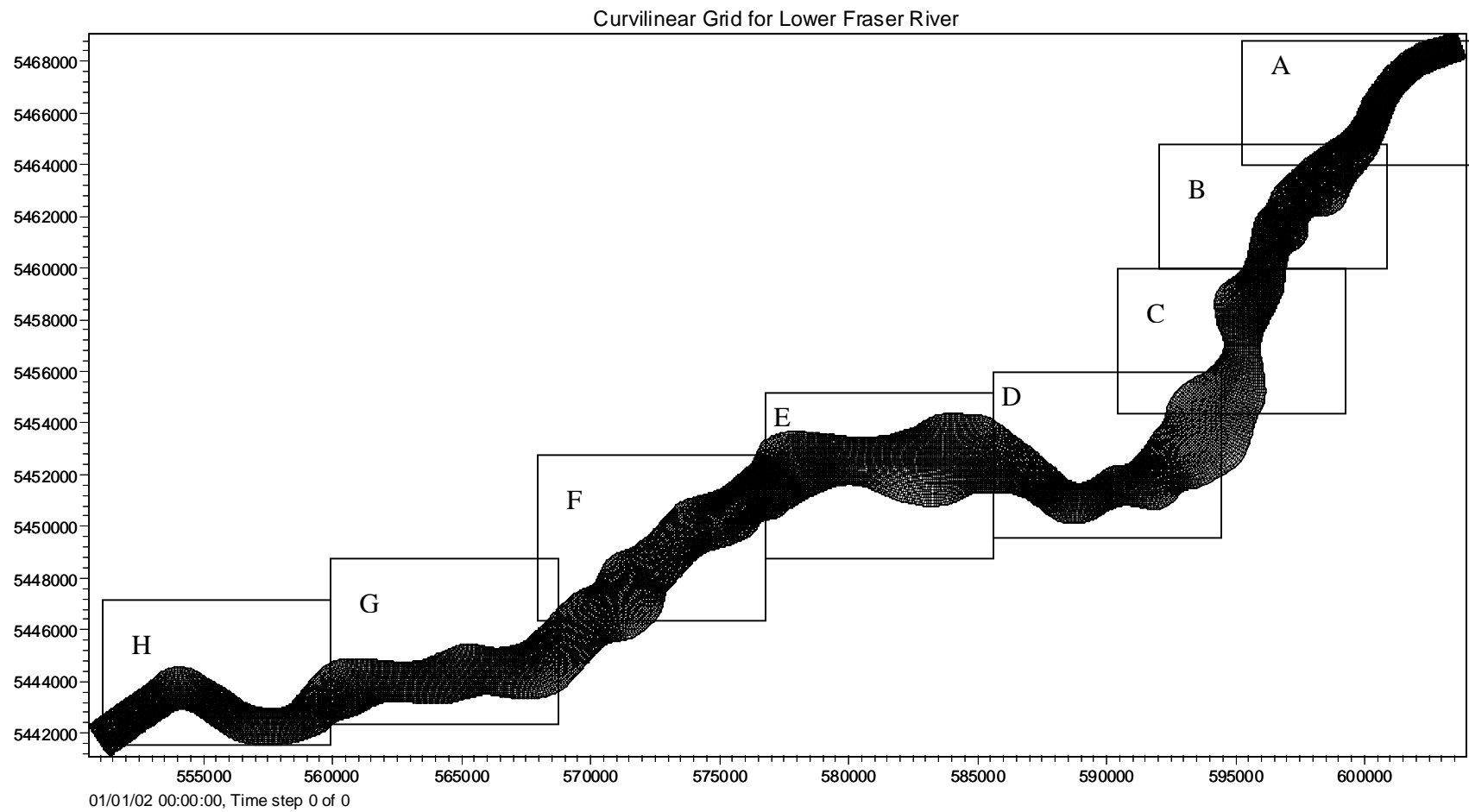
Figure 4.6: Curvilinear grid for Lower Fraser River gravel reach from Laidlaw to Mission (grid size showed in detail in Appendix E).
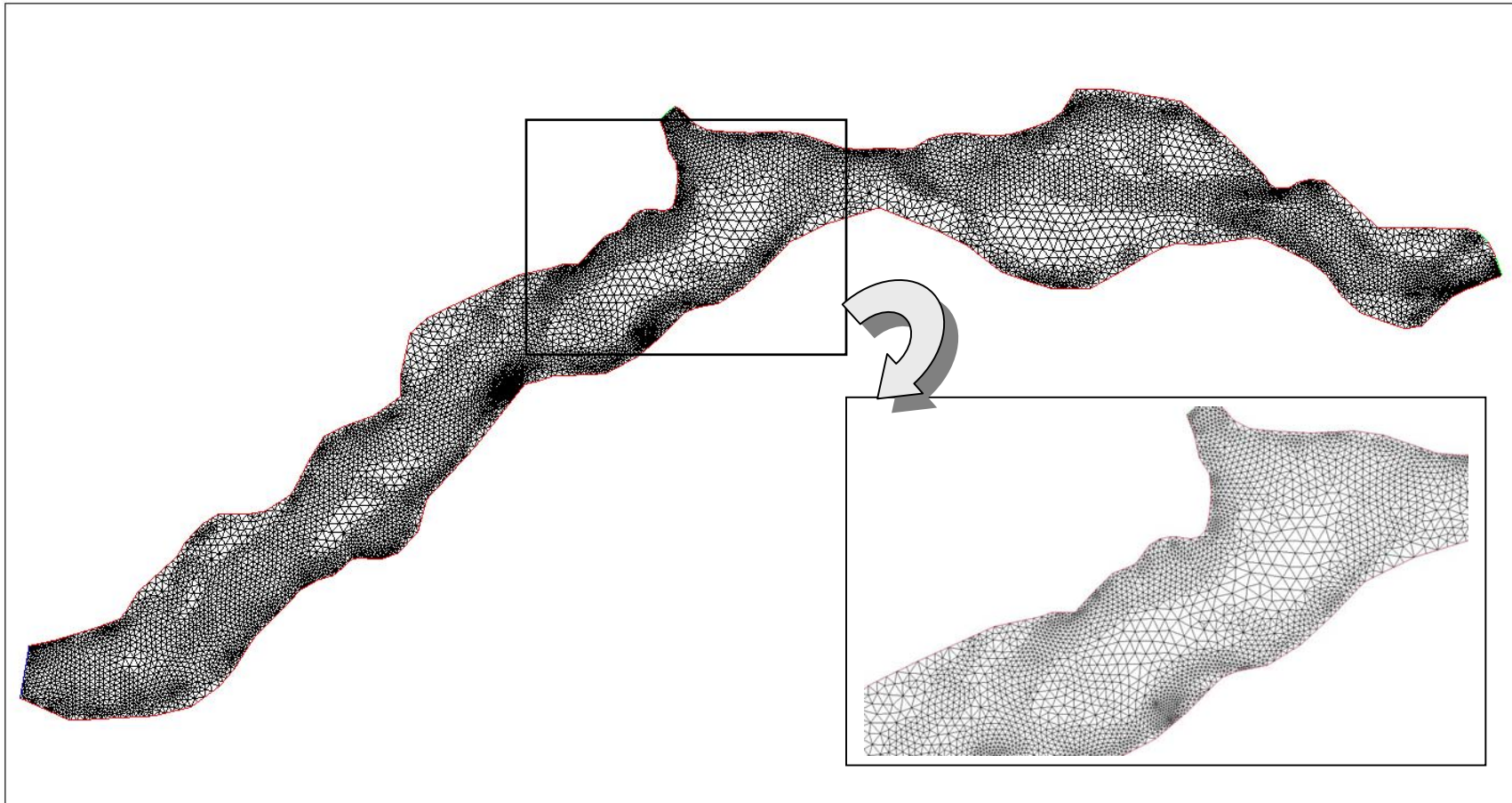
Figure 4.7: River 2D mesh from Agassiz to Sumas (mesh size variation showed in inset picture).

4.3.3 River Bathymetry Preparation

River bathymetry describes the channel bed geometry in a structural or non-structural grid. Accurate representation of the riverbed topography is the most important step in any two-dimensional model development (DHI, 2004; Steffler, 2000). Most of the two-dimensional hydrodynamic models (e.g. MIKE 21C or River2D) require high quality bathymetric survey data for hydrodynamic and morphological simulation. To prepare river bathymetry riverbed elevations data have to be imported into the computational grid in such a way that a river bottom elevations must be assigned in each computational grid cell. A digital Elevation Model (DEM) prepared from 1999 survey data was used to prepare the bathymetry for this study. The DEM was about 70 km long from Mission to Laidlaw, covering the entire gravel reach of Lower Fraser River. The resolution of the DEM was 25m × 25m and all grid points (x, y, and z) were in UTM (NAD-83) format.

After importing this DEM into the grid, most of the grid cells had specified bottom elevation values but a few cells did not. As a result, some degree of interpolation was necessary to confirm that all blank cells have bed elevation data. A maximum 30 m interpolation radius was used to interpolate and fill the blank cells. If any cell was left blank after interpolation, it was investigated and filled manually. Specially, some areas with high ground elevation (e.g. Harrison Hill near Harrison River) were found empty in the grid because they were outside the survey limit. A permanent land value was assigned for those areas so blank cells were filled out but remained out of computation. A permanent land value declaration is necessary in MIKE 21C. Any cell elevation equal to or above this land value is considered permanent land by the model and remains out of computation during simulation. The no flow boundary along the river is also assigned by the permanent land values. Land declaration was not necessary in River2D bathymetry preparation. Complete bathymetry of the Lower Fraser River gravel reach from Laidlaw to Mission in MIKE 21C is shown in Figure 4.8. Bed elevation between -20 to +25 has shown in legend. No sudden expansion or contraction was allowed near the upstream or downstream boundary in MIKE 21C. Thus, some degree of artificial manipulation of grid cell
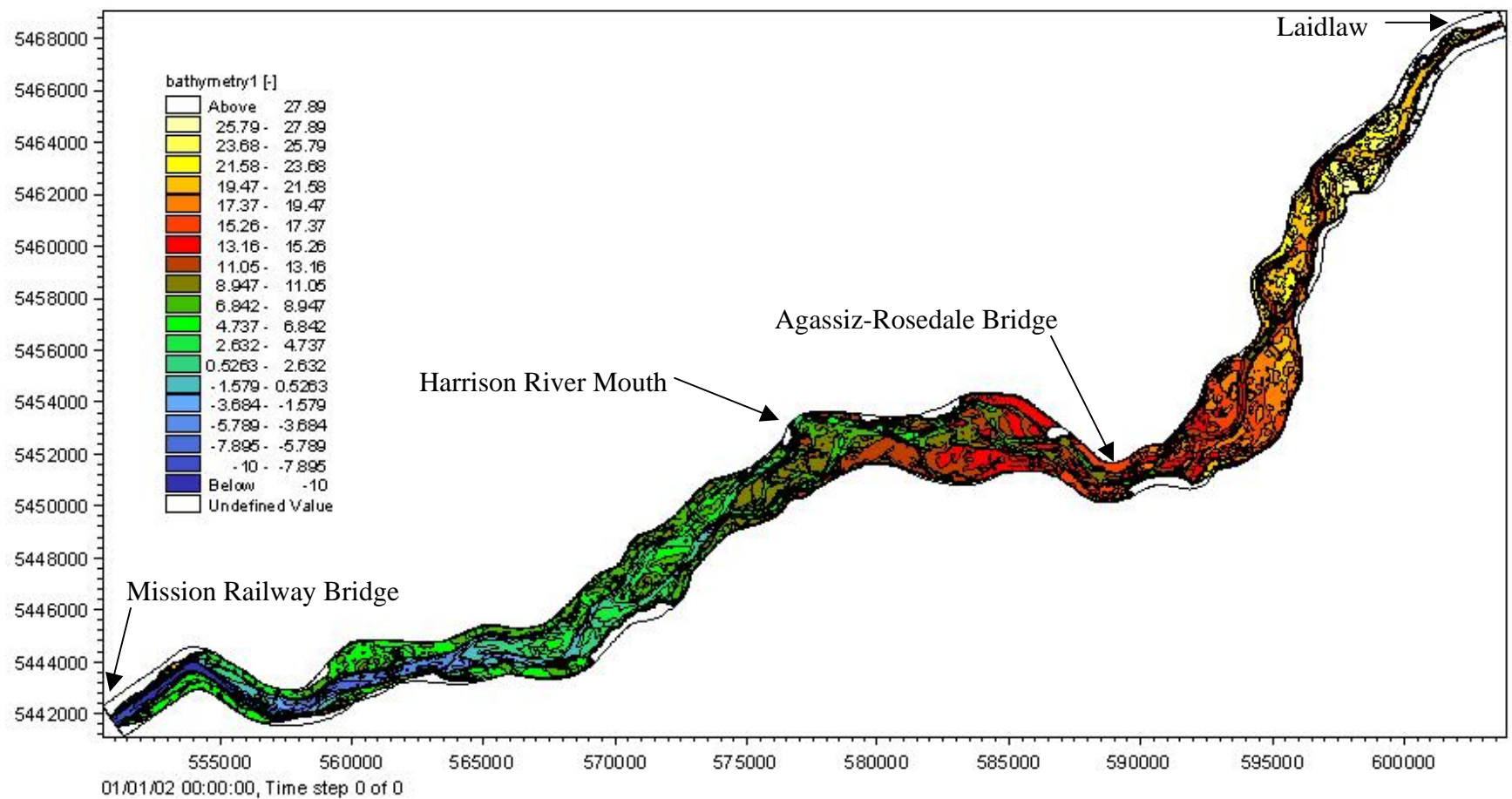
Figure 4.8: Bathymetry of the Lower Fraser River gravel reach from Laidlaw to Mission.
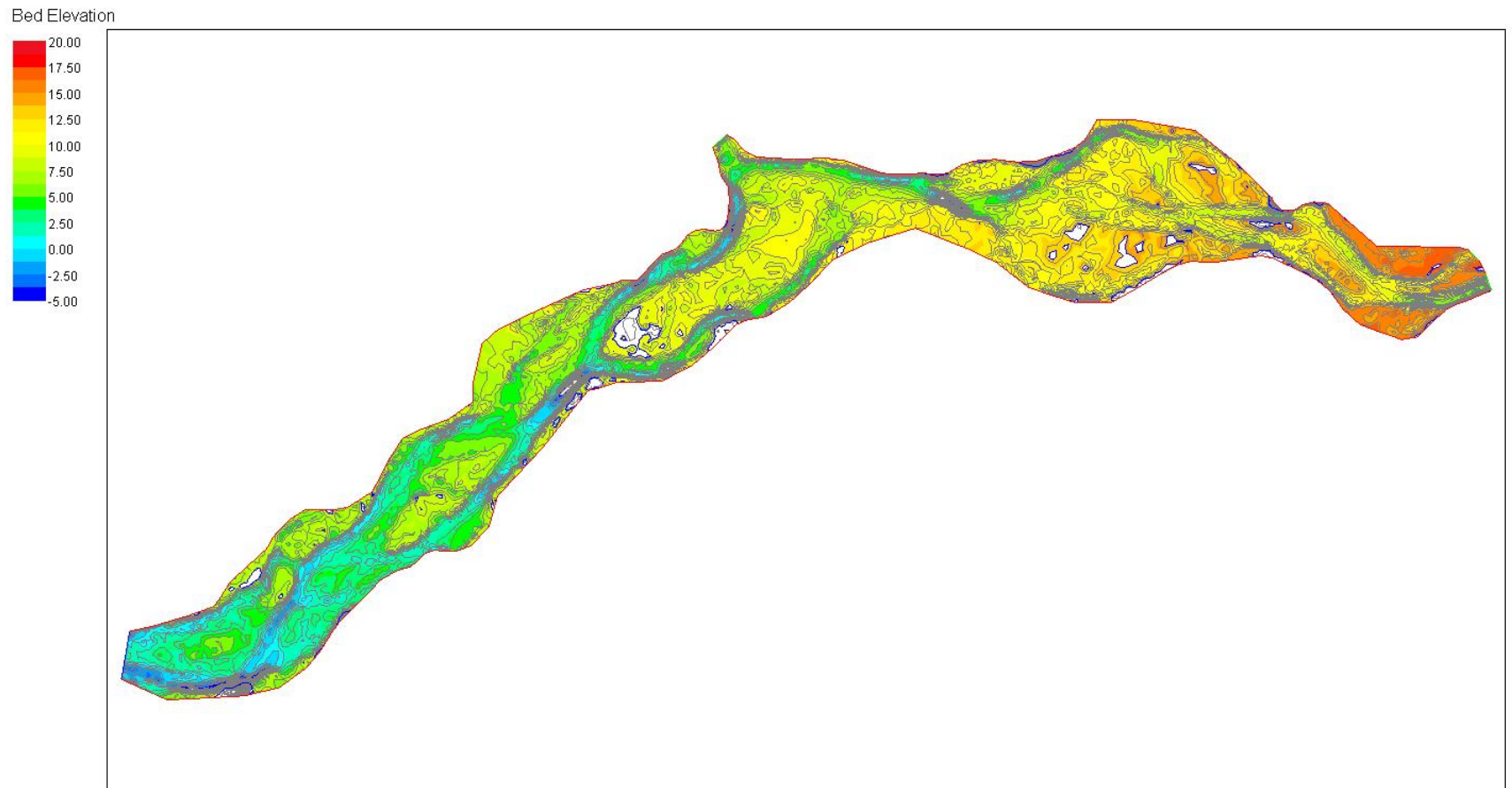
Figure 4.9: River 2D bed elevations from Agassiz to Sumas Mountain.

elevation was required near the inflow and outflow boundary locations to make sure the transitions are gradual along the main channel. Bathymetry of the Lower Fraser River gravel reach from Agassiz to Sumas Mountain in River2D has shown in Figure 4.9.

After preparation of the bathymetry, several "circular holes" were appeared in the channel bed which clearly viewed from 1999 DEM contour plot of the model bathymetry. These are artifacts of the contouring algorithms and is a consequence of survey transects being 200 m apart with no survey points between two adjacent transects in 1999 survey. This was rectified in the 2003 bathymetry survey by adding additional survey points between two adjacent transects.

4.3.4 Hydrodynamic Boundary Conditions

Both MIKE 21C and River2D models require boundary conditions at all open boundary points in the grid. The hydrograph of water discharge was required at the upstream boundary. The water level time series or a stage vs. discharge rating curve was required at the downstream boundary. Actual values of water level or discharge can be specified at each boundary in two different ways, as constant value or as time series. If necessary, user specified flow directions (known as tilting angles) could be set at the open boundary in MIKE 21C. All significant inflows from tributaries were incorporated into the model as inflow boundaries. The locations of all open boundaries were specified in the model by assigning the starting and the end cell numbers (i, j format) of the grid for each boundary. Assigned total input discharge for an open boundary was distributed among all the boundary cells in the same line. A single water surface elevation was specified for all cells along the downstream boundary line.

Since there is no significant attenuation in the flood peak between Hope and Agassiz (Millar and Barua, 1999), discharge at Hope was used as the upstream boundary condition for both Laidlaw and Agassiz during hydrodynamic and bedload simulations, respectively. The mean daily water level data at Mission were used as the downstream boundary during hydrodynamic model calibration. A water level (at Sumas) vs. discharge (at Laidlaw) rating-curve at Sumas Mountain was generated from the calibrated model. Water levels from this

rating curve were used as the downstream boundary condition during bedload simulation.

Two significant tributary discharges, one from Harrison River and another from Chilliwack River, were incorporated into the model as inflow boundaries. Harrison discharge data were available at Harrison Hot Springs and not at the confluence. Exact corrected Harrison River discharge was used for hydrodynamic model calibration but a value of 10% of Fraser River discharge at Hope was used as Harrison River discharge during sediment transport simulation. Chilliwack River discharge data were available at Vedder Crossing. Chilliwack River discharge is 1-2% of the Fraser River discharge during peak flow (UMA, 2001b). Therefore, Chilliwack River discharge may not have any significant effect during Fraser River peak flow. However, the mean daily value of Chilliwack River discharge was included in the hydrodynamic model calibration to ensure the simulation accuracy. During the sediment transport simulation, Chilliwack River discharge data were not needed, as the downstream boundary was set at Sumas Mountain upstream of the Chilliwack River and Lower Fraser River confluence.

Initial conditions are necessary for hydrodynamic flow simulation. An initial water surface profile for the entire model may be generated by linear interpolation from the downstream water level elevation and an assigned water level elevation at the upstream boundary. The whole purpose of the initial condition is to provide an estimated water surface profile elevation for each model cell at the beginning of the simulation.

No lateral inflow (rainfall generated runoff) from the drainage basin was considered for the hydrodynamic model (i.e. no source/sink term added). Default wetting and drying depth 0.2 m and 0.3 m, respectively were used for all simulations. A no-flow boundary along the Lower Fraser River was set by declaring the first and last row of grid cells as permanent land. Later two openings were made in the no-flow boundaries to assign the Harrison River and Chilliwack River inflows into the model. For River2D, the boundary conditions were set in a similar way except the upstream and downstream boundaries were set at Agassiz and Sumas Mountain, respectively.

4.4 Hydrodynamic Model Simulation

4.4.1 Hydrodynamic Model Testing and Debugging

After model development, model testing was carried out to test the model performance. A schematic diagram for the hydrodynamic model simulation is shown in Figure 4.10.
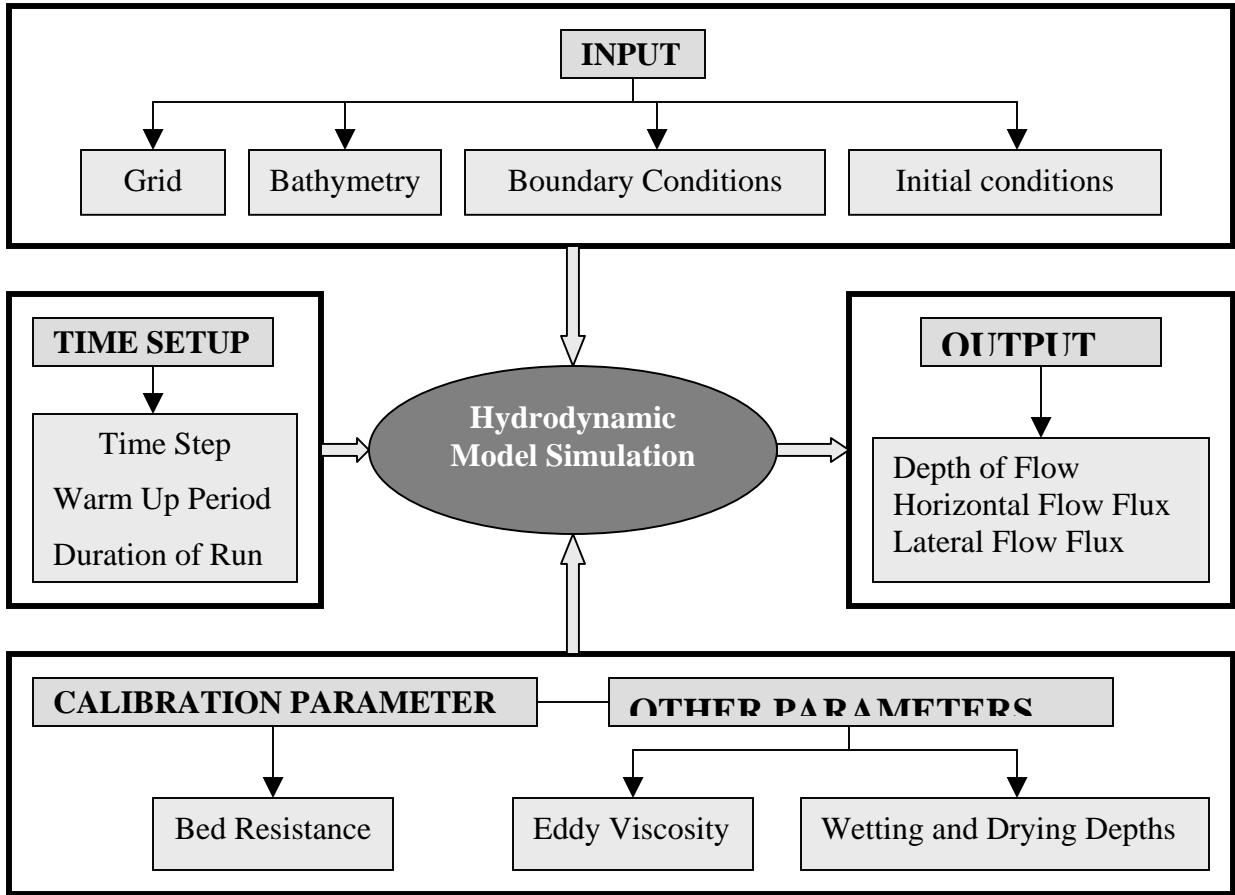
Figure 4.10: Schematic diagram of hydrodynamic model simulation (DHI, 2002).

The hydrodynamic model testing was carried out for the entire 70 km gravel reach. Initially, a constant moderate discharge (5000 m^3/s) at Hope and corresponding downstream water level at Mission with a small time step (2 sec) was tested to assess the preliminary performance of the hydrodynamic model.

It is very usual that the hydrodynamic model fails to run due to numerical instability at the very beginning of the simulation. Two practical reasons are inadequate bathymetry in some areas and inappropriate time step. When the water surface gradient is very steep between two adjacent cells just shortly after the beginning of a simulation, then numerical instability commences. Relatively smoother bathymetric transition from one cell to the other enhances gradual transition of flow, which guarantees the stability of the simulation. Manual bathymetric editing, right time step setting and a relatively longer warm up period setting always help to avoid instability problems. The effort required for debugging is unpredictable, because it could take a few or many test simulations to resolve failed executions (crashes) and numerical instabilities. A sample check is made to see whether the results are reasonable or make sense. A log of computer file development and model simulations was also established and maintained to facilitate an organized approach to management of model revisions. This log is the record of changes made at each step of model development and any problems found in the results.

4.4.2 Sensitivity Analysis of Hydrodynamic Model Parameters

Before making any predictions using the model, it is necessary to calibrate and validate the model so that the reliability of the predictions can be made as accurate as possible. Two selected hydrodynamic models involve calibration parameters such as channel bed roughness. Any calibration parameter has a physical meaning and should not be arbitrarily given values outside its realistic range to obtain an agreement with the observed data. Therefore, some degree of sensitivity analysis of the calibration parameter and other model parameters such as eddy viscosity coefficient, time step and wetting and drying depths was necessary before starting the calibration and simulation of the hydrodynamic model.

The first model parameter was simulation time step. Appropriate time step is necessary for the stable solution not for improving the result. Sensitivity analysis of model time step was performed to assess the stability of the hydrodynamic simulation. Although the numerical scheme of the MIKE 21C model is based on an implicit scheme, computational time step has to be specified in such a way that maximum accuracy in the model results will be achieved without

sacrificing the quality of results (numerical diffusion). Tests were also made to assess the appropriate time step of the computations by gradually increasing the initial time step for achieving stability and convergence. Time step sensitivity was tested by increasing the time step values for higher and lower discharge values. The minimum and maximum range of flows was 4,000-15,000 m^3/s in this study.

The second model parameter was the Manning-Strickler coefficient "N" (1/n in North American literature) in MIKE 21C and bed roughness element height k_s in the River2D. A global Manning-Strickler "N" value for the entire reach and distributed values were tested. It is commonly believe that the bed roughness parameter is the most sensitive so the appropriate value(s) of bed roughness will usually be determined by the calibration test over the whole range of values.

The third important model parameter was "eddy viscosity" which basically controls the size of eddies in the model grid. It is normally believed that the eddy viscosity coefficient is less sensitive and used to improve the stability of the solution. Thus, for simplicity and because of lack of field data a constant eddy viscosity value (global) is often preferred by river modelers in practical model application. However, it is difficult to determine which constant value will be appropriate for a particular application. The best possible solutions are to review the literature and software manual and the range of discharges to be simulated with the model. However, most of the river hydrodynamic application sensitivity of the eddy viscosity coefficient has to be tested. Different wetting and drying depths were also used in the model to test the sensitivity in the model results.

4.4.3 Hydrodynamic Model Calibration

Calibration was performed by a steady-state simulation with the 23 June, 1999 freshet event, which was considered the most complete record to date. Water discharges from Lower Fraser River at Hope, Harrison River at the confluence and Chilliwack River at the Vedder crossing were used as model inflow boundaries. Since there is no significant attenuation in the flood peak between Hope and Mission (Millar and Barua, 1999), the same discharge data at

Hope were used at Laidlaw as the upstream boundary condition. Harrison River discharge data at Harrison Hot Springs were corrected with Harrison Lake water level and Lower Fraser River discharge at Hope and applied in the model calibration. Chilliwack River discharge at Vedder Crossing was used directly in the model calibration. The mean daily water level data at Mission were used as the downstream boundary condition. The Mission gauge has a modest tidal influence. A summary table of the boundary conditions is presented in Table 4.5.

Table 4.5: Summary of the boundary conditions for the Lower Fraser River two-dimensional hydrodynamic model calibration (values represent the 23 June, 1999 freshet event).

Boundary Conditions	Boundary Type	Values	Unit
Upstream Boundary	Discharge at Hope	11,000	m^3/s
Downstream Boundary	Water Level at Mission	6.26	m Geodetic
Tributary Inflows	Discharge at Harrison Mouth	1140	m^3/s
	Discharge from Chilliwack River	235	m^3/s

Simulation results were compared with the various observed water level data obtained from staff gauge reading along the Lower Fraser River until a reasonable agreement between observed and computed data was reached. Water level may vary from one bank to the other or between two adjacent branches separated by the gravel bar or island. Therefore, the exact location (x, y coordinates) of water level gauges was a primary requirement for two-dimensional model calibration and verification. Data from 15 gauges were used for model calibration. A total of 12 gauges were from Ministry of Environment B.C. (MoE, B.C.) and 2 gauges were from District of Kent and 1 from City of Chilliwack (Table 4.3).

4.4.4 Hydrodynamic Model Verification:

The hydrodynamic model has to be verified against some observed data set rather than the calibration data set. Two-stage verification (peak and low discharge) is ideal for the model performance test but many gauge sites are virtually dry during low flow and MoE collect data only in peak flow season. Thus, no measured gauge water level data were available during that period. As a result, one-stage verification was considered with high flow. The peak flood

discharge (10,090 m^3/s) on 18 June, 2002 was used for model verification. On that day only B.C. MoE, gauges were in operation. As a result, Water level data from nine B.C. MoE, gauges were used for the model verification test.

A depth-averaged velocity verification test was performed for discharges above the sediment transport threshold discharge (>5000 m^3/s). The objective was to determine how the model predicts velocity and how it compares with observed data. As part of the hydrographic survey, Public Works Canada used an acoustic Doppler current profiler (aDcp) to collect velocity direction and magnitude information in the Lower Fraser River gravel reach during July 30 to August 11, 1999. The velocity information is based on a single ping at each vertical profile and one measurement was made approximately every meter. Thus, every ten values of velocity and of depth along each transect were averaged to reduce errors associated with individual point measurements. Since no averaging was done in the field, spatial averaging was performed in a spreadsheet.

Unfortunately, most of the surveys were carried out after high freshet flow in a relatively low flow condition, which was below the sediment transport threshold discharge. So, only a few aDcp survey data sets were practically available to verify the results. Three sets of aDcp velocity transects 17, 18 (A and B) and 19 (A and B) data near Agassiz-Rosedale Bridge with a discharge 6,100 m^3/s at Hope were selected for velocity verification (Figure 4.11).
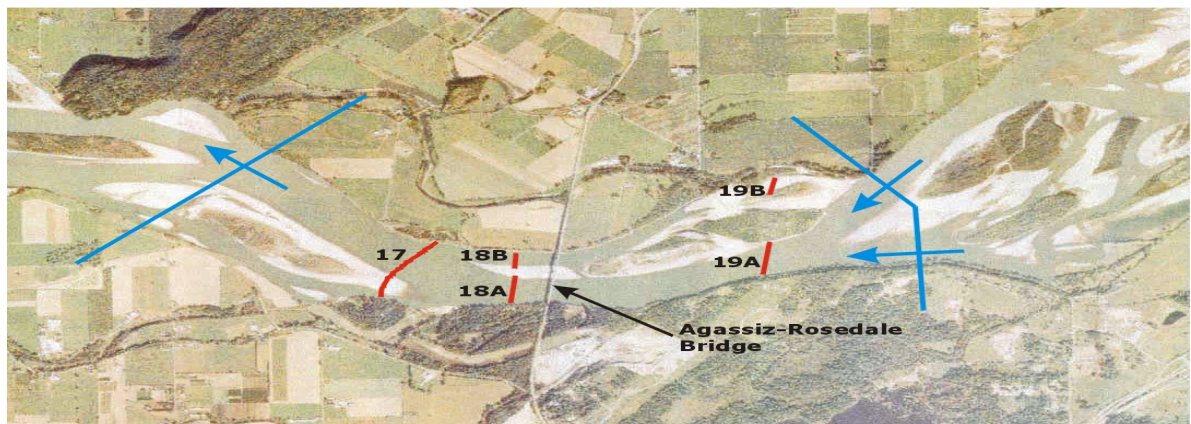
Figure 4.11: ADCP transect locations in the Agassiz-Rosedale reach (after UMA, 2001a)

A single MIKE 21C model grid cell could be large enough (for example, 20 m × 30 m) to contain two or three vertical aDcp data points. In this case, the data points close to the center of the cell were chosen for the verification. The processed aDcp velocity data set was provided by Mr. Faizal Yusuf, P. Eng., BC Hydro (Yusuf, 2001). Results are presented in section 5.1.3.

4.5 Sediment Transport Simulation

4.5.1 Grid Extraction for Sediment Transport Simulation

A new grid and corresponding bathymetry and bed roughness between Agassiz-Rosedale and Sumas Mountain (approx. 35 km) was extracted from the calibrated hydrodynamic model and used for gravel transport and morphological simulation (see Figures 4.12). Frame A and B are shown in detail in Appendix F. There were 30,031 (509 × 59) cells in the sediment transport grid. The sediment transport bathymetry was exactly the same as in the hydrodynamic model except near the upstream and downstream boundaries. Some modification was done near the upstream and downstream boundaries to satisfy the MIKE 21C boundary requirement that no sudden expansion and contraction be allowed near the boundary. To satisfy this requirement some higher elevation cells were assigned as no-flow boundary near the upstream and downstream boundaries.

The upstream boundary was set about two and half kilometers upstream of the Agassiz-Rosedale Bridge near Herrling Island. The objective was to match the simulated bedload transport rate with the observed bedload transport rate (McLean and Church, 1999a) at the Agassiz-Rosedale Bridge. At this section Lower Fraser River inflow was divided by Herrling Island. The maximum inflow is passing through the upper branch of Herrling Island and an insignificant amount of inflow enters through the lower side channel (Yusuf, 2001). Ultimately, these divided flows merge together near the Agassiz-Rosedale Bridge. For the simplicity, the total inflow was set at the upper branch and lower branch was sealed. The Fraser River discharge at Hope was set at this new boundary location as the upstream boundary condition. However, Chilliwack River discharge was not included during sediment transport simulation as it was downstream from the downstream boundary. Harrison River inflow was considered to be

one tenth of the Fraser River discharge during all sediment transport simulations. No bathymetric modification was required near the Harrison River.

The downstream boundary was set near Sumas Mountain, which is virtually the end of the gravel reach (McLean and Church, 1999a). A stage-discharge rating curve at Sumas Mountain was used as the downstream boundary. This rating curve was prepared from the main 70 km long hydrodynamic model simulation with a series of discharges at Hope and corresponding water levels at Mission. Figure 4.14 shows the stage-discharge rating curve at Sumas Mountain. For steady state discharge the downstream water level boundary at Sumas Mountain was directly selected from this rating curve during sediment transport simulation. A new bed roughness file for the sediment transport simulation was extracted from the 70 km long hydrodynamic model. No modification was required as it was already calibrated.
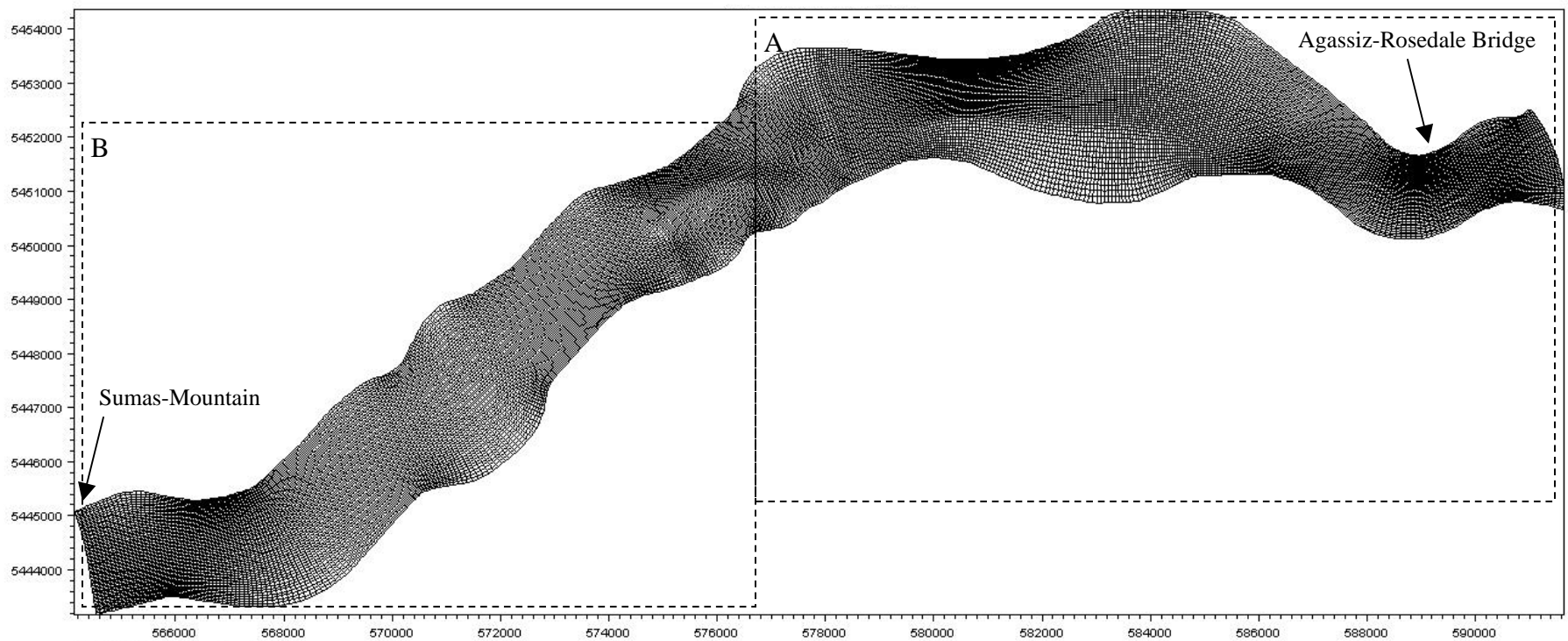
Figure 4.12: Sediment transport grid (Agassiz to Sumas Mountain) extracted from the hydrodynamic model grid (grid size variation in Frame A and B showed in detail in Appendix F).
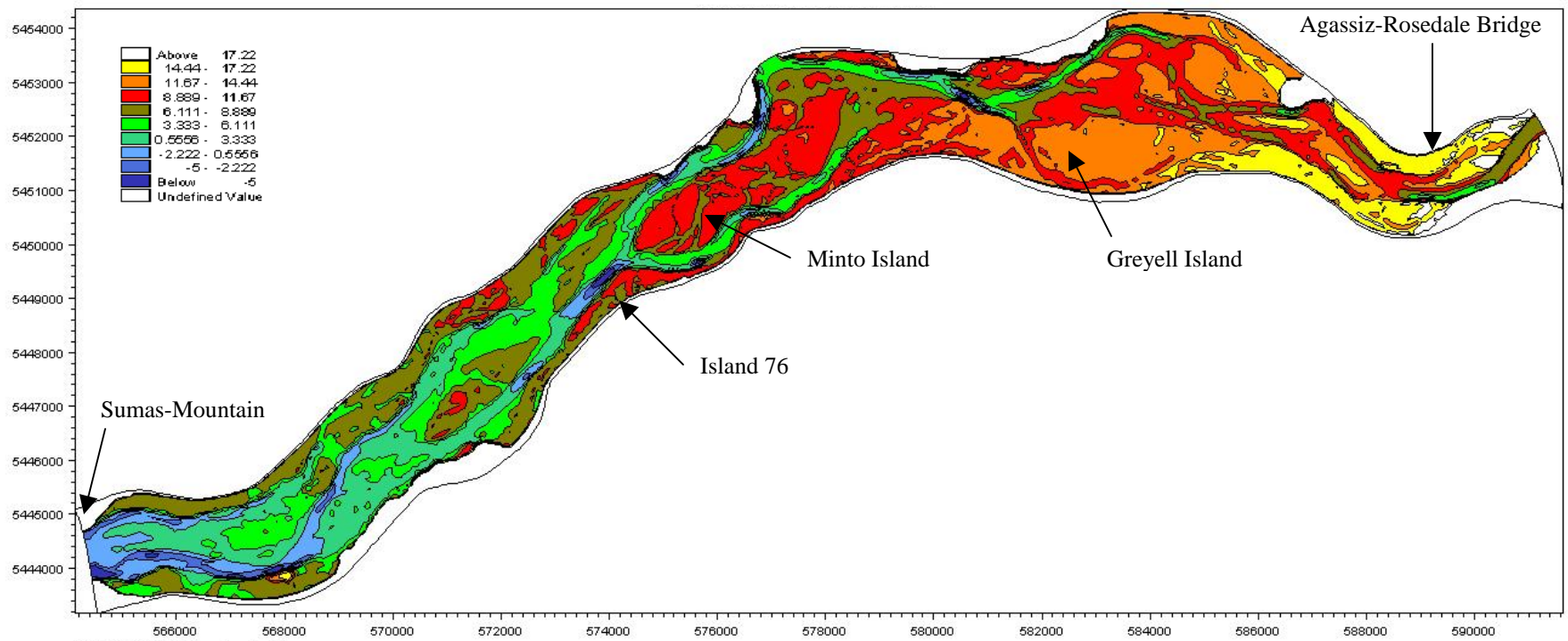
Figure 4.13: Bathymetry of the Lower Fraser River gravel reach from Agassiz to Sumas Mountain.
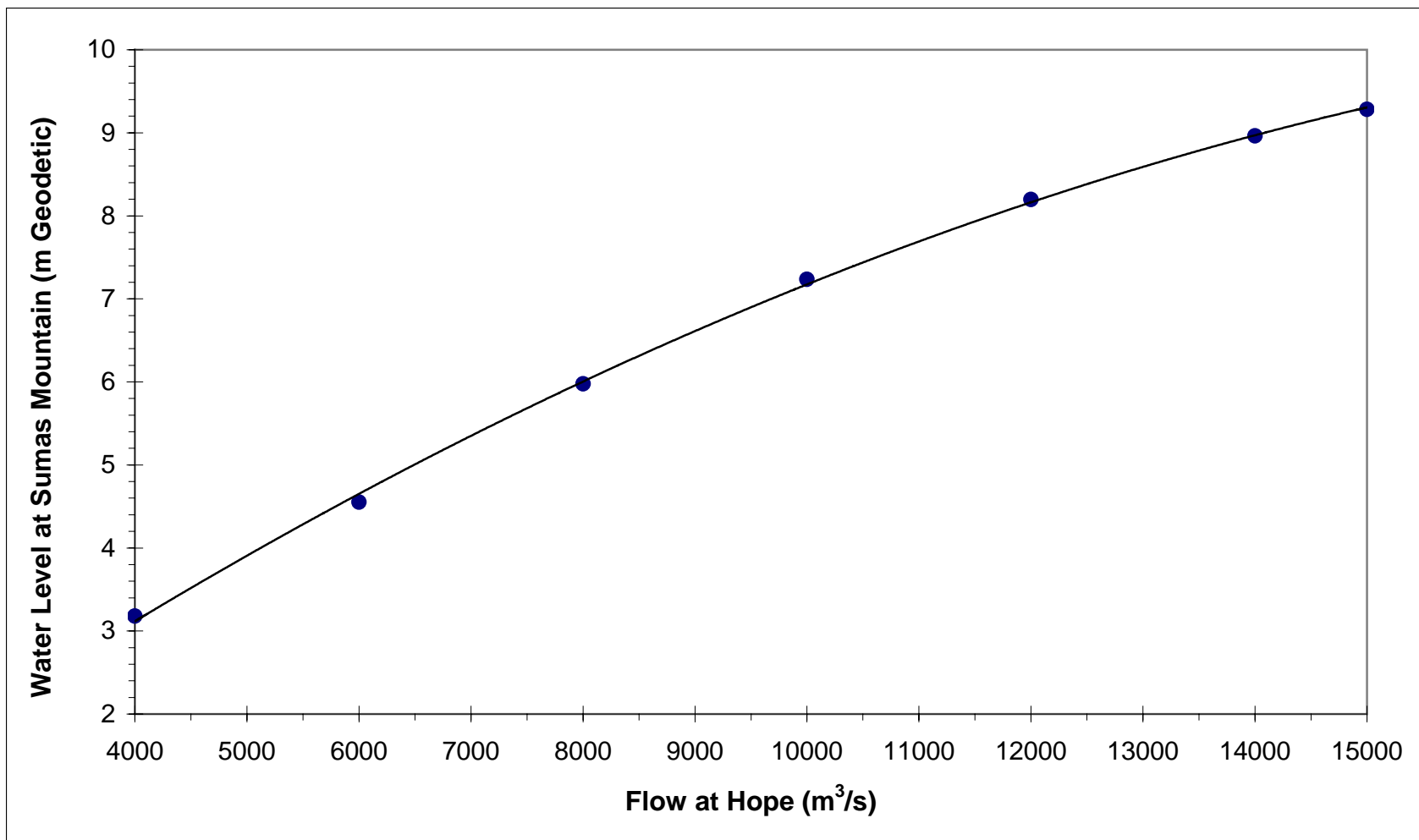
Figure 4.14: Discharge vs. water level rating curve at Sumas Mountain computed using the MIKE 21C Hydrodynamic Model.

4.5.2 Sediment Size Distribution Setting

Only non-cohesive bedload transport was modeled and no suspended sediment transport was considered. Detailed information of sediment size fractions and their distribution in percentage at each cell is necessary as an initial condition for sediment transport and morphological simulation. These contents were set as a spatial map file in the model for all nine size fractions. Nine separate spatial map files were used to set the initial sediment size content in the model. Each of those files indicated the percent content for a size fraction in all 12 zones. For example, the file that contained data for size fraction # 9 indicates 0.99% in Zone 1, 0.98% in Zone 2 and 10.15% in Zone 11 (see Table 4.4).

4.5.3 Sediment Transport Boundary Conditions

A sediment transport boundary condition can be set in two different ways in the model – "no supply limit" and "supply limited". In the "no supply-limit" condition, an appropriate amount of sediment enters into the model from the upstream open boundary so that the bed level at the boundary does not change over the entire simulation period. In this case, the whole sediment transport in the model depends on the bed shear stress produced by the river discharge. In the "supply-limited" condition, the model user must specify the bedload discharge at the upstream boundary so a fixed amount of sediment influx will be entered into the model for each discharge simulation. The "no supply limit" boundary was used as the upstream sediment boundary condition.

4.5.4 Layer Thickness of Riverbed

The riverbed comprised three layers of given thickness. The thickness of surface layer (Layer1), middle layer (Layer2) and lower layer (Layer3) were 0.25 m, 0.25 m and 10 m, respectively. The first two layers were expected to exchange bed material in each time step. If only a deep single layer was set in the model, the change of mean grain size was not very significant. The reason for this is that the bed surface grain size accounting routine in the program does not work properly because it is related to the total number of grain and volume of each cell. To avoid this problem the first two layers were thin as compared to the lowest layer.

113

Surface layer thickness was set about 2-3 times the D_{max} value of grain sizes as recommended in many sediment transport studies (DHI, 2002a). The thickness of the lowest layer was set about 10 m deep so that if bed degradation goes below first two layers in any grid cell then the bed would not be exhausted. Otherwise if bed level exhausted in any cell then the model will fail to run. However, the bed aggradation or degradation should not be unrealistic in any cell. To control this problem a maximum bed degradation value 0.01m/day was set into the model. This value was chosen in the model based on long-term average bed level change in Fraser River gravel-bed reach, which is 20 cm/5years (Ham, 2005a). In surface based sediment transport formulas, an assumption is that the transport will occur from the surface layer. Only and after degradation does the subsurface layer become the surface layer. Therefore, an active surface layer will always be present. To maintain this assumption the same surface size distribution was set for all three layers.

4.5.5 Sediment Transport and Morphological Parameters

The mineral density and porosity of the gravel were set to constant values of 2.65 t/m^3 and 0.35, respectively. For transverse sediment transport, the transverse slope coefficient and power were set to 1.25 and 0.5, respectively as suggested for natural alluvial rivers (DHI, 2002a). The helical flow coefficient was set to 1. An advection time step was necessary for helical flow simulation. A value lower or similar to that of hydrodynamic time step was used. Movement of the sediment wave is not as fast as the hydrodynamic wave. Therefore, a sediment transport time step larger than the hydrodynamic time step was generally used (DHI, 2002). A sediment transport time step 3 times larger than the hydrodynamic time step was used for all sediment transport simulation. A scaling factor of 100 or less was preferred for scaled dynamic simulation with steady discharge to reduce the simulation time in long-time morphological simulation. Other morphological parameters were set under the guideline of the MIKE 21C User Manual (DHI, 2002a).

4.5.6 Sediment Transport and Morphological Simulation

Parker's (1990) surface based bedload transport equation was used at the first stage for gravel transport simulation. Sediment transport simulation with Parker's (1990) formula was started with the threshold gravel transport discharge 5,000 m^3/s (McLean and Church, 1999a). Simulation was performed for discharges > 5,000 m^3/s at increments of 1,000 m^3/s up to a maximum of 15,000 m^3/s. A sediment transport time step (10 sec. to 15 sec), usually 2 to 3 times larger than the hydrodynamic time step, was used to maintain the numerical stability of the sediment transport simulation. When these time steps showed stability with higher discharges as well as lower discharges, then sediment transport calibration was begun.

Sediment transport parameters such as the dimensionless reference shear stress were calibrated against the available measured field data to obtain a good match between observed and estimated values. There were no bedload data in the middle of the reach except at Agassiz-Rosedale Bridge. As a result, these data were used to calibrate the bedload transport capacity at Agassiz-Rosedale Bridge. First of all, the model simulation was performed with Parker's (1990) prescribed dimensionless reference shear stress 0.0386 and simulated bedload discharges were extracted at the Agassiz-Rosedale Bridge and compared with the observed field data. If comparison did not show any match between observed and simulated bedload discharges, then calibration of the dimensionless reference shear stress with an increased or decreased value was performed.

A bedload discharge with a single river discharge value 8000 m^3/s (bankfull) was used primarily to calibrate the dimensionless reference shear stress to get a good match between observed and estimated values at the Agassiz-Rosedale section. When a close match was found between the modeled and observed values, then simulation of other discharges from 5000 m^3/s to 15,000 m^3/s was performed. Parker (1990) used 0.0386 as the dimensionless reference shear stress to develop his equation based on Oak Creek data. More recently, Wilcock and Crowe (2003) showed that the dimensionless reference shear stress values could be significantly lower (e.g., 0.022) depending on percent sand content in the bed material. Based on this idea the dimensionless reference shear stress was lowered to find a good match between the observed

and the modeled data.

In the case of the Wilcock and Crowe (2003) equation, the dimensionless reference shear stress value was calibrated by direct simulation. Total volume balance and thalweg elevation match along the channel was used to calibrate the sediment transport and morphological model. A direct sediment transport and morphological simulation between 1999 and 2003 was performed using the 1999 bathymetry as the initial riverbed and all the discharges > 5000 m^3/s. The total number of days when discharge equaled or exceeded 5000 m^3/s was found to be 248 days within this period (1999-2003). Figure 4.15 shows all the discharges larger than or equal to 5000 m^3/s between 1999 and 2003 in a sequential order (plotted without calendar date). The dark line in Figure 4.15 shows all the discharges in ascending order.

Usually small hydrodynamic time step (2 - 5 sec) is a requirement to maintain numerical stability in a two-dimensional model. As a result, a complete unsteady flow simulation with 248 days was not feasible with present computational power (CPU time in the order of 2 weeks to complete one simulation). To reduce the total simulation time the unsteady discharge hydrograph at Hope was converted to a series of steady discharges with a 500 m^3/s interval. Figure 4.16 shows all the converted steady discharge hydrograph with the values larger than or equal to 5000 m^3/s between 1999 and 2003 in ascending order. In Table 4.6 the median value of a discharge range and corresponding duration, downstream water level elevation and tributary inflow are shown. For example, the discharge between 5000 and 5500 m^3/s with an average value 5243 m^3/s occurred during 70 days between 1999 and 2003. Due to this conversion, unsteady bed level change history may be lost but the total change is assumed to be the same at the end of the simulation. The steady simulation was performed step by step starting from lower discharges to higher discharges. The simulated riverbed from one steady discharge was set as an initial riverbed condition for the next hydrograph simulation. This process continued up to the final hydrograph. As a result, the bed elevation changes from one simulation were transferred to the next simulation. The final riverbed reflected the effect of all discharges.

Hydrograph at Hope (Q ≥ 5000m³/s)
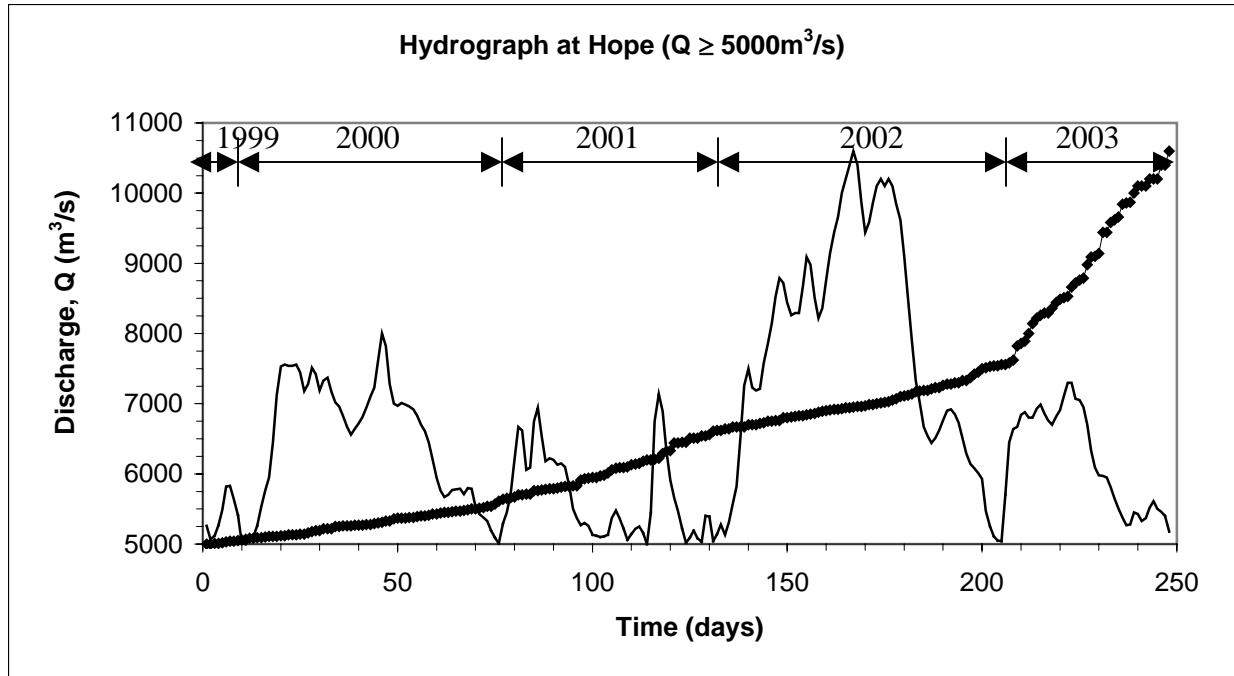
Figure 4.15 shows all the discharges larger than or equal to 5000 m³/s between 1999 and 2003 (dark line shows all of them in ascending order).

Steady Hydrograph at Hope (Q ≥ 5000m³/s)
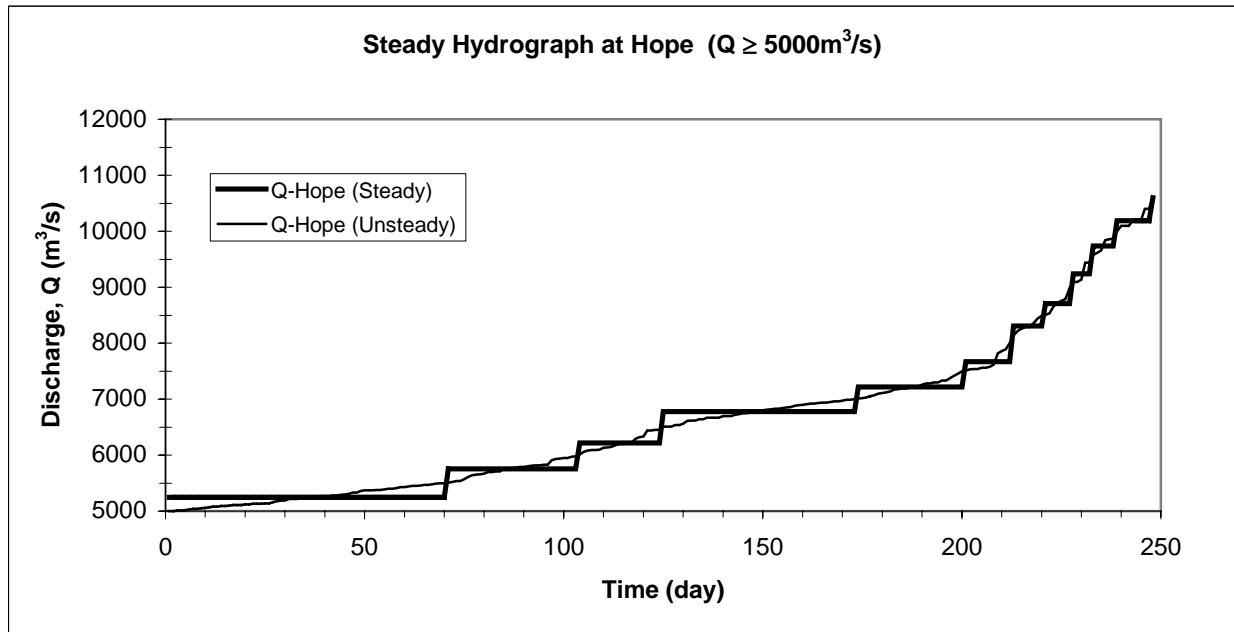
Figure 4.16: Unsteady discharge hydrograph at Hope converted to a series of steady discharge hydrographs (500 m³/s interval).

117

Table 4.6: Median values of the steady discharges (column4) and their durations (column2).

No. (-)	No of days (-)	Q-Range (m³/s)	Q-Hope (m³/s)	WL-d/s (m-GSC)	Q-Harrison (m³/s)
1	70	5000-5500	5243	4.10	721
2	33	5501-6000	5755	4.47	794
3	21	6001-6500	6218	4.84	783
4	49	6501-7000	6776	5.20	878
5	27	7001-7500	7217	5.54	808
6	12	7501-8000	7668	5.86	738
7	8	8000-8500	8311	6.31	1001
8	7	8501-9000	8707	6.41	906
9	5	9001-9500	9242	6.78	1139
10	6	9501-10000	9738	7.02	1230
11	9	10001-10500	10189	7.23	1242
12	1	10501-11000	10600	7.34	1100

The final bed level was compared with the 2003-surveyed Lower Fraser River riverbed. The dimensionless reference shear stress value was calibrated to obtain a good match between the observed and modeled bed. A volume balanced was performed to obtain the net volume change over the 4 years or between two consecutive survey periods.

4.5.7 Gravel Bedload-Discharge Rating Curve

The bedload discharge obtained from the Wilcock and Crowe (2003) equation was used to develop the rating curve. A gravel bedload rating-curve was developed from the model-derived equilibrium transport rates at Agassiz-Rosedale Bridge cross section just near the upstream boundary by fitting an equation of the form:

$$G_b = aQ^b \ \dots\dots\dots\dots\dots\dots\dots\dots\dots\dots\dots\dots\dots\dots\dots\dots\dots\dots\dots\dots\dots\dots\dots\dots\dots\dots \ (4.1)$$

where,

G_b = gravel transport rate (t/d),

Q = discharge (m³/s), and coefficients a and b were empirically derived from curve fitting.

This rating curve was compared with the existing rating curve prepared by McLean and Church (1999) with 20 years observed data collected by Water Survey of Canada at the Agassiz-Rosedale Bridge.

4.6 Computational Gravel Budget

4.6.1 Method 1: Integration of Flow Duration Curve and Bed-Load Discharge Rating Curve

The mean annual bedload influx or transport rate at a river reach can be obtained by integrating the bedload rating-curve with the flow duration-curve. This method is a statistical method because it depends on flow frequency (probability of occurrence of discharge events). A flow-duration curve is basically a histogram representing the range of flows on the x-axis and their frequencies on the y-axis. A flow duration curve (histogram) was developed from 89 years of Fraser River discharge data measured at Hope (1912-2001) and was used in the sediment budget calculations (Figure 4.17).
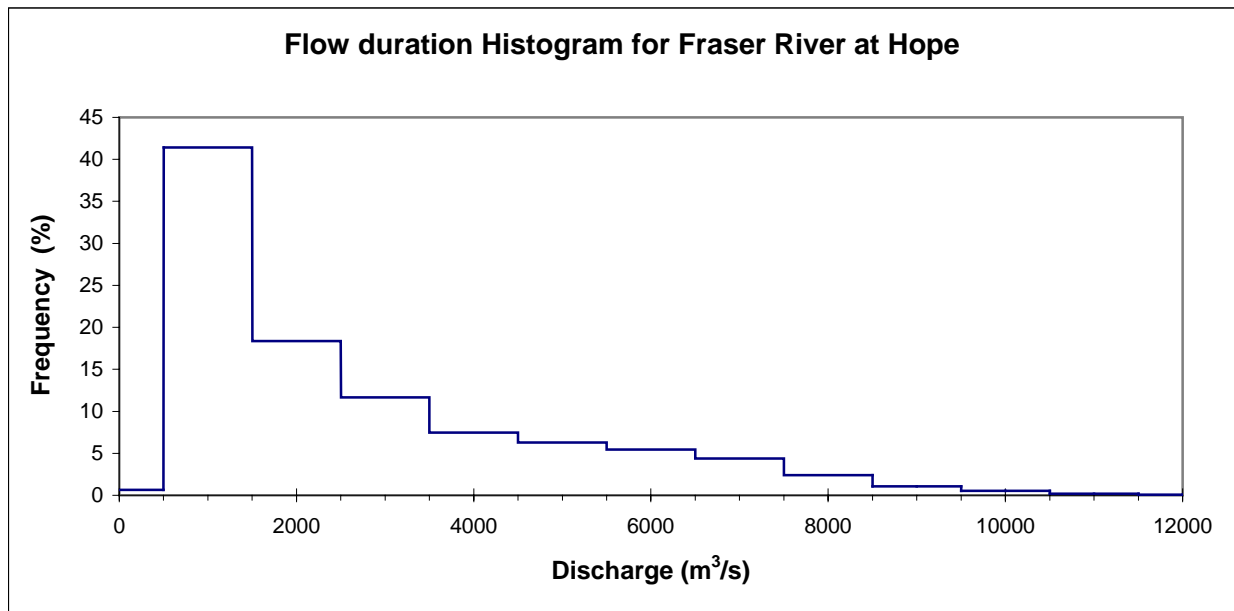
Figure 4.17: Fraser River flow duration curve at Hope (1912-2001).

The frequency of each selected discharge event can be obtained from the flow duration curve. The flow ranges (1000 m³/s classes) > 5000 m³/s and their frequencies are used. For example, a flow of 7000 m³/s flow has a frequency of 5% in Figure 4.16. A mean annual transport rate at a section of the river was obtained by integrating the flow duration curve with the sediment discharge rating-curve as follows:

$$G_{bT} = \sum_{i=1}^{n} G_{bi}\, p_i * 365.25 \ldots\ldots\ldots\ldots\ldots\ldots\ldots\ldots\ldots\ldots\ldots\ldots\ldots\ldots\ldots\ldots\ldots\ldots\ldots\ldots\ldots\ldots\ldots\ldots\ldots\ldots\ldots\ldots\ldots\ldots \quad (4.2)$$

where,

G_{bT} = average annual gravel load (t/y),

G_{bi} = transport rate (t/d) from the rating curve corresponding to Q_i (individual discharge),

p_i is the proportion of the time the flow is within the range represented by Q_i (where, $\sum p_i = 1.0$),

365.25 is the conversion factor for the number of days in a year.

Annual gravel influx at Agassiz-Rosedale Bridge was calculated using this formula. A distributed sediment budget along the channel was prepared. Transport rates were integrated across the channel to provide a cross-sectional total.

4.6.2 Method 2: Direct Simulation, Visual and Thalweg Comparison and Volume Balance

Method 2 is a direct simulation and comparison method. This method can be applied when two sets of digital elevation models or river bathymetric survey data are available over a short period. An unsteady flow and sediment transport simulation over a specific period was performed using the earlier bathymetry as the initial riverbed. Then, the simulated river bathymetry was compared to the observed bathymetry. For example, unsteady flow and sediment transport simulation between1999 to 2003 can be performed by setting the 1999 river bathymetry (riverbed)) as the initial riverbed and then the simulated river bed can be compared with the observed 2003 river bed. This process will continues until a satisfactory result is found by tuning the calibration parameters.

Bathymetric changes were computed using the calibrated MIKE 21C morphological model by simulating gravel transport and deposition between 1999 and 2003. First of all, the 2003-surveyed bed level was imported into the model grid to prepare the observed bathymetry. Then, the initial bed level (1999) was subtracted from this bed (2003 bed) to obtain the observed erosion or deposition depths in each cell. The positive depths and the negative depths indicate aggradation and degradation, respectively. Secondly, a new river bed bathymetry similar to 2003 bathymetry was obtained by simulating the steady flow hydrograph (converting from unsteady flow) from the known initial bed level (1999 bathymetry). As mentioned earlier, all unsteady discharges within 500 m^3/s interval were represented by an equivalent steady discharge and corresponding duration. The simulated model bathymetry was obtained by simulating all the steady time series data above 5000 m^3/s.

The simulated modeled bathymetry has compared with the observed 2003 bathymetry to verify how accurately the model can predict gravel transport and bed level changes. A two-dimensional map with this new bed elevation along the channel was prepared. Instead of riverbed elevation, observed and simulated riverbed elevation change maps can be compared. This permits direct comparison with the morphological changes identified from the bathymetric surveys. Visual comparison was performed in the MIKE 21C result viewer. Various color legends were used to visualize them as best as possible but this exercise is limited by the MIKE 21C in-built result-view map's color resolution. Perfect visual matching is impossible for a large two-dimensional morphological model application but a reasonable match is acceptable (Enggrob, 1998).

Visual matching is a qualitative method even though it is produced from bed-level change data. The result is acceptable or not depending on the modeler's judgment, the resolution of the map and also the purpose of the comparison. The practical limitation of this method is computational power and availability of flow data with the desired interval (e.g. hourly data). Dimensionless reference shear stress was tuned as a calibration parameter to obtain a good match between observed and simulated bed. Two more techniques may be used to calibrate the sediment transport model, thalweg elevation matching and volume balance. Both methods are

described below.

This type of calibration technique is often found in cross-section based one-dimensional sediment transport and morphological model calibration (Krishnappan, 1981). The procedure described in Method 2 will be applied in this case except a one-dimensional bed-profile will be used instead of a two-dimensional visual bed-level change map. In this method, simulated point bed elevations along the channel are compared with the observed point bed elevations. Normally the points are selected at the deepest points along the channel that is called 'thalweg'. If the visual comparison method does not provide satisfactory result then this may be a useful option to calibrate the model. The bed elevations in the thalweg were extracted from both 2003 simulated and 2003 observed bathymetries and plotted together for comparison.

Volume balance is a quantitative approach to calibrate the sediment transport model. After following the simulation procedure described in Method 2 a volume balance was performed to find out the net sedimentation in the model reach. The area of each cell was calculated from the grid geometry and their coordinates. Then the depth change in each grid cells are multiplied by the corresponding cell areas. These represent the aggradational or degradational volumes for each cell. If the depth change is zero in any cell, then it indicates that there was no net change between two subsequent survey periods. The volume balance was performed to find the net sedimentation in the reach (or, over a specific zone). The total volume balance was performed in the following way:

$$V_{net} = \frac{1}{N_y}\left[\sum_{i=1}^{n} V_a - \sum_{i=1}^{m} V_d\right] \dots\dots\dots\dots\dots\dots\dots\dots\dots\dots\dots\dots\dots\dots\dots\dots\dots\dots\dots \text{(4.3)}$$

Where,

V_{net} = net aggradation or degradation volume per year in cubic meters,
N_y = difference between two survey periods in years,
V_a = aggradation volume in a cell,

V_d = degradation volume in a cell,

n = total number of aggradation cells and

m = total number of degradation cells.

A positive value of V_{net} will indicate overall aggradation in the reach. Similarly, a negative value will indicate net degradation in the reach. To calculate the depths in each cell the old bed elevations (1999) were subtracted from the simulated bed levels. The net volume change was calculated by using the equation (4.3).

It is obvious that simulated bathymetry will never be exactly the same as the observed bathymetry but it should at least show a similar trend and the overall volume balance should also be similar to the observed one. Tuning of the dimensionless reference shear stress as a calibration parameter and performing the calibration (visual matching, thalweg elevation matching and volume balancing) to obtain a good match between observed and simulated bed is a tedious task. As mentioned earlier visual matching was a qualitative method so much emphasis was given to thalweg matching and volume balancing. When the results obtained from these two methods showed close match with the observed results, then the model was considered to be calibrated model and used for gravel extraction scenario simulation.

4.7 Identification of Aggradation and Degradation Zones

Aggradation and degradation zone identification can be done by direct comparison of two bathymetric surveys. The volume change in each model cell was calculated by taking the difference between two cells and multiplying it by the cell area. This volume may be negative or positive. The net volume was calculated over a certain length along the river. Some researchers have averaged it over a kilometer length (Ham, 2005a and McLean et al., 1999a). As a result, the net simulated volume was calculated approximately over one km length unit starting from Sumas Mountain to Agassiz-Rosedale Bridge. A 2-D map can be prepared to present these aggradation and degradation zones.

4.8 Gravel Extraction Scenario Simulation (Scaled Dynamic Simulation)

Land and Water BC (LWBC) identified potential gravel removal sites for the time frame 2003-2008 (KWL, 2003). Most of the proposed potential gravel extraction sites were located within the study area (Agassiz to Sumas Mountain). DFO approval is mandatory to finalize any of these removal site locations without adversely impact the existing aquatic habitat in this reach. Some DFO approved design drawings were obtained in Fall, 2005 (KWL, 2003, nhc2004) and a strategy was set to incorporate these removal sites into the sediment transport and morphological model. The objective was a series of morphological simulations performed to predict the potential morphological changes with the proposed removal plan. These results are important to determine the effectiveness of the removal plan and the possible future morphological changes after the removal.

Most of the removal operations were started after 2003. As a result, the morphological change has to be detected from 2003 and onward. A new bathymetry was prepared with 2003 survey data for this purpose. It was assumed that the 1999 hydrodynamic calibration would still be valid and applicable for the 2003 model. It was not possible to set the actual volume removal nor the exact irregular shape area in the model because the model grid size cannot be changed. However, the approximate equivalent area and the removal elevations could be set exactly into the model. Removal elevations for all the sites were determined from the DFO supplied gravel removal design drawings (Busto, 2005). All these elevations were set in the model bathymetry. To do so, the 2003 bathymetry was edited and the bed elevation levels were set at the ultimate extraction elevations (river bed elevation after removal) for those selected extraction locations. This new adopted bathymetry was set as an initial bed for the morphological model simulation.

The morphological changes were determined for each year. The simulated bed after one year was set as an initial bed for the next year's simulation. The second year bed was set for the third year simulation and so on up to 10 years. To simulate 10 years of change "average" flow conditions were assumed. A flow duration curve was developed for the entire daily discharge record at Hope (Table 4.7) to provide the proportion of the flow for each discharge interval. For

124

example, daily flows between 9,501-10,500 m³/s occur an average 0.525% of the time. Over 10 years this is assumed equivalent to 19.2 days of transport at a discharge of 10,000 m³/s.

Table 4.7: Discharges and their corresponding frequency of occurrence over a year's time.

Discharge -Range	Average Interval Values	Frequency	P	P	No. of days/10 yr.
(m³/s)	(m³/s)	(days)	(%)	(-)	(days)
14501-15500	**15000**	2	0.006	0.000	-
13501-14500	**14000**	4	0.012	0.000	-
12501-13500	**13000**	5	0.015	0.000	0.6
11501-12500	**12000**	20	0.061	0.001	2.5
10501-11500	**11000**	64	0.195	0.002	10
9501-10500	**10000**	172	0.525	0.005	20
8501-9500	**9000**	352	1.074	0.011	40
7501-8500	**8000**	787	2.401	0.024	90
6501-7500	**7000**	1433	4.371	0.044	160
5501-6500	**6000**	1790	5.460	0.055	200
4501-5500	**5000**	2065	6.299	0.063	230
3501-4500	**4000**	2446	7.461	0.075	270
2501-3500	3000	3827	11.674	0.117	-
1501-2500	2000	6022	18.369	0.184	-
501-1500	1000	13581	41.427	0.414	-
<500	500	213	0.650	0.006	-
Total =		32783	100	1	

A full 10-year hydrodynamic simulation would require an unreasonable amount of CPU time. Based on Courant stability conditions, and for the grid size and water depth, we can expect that a dynamic time step of 5 seconds may be required. We cannot easily run a dynamic simulation that will require half a millions time steps. To reduce this CPU time an advanced technique called "scaled dynamic simulation" was applied in MIKE 21C model. A scale factor 100 with this 5 seconds hydrodynamic time step can significantly reduce the total simulation time step to 25,000. The scaled dynamic time means that the HD engine will use a specified HD time step, and then the results will be scaled by a factor before being applied in the sediment transport and morphological calculations. This permits a much longer time step, however any

hydrodynamic response in the system will behave as if the simulation is being run at the HD time step. This technique is applicable only if the discharge is constant over a long period.

Generally, morphological time scales are much longer than the hydrodynamic time scales. If considering only a hydrodynamic simulation, without morphological change, it can be considered as a steady-state problem. If there is any morphological change then by definition the simulation will be unsteady even though discharge is constant. However, for practical simulation, a scale factor can be used (DHI, 2002a). In this work a scale factor of 100 was used for all solutions, which means that the wave celerity across the model has to be considered.

A set of visual maps of year-by-year simulations with new bed level and corresponding depth changes was prepared. In the case of small bed level changes, it could be very difficult to determine the changes visually from one year to the next. To determine the exact amount of change from the 2003 bed to the simulated bed a spreadsheet analysis was performed. From this analysis future aggradation or degradation for each removal sites was determined over the years. The analysis was as follows:

Bedlevel changes without gravel removal (in m) = Simulated bed elevation without gravel removal – 2003 bed elevation ……………………………………………...………… (4.5)

Bedlevel changes with gravel removal (in m) = Simulated bed elevation after gravel removal - 2003 bed elevation after gravel removal…...…………………………………………… (4.6)

An approximate recovery time was determined for each removal site. The recovery time was basically how much time in needed to recover the bed to its original state after gravel removal from a site. As the maximum simulation period was up to ten years, if the bed does not recover to its original state within this time the recovery time was considered to be more than 10 years. After gravel extraction, the channel shape may change due to bank erosion or gravel deposition on the bank or submerged bar top inside the channel. A few cross-sections upstream and downstream of each removal site were extracted from the simulated bathymetry and

compared with the original 2003 cross-section shape. Therefore, morphological changes such as bankline shift or bed aggradation/degradation in a section of the channel may be determined.

4.9 Hydrodynamic Simulation of Flood Profiles after Gravel Extraction

Two hydrodynamic simulations were carried out separately with the original 70 km long model to see how gravel removal affects the design flood surface profile along the Lower Fraser River gravel reach. Lower Fraser River design flood level is the water surface profile with 17,000 m^3/s discharge at Hope plus 0.6 m free board. No free board was added in the simulation results because we want to compare the true water levels in the river. The first simulation was conducted with the existing 2003 survey bed and the second simulation was with the 2003 bed after gravel extraction. A new bathymetry was prepared from the 2003 survey data for the entire 70 km length. The upstream bathymetry from Herrling Island to Laidlaw remained the same because no new survey was done for that area in 2003 and it was assumed that there were not much morphological changes occurring in this area from 1999 to 2003. The design discharge at Hope and corresponding water level at Mission were set in the model and the model was run for 5 days to obtain a steady state water level. Two water surface profiles were extracted from those models and plotted on the same figure to compare them. The difference between two water surface elevations was also plotted in the same figure. Zero difference will indicate no change and positive and negative difference will indicate increased and decreased flood profile levels, respectively.

5 RESULTS AND DISCUSSION

5.1 Hydrodynamic Model Calibration and Verification Results

5.1.1 Sensitivity Analysis of Model Parameters

By trial, it has been found that larger time step ranges between 10 and 20 seconds were suitable for high flow simulation and smaller time steps 5 to 10 seconds, for lower discharge simulation. Model simulation with lower discharges faces severe numerical instability problems when the hydrodynamic (HD) time step is greater than 10 seconds, and showed good stability with a value of less than 6 seconds. A large range of discharge will be simulated in the model so a smaller time step was preferable to cover the whole range of flows. The hydrodynamic time step 5 second was used for the MIKE 21C hydrodynamic model calibration and simulation. This smaller time step guaranteed the numerical stability, however more CPU time was required. In River2D, the initial time step was assigned as 5 seconds and the model itself readjust to larger time steps while simulation is in progress.

For large rivers, the value of the roughness coefficient Manning-Strickler "N" typically ranges from 30 to 50 (n = 0.033 to 0.020). The sensitivity to water level is demonstrated at the Agassiz-Rosedale Bridge (Gauge #22) in Table 5.1.

Table 5.1: Simulated and corresponding observed water levels with different Manning-Strickler "N" values at Agassiz-Rosedale Bridge (Gauge #22) with a discharge 11,000 m^3/s at Hope.

Manning's-Strickler N	Manning's n	Observed WL	Simulated WL	Difference
(-)	(-)	(m Geodetic)	(m Geodetic)	(m)
30	0.033	17.00	17.51	0.51
35	0.029	17.00	17.47	0.47
40	0.025	17.00	17.43	0.43
45	0.022	17.00	17.28	0.28
50	0.020	17.00	17.11	0.11

About 0.4 m water surface elevation variation was associated with Manning-Strickler "N" values over the range from 30 to 50. The bed roughness coefficient is the most sensitive

model parameter and must be determined from the calibration.

Typical values of the eddy viscosity coefficient in MIKE 21C hydrodynamic and morphological model applications range between 0.5 and 10 m^2/s based on river gradients and grid sizes. Water levels and horizontal and lateral velocities were observed in a model cell with different eddy viscosities for a constant bed roughness values (Manning-Strickler value, $N = 40$). A grid cell near Carey point (Gauge # 39 in Figure 4.9) was selected for this test. The main reason was water level near Carey point showed a close match to the observed values with this preliminary Manning-Strickler value and 11,000 m^3/s discharge at Hope (Table 5.2).

Table 5.2: Simulated water levels and velocities with different eddy viscosity coefficient E, near Carey Point with a discharge at Hope 11,000 m^3/s and a constant Manning-Strickler "N" = 40.

E (m²/s)	Simulated WL-EL (m Geodetic)	Observed WL (m Geodetic)	WL difference (m)	Simulated U_x (m/s)	Simulated U_y (m/s)
0.5	13.21	13.42	-0.21	0.54	0.56
1	13.21	13.42	-0.21	0.54	0.56
5	13.23	13.42	-0.19	0.58	0.83
10	13.24	13.42	-0.18	0.84	0.91
20	13.25	13.42	-0.15	0.90	0.99

The simulated water level does not match accurately the observed water level because the model was not yet calibrated, but it indicates sensitivity for different eddy viscosity values. The change of simulated water level elevation and velocity was 6 cm and 0.4 m/s, respectively, over following a 40-fold increase in eddy viscosity coefficient (E) values. Very larger values of eddy viscosity (such as 100 m^2/s) cause numerical instability in the model. It is not entirely clear that what has caused the instability. Therefore, a preferable eddy viscosity value will lie within the range 0.5 to 20 m^2/s. The discharges will not be constant for the model application and grid size also will vary along the channel so a smaller value of eddy viscosity could guarantee numerical stability for the whole range of discharge simulation.

The sensitivity analysis together with experience from several tests with MIKE 21C indicates that the eddy viscosity has only a relatively minor influence compared to the bed

resistance. The eddy viscosity influences the flow distribution in a cross section by transferring momentum from areas with a high flow velocity to areas with lower flow velocity. River flow is strongly friction dominated, so the effect of turbulence is fairly small. However, due to the modeling of the river flow, the eddy viscosity will tend to have a stabilizing effect on the solution (DHI, 2002b). The velocity-based formulation of the eddy viscosity in MIKE 21C was used. In sand bed river applications, 1 to 2 m^2/s is a commonly used value for MIKE 21C (DHI, 2002a). Therefore, a conservative value of eddy viscosity, 5 m^2/s, was used for application in the gravel-bed reach for all simulations.

Wetting and drying depths parameter did not show any sensitivity during high flow simulation. However, these parameters showed some sensitivity with flow < 3000 m^3/s. The sediment transport model simulation will be carried out with flow at least 5000 m^3/s, which is the bedload transport threshold. Therefore, the default wetting and drying depths 0.2 m and 0.3m, respectively, were used for the simulation.

5.1.2 Hydrodynamic Model Calibration Results

After running the model with the 23 June, 1999 freshet event (11,000 m^3/s), water level elevations were extracted at specific gauge locations. The simulated water levels were plotted against the observed water levels (see Figure 5.1). Figure 5.1 is somewhat misleading, because most of the water level variation is directly related to the bed elevation. To avoid this problem, water level differences were calculated by subtracting observed water level from simulated water level elevation (Table 5.3).
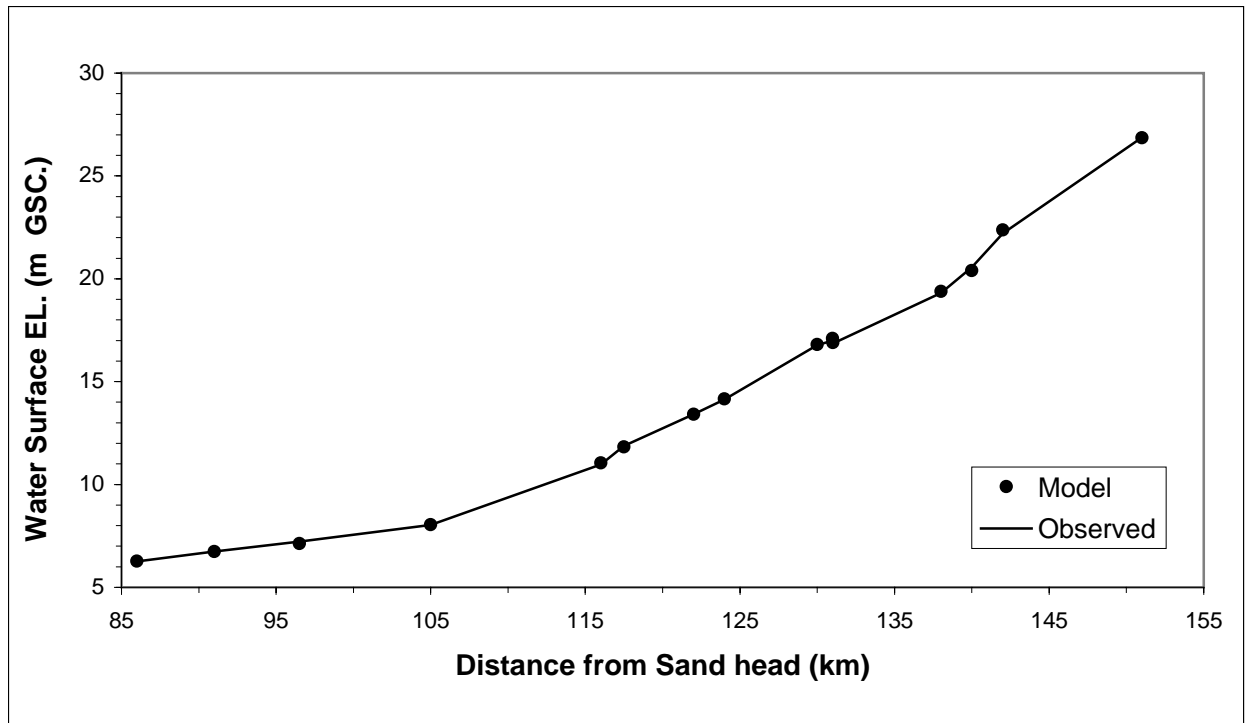
Figure 5.1: Location of gauges used to compare modeled and observed water surface elevations.

Table 5.3: Comparison of model and observed water surface elevations.

Gauge#	Gauge name	UTM (NAD-83) Easting	UTM (NAD-83) Northing	Distance (m GSC)	Model (m GSC)	Observed (m GSC)	Difference (m)
Mission	At Mission railway bridge	550850.90	5441885.49	86	6.28	6.26	0.02
12	Dewdney Pump Station	555515.14	5443361.58	91	6.74	6.75	-0.01
15	Robson Pump Station	560137.92	5444705.24	96.5	7.13	7.22	-0.09
41	Quaamitch Slough	565815.10	5446038.81	105	8.04	8.03	0.01
40	Minto landing area	555356.65	5450551.91	116	11.05	10.97	0.08
Kent # 8	Scowlitz	558085.96	5453444.41	117.5	11.83	11.88	-0.05
39	Carey Point	581543.88	5452039.58	122	13.41	13.42	-0.01
20	Hammersley PS	583390.31	5454396.88	124	14.16	14.13	0.03
Chwk # 2	Chip Intake	587554.10	5450768.03	130	16.81	16.78	0.03
22	Agassiz Rosedale Bridge	589212.55	5450812.53	131	17.10	17.00	0.10
Kent # 5	Agassiz Rosedale Bridge	589160.56	5451288.6	131.01	16.90	16.86	0.04
21	Maria Slough	592145.22	5455771.97	138	19.40	19.31	0.09
44	Herrling Island	596094.00	5455526.00	140	20.39	20.55	-0.16
42	Seabird Island	594160.00	5458600.00	142	22.38	22.20	0.18
43	Johnson Slough	599239.59	5463803.04	151	26.86	26.87	-0.01

131

The target water level elevation difference was ± 0.10 m. Water level differences were within this range except at gauges 42 and 44 (Table 5.3). Gauge 42 showed a maximum difference of 18 cm. This gauge was on the flood plain and near a sharp bend so a water level discrepancy may occur during high flow simulation in such a critical place. Gauge 44 was in a narrow side channel of Herrling Islands beside Highway #1. The exact gauge location was very close to the no flow boundary of the model. As a result, the result extraction was done slightly north from the exact location. Hence, the discrepancy between the observed and modeled values is higher. Water level difference at Gauge 15 near Robson Pump station was –0.09m. The observed value may be affected by the pump station operation at higher Lower Fraser River stage. Whatever the reason, where the water level match showed some discrepancy will remain out of main sediment transport simulation zone (Sumas Mountain to Agassiz Bridge). MIKE 21C model has captured the super-elevation at Agassiz-Rosedale bend. The difference between water surface elevations at this point was 0.14 m, which is close to the result (0.16 m) found by Yusuf (2001). Overall calibration results achieved the targeted difference ± 0.10 m. A spatially varying or distributed Manning's-Strickler "N " in the model domain showed the best calibration results (Figure 5.2).

In River2D, different roughness element heights k_s were set according to Figure 5.3 to achieve a reasonable calibration. For floodplain, k_s value 0.64 (cm) was set. Only 7 water level gauges were available in the short test reach. Water surface elevations are shown in Figure 5.4. The results from River2D and MIKE 21C are compared in Table 5.4.
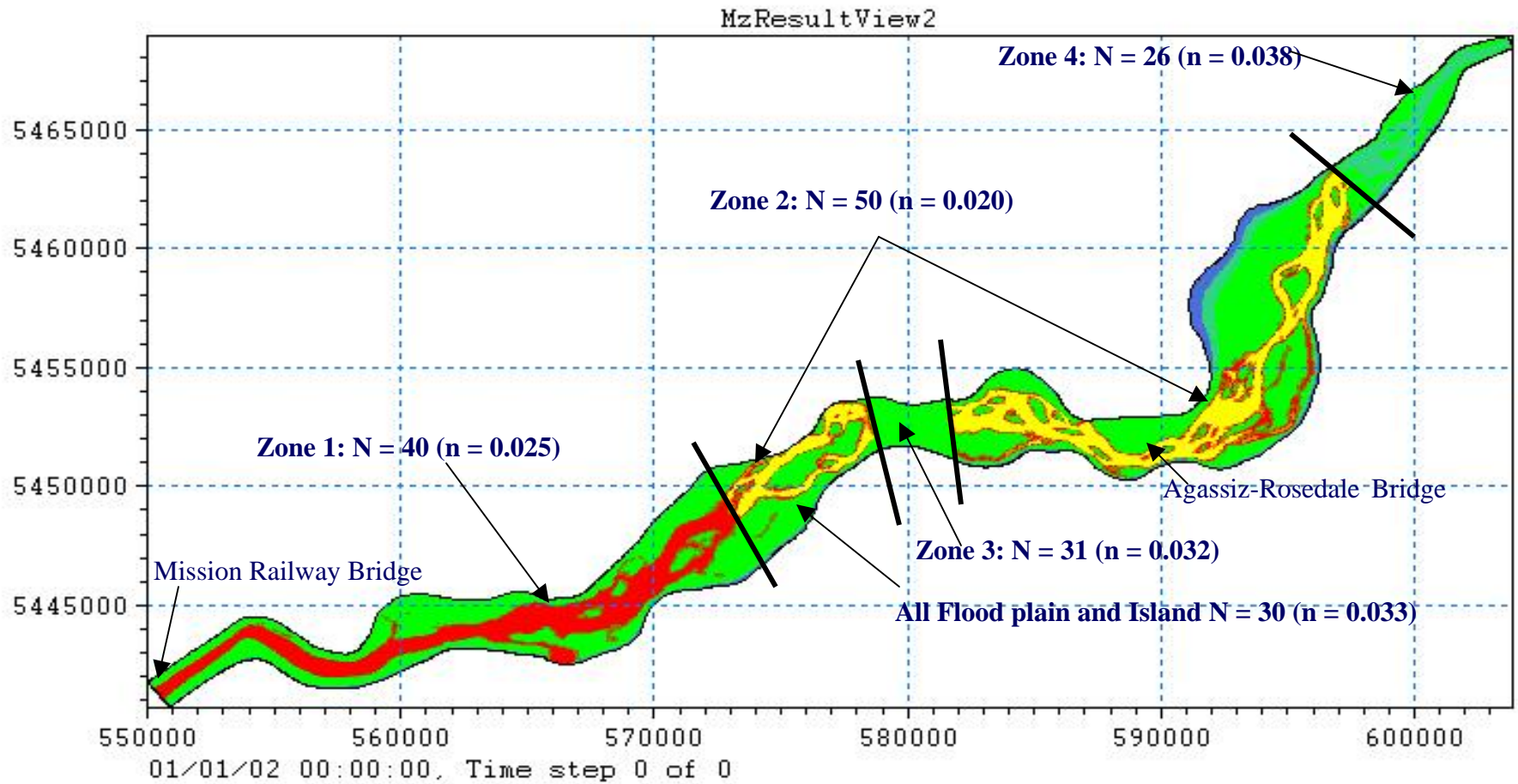
Figure 5.2: Bed roughness Map (Manning Strickler "N" values used for MIKE 21C hydrodynamic model calibration).
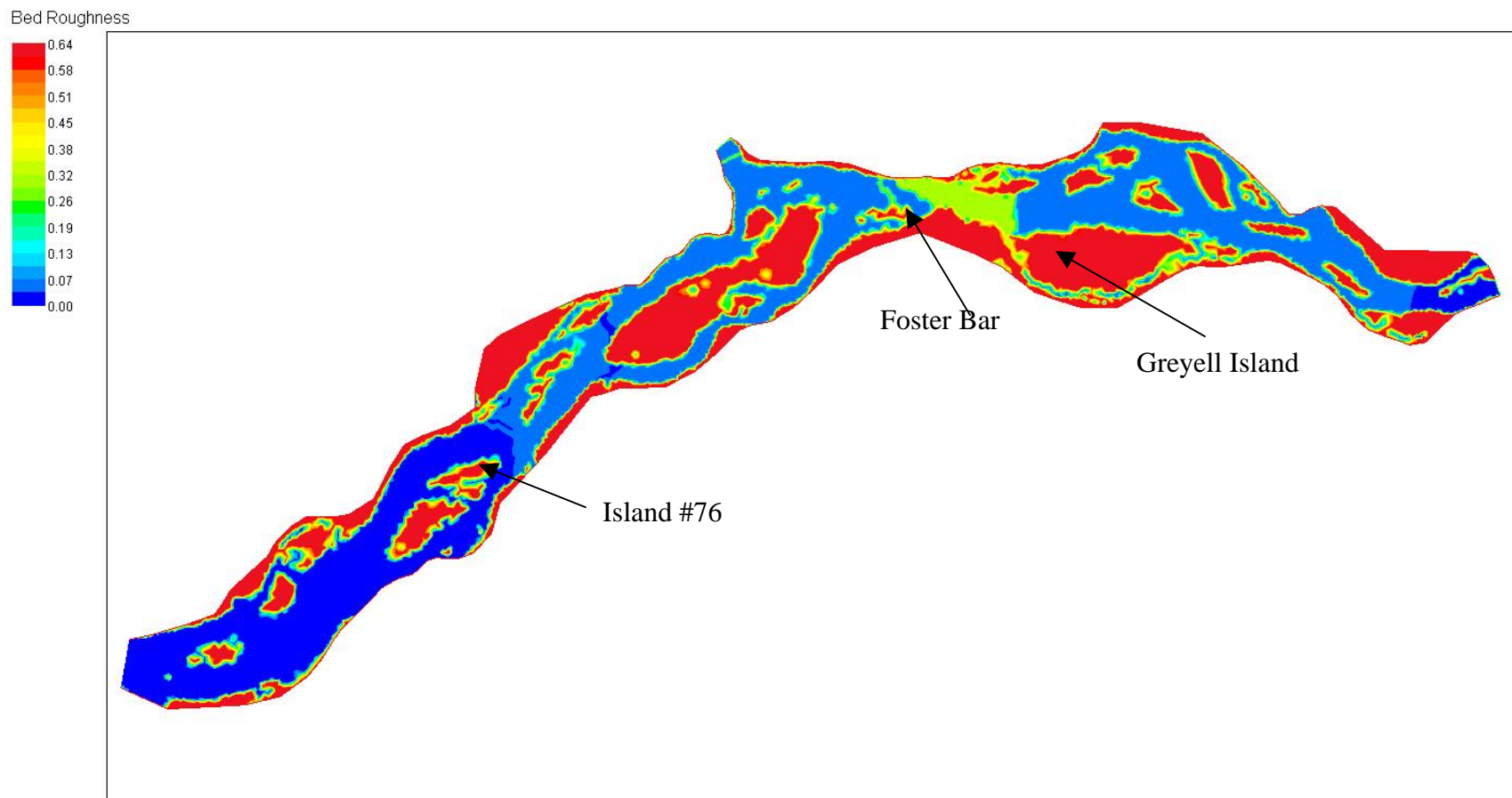
Figure 5.3: Bed roughness Map (Roughness element height "k_s" (cm) values used for River2D hydrodynamic model calibration).
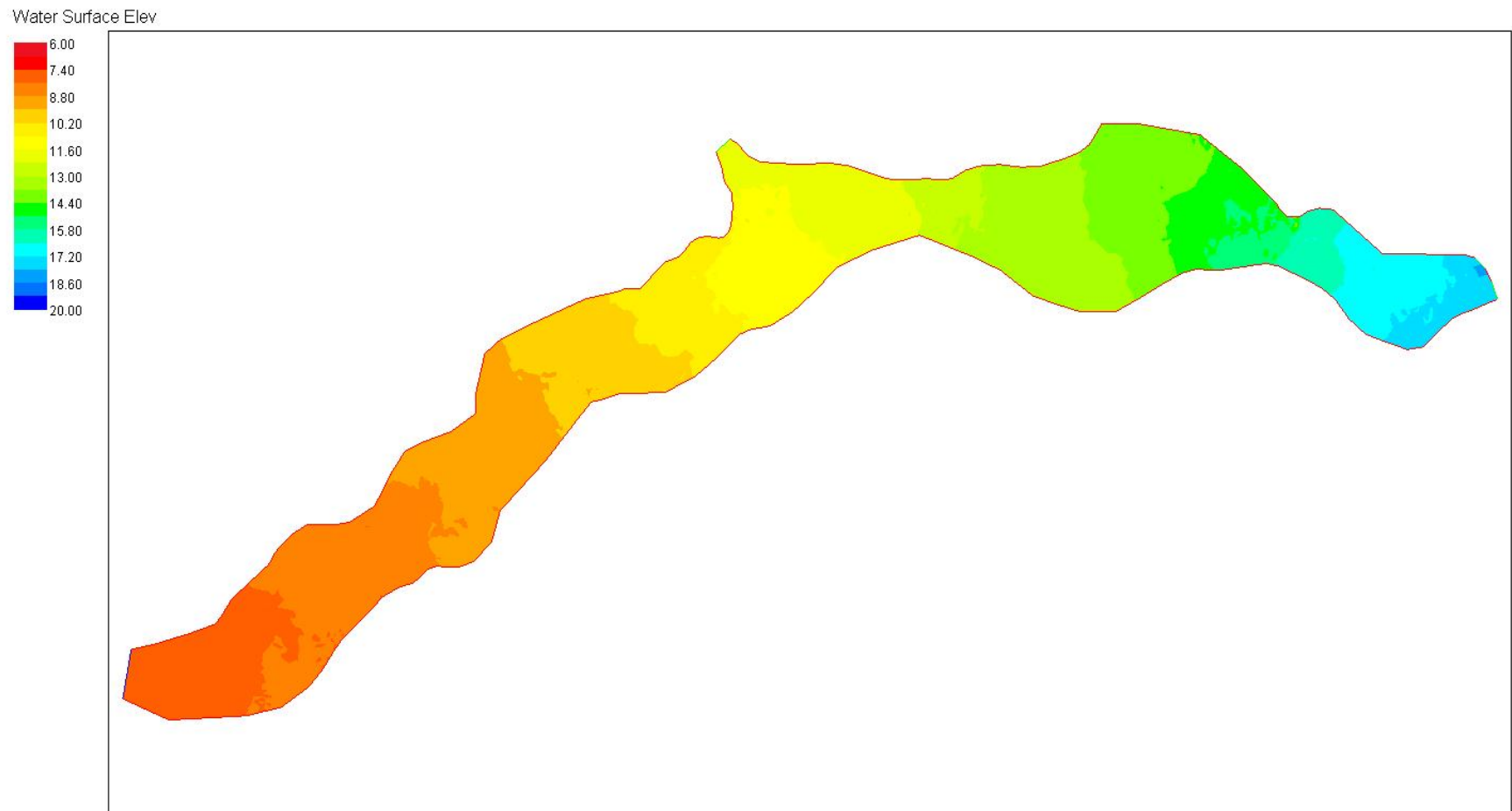
Figure 5.4: Calibrated Water Surface Elevations along the Lower Fraser River in River2D (Agassiz -Sumas Mountain).

Table 5.4: Comparison of River2D and MIKE 21C model water level calibration.

Gauge ID	Gauge Name	Obs. WL. (m Geodetic)	Simulated WL. River 2D Model (m Geodetic)	Difference (Sim.-Obs.) (m)	Simulated WL. MIKE 21C Model (m Geodetic)	Difference (Sim.-Obs.) (m)
41	Quaamitch Slough	8.03	8.04	0.01	8.04	0.01
40	Minto Landing area	10.97	11.06	0.09	11.05	0.08
Kent 8	Scowlitz	11.88	11.91	0.03	11.83	-0.05
39	Carey Point	13.42	13.34	-0.08	13.41	-0.01
Chwk # 2	Chip Intake	16.96	16.87	-0.09	16.81	-0.15
Kent # 5	Agassiz Rosedale Br.	16.86	16.99	0.13	16.90	0.04
22	Agassiz Rosedale Br.	17.00	17.23	0.23	17.10	0.10

Both model calibration results compare well. Even though MIKE 21C uses the Manning roughness coefficient and River2D use roughness element height, both models showed similar pattern in terms of distributed roughness value settings. Three different roughness zones from Agassiz-Rosedale Bridge to Sumas Mountain are visible in Figure 5.2 and Figure 5.3. Both models need higher roughness values between Greyell Island and Foster Bar area. MIKE 21C model showed 4 roughness zones as it covers a larger area than River2D does. In River2D, roughness zone settings can be done more accurately than in MIKE 21C because of the finite element mesh. However, zone setting and refinement is time consuming. In MIKE 21C, zone setting and refinement is much more easier than those operation in River2D due to the sophisticated inbuilt operation options under the tools menu.

5.1.3 Hydrodynamic Model Verification Results

The calibrated MIKE 21C hydrodynamic model was verified against 18 June 2002 peak observed data. The Hope, Harrison and Chilliwack discharges and Mission water level were set as 10,000 m^3/s, 1220 m^3/s, 237 m^3/s and 5.86 m Geodetic, respectively. A fairly good match between observed water levels and simulated water levels was found - within ± 0.20 m (Table 5.5).

Table 5.5: Comparison of model and observed water surface elevations: verification test.

Gauge No.	Location	Observed WS-EL (m)	Model WS-EL (m)	Difference (m)
11	Mission Bridge	5.85	5.88	0.03
12	Dewdney PS	6.29	6.34	0.05
15	Robson PS	6.75	6.76	0.01
41	Quaamich Slough	7.55	7.62	0.07
40	Minto Channel	10.52	10.74	0.18
39	Carey Point	12.9	13.10	0.20
Chk2	Chip Intake.	16.46	16.57	0.11
22	Agassiz-Rosed. Br.	16.6	16.80	0.20
44	Herrling Island	20.07	20.25	0.18
43	Johnson Slough	26.5	26.64	0.14

Gauges 40, 39, 22 and 44 show nearly 20 cm water level discrepancy. Minto channel, Carey Point and Herrling Island gauges are located in side channels. The water levels and flow rates at these locations depend on the total flow and the amount that passes through the adjacent main channels. Therefore, higher discrepancies between observed and simulated water level were expected from these gauges. MIKE 21C has over estimated water level near Gauge 22 due to the sharp bend. However, model performance was verified reasonably well, at least in terms of water levels.

All simulated depth-averaged velocity data from MIKE 21C and River2D models were extracted from specific locations (x, y coordinates) and compared to observed aDcp velocities obtained from Agassiz-Rosedale bend (Figure 5.5A and Figure 5.5B). The mean errors (*ME*) for the velocity comparisons were calculated and are shown in Figures 5.5A and Figure 5.5B. A parameter that indicates the symmetry of the data about the 1:1 line was determined as follows:

$$ME = \frac{\sum_{i}^{N_p}\left(\frac{V_{\text{mod}i} - V_{ADCPi}}{V_{ADCPi}}\right)100\%}{N_p} \dots\dots\dots\dots\dots\dots\dots\dots\dots\dots\dots\dots\dots\dots\dots\dots\dots \text{ (5.1)}$$
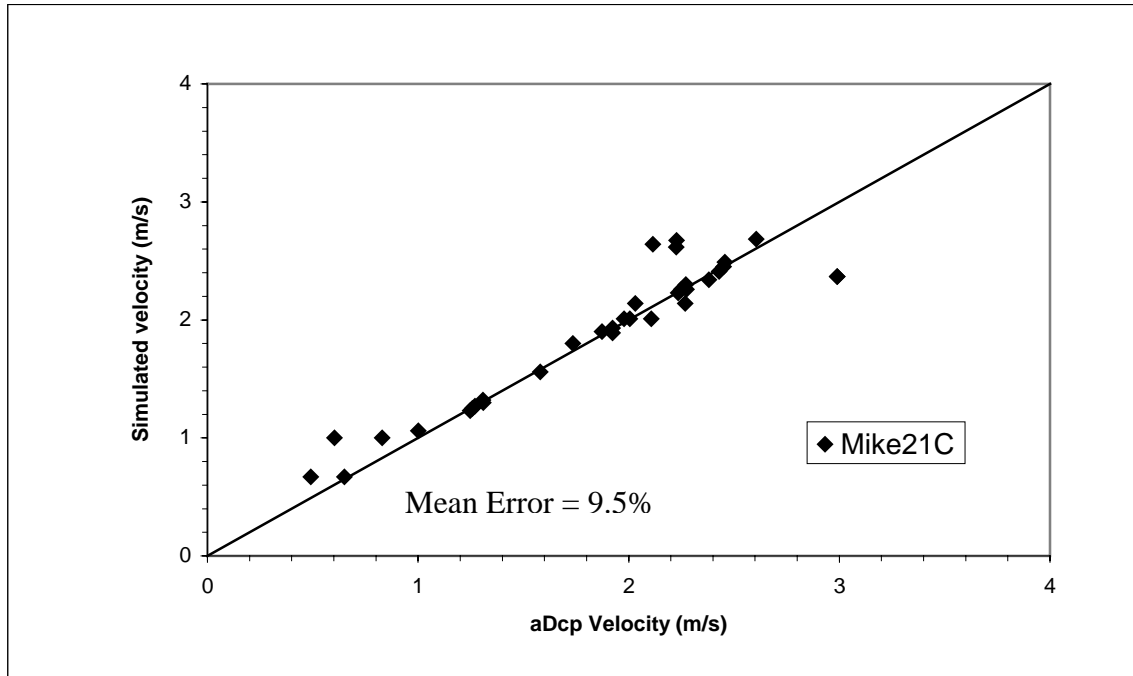
Figure 5.5 (A): Simulated velocity versus aDcp velocity near the Agassiz-Rosedale reach using the calibrated MIKE 21C Model.
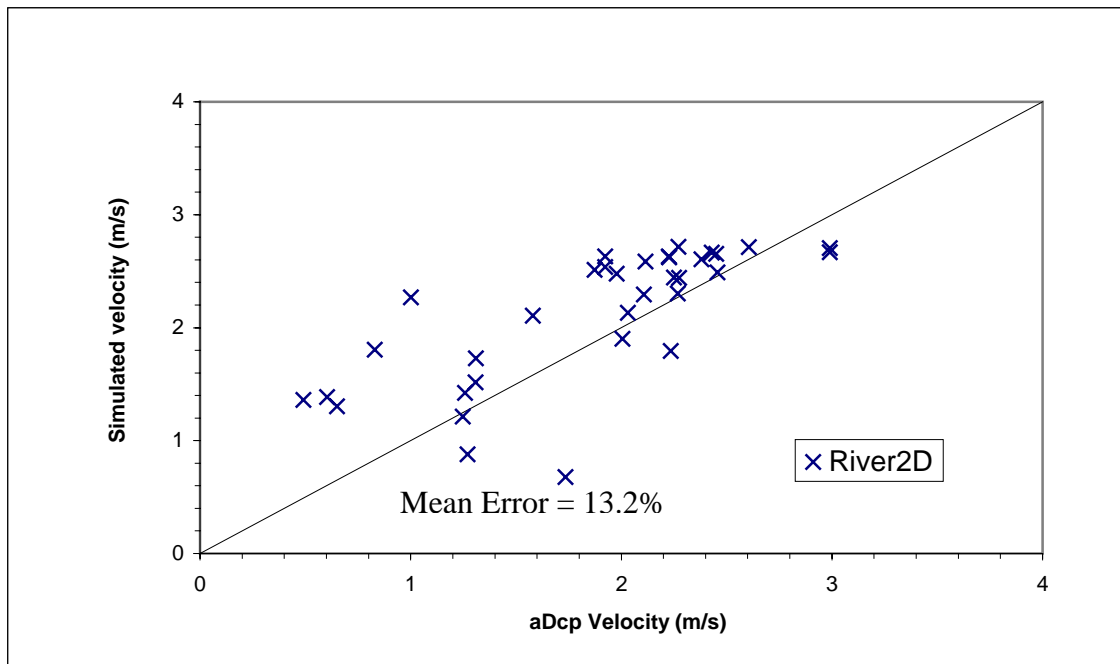

Figure 5.5 (B): Simulated velocity versus aDcp velocity near the Agassiz-Rosedale reach using the calibrated River2D Model.

In the above equation the modeled and aDcp velocities are represented by V_{mod} and V_{ADCP}, respectively and N_P is the total number of points included in the calculation.

From Figure 5.5 it is clear that the simulated velocities with MIKE 21C showed somewhat better agreement than the velocities from River2D. The MIKE 21C velocity was extracted from a larger grid cell as compared to River2D's small finite element cell. It should be mentioned here that for this comparison, only aDcp velocity verticals in the main channel were used. Actually, observed velocities depend on the instantaneous unsteady discharge during data collection but the simulated discharge was a steady mean daily discharge so some discrepancy may be expected. It is not clear why the MIKE 21C model shows a better result. It might be grid cell size, bed friction factor, or proximity of the upstream boundary to the aDcp data site for River2D, as that model simulates only the Agassiz to Sumas Mountain reach.

5.2 Sediment Transport Simulation

The sediment transport simulation was started with the threshold gravel transport discharge of 5,000 m^3/s. For flows less than 5,000 m^3/s, no significant gravel transport occurs in Lower Fraser River (McLean et al., 1999a). Care has to be taken to identify anomalous cells where large shear stress and large transport rates are indicated, even during low flows. This typically occurs where flow becomes shallow along bars and the edge of exposed gravel bars. This high shear stress is a problem in two-dimensional model application and difficult to control without implementing a shear stress check. To control this problem the code has been modified so that the model will not calculate bedload discharge in a cell when shear stress value exceeds a certain prescribed value. This value was set based on the probable averaged maximum and minimum velocity values that may occur in the Lower Fraser River gravel reach. Even with this control unreasonable high shear stresses were occasionally simulated in shallow water depths and near the bank. These cells are referred to as bad cells. These cells were identified by a two-dimensional bedload discharge vector plot. In a two-dimensional plot, a large, over-shooting vector indicates the bad cells. All these cells were sorted out manually and excluded from the bedload discharge calculation, which is a tedious process. Due to the local high shear stress, the model produced a small bedload discharge when flow was less than 5000 m^3/s. Therefore, it

may be assumed that the threshold water discharge value probably lies between 4000 and 5000 m^3/s in this gravel reach to initiate the bedload discharge.

For each cell bedload transport rates generally increase to a maximum just shortly after the beginning of simulation, and then decrease with time as the bed surface coarsens (Figure 5.6). Bedload transport time-series in two different locations (Agassiz-Rosedale Bridge and Carey Point) along the gravel reach are shown in Figure 5.6. Approximate steady state transport rate for all size fractions was reached generally after 15-18 days or more of model time, which represents a condition of equilibrium transport. Any bedload transport result for a specific discharge was extracted from this equilibrium part.
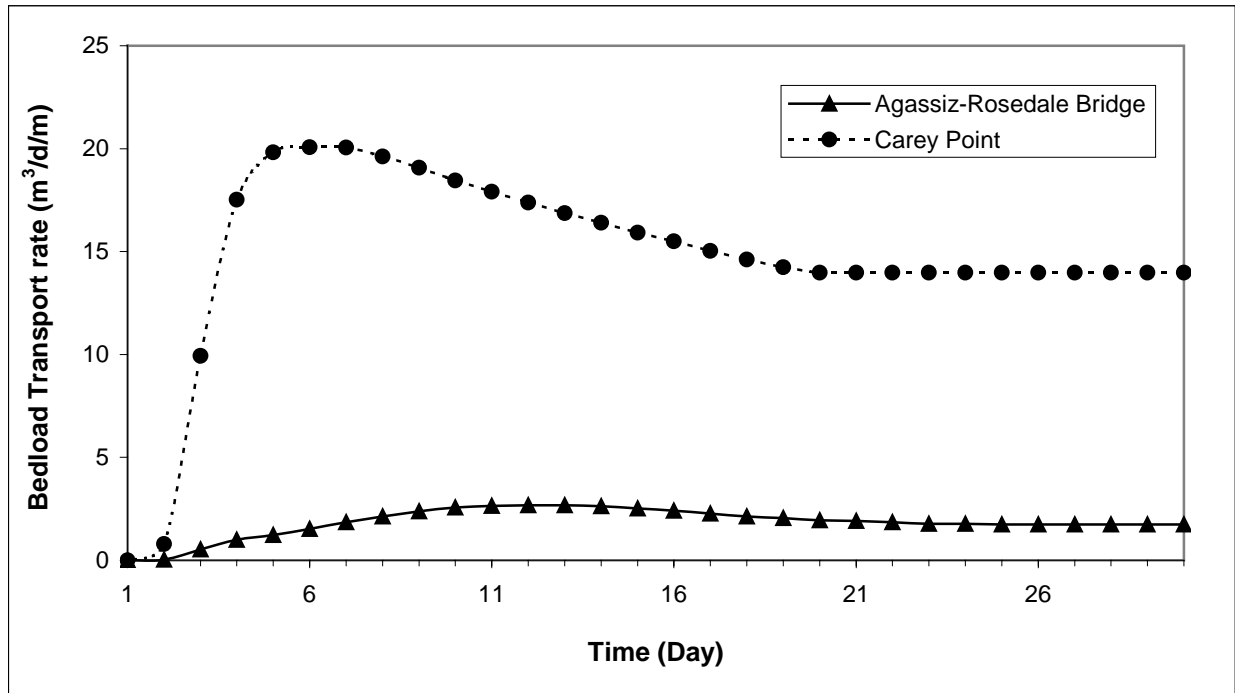
Figure 5.6: Bedload transport rate at Agassiz-Rosedale Bridge and near Cary Point over 30 days simulation period for Q = 8000 m^3/s.

5.3 Bedload Transport Rating Curve at Agassiz-Rosedale Bridge

To validate the model a gravel bedload rating-curve was developed from the model-derived equilibrium transport rates at a cross section at Agassiz-Rosedale Bridge just near the upstream boundary of the sediment transport model (Figure 4.13). The dimensionless reference shear is used as a calibration parameter in the sediment transport model. Parker (1990) used 0.0386 as dimensionless reference shear stress to develop his surface based transport model using data from Oak Creek, Oregon. The Wilcock and Crowe (2003) equation is used here to simulate the bedload transport. It is based on Parker (1990) surface-based relation and might best be described as a modified Parker surface-based transport function.

The resultant bedload rating curve developed using the Wilcock and Crowe (2003) formulation, using the original dimensionless reference shear stress value of 0.0386 is shown in Figure 5.7. Clearly the model is underestimating the transport rate by an order of magnitude or more. Therefore, a dimensionless reference shear stress calibration was necessary. Wilcock and Crowe (2003) showed that dimensionless reference shear stress value could be substantially lower in gravel-bed rivers with higher sand content of the bed, and that the dimensionless reference shear stress of gravel-bed river might as low as 0.020 depending on the percentage of surface sand content in the riverbed (Wilcock and Crowe, 2003).

Trial values of dimensionless reference shear stress as low as 0.020 were used during the calibration procedure and compared to the observed data. A close match with the observed data was achieved with a dimensionless reference shear stress 0.025. As a result, a complete simulation was performed for all discharges starting from 5,000 m^3/s to 10,000 m^3/s. Despite, the scattered nature of field data the computed rating curve passes through the middle of those data (Figure 5.8).

The simple regression equation fitted through the simulated bedload discharge data is as follows:
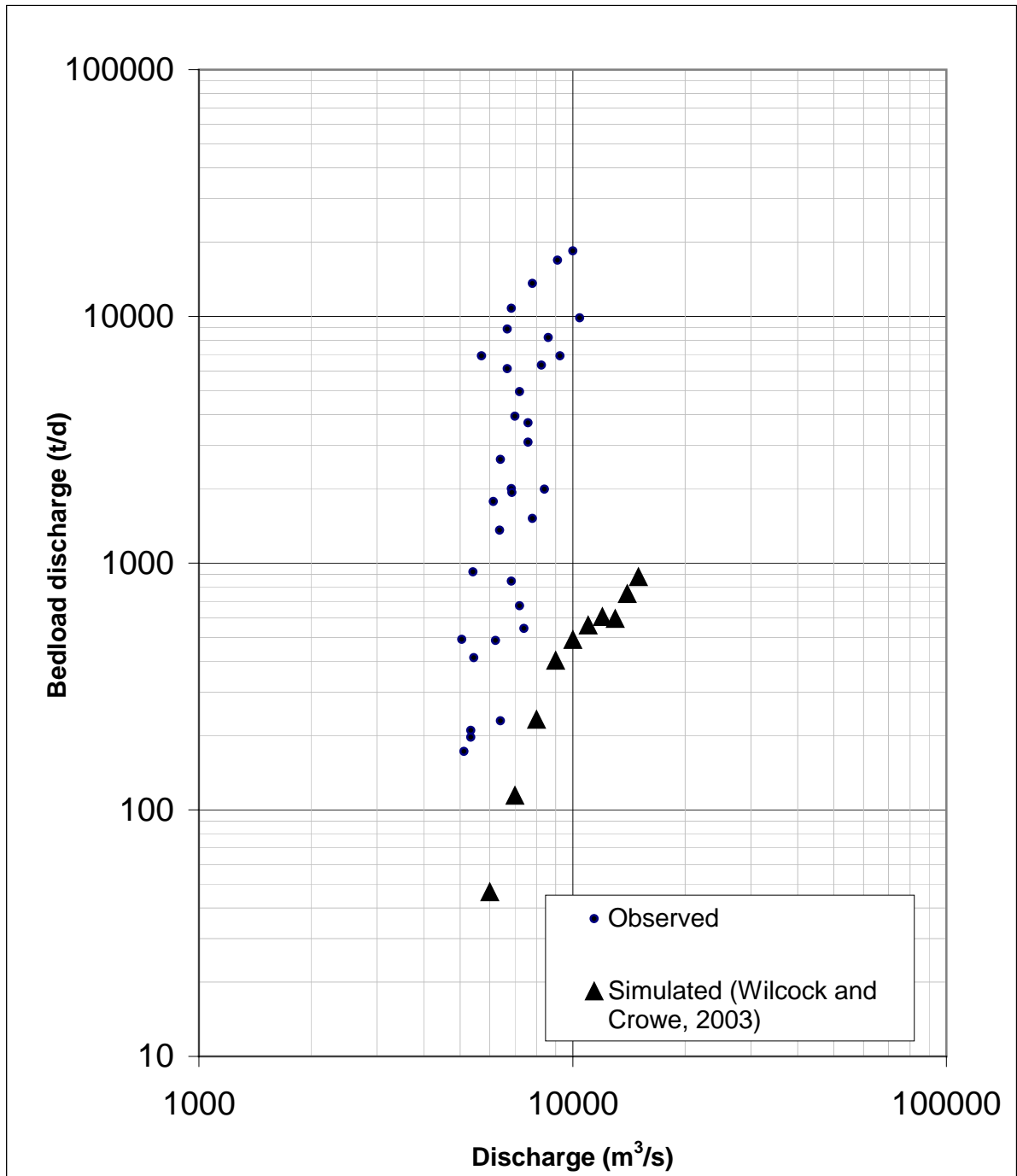
Figure 5.7: The bedload vs. discharge rating curve at Agassiz-Rosedale Bridge calculating using Wilcock and Crowe (2003) equation and a value of $\tau_{ref} = 0.0386$.
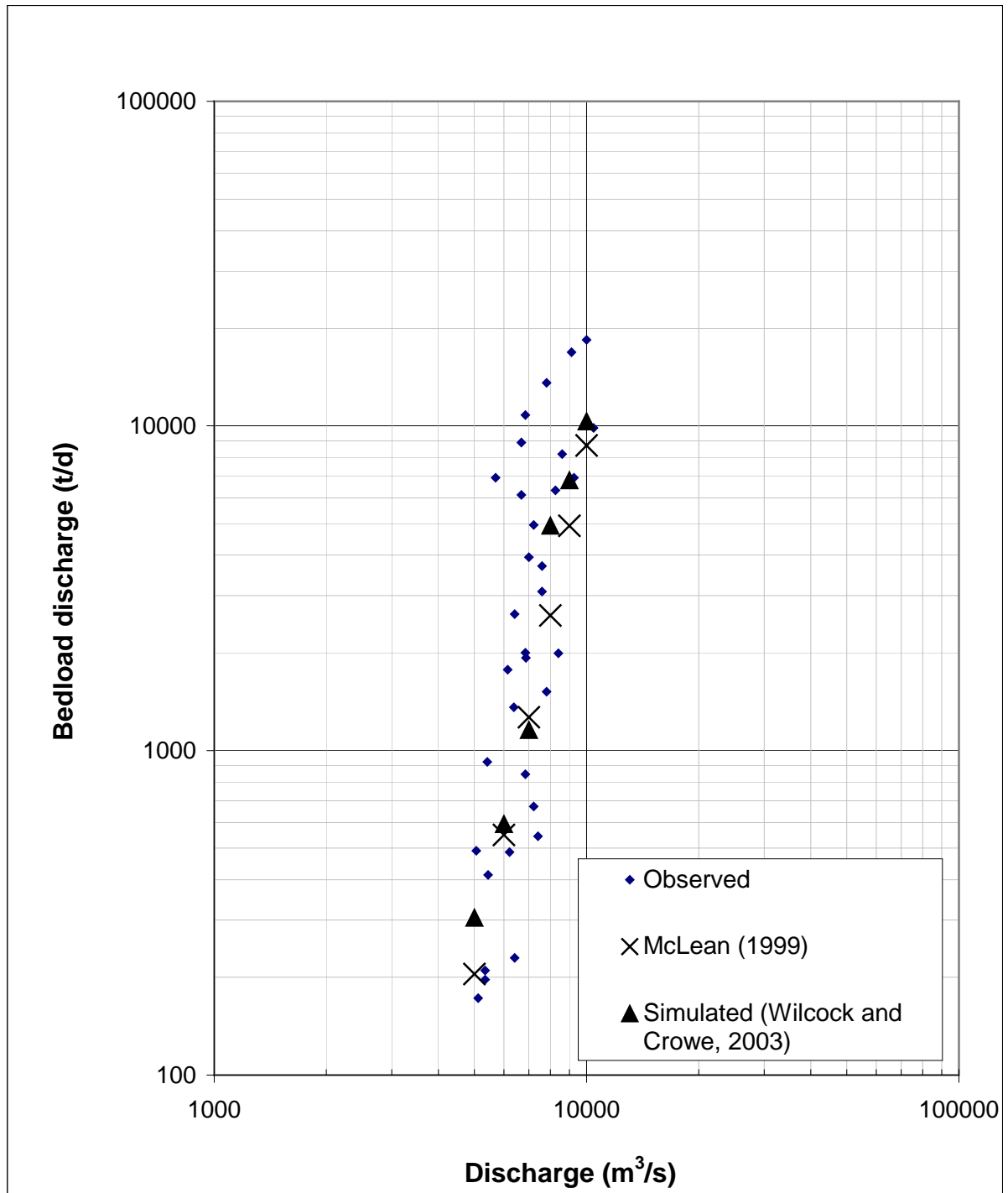
Figure 5.8: The bedload vs. discharge rating curve at Agassiz-Rosedale Bridge calculating using Wilcock and Crowe (2003) equation and a value of $\tau_{ref} = 0.025$.

$$g_b = 4 \times 10^{-18} Q^{5.36}$$ …………………………………………..……….………….………………. (5.2)

This is similar to the previously developed bedload rating curve by McLean et al. (1999).

$$g_b = 2 \times 10^{-18} Q^{5.41}$$ …………………………………………..……….…………………….………. (5.3)

where,

g_b = gravel transport rate (t/d),

Q = discharge (m^3/s),

For comparison, McLean et al. (1999a) line is shown Figure 5.8. This low reference shear stress is consistent with the presence of 10-20% sand in the surface materials. The reason for lower dimensionless reference shear stress was explained in sub-section 2.5 in Chapter 2. A value of τ_c = 0.025 is assumed in all subsequent calculations.

5.4 Computational Gravel Budget

5.4.1 Method 1: Integration of Flow Duration Curve and Bedload Discharge Rating Curve

Method 1 was an integration of flow duration curve and bedload discharge rating curve. In this method, gravel transport capacity was integrated across the channel to provide a cross-sectional total. Raw model output from MIKE 21C has been smoothed by averaging transport rates over five cross-sections immediately upstream and downstream. A gravel bedload rating-curve was developed from the model-derived equilibrium transport rates at a cross section of Agassiz-Rosedale Bridge near the upstream boundary by fitting the Equation 5.1 and coefficients a and b were empirically derived from curve fitting. A flow duration curve was prepared with 89 years (1912-2001) of water flow records at Hope. The probability of each selected discharge event was obtained from the flow duration curve. A mean annual transport rate at Agassiz-Rosedale Bridge was obtained by integrating the flow duration curve with the sediment discharge rating-curve (Equation 5.1) as described in Equation 4.2 (Table 5.6).

Table 5.6: Mean annual gravel influx (t/y) at Agassiz-Rosedale Bridge.

Representative flow for each interval (+/- 500 m^3/s), Q (m^3/s)	Percentage of time in this flow range, P_i (-)	Bedload Transport, g_b (McLean) (t/y)	Bedload Transport, g_b (Model) (t/y)
15000	0.000092	2610	3471
14000	0.000122	2396	3196
13000	0.000122	1605	2147
12000	0.000610	5204	6986
11000	0.001952	10400	14013
10000	0.005246	16690	22580
9000	0.010737	19316	26250
8000	0.024006	22836	31190
7000	0.043710	20191	27735
6000	0.054600	10954	15147
5000	0.062988	4713	6567
Annual gravel transport rate, G_{bT} =		**116,916**	**159,281**

In order to obtain the bedload transport results in t/y, the mean daily bedload discharges were multiplied by the 365.25 and probability of the discharge. Based on this rating curve the analysis found an average annual gravel influx at Agassiz-Rosedale Bridge is 159,000 t/y, which is higher than the McLean and Church (1999) gravel influx estimation based on 20 years observed data (Table 5.6). However, it must be stressed that this gravel influx estimate is highly dependent on the dimensionless reference shear stress (τ_{ref}), which is treated here as a calibration parameter.

The average annual gravel influx obtained from McLean and Church (1999) rating curve was 117,000 t/y. The result based on computational method showed 40,000 t/y more gravel transport than the result based on the empirical rating curve. McLean et al. (1999a) adjusted annual load based on sampler calibration and assigned an error bound of 40% around the annual estimates (Ham, 2005a). The most recent estimation also has shown much higher mean annual gravel influx at Agassiz-Rosedale Bridge (Ham, 2005a). Therefore, a higher mean annual bedload transport rate at Agassiz is expected. There are some discrepancies between observed annual transport rate and computed annual transport rate in individual discharges. Since McLean and Church (1999) obtained their rating curve using the bedload data for maximum

discharge up to 10,000 m^3/s. Annual bedload transport rate for discharges beyond 10,000 m^3/s was calculated by using the rating-curve equation (Equation 5.2).

This method is a statistical method because it depends on flow frequency (probability of occurrence of a discharge event). It basically produces a section averaged bedload discharge at a station that is comparable with one-dimensional model output. However, this method takes into account the cross-sectional distribution over a short distance of length (20-50 m) during integration that could minimize the averaging effect (Li and Millar, 2004). A distributed gravel budget may be produced for the entire reach by applying this technique (Li, Millar and Islam, 2008, Islam and Millar, 2005).

5.4.2 Method 2: Direct Simulation, Visual and Thalweg Comparison, and Volume Balance

In the Result View Editor of MIKE 21C, the bed level changes between 1999 to 2003 for observed and simulated results were visually compared to see if there any similarity between them. Observed and simulated bed level change maps are shown in Figure 5.9 (A) and Figure 5.9 (B). Figure 5.9 (C) shows the change between 2003 simulated and 2003 observed bathymetry [the difference between Figure 5.9 (A) and Figure 5.9 (B)]. There is considerable discrepancy between the two maps. It was expected that the two results would not be matched exactly but may show some similar pattern. There might be several reasons for disagreement between the observed and simulated bathymetry such as simplified flow hydrograph, simplified bathymetry and variable local shear stress in the real time situation. However, a very close visual match could not guarantee that the transport rate would be similar in both cases.

Observed Bedlevel changes (1999-2003)
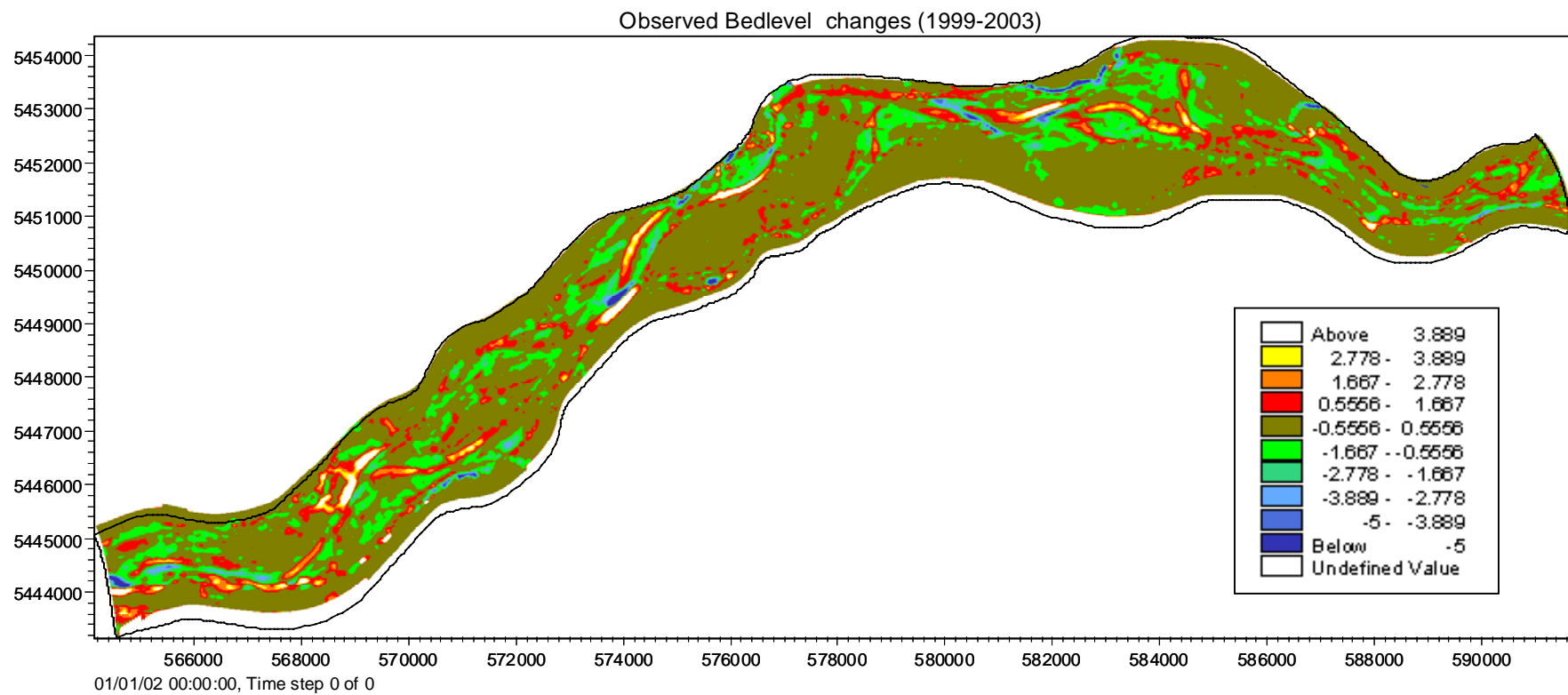
01/01/02 00:00:00, Time step 0 of 0

Figure 5.9 (A): Observed bedlevel changes (in m) from 1999 to 2003 and positive values indicate aggradation. [1999 and 2003 DEM supplied by Darren Ham, Department of Geography, UBC].
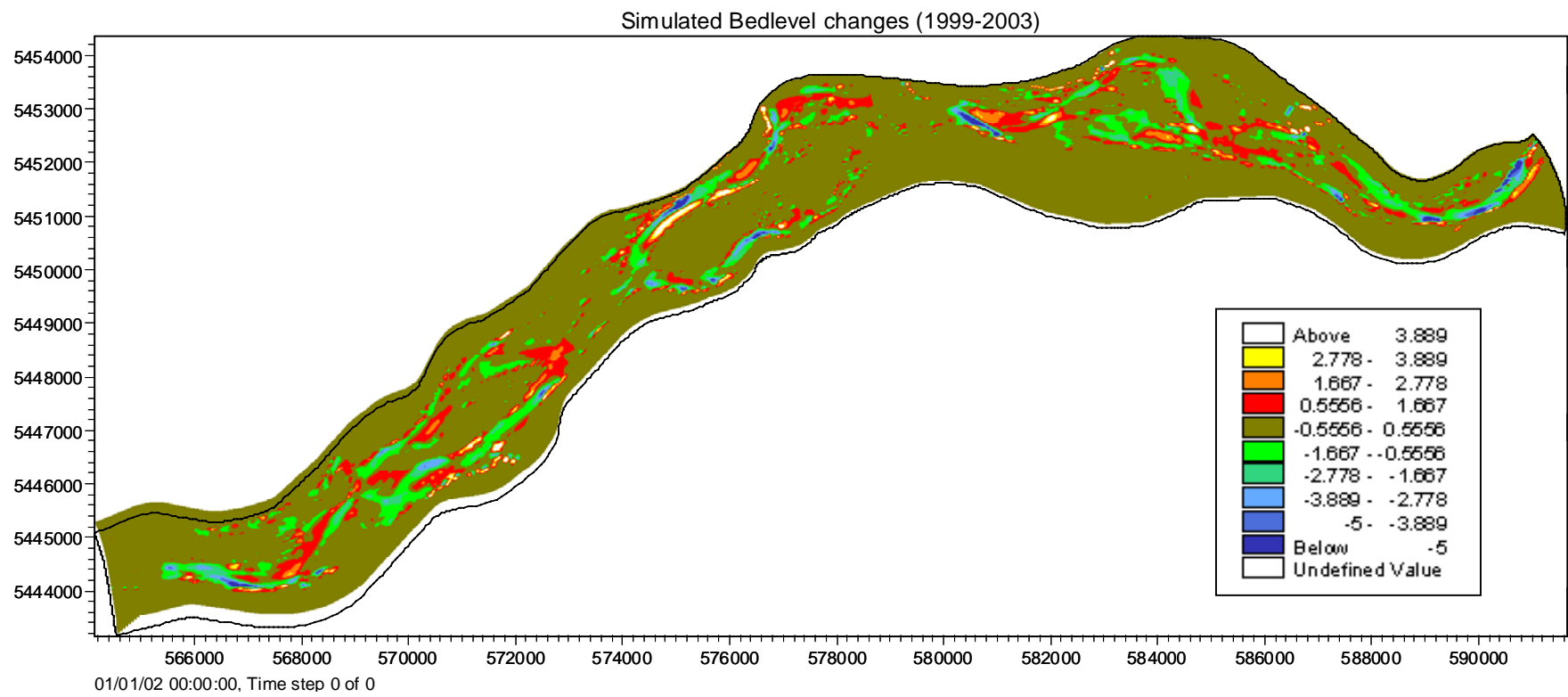
Figure 5.9 (B): Simulated bedlevel changes (in m) from 1999 to 2003 and positive values indicate aggradation.
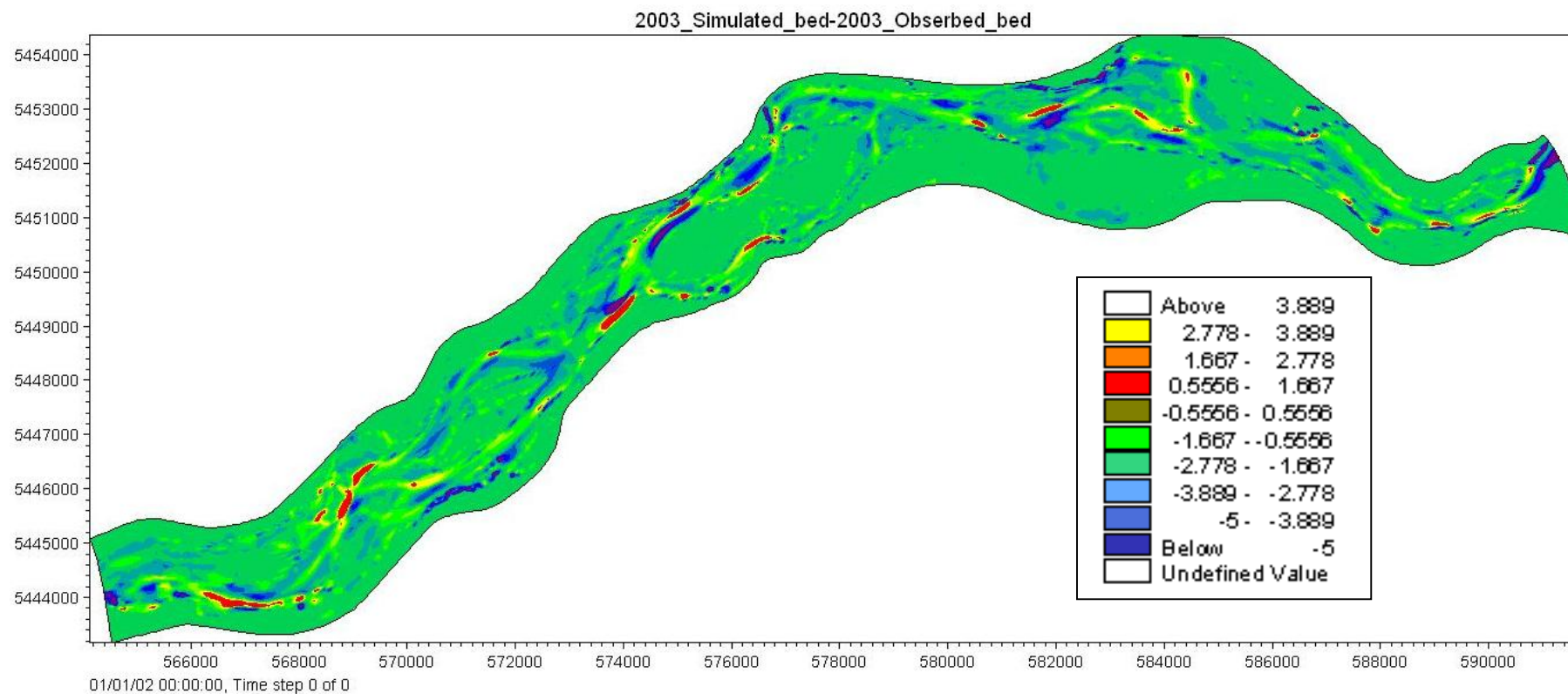
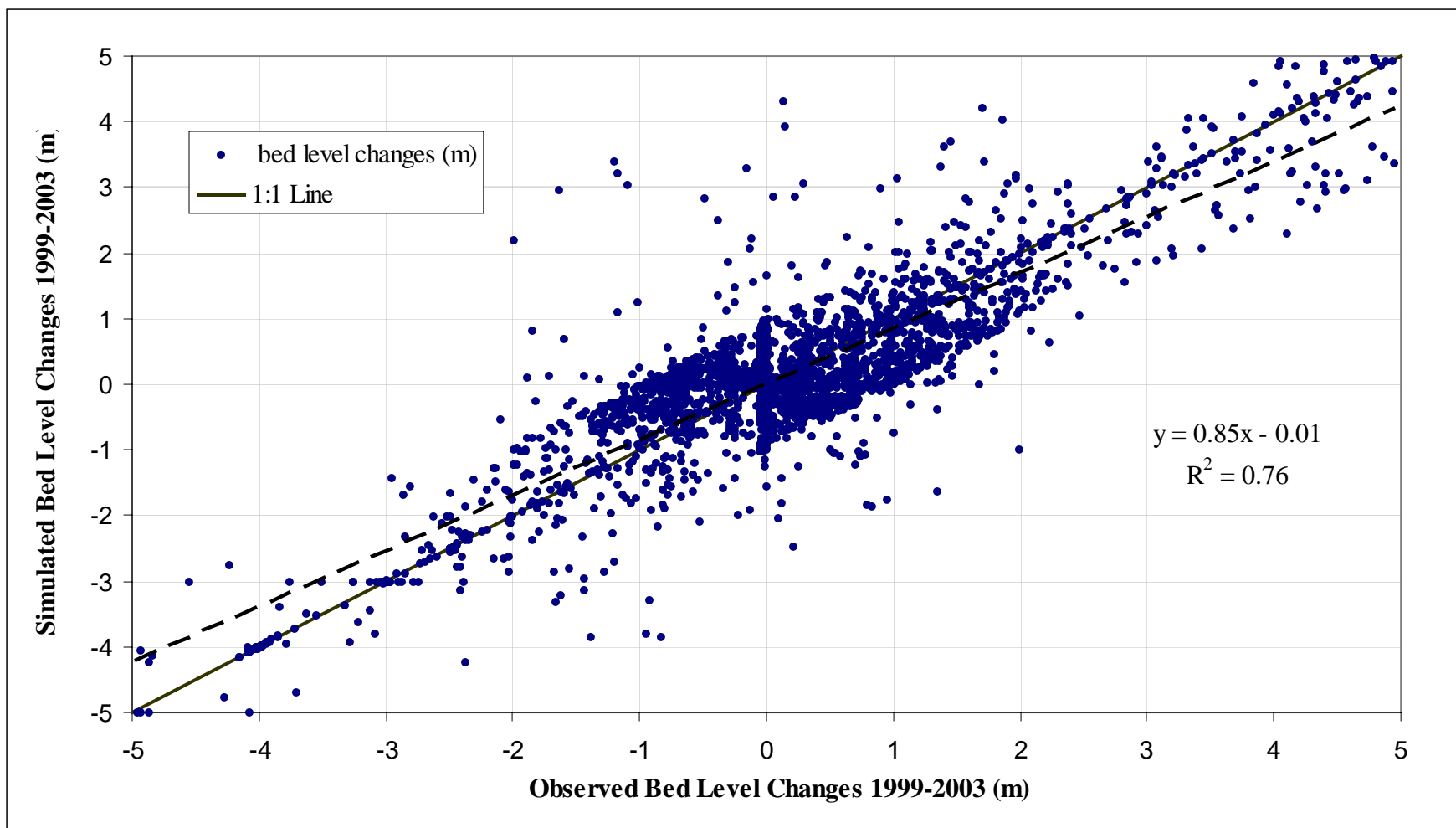Figure 5.9 (C): Showing the difference between Figure 5.9 (A) and Figure 5.9(B) [Change (in m) = 2003 simulated bed - 2003 Observed bed].

Figure 5.9 (D): Showing observed and simulated bed level changes between 1999 and 2003.

The observed bed level changes along the Lower Fraser River gravel reach between 1999 and 2003 was compared with the simulated bed level changes for the same period to verify the performance of MIKE 21C model. Total number of model cells is more than 30,000 including riverbank and floodplains areas which are difficult to plot all together (30,000 x 30,000 data points). To avoid this problem a random sampling along the channel was done. Observed and simulated bed level changes (in m) data were extracted in such a way that entire channel length is covered by the samples without a substantial distance gap between two sampling areas. This data set excluded the floodplain cells those were never inundated during the simulation (called "Permanent Land Cell" in MIKE 21C Model) but inundated bars and floodplains are included. The observed and simulated bed level changes data were plotted and shown in Figure 5.9 (D). Some large outlier values were identified and removed after plotting. A trend line with R^2 value and a 1:1 line are fit through the data points. The root mean square error (RMSE) value is also calculated for the sample data.

The R^2 value for the regression equation is 0.76 and the RMSE is 0.63 m. Approximately 95% of the data points cluster within the $\pm$ 2 m range from the origin (0, 0). The MIKE 21C model predicts the pattern of erosion and deposition over the main active channel area fairly well. Modeled bed level changes may not be accurate near the shoreline, which produce large discrepancy between observed and simulated values. Some unresolved issues in morphological modeling such as over-shooting phenomenon along the riverbank during bedload transport simulation, limitation of the transport equation and inherent chaotic nature of the bar growth in the real river limit the MIKE 21C model's ability to reproduce the similar results as the observed bed level changes as expected. This bed level change statistics is also warned that some degree of manual data sorting and judgment is required prior to perform an average volume balance calculation over a specific reach area using the model output.

Another traditional way of validating simulated bathymetry with the observed bathymetry is thalweg comparison. This technique is often used in one-dimensional morphological model result verification. In a one-dimensional model, thalweg comparison

locations must be selected at the cross-sections. In a two-dimensional model, the thalweg elevations can be extracted from the deepest point of the bathymetry from upstream to downstream. Thalweg comparison was considered as an alternative option to verify the sediment transport and morphological model. Figure 5.10 shows the thalweg along the Lower Fraser River gravel reach with a dotted line. The same cell reference numbers were used to extract the thalweg elevation from the observed and simulated bathymetries. The distance between two thalweg points was calculated from the grid file and the actual distance of each thalweg point was measured from a reference point (km 0 at Sand Heads) near Fraser River mouth at Georgia Strait. Then, a distance versus elevation curve was plotted from Herrling Island (km 133) to Sumas Mountain (km 100) in Figure 5.11.

The simulated thalweg elevations match fairly well with observed thalweg elevations except at a few locations (Figure 5.11). The calculated RMSE value between observed and simulated bed elevations is 0.41 m. It should be noted here that the thalweg match might be very different near the upstream and downstream boundaries as the bed elevations of these sections were modified manually to satisfy the hydrodynamic boundary criterion. The shear stress based sediment transport model works well where velocity and shear stress remain within a reasonable limit. In the edge of the river where velocity may be higher due to the shallow depth of water, causing high shear stress and large transport in that cell that is not realistic at all. These cells can be identified in a spatial velocity plot in the MIKE 21C Result view editor where one velocity vector is shooting off from the cell (not shown in the thesis). During result processing in the spreadsheet analysis, these types of cells were excluded or bed elevation may be chosen from the nearest cell. This was a tedious process but no other alternative was found reliable. The comparison of the elevation changes through the thalweg showed that model simulation works better through the relatively deepest part of the channel where velocity and depths are less erroneous. There are some discrepancies still remaining between the observed and the simulated bed elevation changes. As mentioned earlier, positive depth change and negative depth change represent aggradation and degradation, respectively. Figure 5.11 shows an overall riverbed aggradations between Agassiz-Rosedale Bridge (km 130) and Nicomen Island (km 105), 5 km upstream from the Chilliwack River
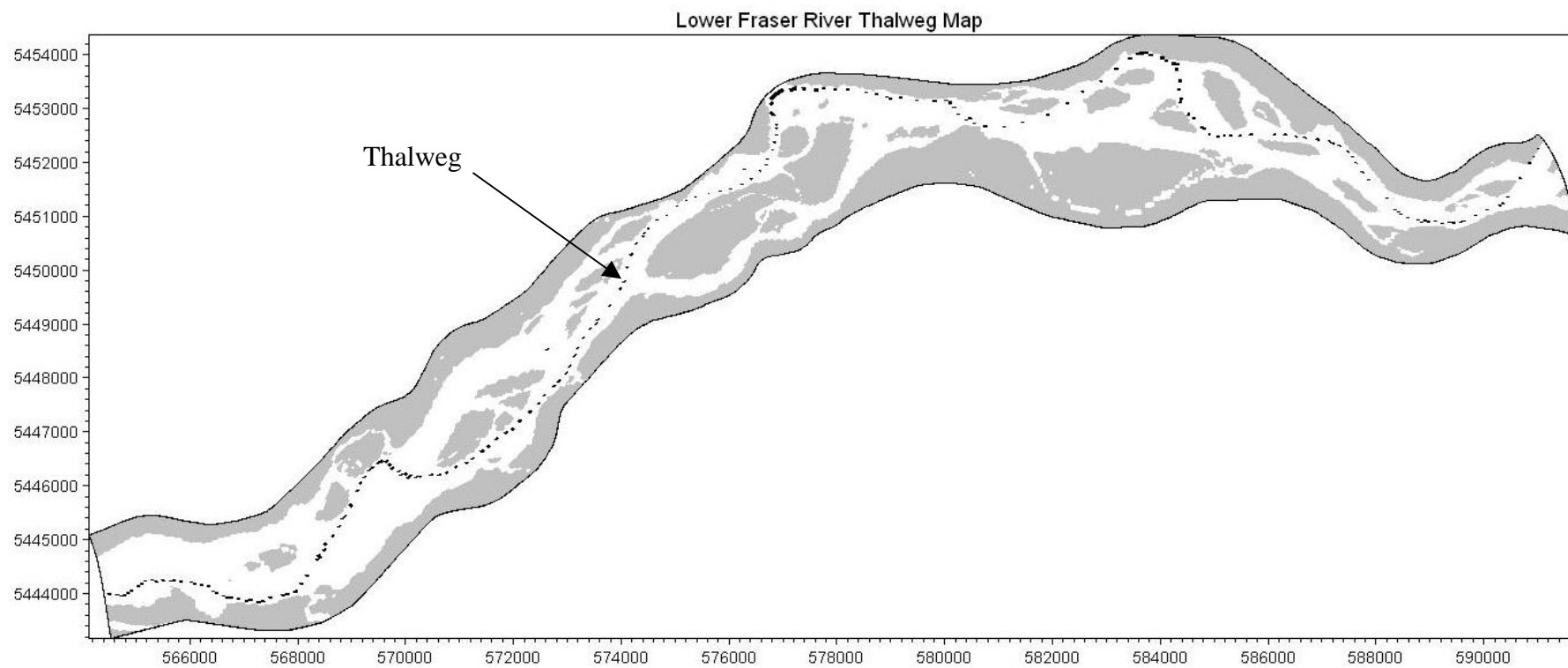
Figure 5.10: Thalweg between Agassiz and Sumas Mountain along the Lower Fraser River has shown with dotted line.
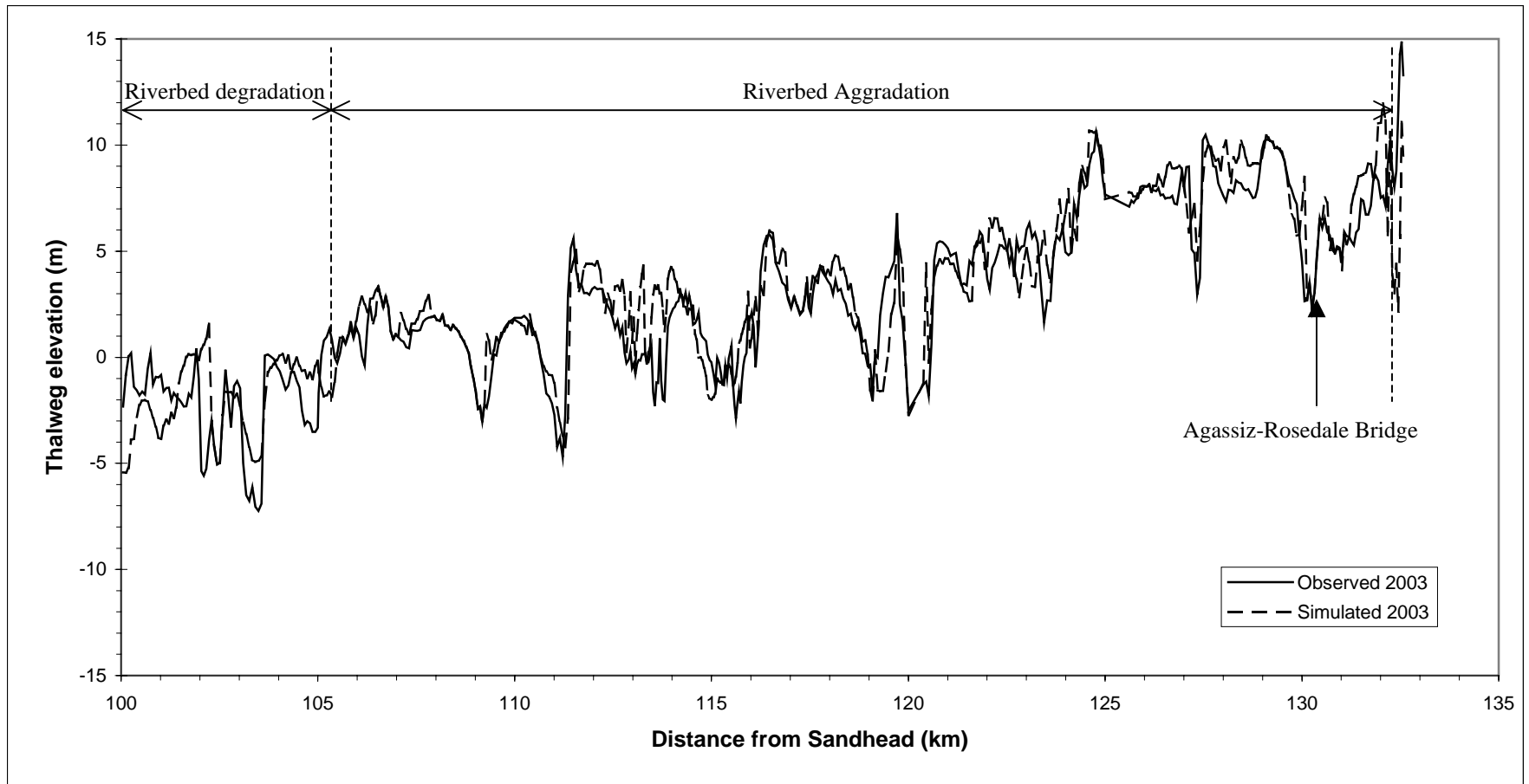
Figure 5.11: Comparison of 2003 observed and simulated thalweg elevation along the Lower Fraser River (Agassiz to Sumas Mountain).

confluence with Lower Fraser River. However a few local degradation zones were found within this 25 km long gravel deposition zone. Similar results were observed using the morphological approach (Ham, 2005a).

The observed and simulated volume changes in each MIKE 21C model cell between 1999 and 2003 were calculated in a spreadsheet. To validate the model and compare the results with the results obtained from the morphological approach (Ham, 2005a), the entire model area was divided into 33 zones. Cell boundaries used in the morphological approach are superimposed on the MIKE 21C model study area shown in Figure 5.12. The approximate length of each area is 1 km and corresponding cell number is similar to the number used in the morphological approach (Ham, 2005a). Cell number 16 starts at the upstream side of the Chilliwack River confluence and cell number 48 ends 3 km upstream of the Agassiz-Rosedale Bridge (Figure 5.12). A total of 33 cells (Cell #16 to # 48) cover the sediment transport model area.

A net volume change was calculated over each 1 km wide area for both observed and simulated cases. It was total volume of deposition minus total volume of erosion over each cell (1 km). These values were plotted against the result obtained from the morphological method (Figure 5.13). Positive values and negative values indicated aggradation and degradation volume respectively. Even though there are some discrepancies among the results, all three results follow a similar trend. The most appropriate comparison is between the values obtained directly from the MIKE 21C observed (Processed in the MIKE 21C Grid) and simulated changes. The results from Ham (2005a) are also shown. Note that Ham (2005a) used different assumptions and different algorithms to process the bathymetric data.
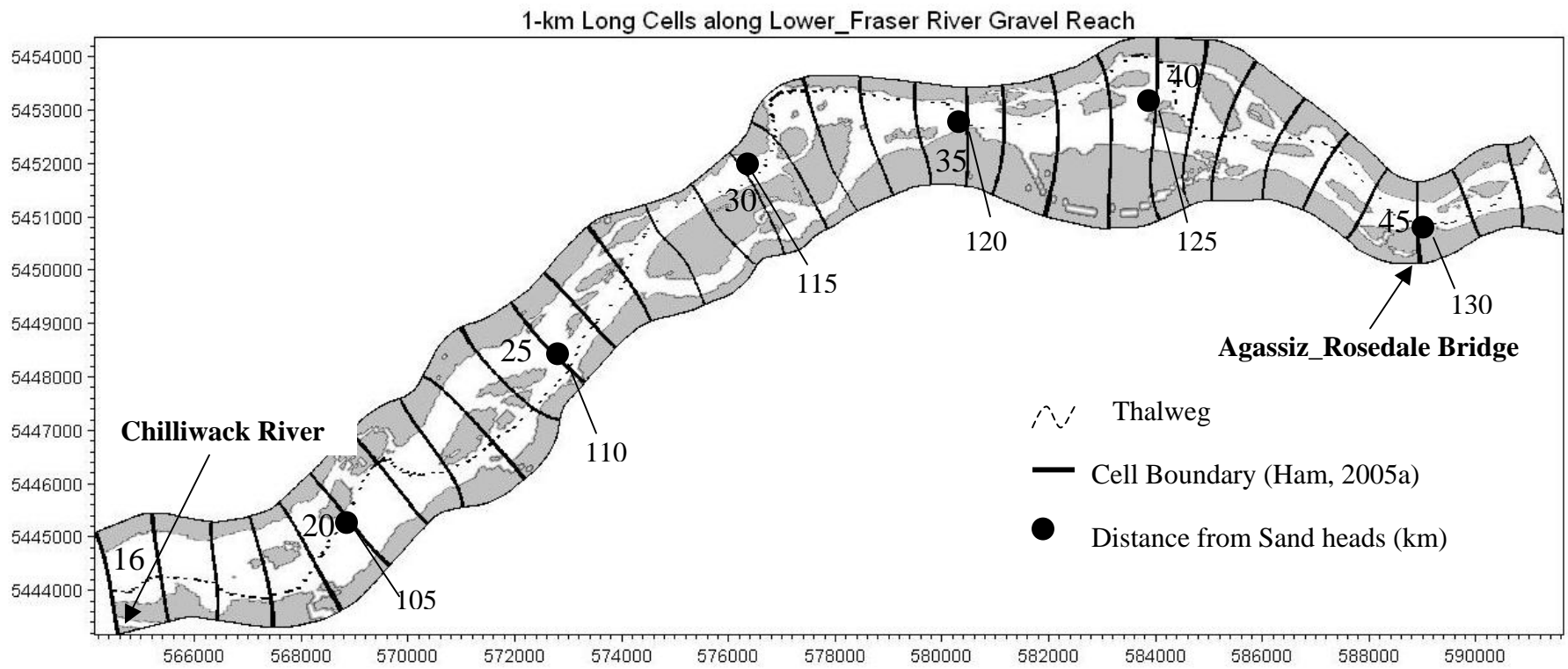
Figure 5.12: Approximate locations of 1-km long cell boundaries (Ham, 2005a) along the Lower Fraser River gravel reach superimposed on MIKE 21C gravel transport simulation model study area (cells 16- 48).
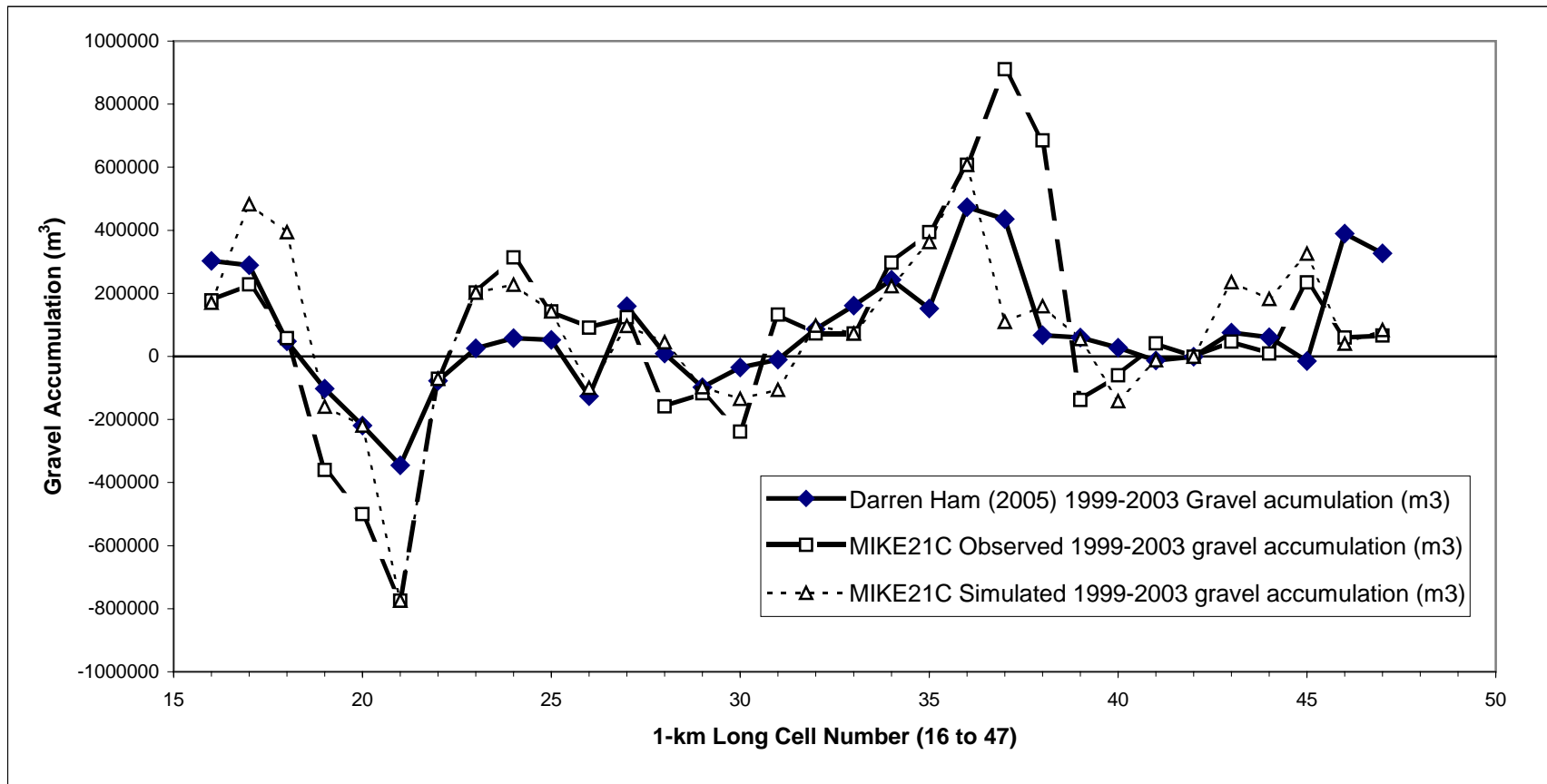
Figure 5.13:Comparison of 1999-2003 observed and simulated gravel transport volume over 1-km long area with the volume obtained from morphological method (Ham, 2005a) for cell #16- #47.

Finally, the net average volume for the entire gravel reach was calculated by the summation of all positive or negative volumes in each cell along the river. The net observed and simulated values (1999-2003) are shown in Table 5.7. The average net volume and volume per year based on the morphological method (Ham, 2005a) are also presented in Table 5.7 for comparison.

Table 5.7: The net observed and simulated gravel budget.

Gravel Budget	(m^3)	(m^3/yr.)
Net observed volume change (1999-2003)	2,551,000	638,000
Net simulated volume change (1999-2003)	2,502,000	626,000
(1999-2003) Long time average (Ham, 2005a)	2,460,000	616,000

The net observed and simulated volumes in MIKE 21C were 2,551,000 m^3 and 2,502,000 m^3 over the 4 years period, respectively. The mean annual observed and simulated gravel influxes were 638,000 m^3/y and 626,000 m^3/y, respectively. Both observed and simulated results show positive values, which means that riverbed has aggraded. The simulated volume is not significantly lower than the observed volume. It cannot be strongly argued that the model underestimates the observed result because some model cells were excluded from the calculation due to the unrealistic velocity or bedload transport. In the computational gravel budget, equilibrium transport rate was calculated as a function of discharge only but actually transport rate also depends on the sediment availability. Moreover, a surface based gravel transport equation was used which assumes that the net changes are due to gravel transport only and sands are in suspension while bedload transport occurs. Practically, small portions of sand are part of the total observed volume change. As a result, mean annual gravel influx based on the gravel transport function produced a lower volume over 4 years than the observed influx.

This computational gravel budget results has a fairly close match with the 1999-2003 morphological based gravel budget 616,000 m^3/y (Ham, 2005a). It should be mentioned here that the channel and floodplain area contain under each 1-km long cells in the sediment transport simulation model are not 100% similar to the areas considered in the morphological

based method (Ham, 2005a). It is also noticed that MIKE 21C model sediment transport simulation performance near the sharp bank line shift is poor (Figure 9). Even though same DEM's were used in both methods but more sophisticated surface generation technique (for example, 3D-TIN) was used in morphological based method. Therefore, it is very usual that some sorts of discrepancy may occur between observed volumes in MIKE 21C and volumes obtained from morphological method (Figure 5.13). Nonetheless, the net deposition simulated with MIKE 21C model compares well with the observed values and values obtained from morphological method.

5.5 Aggradation and degradation zone identification

Aggradation and degradation zones were identified by direct comparison of simulated bathymetry to the observed 1999 bathymetry as described in sub-section 4.7. The net simulated volume was calculated over one kilometer lengths starting from Sumas Mountain to 3 km upstream of Agassiz-Rosedale Bridge to compare the results with the results obtained from the morphology based method (Ham, 2005a). Positive or negative volume over a 1 km long cell indicates approximate aggradation or degradtion respectively, for that cell. Finally, the nominal aggradation rate (m/y) over each 1-km long cell was determined assuming a nominal active channel width of 500m (Fig. 5.14). A comparison is shown with the Ham (2005) results. Except in one spot, simulated model shows similar aggradation and degradation zones, but the rate may vary (Figure 5.14). It is noted that simulation results may not be very reliable near the upstream boundary due to the boundary effect. A 2-D map was prepared to present these aggradation and degradation zones along the Lower Fraser River gravel reach (Figure 5.15). In Figure 5.15 the number of aggradation zones is found to be more than the number of degradation zones. Thus, MIKE 21C is well-calibrated and reliable for sediment transport and sedimentation zone identification.

The next step is to apply the MIKE 21C model to investigate a range of gravel removal scenarios, and to assess local morphological changes with and without gravel removal operation over 10 years.
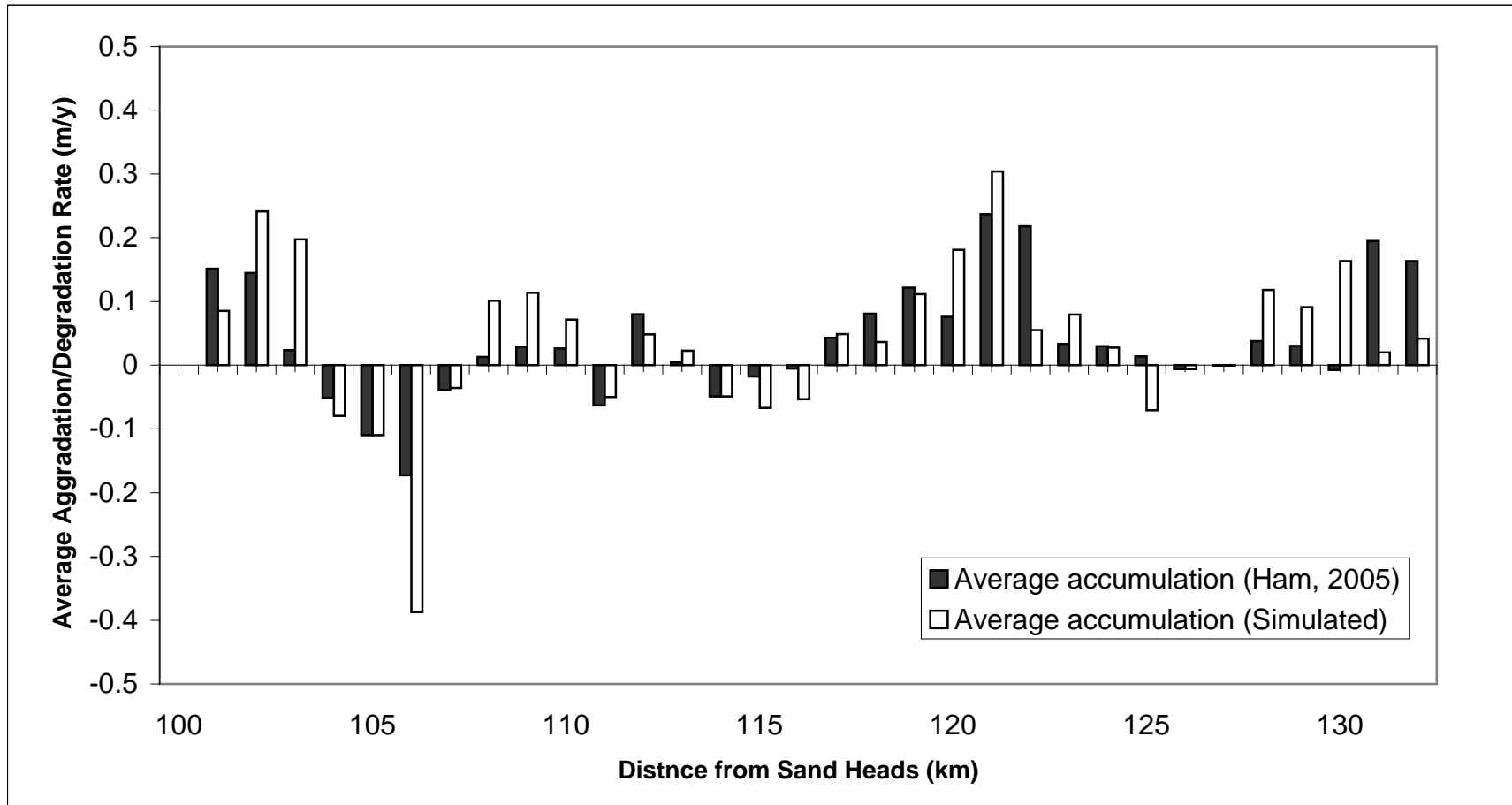
159

Figure 5.14: Nominal aggradation and degradation depths along the Lower Fraser River gravel reach (Cell length is 1 km and nominal width is assumed to be 500 m). Note MIKE 21C results are characteristically more extreme, both positive and negative.
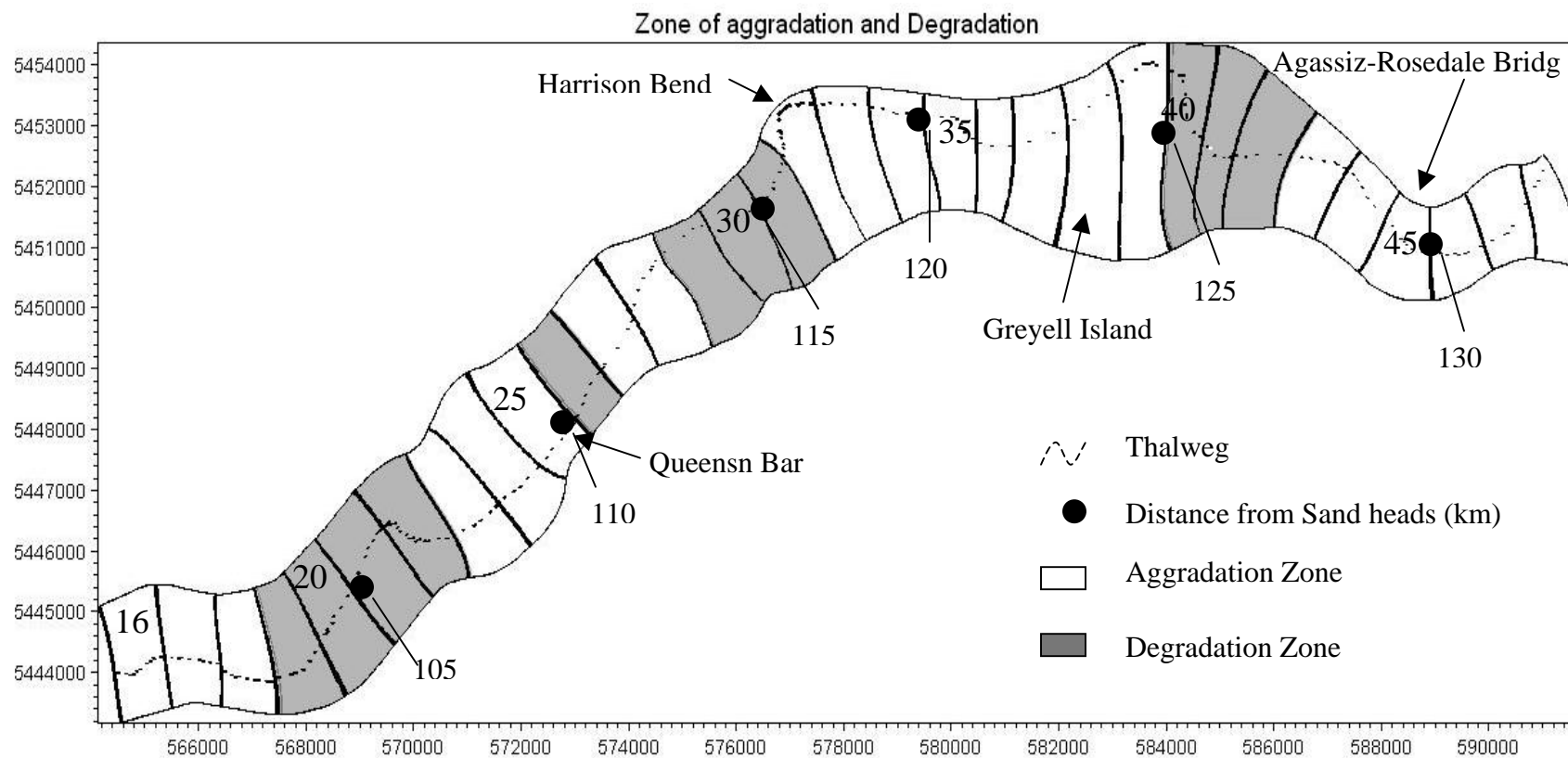
Figure 5.15: Approximate locations of aggradation and degradation zones along the Lower Fraser River gravel reach (cell 16- 47).

5.6 Morphological Effects Due to Gravel Extraction

5.6.1 Morphological Changes Near Queens Bar

The consequence of gravel removal on Queens Bar and in the near by main channel was investigated by model application. First of all, deposition or erosion was observed visually on the removal site. A snap shot of simulated bed level changes after each year was taken for visual comparison. Figure 5.16 presents morphological changes with and without gravel removal after 1, 5 and 10 years respectively. Cross-section details are shown in Appendix-A. Morphological changes inside the channel were calculated by comparing the depths and cross-sections (Figure A.2).

The simulation show that Queens Bar would naturally degrade at the removal site without any excavation. The degradation rate would gradually increase and come to a stable condition at the ninth year then it would decrease slightly (Figure 5.17). The maximum degradation depths are –1.50 m and –2.19 m without and with removal, respectively (Table 5.8). For the case with gravel removal, gravel will accumulate gradually at the removal site. The accumulation depths become stable after the 6th year. Beyond about Year 8, there would be no significant difference between the cases with and without gravel removal.
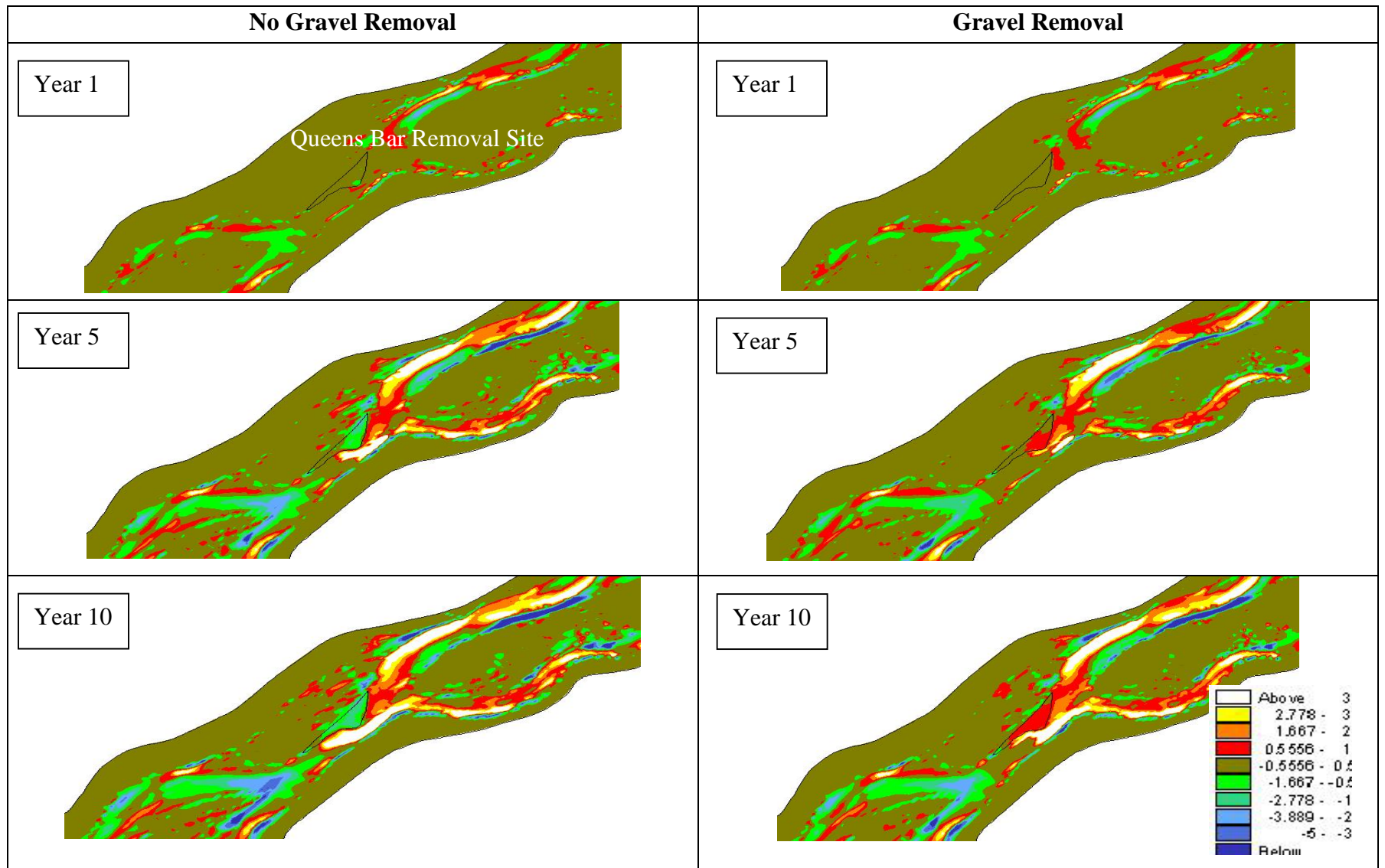
Figure 5.16: Bed level changes near Queens bar without and with gravel removal (Year 1, Year 5 and Year 10).
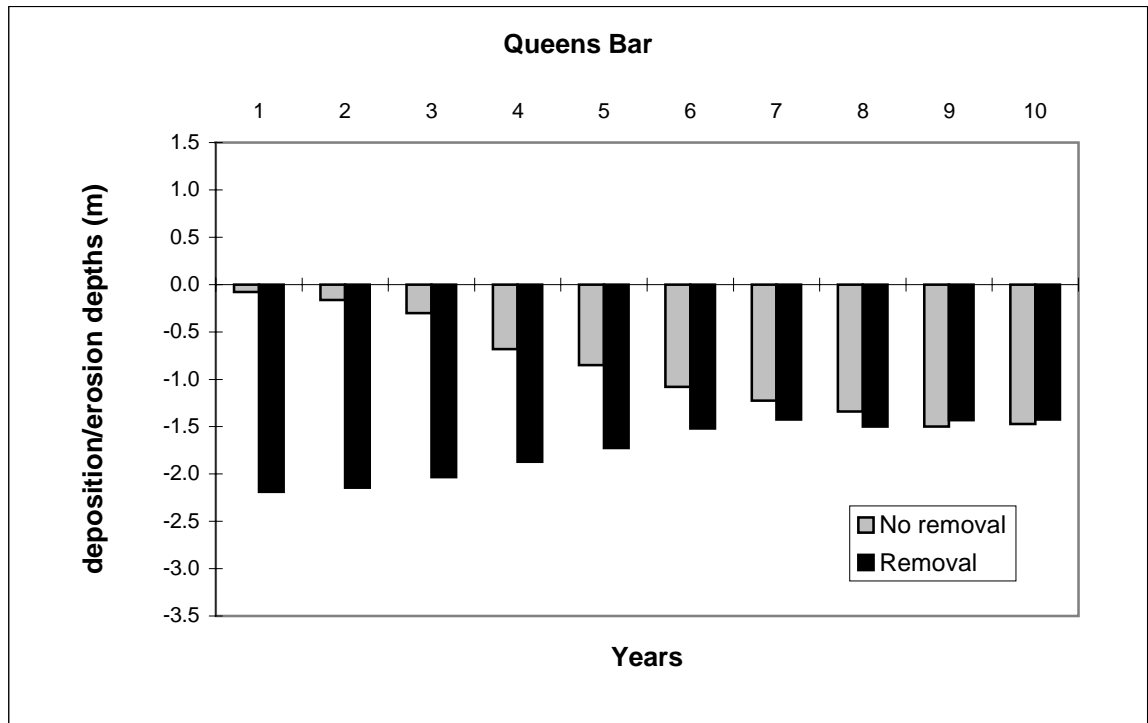
Figure 5.17: Average gravel accumulation at Queens Bar without and with gravel removal.

Table 5.8: Average gravel accumulation at Queens Bar with and without gravel removal.

Year (-)	Accumulation depths (without gravel removal) (m)	Accumulation depths (with gravel removal) (m)
0	0.00	-2.18
1	-0.08	-2.19
2	-0.16	-2.15
3	-0.30	-2.03
4	-0.68	-1.87
5	-0.85	-1.72
6	-1.08	-1.52
7	-1.22	-1.42
8	-1.34	-1.50
9	-1.50	-1.43
10	-1.47	-1.42

5.6.2 Morphological Changes Near Harrison Bar

A snap shot of bed level changes after each year was taken from the simulation model for four removal sites on Harrison Bar denoted as Harrison Site 1 (Harrison inside channel), Harrison Site 2, Harrison Site 3 and Harrison Site 4 for visual investigation. Figure 5.18 presents morphological changes without and with gravel removal after 1, 5 and 10 years respectively. A total of eight cross-sections have been used to assess morphological changes. Cross-section locations and details are shown in Appendix B.

Removal Sites 1 and 2 would degrade over the ten-year simulation with no gravel removal. Modeling indicates that there would be little infilling of the removal pits (Figures 5.19 and 5.20). After 10 years, the natural degradation would approach the removal depths. The maximum erosion depths will be -0.75 m and –1.26 m without and with any gravel removal condition, respectively at Harrison Site 1 (Table 5.9). The maximum deposition and erosion depths will be 0.32 m and –1.53 m, respectively at Harrison Site 2 (Table 5.10)

In the absence of gravel removal, Harrison Sites 3 and 4 would show modest aggradation (Figure 5.21 and 5.22). At Harrison site 3, gravel removal appears to enhance aggradation, and after 10 years it would have aggraded higher than the base case. The maximum accumulation depths are 1.02 m and 0.98 m without and with removal, respectively (Table 5.11). At Harrison Site 4, the removal pit would slowly aggrade to within 0.6 m of the original bed surface after 10 years. The maximum accumulation rate is 0.68 m and 2.01 m without and with gravel removal, respectively for Site 4 (Table 5.12).

There do not appear to be significant off-site differences between the two cases with and without gravel removal.
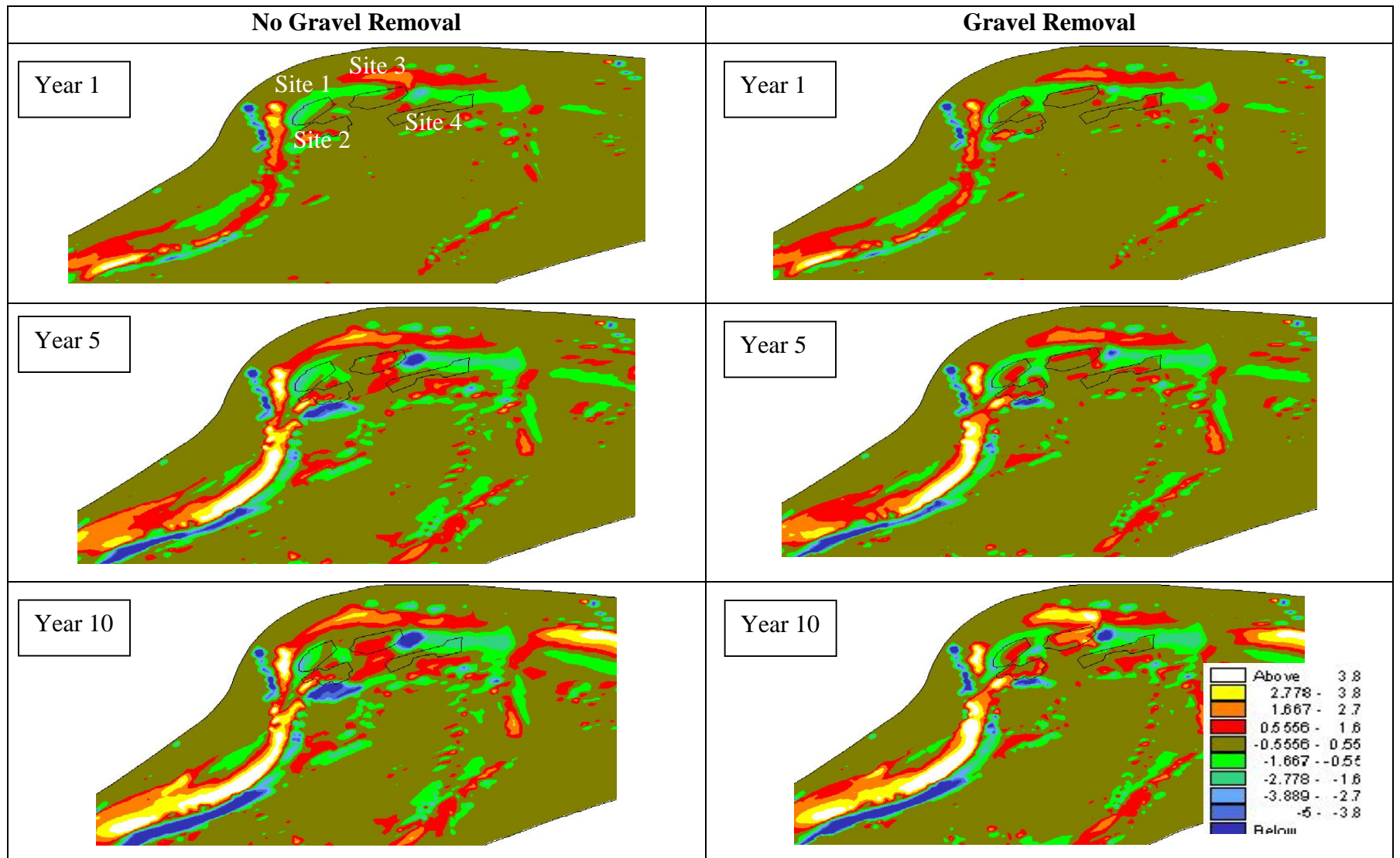
Figure 5.18: Bed level changes of 4 removal sites near Harrison Bar without and with gravel removal (Year 1, Year 5 and Year 10).
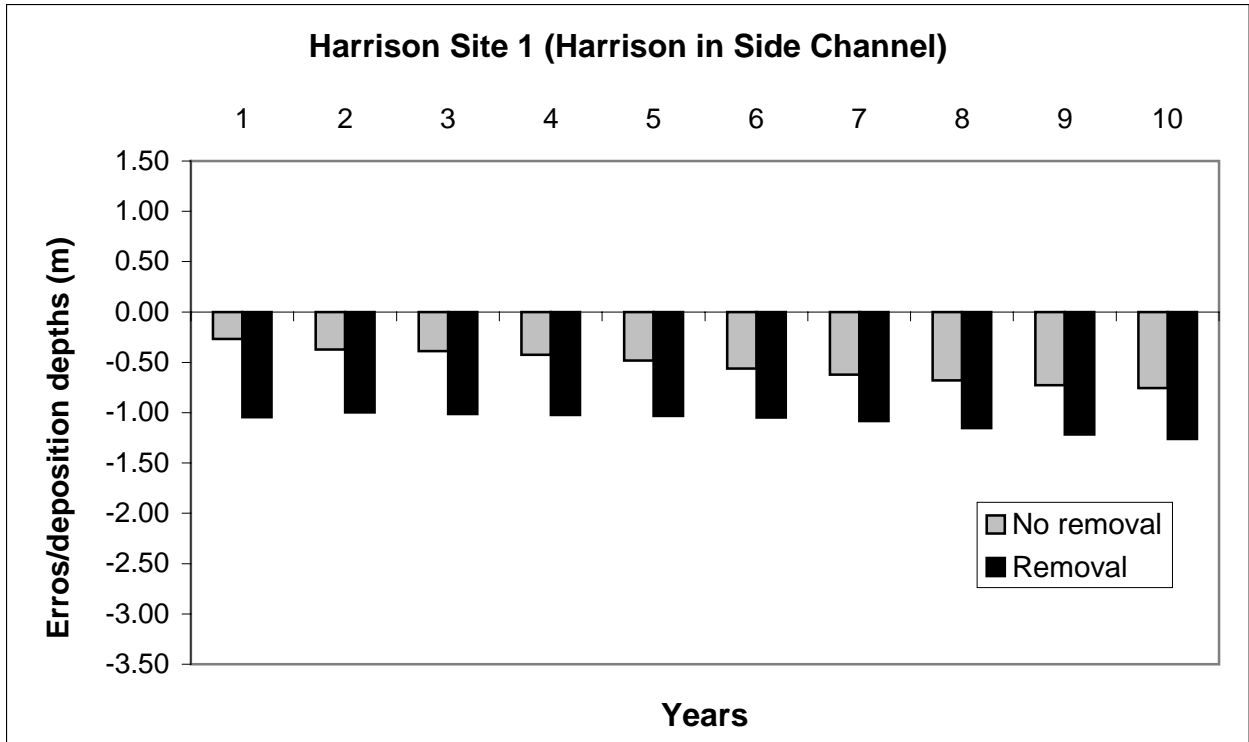
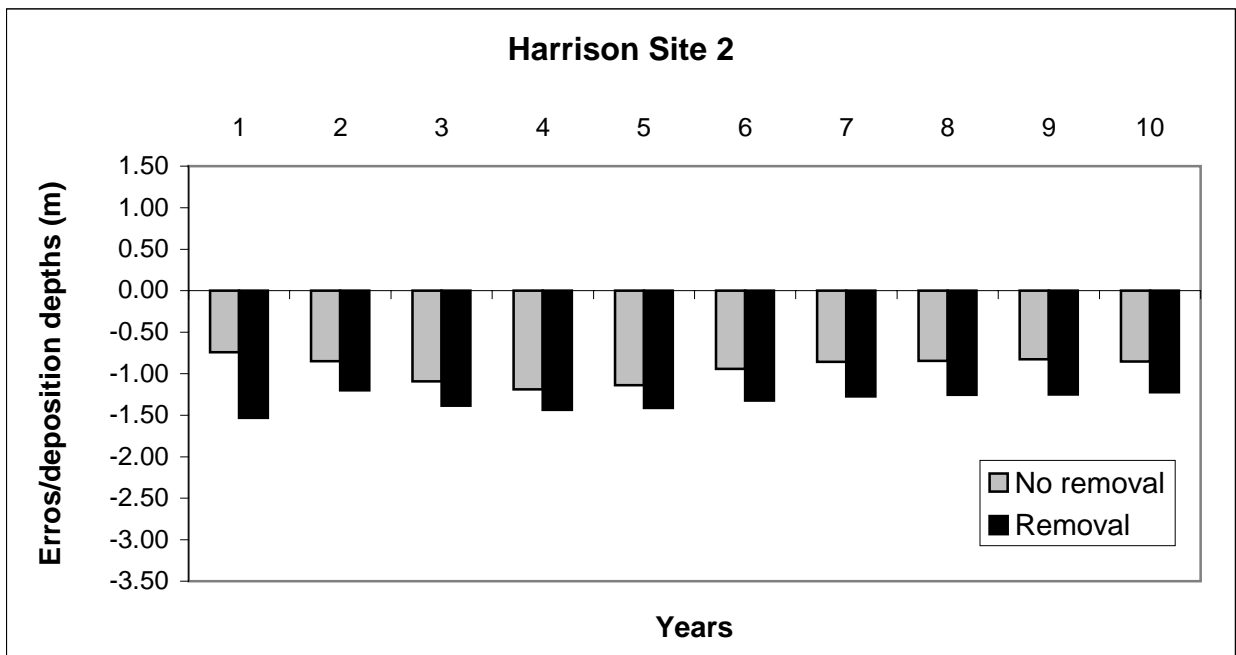Figure 5.19: Average gravel accumulation at Harrison Site 1 with and without gravel removal.

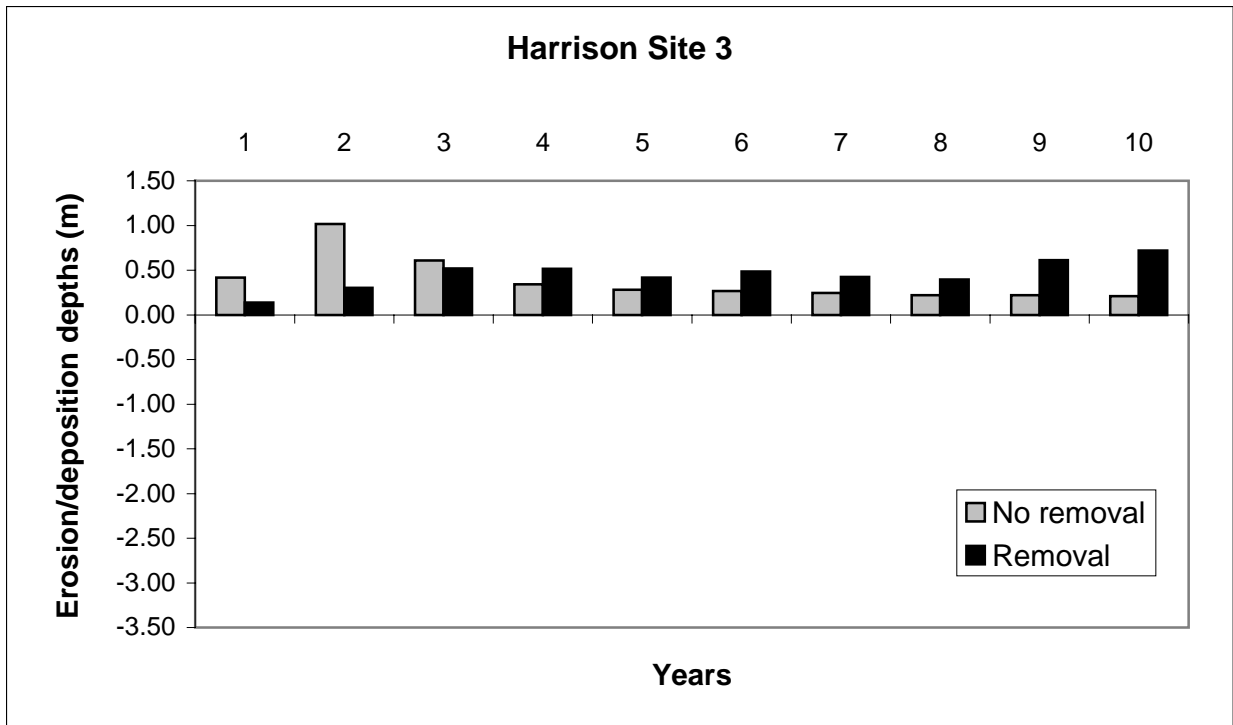Figure 5.20: Average gravel accumulation at Harrison Site 2 with and without gravel removal.

Figure 5.21: Average gravel accumulation at Harrison Site 3 with and without gravel removal.
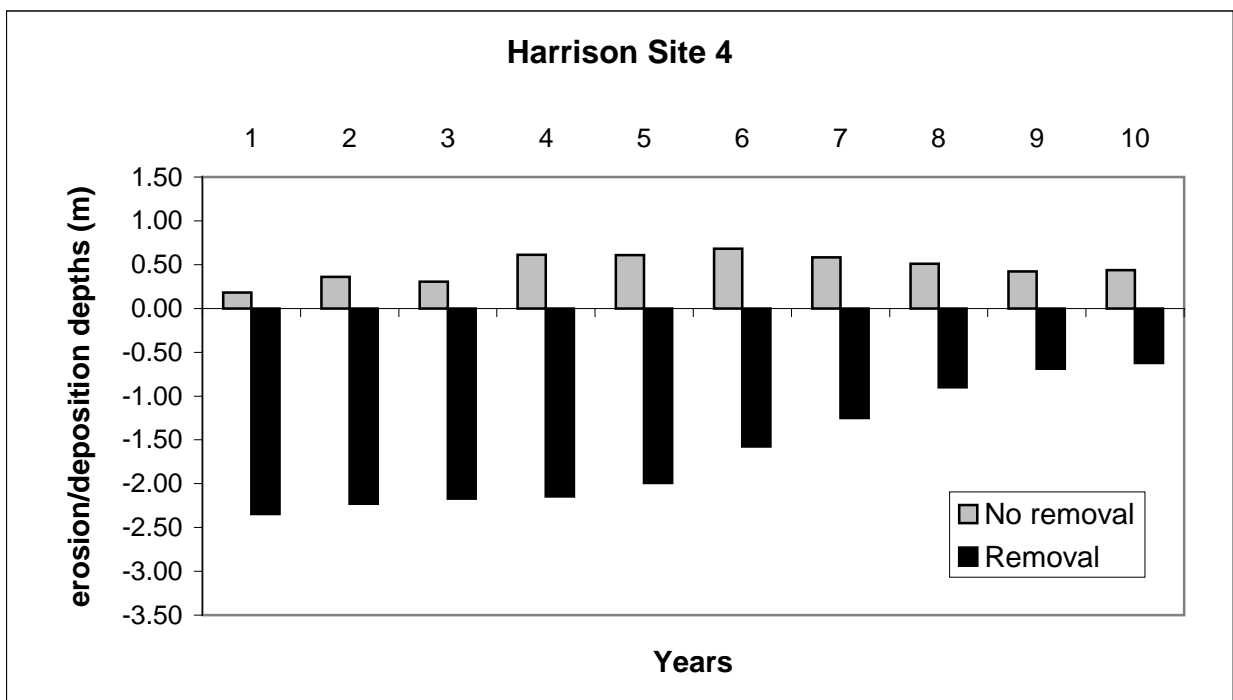

Figure 5.22: Average gravel accumulation at Harrison Site 4 with and without gravel removal.

Table 5.9: Average gravel accumulation at Harrison Bar with and without gravel removal at Harrison Site 1.

Year (-)	Accumulation depths (without gravel removal) (m)	Accumulation depths (with gravel removal) (m)
0	0	-1.04
1	-0.27	-1.04
2	-0.37	-1
3	-0.39	-1.01
4	-0.42	-1.02
5	-0.48	-1.03
6	-0.56	-1.05
7	-0.62	-1.08
8	-0.68	-1.15
9	-0.72	-1.22
10	-0.75	-1.26

Table 5.10: Average gravel accumulation at Harrison Bar with and without gravel removal at Harrison Site 2.

Year (-)	Accumulation depths (without gravel removal) (m)	Accumulation depths (with gravel removal) (m)
0	0	-1.53
1	-0.74	-1.53
2	-0.85	-1.20
3	-1.09	-1.38
4	-1.19	-1.43
5	-1.14	-1.41
6	-0.94	-1.32
7	-0.86	-1.28
8	-0.85	-1.26
9	-0.83	-1.25
10	-0.85	-1.22

Table 5.11: Average gravel accumulation at Harrison Bar with and without gravel removal at Harrison Site 3.

Year (-)	Accumulation depths (without gravel removal) (m)	Accumulation depths (with gravel removal) (m)
0	0	-1.5
1	0.42	0.14
2	1.02	0.30
3	0.61	0.52
4	0.34	0.51
5	0.28	0.42
6	0.27	0.48
7	0.25	0.43
8	0.22	0.40
9	0.22	0.61
10	0.21	0.72

Table 5.12: Average gravel accumulation at Harrison Bar with and without gravel removal at Harrison Site 4.

Year (-)	Accumulation depths (without gravel removal) (m)	Accumulation depths (with gravel removal) (m)
0	0	-2.35
1	0.18	-2.35
2	0.36	-2.23
3	0.30	-2.17
4	0.61	-2.15
5	0.61	-1.99
6	0.68	-1.57
7	0.58	-1.25
8	0.51	-0.90
9	0.42	-0.69
10	0.44	-0.62

5.6.3 Morphological Changes near Gill and Hamilton Island Complexes

A snap shot of bed level changes after each year was taken from the simulation model for three removal sites at Gill Bar and two sites at Hamilton Bar for visual investigation. Figure 5.23 presents morphological changes near Gill Bar and Hamilton Bar without and with gravel removal after 1, 5 and 10 years respectively. A total of 16 cross-sections have been taken to identify the morphological changes inside the channel by comparing the depths. Cross-section locations and details are shown in Appendix C. The following results were found after 10 years simulation.

The Gill West removal site will degrade over the first 2 years with and without gravel removal (Figure 5.24). Maximum degradation depths are -1.77 m and -1.24 m in the 2nd year with and without any gravel removal respectively (Table 5.13). There would be infilling of the removal pit after the second year continuing up to the tenth year. After 10 years, the removal pit may fully infill to near its original base level.

The Gill North removal site will aggrade over the first two years then it will recover to its base level after the 3rd year without gravel removal (Figure 5.25). This site will again naturally degraded from the 6th year without gravel removal. Maximum aggradation and degradation depths are 0.52 m and –0.05 m, respectively (Table 5.14). Similarly, the removal site will aggrade over the first three years to exceed the base level at the 4th year with gravel removal. Gravel buildup will gradually decrease from the 6th year to 10th year. Maximum aggradation and degradation depths are 0.43 m and –0.67 m respectively (Table 5.14). The infill time of this site is about 2 to 3 years for both cases but gravel will be eroded away after the 6th year.

The Gill East removal site will be degraded over the first 3 years both with and without gravel removal (Figure 5.26). Maximum degradation depths are –3.02 m and –3.12 m with and without removal respectively (Table 5.15). The removal pit will infill after 5 years and 3 years with and without gravel removal. This site will not reach its base level after 10 years of simulation period.

171

The Hamilton South removal site will degrade without gravel removal (Figure 5.27). Maximum degradation depth is 0.84 m in the 8th year (Table 5.16). The removal site will degrade up to the 3rd year after gravel removal then aggrade again in the 4th year. After the 4th year it will slowly degrade up to the 7th year and remain constant up to the 10th year (Figure 5.27). The accumulation process varies approximately over a 3-year cycle, which indicates that the site is not stable. Maximum degradation depth is –1.33 m (Table 5.16). The removal pit will not infill back to its original state over the 10 years simulation period.

The Hamilton North removal site will aggrade over the 10 years with and without gravel removal (Figure 5.28). Maximum aggradation depths are 0.53 m and 0.39 m with and without gravel removal, respectively (Table 5.17). Aggradation will gradually increase over the first 4 years then it will be stable over the next 6 years simulation period in both cases. This continuous but slow gravel accumulation indicates that the removal pit will not infill back to its original state over the 10 year simulation period after gravel removal. However, the stability of accumulation or slower deposition rate after the first few years indicates that gravel removal is very effective in this site and may take a very long period to recover at its original state.
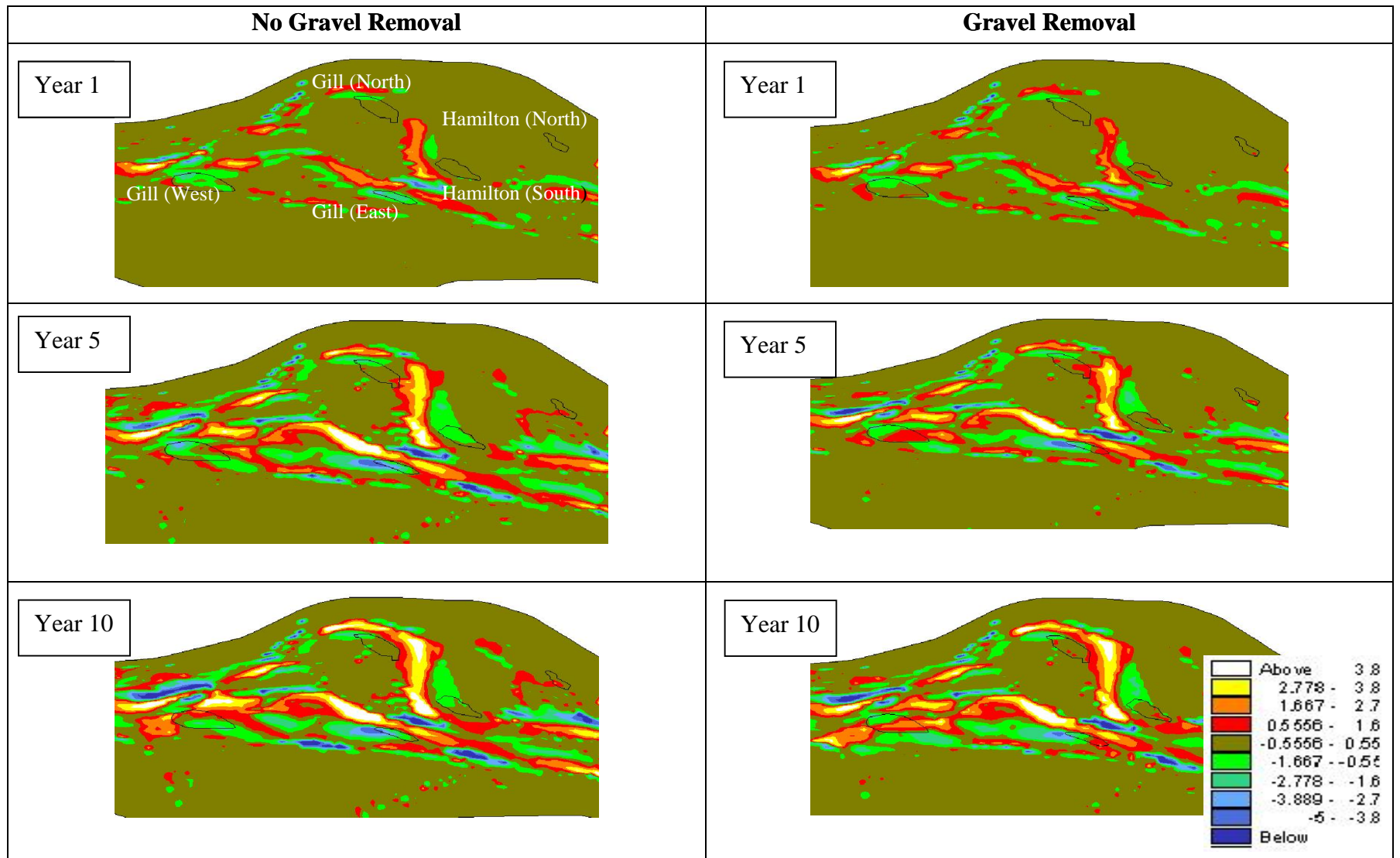
Figure 5.23: Bed level changes of removal sites near Gill Bar and Hamilton Bar without and with removal (Year 1, Year 5 and Year 10).
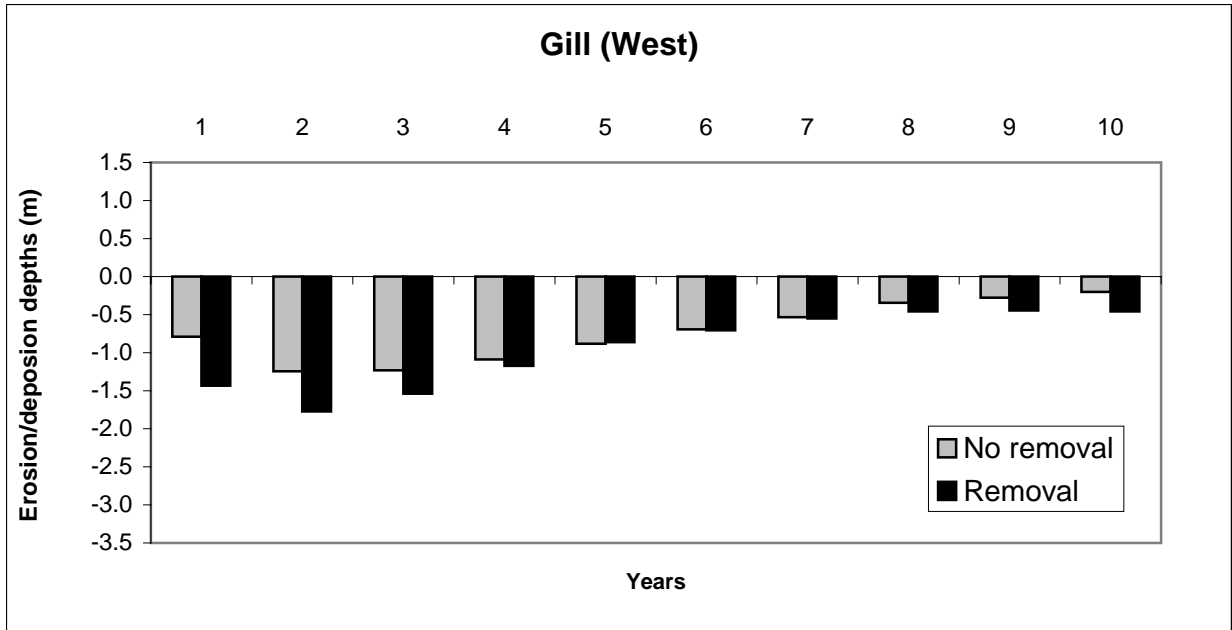
Figure 5.24: Average gravel accumulation at Gill Bar (West) removal sites with and without gravel removal.
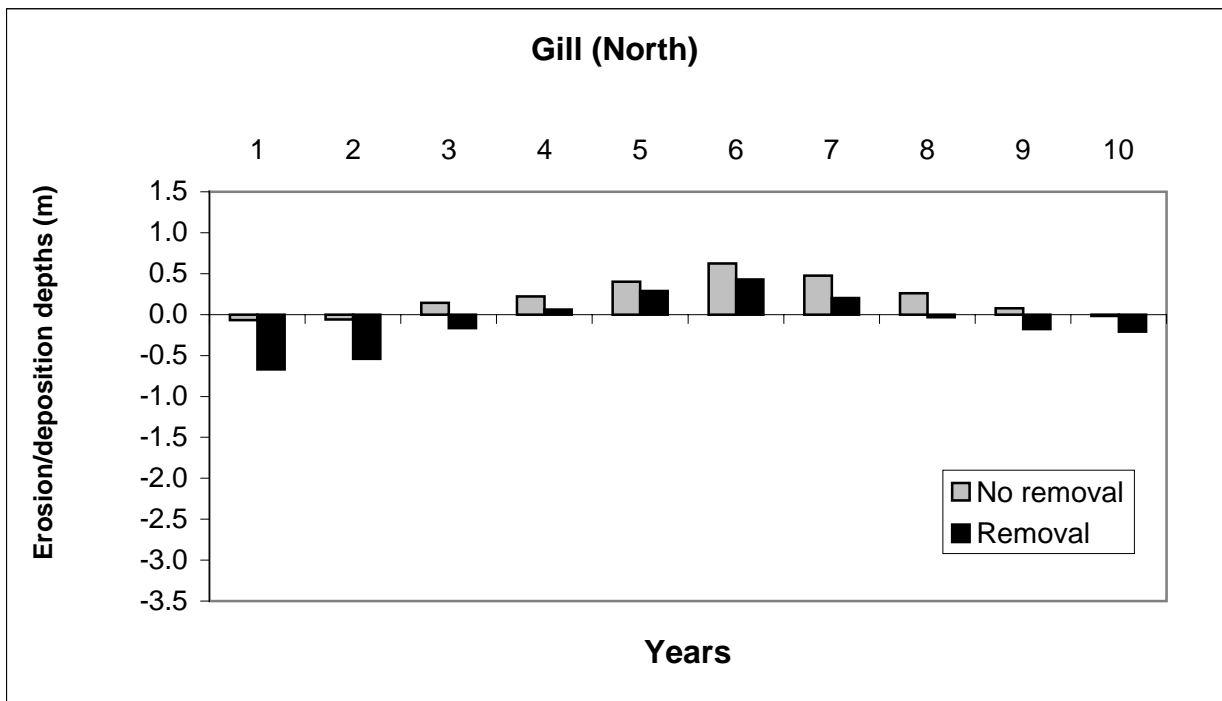

Figure 5.25: Average gravel accumulation at Gill Bar (North) removal sites with and without gravel removal.
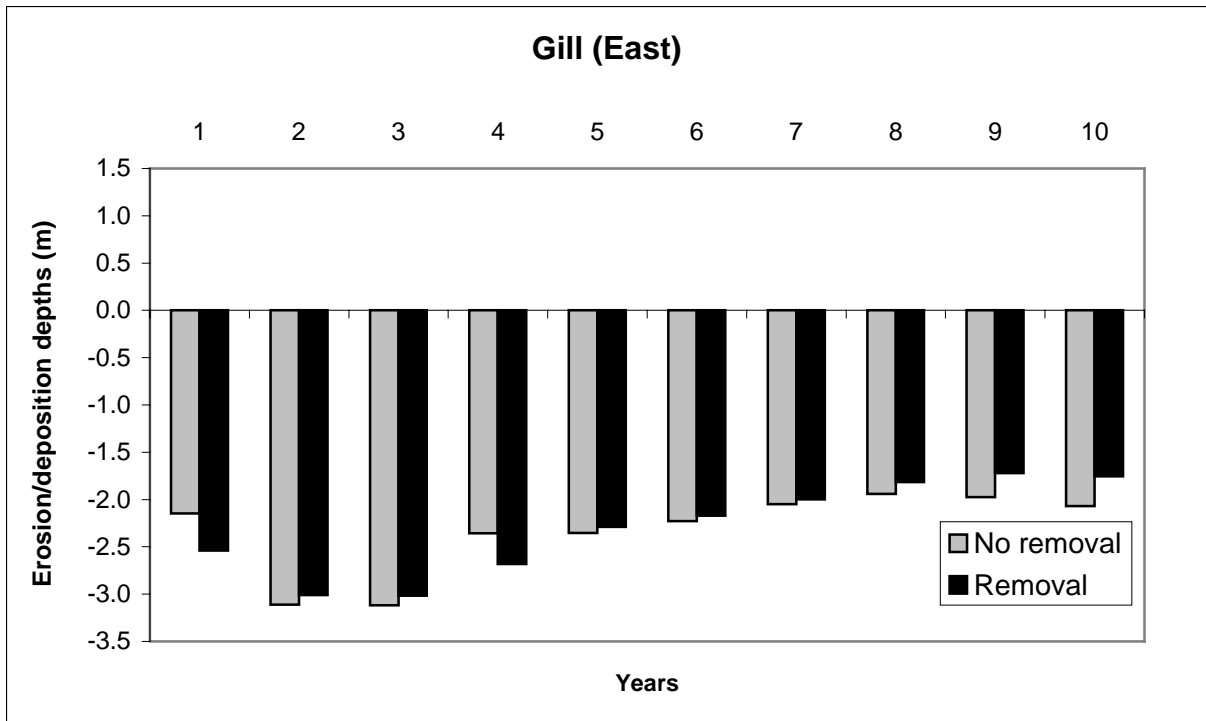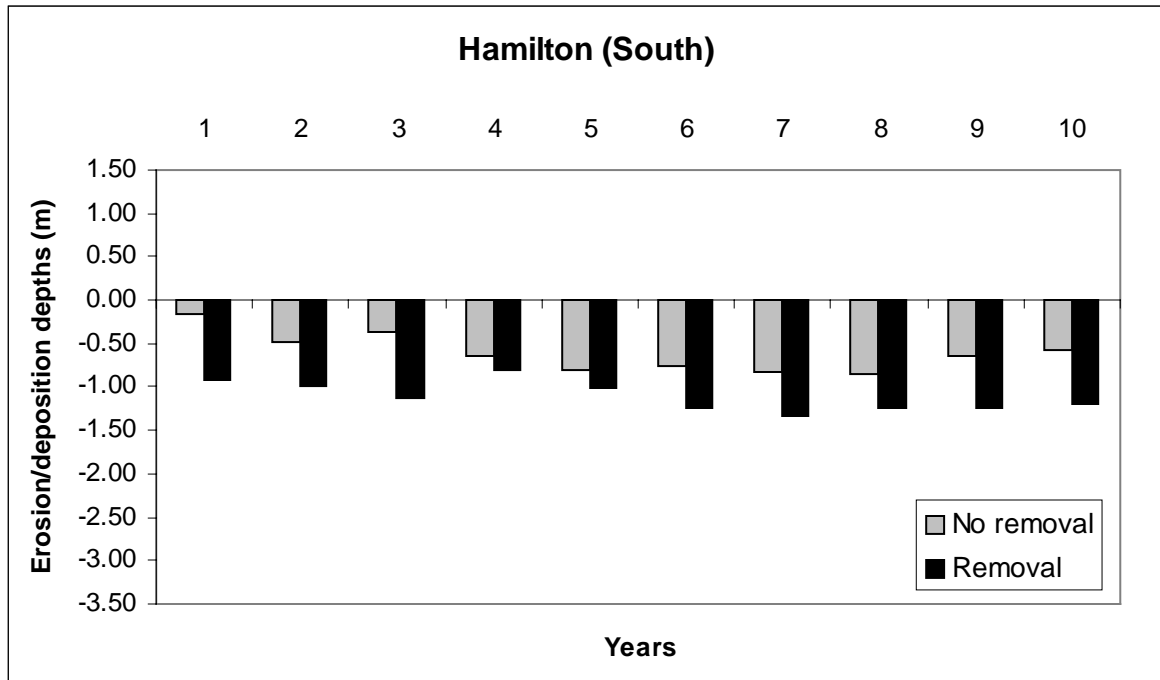
Figure 5.26: Average gravel accumulation at Gill Bar (East) removal sites with and without gravel removal.

Figure 5.27: Average gravel accumulation at Hamilton Bar (South) removal site with and without gravel removal.

Figure 5.28: Average gravel accumulation at Hamilton Bar (North) removal site with and without gravel removal.

Table 5.13: Average gravel accumulation at Gill Bars (West) with and without gravel removal.

Year (-)	Accumulation depths (without gravel removal) (m)	Accumulation depths (with gravel removal) (m)
0	0	-1.43
1	-0.79	-1.43
2	-1.24	-1.77
3	-1.23	-1.54
4	-1.09	-1.17
5	-0.88	-0.86
6	-0.69	-0.70
7	-0.53	-0.55
8	-0.35	-0.46
9	-0.28	-0.45
10	-0.20	-0.46

Table 5.14: Average gravel accumulation at Gill Bars (North) with and without gravel removal.

Year (-)	Accumulation depths (without gravel removal) (m)	Accumulation depths (with gravel removal) (m)
0	0	-0.67
1	-0.07	-0.67
2	-0.06	-0.54
3	0.14	-0.17
4	0.22	0.06
5	0.40	0.29
6	0.62	0.43
7	0.48	0.20
8	0.26	-0.03
9	0.08	-0.18
10	-0.02	-0.21

Table 5.15: Average gravel accumulation at Gill Bars (East) with and without gravel removal.

Year (-)	Accumulation depths (without gravel removal) (m)	Accumulation depths (with gravel removal) (m)
0	0	-2.54
1	-2.15	-2.54
2	-3.11	-3.01
3	-3.12	-3.02
4	-2.36	-2.68
5	-2.35	-2.29
6	-2.23	-2.17
7	-2.05	-2.00
8	-1.94	-1.82
9	-1.97	-1.72
10	-2.07	-1.76

Table 5.16: Average gravel accumulation at Hamilton Bar (South) with and without gravel removal.

Year (-)	Accumulation depths (without gravel removal) (m)	Accumulation depths (with gravel removal) (m)
0	0	-0.92
1	-0.17	-0.92
2	-0.48	-0.99
3	-0.37	-1.12
4	-0.65	-0.81
5	-0.80	-1.01
6	-0.75	-1.24
7	-0.84	-1.33
8	-0.84	-1.24
9	-0.65	-1.24
10	-0.57	-1.19

Table 5.17: Average gravel accumulation at Hamilton Bar (North) with and without gravel removal.

Year	Accumulation depths (without gravel removal)	Accumulation depths (with gravel removal)
(-)	(m)	(m)
0	0	-1.45
1	0.09	-1.45
2	0.12	-1.34
3	0.16	-1.33
4	0.34	-1.30
5	0.36	-1.17
6	0.36	-1.11
7	0.37	-1.05
8	0.38	-1.03
9	0.39	-1.02
10	0.39	-1.02

5.6.4 Morphological Changes Near Big Bar

A snap shot of bed level changes after each year was taken from the simulation model for two removal sites at Big Bar for visual investigation. Figure 5.29 presents morphological changes near Big Bar (South) and Big Bar (North) without and with gravel removal after 1, 5 and 10 years respectively. A total of 7 cross-sections have been taken to identify the morphological changes inside the channel by comparing the depths. Cross-section locations and details are shown in Appendix D. The following results were found after 10 years simulation.

The Big Bar (South) removal site will aggrade over the 10 years with or without gravel removal (Figure 5.30). The aggradation will increase rapidly over the first 4 years then it will decrease slowly up to sixth year and again gradually increase onward up to the 10th year without any gravel removal. The net gravel deposition will be nearly zero over the first two years after gravel removal, then the removal pit will aggrade slightly and remain in an equilibrium state over the next 8 years. Maximum aggradation depths are 0.59 m and 0.80 m

without and with gravel removal, respectively (Table 5.18). In general, gravel deposition will continue at this site immediately after the removal so the pit will infill back quickly and generally aggrade over the 10 years simulation period. However, gravel removal will damp the overall aggradation rate.

The Big Bar (North) removal site will naturally degrade over the 10 years without gravel removal (Figure 5.31). The degradation will increase gradually over the 10 years and will reach its maximum rate at the 10th year. The removal pit will also degrade over the 10 years with gravel removal. The erosion rate will remain constant for the first five years after gravel removal then it will increase rapidly up to the tenth year. Maximum degradation depths are -1.36 m and -1.13 m without and with gravel removal, respectively (Table 5.19). The site will degrade continuously and the removal pit will not infill back to its original state over the 10 years.

A total of seven cross-sections were extracted and analyzed to observe the changes upstream and downstream of the gravel removal site for both removal and no removal cases (Figure D.3.1 to D.3.4). Three cross-sections were across the Big Bar South and the rest were across the Big Bar North (Figure D.2). Gravel will be deposited on both side of the removal areas and the bar will become wider and flatter. As a result, the riverbed will be shallower on both sides of the South bar and the thalweg will be shifted toward the Big Bar side. This situation is very prominent at the downstream side of the Big Bar South removal site.

Due to the erosion on the Big Bar North removal site, eroded materials will be deposited inside the main Lower Fraser River channel bed. As a result, a shallow and wider channel on the left side and a deep narrow channel on the right side will be formed near the Big Bar North removal site. There is not much morphological difference between the two riverbeds with or without removal.
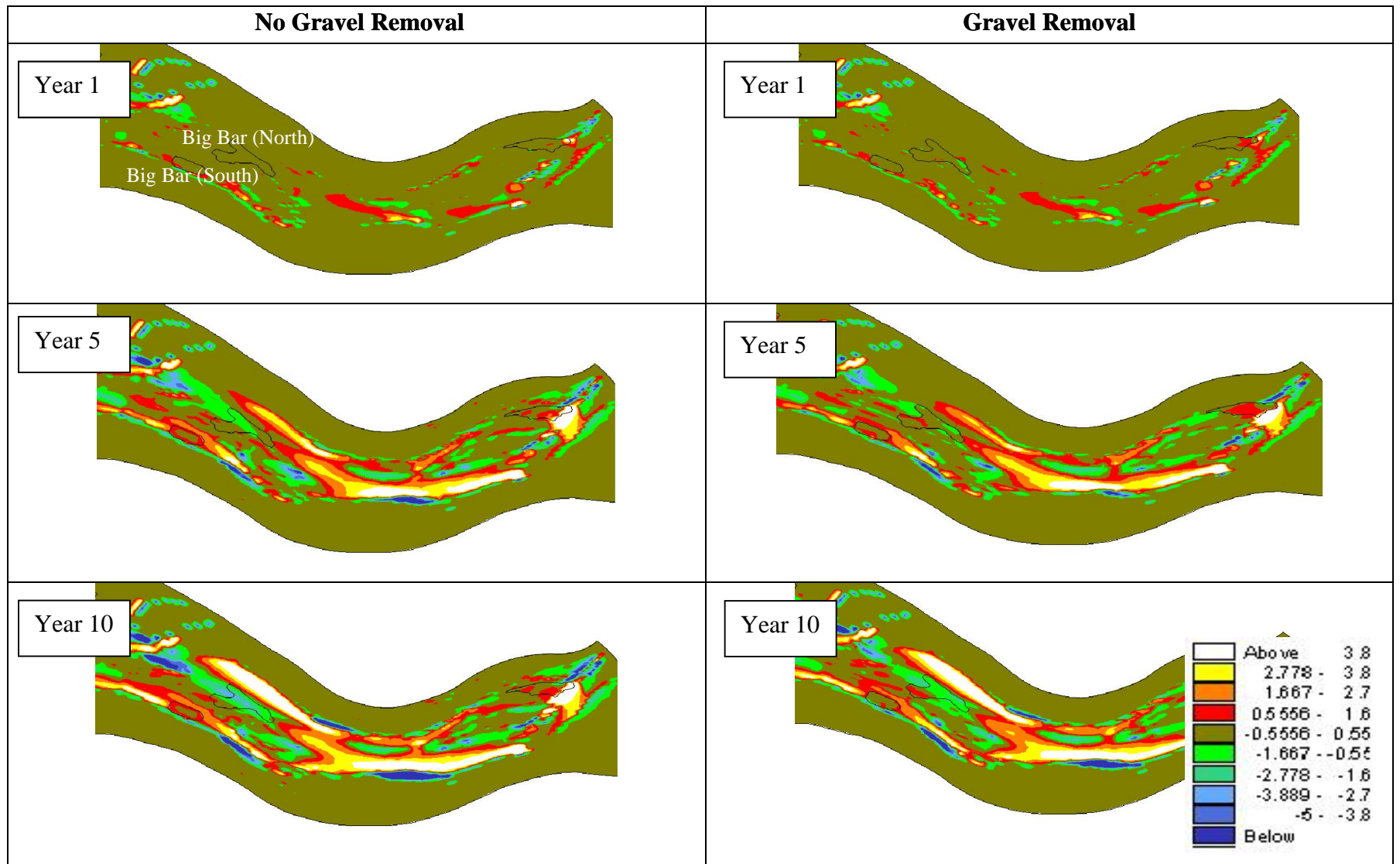
Figure 5.29: Bed level changes near Big Bar without and with gravel removal (Year 1, Year 5 and Year 10).
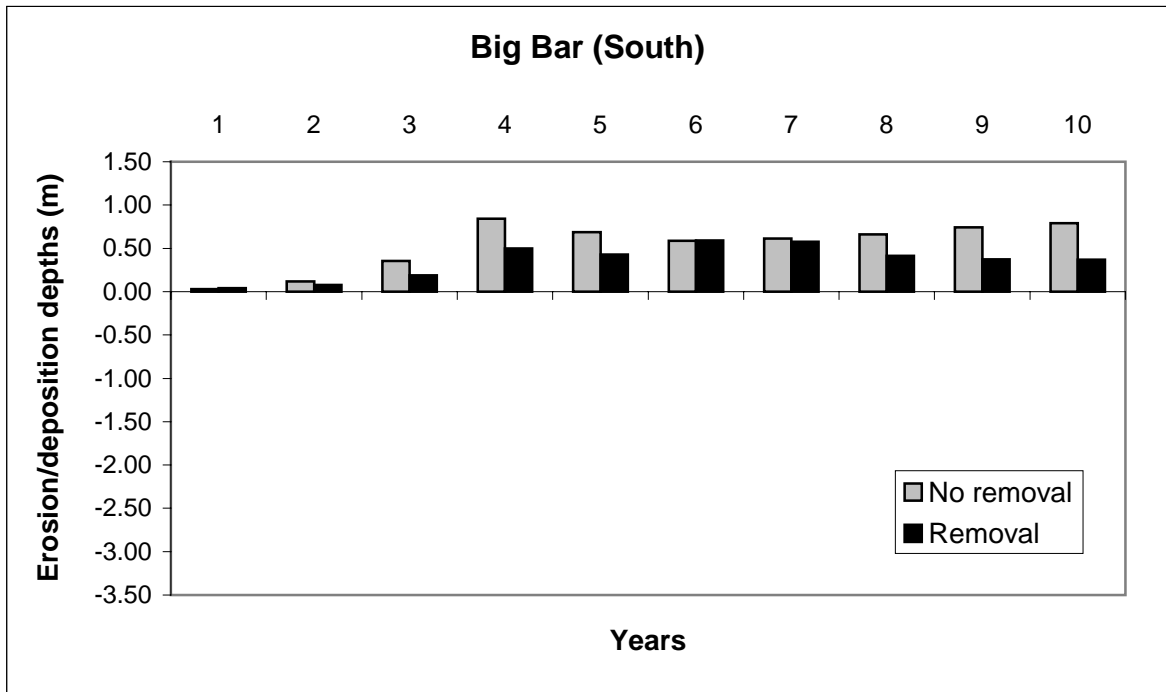
Figure 5.30: Average gravel accumulation at Big Bar (South) with and without gravel removal.
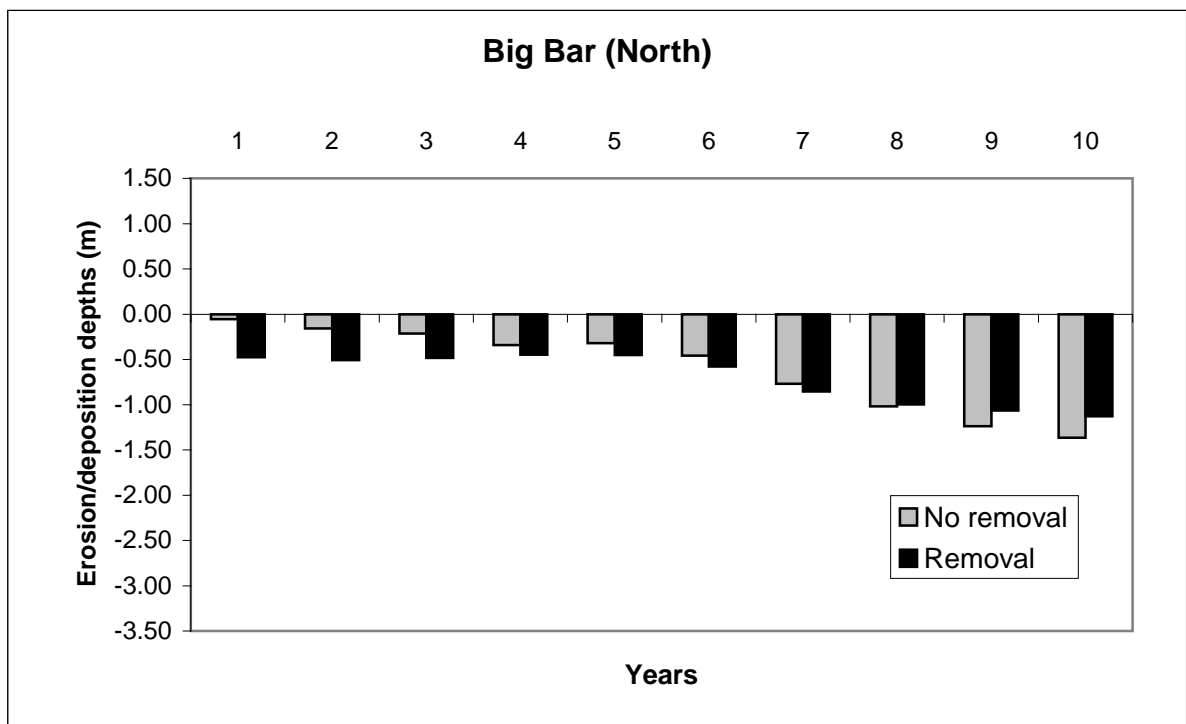

Figure 5.31: Average gravel accumulation at Big Bar (North) with and without gravel removal.

Table 5.18: Average gravel accumulation at Big Bar (South) with and without gravel removal.

Year (-)	Accumulation depths (without gravel removal) (m)	Accumulation depths (with gravel removal) (m)
0	0	-1.1
1	0.03	0.04
2	0.12	0.08
3	0.35	0.19
4	0.84	0.50
5	0.69	0.43
6	0.59	0.59
7	0.61	0.58
8	0.66	0.41
9	0.74	0.37
10	0.80	0.37

Table 5.19: Average accumulation of gravel on Big Bar (North) with and without gravel removal.

Year (-)	Accumulation depths (without gravel removal) (m)	Accumulation depths (with gravel removal) (m)
0	0	-0.2
1	-0.06	-0.48
2	-0.16	-0.51
3	-0.22	-0.48
4	-0.34	-0.45
5	-0.32	-0.45
6	-0.46	-0.58
7	-0.77	-0.85
8	-1.02	-1.00
9	-1.24	-1.07
10	-1.36	-1.13

5.6.6 Summary of Morphological Changes After Gravel Extraction

The morphological changes accompanying gravel removal from Queens Bar, Harrison Bar, Gill and Hamilton Islands and Big Bar are summarized in Table 5.20. Except for two of the sites (Harrison Site 3 and Big Bar South), gravel removal work may have some positive impact on flood management at least for the next 10 years from 2003 onward. Fresh gravel will be accumulated on all removal sites except Gill (East) and Big Bar (North). Erosion will continue on these two sites after gravel removal. Channel shape changes upstream or downstream of all the gravel extraction sites are not similar. Some sites such as Queens and Big Bar, are highly sensitive to the extraction, and some such as Gill (North) Bar, are not. Visual comparison of morphological changes (e.g. Figure5.9) were good for presentation but very difficult to quantify the exact amount of changes between two cases as compared to other means of quantification such as spreadsheet analysis (e.g. Table 5.18 and 5.19).

All the results are based on a shear stress based sediment transport equation (Wilcock and Crow, 2003), which is a function of channel discharge and roughness only. The discharge and sediment size time series are based on historical flows, however the future 10 years of real flow may be significantly different. Therefore, there is no guarantee that the estimated morphological changes will occur after gravel removal from those sites. There are some sites shows degrading anyway without or with gravel removal. These sites may be put under watch for next few years before implementing the gravel extraction plan to investigate the validity of the model result. Many hypothetical gravel extraction scenarios may be tested with calibrated MIKE 21C model which is the most important use of this model.

Table 5.20: A short summary of effectiveness of gravel extraction.

Removal Sites	Removal amount	Aggradation depths (after 1 yr)		Aggradation depths (after 5 yrs)		Aggradation depths (after 10 yrs)		Recovery time
		No Removal	Removal	No Removal	Removal	No Removal	Removal	
	(m^3)	(m)	(m)	(m)	(m)	(m)	(m)	(year)
Queens Bar	500,000	-0.08*	-2.19	-0.85	-1.72	-1.47	-1.42	>10
Harrison Site 1	161,000	-0.27	-1.04	-0.48	-1.03	-0.75	-1.26	>10
Harrison Site 2	122,000	-0.74	-1.53	-1.14	-1.41	-0.85	-1.22	>10
Harrison Site 3	53,000	0.42	0.14	0.28	0.42	0.21	0.72	1
Harrison Site 4	156,000	0.18	-2.35	0.61	-1.99	0.44	-0.62	>10
Gill (West)	52,000	-0.79	-1.43	-0.88	-0.86	-0.20	-0.46	>10
Gill (North)	20,000	-0.07	-0.67	0.40	0.29	-0.02	-0.21	4
Gill (East)	50,000	-2.15	-1.06	-2.35	-2.29	-2.07	-1.76	>10
Hamilton (South)	4,200	-0.17	-0.92	-0.80	-1.01	-0.57	-1.19	>10
Hamilton (North)	44,000	0.09	-1.45	0.36	-1.17	0.39	-1.02	>10
Big Bar (South)	50,000	0.03	0.04	0.69	0.43	0.80	0.37	1
Big Bar (North)	20,000	-0.06	-0.48	-0.32	-0.45	-1.36	-1.13	>10

* Negative (-) value indicates the degradation.

5.7 Effects of Gravel Extraction on Flood Profiles

As mentioned in the methodology section, the water surface elevations in each 1 km interval were extracted for the 70 km long flood profiles between Mission and Laidlaw. The first simulation was based on 2003 surveyed bed bathymetry and the second simulation was 2003 surveyed bathymetry after gravel removal. Two water surface profiles were plotted and compared against each other (Figure 5.32). Due to the scale, no apparent difference has been observed between them. As a result, the differences were calculated separately and plotted on the same figure using a secondary axis to identify the water surface elevation increases or decreases.

The flood profile has been changed between Herrling Island (at km 142) and Mission (at km 85) after gravel removal. The flood profile has dropped in this reach after gravel removal except of a few locations. The maximum drop is 15 cm near Quaamitch Slough (at km 105). The maximum water level increase is 7 cm just downstream of Hamilton Island (at km128). The other increased water levels are 1 cm at Island # 76 (at km 108), 5 cm near Minto Island (at km 115) and 1 cm near Foster Bar (at km 120). The increase of water level is negligible except near Hamilton Island (at km128) and Minto Island (at km 115).

All gravel removal sites approved by the DFO were not considered in this study and the simulation considered the condition immediately after removal. It is difficult to set the exact removal area in a curvilinear grid 2D-model but bed elevation after removal can be set accurately in the grid cell. The water surface profile elevations presented here are based on the removal sites, considered in this study. A positive effect on design flood profile is observed immediately after gravel removal. However, the effectiveness of gravel removal depends on the removal amount, number of locations and recovery time. The effectiveness of this measure on flood risk reduction obviously will decline over the years. Therefore, from these simulation results it can be concluded that continuous gravel removal operations from various large accumulation sites may be necessary to ensure reduction of flood risk in this reach.
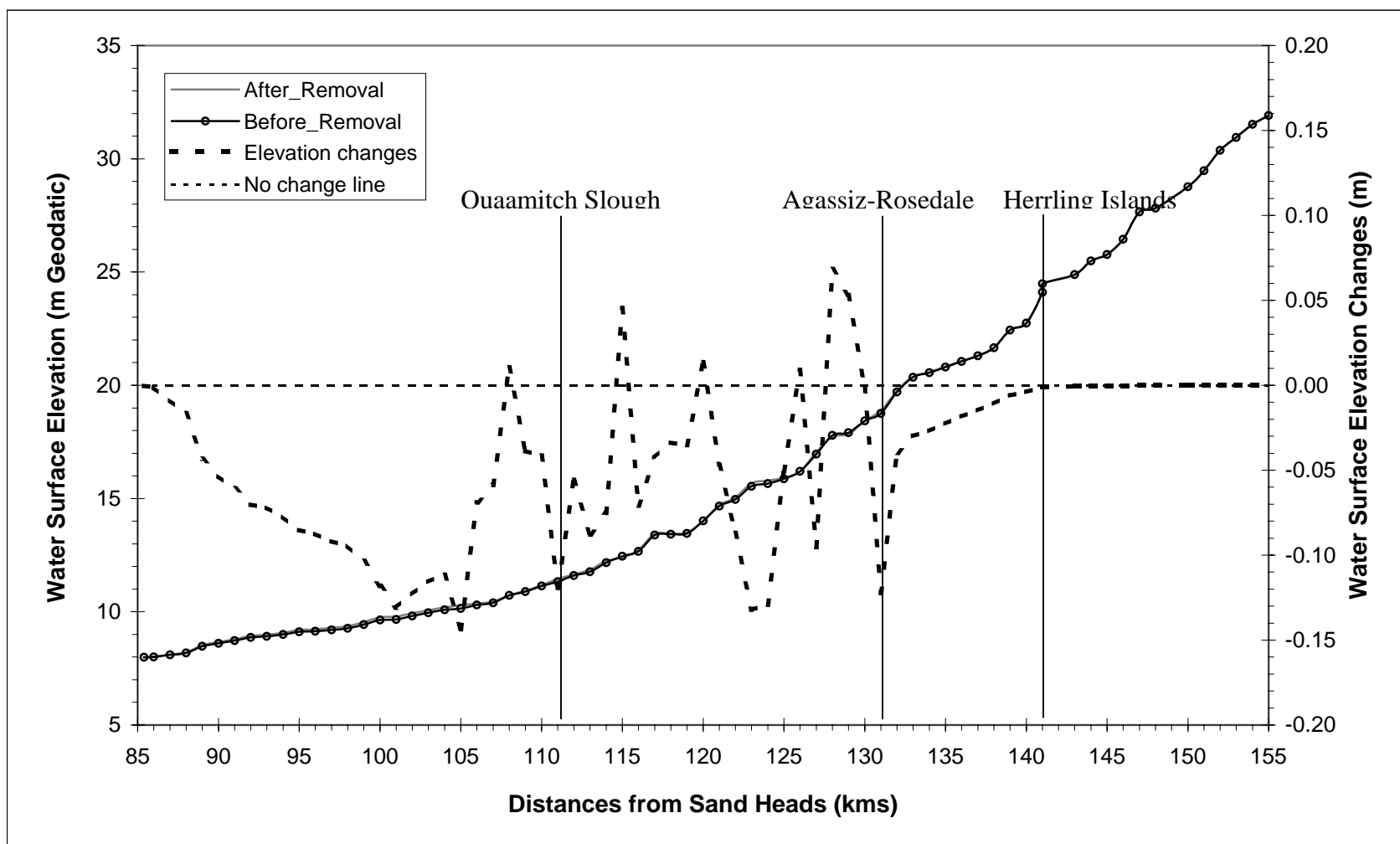
Figure 5.32: Comparison of water surface profiles before and after gravel removal with Lower Fraser River discharge of 17,000 m³/s.

6 CONCLUSIONS AND FUTURE WORK

6.1 Summary of Hydrodynamic and Sediment Transport Model Development

This study begins with the key objective of practical application of a two-dimensional depth-averaged hydrodynamic and morphological modeling technique to investigate the potential uses for gravel bedload transport simulation and bed level change prediction for a large wandering gravel-bed river. This objective was fulfilled very well. A curvilinear grid based two-dimensional depth-averaged numerical model based on MIKE 21C was developed for the entire Lower Fraser River gravel reach between Mission and Laidlaw for hydrodynamic calibration. It incorporates fully unsteady flow, bedload transport via transport formulation, dynamic bed level changes through a simple sediment continuity equation (Exner equation) and also includes an analytical model for computing the secondary currents, and thus provides three-dimensional effects for a two-dimensional model. The MIKE 21C model was mainly developed for sand-bed river application and there was no in-built gravel transport formulation which can simulate sediment transport for gravel-bed rivers. Therefore, a relatively recent gravel transport formula the Wilcock and Crowe (2003) surface based gravel transport formula which is best described as a modified Parker (1990) gravel transport formulation was coded and incorporated into the MIKE 21C sediment transport and morphological module.

The key steps of a typical two-dimensional model development were followed in this study, beginning with the grid generation, bathymetry preparation, initial and boundary conditions setting, riverbed roughness calibration and ending with successful model simulation. The grid generation process was consists of number of generating small sub-grids and merging them together to form a larger grid with various cell sizes. Orthogonal curvilinear grid (mesh) generation for a large braided river, which consists of various sizes of bars and islands, takes a significant amount of time. There were a total of 64,310 (1090 × 59) cells in the grid for the entire 70 km gravel reach. The reach length of the Lower Fraser River which has been used in the two-dimensional sediment transport and morphological simulation model with 15-30 m variable grid spacing was considerably larger than any previously used simulation model in this reach. A pre-prepared digital elevation model (DEM) data was imported into the grid to create

the riverbed topography as accurately as possible. Two separate DEM's, one from 1999 Public Works Canada (PWC) survey data and the other from 2003 PWS survey data were used for model development. Initially 1999 PWC survey data were used for model development and calibration and 2003 PWC survey data were used for gravel removal scenario simulation.

Hydrodynamic calibration of such a large two-dimensional model is a tedious task. Sensitivity analysis was performed to determine the most sensitive calibration parameter. The riverbed roughness coefficient appeared to be more sensitive than any other model parameters such as eddy viscosity or, simulation time step. A distributed Manning-Strickler bed-roughness map produced the best model calibration results in MIKE 21C. The simulated water surface elevation was calibrated within ± 0.10 m against the observed data. In River2D, bed-roughness element heights "k_s" were used and calibration results were comparable with the MIKE 21C model calibration results. Both models show a similar pattern in terms of distributed bed-roughness values. In the bed-roughness map, three different roughness zones were identified between the Agassiz-Rosedale Bridge and Sumas Mountain. Both models need higher bed-roughness values between Greyell Island and Foster Bar area.

The calibrated MIKE 21C hydrodynamic model was verified against an individual set of observed data (18 June, 2002 data). A match between observed water levels and simulated water levels was found within ± 0.20 m. Simulated depth-average velocities were extracted from specific locations (x, y coordinates) near the Agassiz-Rosedale Bridge and compared with observed aDcp velocities. The simulated velocities with MIKE 21C model showed somewhat better performance than the velocities from the River2D model. It is not clearly understood why MIKE 21C gave better results. The results might be due to grid cell size, bed friction factor, or proximity to the upstream boundary to the aDcp data site. In general, the model was verified in terms of water level and velocity fairly well.

A new sub-grid and corresponding bathymetry and bed roughness between Agassiz-Rosedale and Sumas Mountain (approx. 33 km) was extracted from the calibrated hydrodynamic model and used for the gravel transport and morphological simulation. There were a total of 30,031 (509 col. × 59 row) cells in the sediment transport grid. The sediment

transport bathymetry was exactly the same as hydrodynamic model except near the upstream and downstream boundaries. Fraser River discharges at Hope were set about two and a half kilometers upstream of the Agassiz-Rosedale Bridge near Herrling Island as the new upstream boundary condition and the downstream boundary was set near Sumas Mountain, which is virtually the end of the gravel reach (McLean and Church, 1990). A stage-discharge rating curve at Sumas Mountain was used as the downstream boundary. For all steady-state discharges, the downstream water level boundary at Sumas Mountain was directly selected from this rating-curve during sediment transport simulation.

Sediment transport simulation was started with the threshold gravel transport discharge at 5,000 m^3/s. It is believed that at discharges less than 5,000 m^3/s, no significant gravel transport occurs in Lower Fraser River (McLean et al., 1999a). The flow over shallow depths may create locally high velocity and shear stress, and simulate high bedload discharge for a model cell. Practically, this might not be the case. This unrealistically high shear stress is a problem and difficult to control without implementing a shear stress check. To control this problem the code has been modified in such a way that the model will not calculate bedload discharge in a cell when the shear stress value exceeds a certain prescribed value. This value was set based on the probable averaged maximum and minimum velocity values that may occur in the Lower Fraser River. Even with this control, unreasonably high shear stresses were found in shallow water depths and near the bank. These cells were identified by two-dimensional bedload discharge vector plot. All of these cells were identified manually and excluded from the bedload discharge calculation, a tedious process. Due to the local high shear stress, the model produced a small amount of bedload discharge when flow was less than 5000 m^3/s. Therefore, It may be assumed that the threshold water discharge value probably lies between 4000 and 5000 m^3/s in this reach to initiate bedload transport.

6.2 Summary and Evaluation of the Computational Gravel Budget

One of the key objectives of this study was to prepare a gravel budget for the Lower Fraser River gravel reach by using the computational technique and this objective was fulfilled very well. The surface-based gravel transport formula of Wilcock and Crowe (2003) was selected. The sediment transport model was calibrated against the existing bedload rating curve developed at Agassiz-Rosedale Bridge and was prepared by McLean and Church (1999). Average annual gravel influx at the Agassiz-Rosedale Bridge was calculated by the integration of bed-load discharge rating curve with the flow duration curve. This method was described as "Method 1".

The Wilcock and Crowe (2003) surface-based gravel transport formula uses a dimensionless reference shear stress that was used as a calibration parameter in the sediment transport model. Parker (1990) recommended a dimensionless reference shear stress value 0.0386 (based on Oak Creek, Oregon data) for a gravel-bed river but the simulated bedload discharge based on the Wilcock and Crowe (2003) formulation underestimated the observed values at the Agassiz-Rosedale Bridge. Wilcock and Crowe (2003) showed that the dimensionless reference shear stress value could be substantially lower in gravel-bed rivers with a higher sand content on the bed, and that the dimensionless reference shear stress of a gravel-bed river might as low as 0.020 depending on the percentage of surface sand content in the riverbed (Wilcock and Crowe, 2003). Trial values of dimensionless reference shear stress as low as 0.020 were used during the calibration procedure and compared to the observed data. A close match with the observed data was achieved with a dimensionless reference shear stress 0.025.

Average annual gravel influx at the Agassiz-Rosedale Bridge based on Method 1 was approximately 159,000 t/y (90,000 m^3/y), which is 42,000 t/y higher than the McLean and Church (1999) gravel influx estimation based on 20 years (1966 to 1986) observed data of 117,000 t/y. McLean et al. (1999) adjusted annual load based on sampler calibration and assigned an error bound 40% around the annual estimates (Ham, 2005a). The most recent estimation has shown much higher mean annual gravel influx at the Agassiz-Rosedale Bridge (Ham, 2005a). Therefore, the higher mean annual bedload transport rate at Agassiz is expected.

This method is a statistical method because it depends on flow frequency. It basically produces a section averaged bedload discharge at a station that is comparable with one-dimensional model output.

A distributed gravel budget was produced for the entire reach by applying the Wilcock and Crowe (2003) surface based gravel transport formula and direct simulation and a volume balance method was used to produce a computational mean annual gravel budget for the Lower Fraser River gravel reach. This method was described as Method 2. In Method 2, the bed level changes between 1999 and 2003 for observed and simulated results were compared against each other. Visual comparison and thalweg elevations comparison was used. It was expected that two results would not be matched exactly but may show some degree of similarity between them. However, very close visual match could not guarantee that the transport rate would be similar in both cases. Due to the relatively poor visual comparison of bed level changes, a thalweg elevation comparison was performed as an alternative approach to verify the sediment transport and morphological model. Simulated thalweg elevations match fairly well with the observed thalweg except at a few locations. The thalweg near upstream and downstream boundaries did not match because of artificial manipulation of bathymetry near the boundaries. From this observation it can be stated that the shear stress based two-dimensional model works well in relatively deeper parts of the channel (thalweg) where velocity and shear stress remain within a reasonable limit.

A volume balance was performed to find the net sedimentation in the model reach. To validate the model and compare the results with the results obtained from the morphological approach (Ham, 2005a), the entire model area was divided into 33 zones. The approximate length of each area was 1 km and the cell number was similar to the number used in the morphological approach (Ham, 2005a). The erosion or deposition depth in each model cells was calculated by comparing the initial bed elevation and final bed elevation. Then, erosion or deposition volume for a model cell was calculated by multiplying the depth changes by the cell area. A net volume was calculated over each 1 km wide zone for both observed and simulated cases as total volume of deposition minus total volume of erosion over each zone (1 km). For comparison, these values were plotted against the result obtained from the morphological

method. Even though there are some discrepancies among the results, observed, simulated and morphologically based results follow a similar trend. The most appropriate comparison was between the values obtained directly from the MIKE 21C observed and simulated changes.

The net volume change over a period was total volume of deposition minus total volume of erosion for that period. If the net volume is positive, then accumulation is occurring and if the net volume is negative then the zone is degrading. The net observed and simulated volumes were 2,550,000 m^3 and 2,500,000 m^3 over the 4 years period, respectively. The mean annual observed and simulated gravel influxes were 638,000 m^3/y and 626,000 m^3/y, respectively. This computational gravel budget results fairly closely matches the 1999-2003 morphological gravel budget of 616,000 m^3/y (Ham, 2005a). Both observed and simulated results show positive values which means the riverbed aggrades. The simulated volume is not significantly lower than the observed volume. In the computational gravel budget, equilibrium transport rate was calculated as a function of discharge only but actually transport rate also depends on the sediment availability. Moreover, the surface based gravel transport equation was used, which assumed that the net changes are due to gravel transport only and sands are in suspension when bedload transport occurs. Practically, small portions of sands are part of the total observed volume change. As a result, mean annual gravel influx based on the gravel transport function produced a lower volume over 4 years than the observed influx. From these results, it can be concluded that the computational method is a useful and cost effective method for gravel budget computation with some of limitations.

Aggradation and degradation zones were identified by direct comparison of simulated bathymetry with the observed 1999 bathymetry as described in sub-section 4.7. The net simulated volume was calculated over one kilometer lengths starting from Sumas Mountain to 3 km upstream of Agassiz-Rosedale Bridge to compare the results with the results obtained from the morphology based method (Ham, 2005a). Positive or negative volume over a 1 km long cell indicates aggradation or degradation respectively, for that zone. Finally, the nominal aggradation/degradation rate (m/y) over each 1-km long zone was determined assuming a nominal active channel width of 500 m. A comparison was made with Ham (2005) results. Except in one place, simulated results showed similar aggradation and degradation patterns but

rate may vary. A total of 21 aggradation, 10 degradation and 2 neutral (no change) zones are found along the gravel reach.

6.3 Summary and Evaluation of the Gravel Removal Operations

A total of 12 gravel removal sites; Queens Bar, Harrison Bar (Site 1, Site 2, Site 3 and Site 4), Gill (East, West and South), Hamilton (South and North), and Big Bar (South and North) were assessed to determine the morphological changes with and without gravel removal. The average depth change between two subsequent years for an extraction site was calculated by summation of the net volume divided by the extraction area for that site. A total of nine sites were found to aggrade slowly and one site aggraded moderately. Two sites were found to aggrade rapidly. Gravel recovery was slow after removal operation on Queens Bar, Harrison Bar (3 sites), Gill Bar, Hamilton Bar and Big Bar sites. Faster gravel recovery was shown on Harrison Site 3 and Big Bar South sites over the 10 years from the extraction date (2003). Fresh gravel will be accumulated on all the removal sites except Gill (East) and Big Bar (North). Erosion will continue on these two sites after gravel removal.

Morphological changes inside the channel were calculated by comparing the depths and cross-section shape from one year to the next year. Channel shape changes at the upstream or downstream of a gravel extraction site depend on the extraction amount, area, and location. Some sites such as Queens Bar and Big Bar, were highly sensitive to the extraction and some sites such as Gill (North) Bar, were not. All results are based on a shear stress based sediment transport equation, which is a function of channel discharge only. The discharge time series was based on historical flow data but the future 10-year's real flow data may be significantly different from that. Hence, there is no guarantee that the predicted morphological changes must occur after gravel removal from these sites. The assessments of the various gravel removal sites present in this thesis are solely case studies. It is also note that there is no better means presently available which can predict the result for the future period. Therefore, simulation model study appears to be an affordable and reasonable option for future morphological change prediction. It is also worth mention here that morphological change prediction is good for a limited period, for example 5 to 10 years (Enggrob, 1998).

6.4 Evaluation of the 2-D Gravel Transport Model as a Flood Management Tool

Bed level aggradation along the Fraser River Gravel above Sumas Mountain is a consequence of ongoing gravel deposition. The long-term, average aggradation rate, based on an annual influx of 250,000m^3 of gravel past Aggasiz-Rosedale Bridge, is in the order of perhaps 1 cm per year. Locally, however, changes in channel alignment and local deposition rates that may be temporarily much greater. The rationale for ongoing gravel removal is to offset the annual gravel influx, and to maintain the bed elevation more or less at its current elevation. Gravel removal would generally have little immediate, significant impact on water levels. Thus, gravel removal has limited capacity to address any current deficiencies in flood protection, and it seems that these must be addressed primarily though dike improvement, or through other non-structural approaches.

The present study demonstrates possible future morphological consequences of gravel removal. This study is not able to assess the direct impact on fisheries habitat as a consequence of gravel removal. Use of this model output in a habitat modeling tool may shed some light on aquatic habitat issues. The present Lower Fraser River flood profile estimation was based on a one-dimensional MIKE 11 model simulation result. For more precise design floodwater surface estimation, the developed two-dimensional numerical model may be applied as a supplement to the existing one-dimensional model.

6.5 Conclusions

1. A distributed gravel budget for the Fraser River gravel reach was computed using the two-dimensional MIKE 21C code that was modified to include the surface-based gravel transport algorithm of Wilcock and Crowe (2003).

2. A key parameter in the bedload transport simulation is the dimensionless reference (or, critical) shear stress in the Wilcock and Crowe (2003) algorithm. This parameter value may range from 0.037 to 0.021, and is sensitive to the sand content in the gravel mixture. For the current study, a comparatively low value of 0.025, consistent with about 20%

sand content in the bulk gravel mixture, was necessary to provide agreement with the next gravel influx volume from 1999-2003 obtained by Ham (2005a) which was obtained from repeat channel surveys.

3. The longitudinal distribution of sediment aggradation and degradation between 1999 and 2003 determined for the computational sediment budget (Figure 5.14) was generally consistent with that determined by Ham (2005a). This suggests that, once calibrated, the computational model can be used to identify broad zones of aggradation, degradation and morphological change.

4. When bed level change comparison between 1999 and 2003 are made on a cell-by-cell basis the R^2 value was 0.76 [Figure 5.9 (D)]. Approximately 95% of the bed level change values were within ± 2 m range. The root mean square error (RMSE) value of the observed and simulated bed level changes is 0.63 m.

5. A number of proposed gravel removals sites were simulated over a 10-year post removal period to determine the effects of removal and the subsequent "recovery" at the site. At present these represent valuable exercise, as there are no data available to verify the performance of the model at such a small scale.

6. The net effect on the design flood level of the gravel removals in this study was local and marginal, less than about 15 cm. This is consistent with the results obtained by UMA (2001a). The justification for gravel removal is to offset continued aggradation and to maintain the current design flood profile.

6.6 Future Work

The main limitations identified in this study are insufficient bedload discharge data, the large scale of the gravel reach, the required time step versus computational power, and spurious shear stress values near the bank during sediment transport simulation. These issues should be investigated in any future research.

Insufficient bedload discharge data was the main limitation for this modeling study. Bedload discharge data was available only one location at Agassiz-Rosedale Bridge which is 23 years old (station discontinued since 1986) and showed high variability between water discharge and bedload discharge (scattered in the bedload rating curve plot). Additional bedload discharge measurement data along the gravel reach between Herrling Island and Mission is required to better calibrate and validate the bedload transport model. Bedload discharge data from four new temporary stations at Cheam View near WSC water level Gauge # 44, Foster Bar, Island 76, Nicomen Island near Gauge # 41 plus two existing stations at Agassiz-Rosedale Bridge and Mission are recommended.

Gravel reach is approximately 33 km in length with an average width of 500 m. For a 25 m^2 grid size (roughly 5 m × 5 m) total 660,000 grid cells are required which would not be feasible to run with a 5-second time step (which is required to satisfy the CFL condition). A direct unsteady simulation from 1999 to 2003 was not possible due to this time constraint, which is a major limitation of using MIKE 21C model. In future study, an assessment of various grid sizes, time-steps, total simulation time and maximum feasible reach length are recommended before applying this tool in Fraser River gravel reach or any other gravel transport study.

Spurious high shear stress values were computed in locations along banks and bar edges where the shallow water depths combine with and high velocities. In this study, maximum shear stress and minimum water depth criteria were established to identify and correct these errors. This issue, common to many 2D models, requires further work to resolve

The simulations of morphological change at and adjacent to gravel removal sites were not verified in this study. It is recommended that several actual gravel removal sites be monitored and resurveyed over several years following removal in order to document actual changes and to provide data to fully assess the ability of two-dimensional morphological models to predict the changes.

REFERENCES

ASCE (2004). ASCE Task Committee on Computational Modeling of Sediment Transport Processes Journal of Hydraulic Engineering, ASCE, July 2004, pp. 597-598.

Ashida, K. and Michue, M. (1971). An investigation of riverbed degradation downstream of a dam. Proceeding, 14th International Association of Hydraulic Research Congress, Vol. 3, Wallingford, U.K., 247–255.

Bathurst, J.C. (1985). Flow Resistance Estimation in Mountain Rivers. Journal of Hydraulic Engineering, ASCE 111(4), 625–643.

Bathurst, J.C. (1993). Flow resistance through the channel network. In: Beven, K., Kirkby, M.J. (Eds.), Channel Network Hydrology. John Wiley and Sons, Chichester, UK, pp. 69–98.

Becchi I. (1979). Some observations on a two-dimensional model of bed-load transport based on the moving layer equation. Meccanica, Springer Netherlands, Vol-14 (March), pp 19-25.

Busto, V. (2005). Gravel Removal Site selection for Lower Fraser River. Personal Communication.

Chang, H.H. (1988). Fluvial Processes in River Engineering, John Wiley and Sons New York, USA.

Chaudhry, M.H. (1993). Open channel Flow. Prentice Hall, Englewood Cliffs, New Jersey, U.S.A.

Church, M. (2001a). River science and Fraser River: who controls the river? In Gravel-Bed Rivers V, M.P. Mosley [Ed]. Wellington: New Zealand Hydrological Society, 607-631.

Church, M. (2001b). Gravel Management in Lower Fraser River. Report prepared for City of Chilliwack.

Church, M. (2003). Sediment Size distribution data -Personal communication.

Church, M. and McLean, D.G. (1994). Sedimentation in Lower Fraser River, British Columbia: implications for management. In The Variability of Large Alluvial Rivers: 221-241, Schumm, S.A. and Winkley, B.R. (eds.), ASCE, Monograph.

Church, M., Ham, D. and Weatherly, H. (2000). Sedimentation and flood hazard in the gravel reach of Fraser River: Progress report 2000. Report for District of Chilliwack, September 2000.

Church, M., Ham, D. and Weatherly, H. (2001). Gravel Management in Lower Fraser River: Report for District of Chilliwack, B.C., October 2001.

Chaudhry, M. (1993). Open channel flow. Prentice-Hall, Inc. New Jersey, USA.

Colby, B. (1957). Relationship of unmeasured sediment discharge to mean velocity, EoS Translation, AGU, 38, pp 707-717.

Cunge, J.A., Holly, F.M., Verwey, A. (1980). Practical Aspects of Computational River Hydraulics, Pitman, London.

Desloges, J.R. and Church, M. (1989). Wandering gravel-bed rivers. The Canadian Geographer, 33(4), 360-364.

De Vriend, H.J. (1977). A mathematical model of steady flow in curved shallow channel. Journal of Hydraulic Research, 15(1), 37–54.

De Vriend, H. (1980). Velocity redistribution in curved rectangular channels. Journal of Fluid Mechanics, 107, 423–439.

De Vriend, H.J. (1987) Analysis of horizontally two-dimensional morphological evolutions in shallow water, Journal of Geophysical Research, 92(C4), 3877-3893, 1987.

DHI Water and Environment (2002a). MIKE 21C – River Hydrodynamics and Morphology – Reference Manual.

DHI Water and Environment (2002b) MIKE 21 Hydrodynamic Module and Scientific Documentation.

DHI Water and Environment (2003). MIKE 21 – Coastal Hydraulics and Oceanography, Hydrodynamic Module– Scientific Documentation, DHI, Agern Alle, Horsholm, Denmark.

DHI Water and Environment (2004). MIKE 21C River Morphology – A short description.

Dietrich, W.E. and Whiting, P.J. (1989). Boundary shear stress and sediment transport in river meanders of sand and gravel. In: Ikeda, S. and Parker, G. (Eds). River Meandering. Water Resource Monograph 12, American Geophysical Union Monograph, pp. 1–50.

Duan, J.G. (2004). Simulation of flow and mass dispersion in meandering channels. Journal of Hydraulic Engineering, 566–576.

Duan, J.G., Julien, P. (2005). Numerical simulation of the inception of meandering channel. Earth Surf. Process. Land Forms 30, 1093–1110.

Duan, J.G., Wang, S.S.Y., and Jia, Y.F. (2001). The applications of the enhanced CCHE2D model to study the alluvial channel migration processes. Journal of Hydraulic Research, 39(5), 469-480.

Duan, G.J., Wang, S.S.Y. and Yafei J. (2002). The applications of the enhanced CCHE2D model to study the alluvial channel migration. Journal of Hydraulic Research, Vol. 39, 2001, No. 5, pp 1-12.

Einstein, H.A. and Barbarossa, N. (1952). River channel roughness. Translation ASCE, 117, 1121-1146.

Engelund, F. (1974). Flow and bed topography in channel bends. Journal of the Hydraulics Division of the American Society of Civil Engineers, 100: 1631–1648.

Enggrob, H.G. (1998). Morphological forecast simulation of Jamuna River in Bangladesh Danish Hydraulic Institute, Hørsholm, Denmark.

Fang, C. (2003). Simulation of Bend Secondary Flow Effect in 2D Depth-averaged Model. Journal of China Institute of Water Resources and Hydropower Research, Vol. 1, No.3.

Fraser Basin Council (2001). Draft Interim Fraser River Management Plan: Hope to Mission, January 2000: pp 5.

Fraser Basin Council (2003). A Snapshot on Sustainability: State of the Fraser Basin Report.

Gessler, D., Hall, B., Spasojevic, M., Holly, F., Pourtaheri H. and Raphelt N. (1999). Application of 3D mobile bed hydrodynamic model. Journal of Hydraulic Engineering, ASCE, vol.125, No. 5, pp 535-549.

Ghanem, A.H., Steffler P.M., Hicks F.E. and Katopodis C. (1996). Two dimensional finite element flow modeling of physical fish habitat, Regulated Rivers: Research and Management, Vol. 12, pp. 185-200.

Gomez, B. and Church, M.A. (1989). Assessment of Bed Load Sediment Transport Formulae for Gravel-bed Rivers. Water Resources Research, Vol. 25, No. 6, p 1161-1186.

Grade, R.J. and Raju R.K.G. (1977). Mechanics of Sediment Transport and Alluvial Stream Problems. Wiley Eastern Ltd., New Delhi, India.

Graf, W.H. (1971). Hydraulics of Sediment Transport. McGraw-Hill, Inc., New York.

Griffiths, G.A. (1981). Flow resistance in coarse gravel-bed rivers, Journal Hydraulic Division ASCE, 107(HY7), 899–918.

Ham, G.D. (2005a). Morphodynamics and sediment transport in a wandering gravel-bed channel: Fraser River, British Columbia. Unpublished Ph.D. thesis, University of British Columbia, 210p.

Ham, G.D. (2005b). Personal communication during his research in Department of Geography, UBC (2002-2005).

Ham, D. and Church, M. (2003). The sediment budget in the gravel-bed reach of Fraser River: 2003 revision. University of British Columbia, Department of Geography. October 2003.

Henderson, F.M. (1966). Open channel flow. Prentice-Hall, Inc., Upper Saddle River, NJ.

Hey, R.D. (1979), Flow resistance in gravel-bed rivers, Journal Hydraulic Division ASCE, 105(HY9), 365–379.

Hicks D.M. and Mason P.D. (1991). Roughness Characteristics of New Zealand Rivers. New Zealand Water Resources, Survey, National Institute of Water and Atmospheric Research, New Zealand.

Hicks, F.E. and Steffler, P.M. (1992). Characteristic dissipative Galerkin scheme for open-channel flow. Journal of Hydraulic Engineering, ASCE, 118: 337-352.

Ikeda, S. and Nishimura, T. (1986). Flow and bed profile in meandering sand-silt rivers. Journal Hydraulic Division ASCE, 112(7), 562–579.

Ikeda, S., Parker, G, and Sawai, K. (1981). Bend theory of river meanders 1: Linear development. Journal of Fluid Mechanics 112: 363–377.

Islam, M. and Hassan, K.I. (2002). Prediction through Mathematical Morphological Modeling for the Design of Engineering Proceedings: Measures, Modeling and Simulation, Editor Hamza, M.H., Published by ACTS, USA.

Islam, S. and Millar, R.G. (2005). Gravel Transport and Morphological Modeling for the Lower Fraser River, British Columbia, 17th Canadian Hydrotechnical Conference, Edmonton, Alberta, CSCE.

Jain, S.C. (2001). Open-Channel Flow. John Wiley and Sons, New York.

Jansen, P.PH., van Bendegom, L., van Den Berg, J., de Vries, M., Zanen, A. (1979). Principles of River Engineering. The non-tidal alluvial river. London, UK Pitman.

Kassem, A.A. (1996). Modeling of Sediment Transport in Unsteady, Two-Dimensional, Open-Channel Flows, unpublished Ph.D. Thesis, Washington State University.

Kassem, A.A. and Chaudhry, M.H. (2002). Numerical Modeling of Bed Evolution in Channel Bends. Journal of Hydraulic Engineering, ASCE, 128(5), 505-514.

Kalkwijk, J.P.T. and de Vriend, H.J. (1980). Computation of the flow in shallow river bends. Journal of Hydraulic Research 18(4), 327–342.

Kellerhals A. M. (1967). Stable channels with gravel beds. Journal of Water and Harbors Division, American society of Civil Engineering, 93(WW1), 63-84.

Kellerhals Engineering Services (1987). Effects of gravel mining on the salmonid resources of the Lower Fraser River. Report prepared for Department of Fisheries and Oceans, Habitat Management Division. 43 p.

Krishnappan, B.G. (1981). Field Verification of an Unsteady Nonuniform Mobile Boundary Flow Model. Proceedings, XIX Congress of IAHR, New Delhi, India, 1981.

Kuipers, J. and Vreugdenhill (1973). Calculation of two-dimensional horizontal flow. Report S163, Part I, Delft Hydraulics Lab, Delft, The Netherlands.

KWL (2001). 2002 Fraser River Gravel Removal- Final Report submitted to British Columbia Ministry of Water, Land and Air Protection by Kerr Wood Leidal Consulting Engineers.

KWL (2002). 2003 Fraser River Potential Gravel Removals- Final Report submitted to Fraser Basin Council by Kerr Wood Leidal Consulting Engineers.

KWL (2003). 2004-2008 Fraser River Potential Gravel Removal Sites- Final Report submitted to Land and Water BC Inc. by Kerr Wood Leidal Consulting Engineers.

Lai C., Baltzer R.A., Schaffranek R.W. (2002). Conservation-form equations of unsteady open-channel flow Journal of Hydraulic Research, Vol. 40, NO. 5, pp567-578.

Lane, S.N., Richards, K.S. (1998). Two-dimensional modeling of flow processes in a multi-thread channel. Hydrological Processes 12, 1279–1298.

Lane S.N., Bradbrook K.F., Richards K.S., Biron P.A. and Roy A.G. (1999). The application of computational fluid dynamics to natural river channels: three-dimensional versus two-dimensional approaches. Geomorphology, 29, 1-20.

Leopold, L.B., Bagnold, R.A., Wolman, M.G. and Brush, L.M. (1960). Flow resistance in sinuous or irregular channels. USGS Professional Paper 282D, 111–135.

Lien, H.C., Hsieh, T.Y., Yang, J.C., and Yeh, K.C. (1999). Bend flow simulation using 2D depth-averaged model. . Journal of Hydraulic Engineering, 125(10), 1097–1108.

Li, S. and Millar, R.G. (2004). A computational distributed gravel budget for the lower Fraser River, British Columbia. Draft submitted for review and presentation at Riverflow 2004, Naples Italy, June 2004.

Li S., Millar R.G and Islam S. (2008). Modeling Gravel Transport and Morphology for the Fraser River, British Columbia, Geomorphology, Elsevier, Volume 95 (3).

Luettich, R. A. Jr., Westerink J.J., Scheffner, Norman W. (1991). ADCIRC: An advanced three-dimensional circulation model for shelves, coasts and estuaries. Report 1: Theory and methodology of ADCIRC-2DDI and ADCIRC-3DL. Final Report prepared for U.S. Army

Corps of Engineers, University of North Carolina at Chapel Hill, Institute of Marine Sciences, Morehead City, NC, 150 pp.

McLean, D.G. and Church, M. (1986). A re-examination of sediment transport observations in the lower Fraser River. Environment Canada, Water Resources Branch, Sediment Survey Section. Report IWD-HQ-WRB-86-62. 56 p + figs + tables.

McLean, D.G. and Church, M. (1990). Sedimentation in Lower Fraser River, British Columbia: Implications for Management. The variability of Large Alluvial Rivers, ASCE: 221-241.

McLean, D.G., Church, M. and Tassone, B. (1999a). Sediment transport along lower Fraser River 1. Measurements and hydraulic computation. Water Resources Research, 35, 8, 2533-2548.

McLean, D.G. and Church, M. (1999b). Sediment transport along lower Fraser River 2. Estimates based on the long-term gravel budget. Water Resources Research, 35, 8, 2549-2559.
McLean, D.G. (1990). Channel Instability on lower Fraser River. Unpublished PhD thesis, University of British Columbia, 290p.

McArdell, B.W. and Faeh, R. (2000). A computational Investigation of River Braiding. Fifth International Gravel-Bed Rivers Workshop, Christchurch and Franz Josef Glacier, New Zeland, 53-93.

Meyer-Peter E. and Muller R. (1948). Formulas for bed-load transport. 2nd Congress of the International Association for Hydraulic Structures Research, Stockholm, 7–9 June, 1948, Proceedings, Appendix 2, 26pp.

Millar, R.G. and Quick M.C. (1993). Effect of bank stability on geometry of gravel rivers. Journal of Hydraulic Engineering, ASCE, vol.119, No. 12, pp 1343-1363.

Millar, R.G. (1999). Grain and form resistance in gravel-bed rivers. Water Resources Research, 37(3), 303-312.

Millar, R.G. and Barua, D.K. (1999). Hydrodynamic model selection study for the Lower Fraser River between Laidlaw and Mission. Submitted to the District of Chilliwack, Chilliwack, BC.

Ministry of Environment, Lands and Parks B.C. (1999). Ortho Imagery: Fraser River Gravel Reach, January 1999.

Molls, T. and Chaudhry, M.H. (1995). Depth-averaged open-channel flow model. Journal of Hydraulic Engineering, ASCE, 121(6), 453–465.

Morvan, H., Pender, G., Wright, N.G. and Ervine, D.A. (2002). Three-Dimensional Hydrodynamics of Meandering Compound Channels. Journal of Hydraulic Engineering, ASCE, Volume 128(5), 654-682.

Nagata, N., Hosoda, T., Muramoto, Y., and Rahman, M. (1997). Experimental and numerical studies on meandering channels with bank erosion. In Eddy Langendoen, Sam S.Y. Wang and J.F.D. Shields, editors, Proceedings of the Conference on Management of Landscape Disturbed by Channel Incision, the University of Mississippi, 262-267.

nhc (1996). Fraser River stability upstream from Agassiz/Rosedale Bridge. Report for Cheam Indian Band, February 1996. 5 pp + figures.

nhc (2000). Flood and Erosion Damage Mitigation Plan, Lower Fraser Valley. Report prepared for FNESS.

nhc (2002). Review of Fraser River Sediment Budget, Final Report. Report prepared for Fraser River Estuary Management Program, 27 p.

nhc (2004). Fraser River Gravel management 2-D Numerical Modeling: Tranmer Bar to Harrison Bar, Final Report submitted to City of Chilliwack, Fisheries and Ocean Canada, Fraser Basin Council, Land Water BC and MoE BC by Northwest Hydraulics Consultants.

nhc (2006). Lower Fraser River Hydraulic Model, Final Report submitted to Fraser Basin Council, by Northwest Hydraulics Consultants.

Odgaard, A. (1989). River meander model. I: Development. Journal of Hydraulic Engineering, ASCE, 115(11), 1433–1450.

Olesen, K.W. (1987). Bed topography in shallow river bends, Communication Hydraulic 917 Geotechnical Engineering 87-1, Delft University of Technology, Delft, Netherlands.

Parker, G., Klingeman, P.C., and McLean, D.G. (1982). Bedload and Size Distribution in Paved Gravel-Bed Streams. Journal of the Hydraulics Division, 108(HY4), 544-551.

Parker, G. (1990). Surface based bedload transport relation for gravel rivers. Journal of the Hydraulic Research, Vol. 28, No. 4. 415-436.

Raphelt, N.K., and Alexander, M.P. (2001). Multidimensional models used in rivers and streams, Coastal and Hydraulics Engineering Technical Note CHETN-VII-2, U.S. Army Engineer Research and Development Center, Vicksburg, MS.

Raudkivi, A. (1998). Loose Boundary Hydraulics, Balkema, Rotterdam, The Netherlands.

Rozovskii, I. (1957). Flow of water in bends of open channels, Academy of Sciences of Ukrainian S.S.R., Translated from Russian, Israel Program for Science Translation, Jerusalem, 1961, 1–233.

Schumm, S.A, (1963). A tentative classification of alluvial river channels: U.S. Geol. Survey Circ.477, 10 p.

Steffler, P. and Blackburn, J. (2002). River2D: Two-Dimensional Depth Averaged Model of River Hydrodynamics and Fish Habitat, University of Alberta, Edmonton, Alberta, Canada.

SWMC/DHI (2000a). Mathematical Morphological Modeling on the Meghna River at Bhairab Bridge, Final Report.

SWMC/DHI (2000b). Morphological Impact in the vicinity of the existing Bhairab Railway Bridge due to dredging.

SWMC (2000). Morphological Forecast Simulation of Jamuna River In Bangladesh. Final Report.

SWMC, (2001). Southwest Road Network Development Project: Construction of Bridge over Arial Khan River, Final Report, Hydraulic Mathematical Modeling Study, February 2001.

Shimizu, Y., Yamaguchi, H., and Itakura, T. (1990). Three-Dimensional Computation of Flow and Bed Deformation. Journal of Hydraulic Engineering, 116(9), 1090-1108.
Shimizu, Y. and Itakura, T. (1989). Calculation of bed variation in alluvial channels. Journal of Hydraulic Engineering, ASCE, Vol. 115, No. 3, 367-384.

Steffler, P.M., and Jin, Y.C. (1993). Depth-averaged and moment equations for moderately shallow free surface flow. Journal of Hydraulic Research, 31(1), 5-15.

Steffler, P.M. (2000). River2D: Introduction to depth averaged modeling and user's manual. University Of Alberta, Edmonton, Alta.

Struiksma N., Olsen K.W., Flokstra C. and De Vriend H.J. (1985). Bed deformation in curved alluvial channels. Journal of Hydraulic Research 23: 57–78.

TELEMAC-2D (1995). TELEMAC-2D Modeling System: TELEMAC-2D Hydrodynamic Computation Software Version 3.0, Users Manual Direction des Etudes et Recherches, (in English).

Thorne, C.R., Zevenbergen, L.W., Pitlick, J.C. (1985). Direct measurement of secondary currents in a meandering sand-bed river. Nature 315, 746–747.

Thorne, C. and Hey, R. (1979). Direct measurements of secondary currents at a river inflection point. Nature (London), 280, 226–228.

UMA Engineering Ltd. (2001a). Fraser River gravel reach hydraulic modeling study. Submitted to the City of Chilliwack, Chilliwack, BC.

UMA Engineering Ltd with Ward & Associates Ltd. and Quick, M.C. (2001b). Fraser and Harrison Rivers hydrologic and hydraulic investigations. Final report prepared for The City of Chilliwack by UMA Engineering Ltd., Victoria.

USACE (1992). Shore Protection Manual, US Army Crops, Vicksburg.

USACE (2000). Users guide to SED2D WES, Version 4.5. U.S. Army Engineer Research and Development Center, USA.

Vanoni, V.A. [ed.] (1975). Sedimentation Engineering. ASCE Manuals and Reports on Engineering Practice. ASCE, New York.

Van Rijn (1987). Mathematical modeling of morphological processes in the case of suspended sediment transport, Delft hydraulics, Communication no. 382.

Van Rijn, L.C. (1993). Principles of sediment transport in rivers, estuaries and coastal seas. Aqua Publications, Amsterdam, The Netherlands.

Vasquez J.A., Millar, R.G. and Steffler, P.M (2005). Two-dimensional finite element river morphology model, Canadian Journal of Civil Engineering, CSCE, 34 (6), 752-760.

Vasquez J.A. (2006). Two-Dimensional Finite Element River Morphology Model, Unpublished Ph.D. thesis, University of British Columbia.

Vreugdenhill C.B. (1994). Numerical Methods for Shallow Water Flow. Water Science and Technology Library, Volume 13, Kluwer Academic Publishers, Dordrecht, The Netherlands.

Water Management Consultant (2001). Harrison Bar pilot channel preliminary investigation. Submitted to the City of Chilliwack, Chilliwack, BC by Water Management Consultants.

Weatherly, H. and Church, M. (1999). Gravel extraction inventory for Lower Fraser River (Mission to Hope) - 1964 to 1998. Report prepared for District of Chilliwack. Department of Geography, The University of British Columbia. 18 p.

Wilcock PR. (1998). Two-fraction model of initial sediment motion in gravel-bed rivers. Science 280: 410–412.

Wilcock, P. (2001). Toward a practical method for estimating sediment-transport rates in gravel-bed rivers. Earth Surface Processes and Landforms, 26, 1395-1408.

Wilcock, P.R., Kenworthy, S.T., and Crowe, J.C. (2001). Experimental study of the transport of mixed sand and gravel. Water Resources Research, 35(12), 3349-3358.

Wilcock, P.R., and Crowe, J.C. (2003). Surface-based Transport Model for Mixed-size Sediment. Journal of Hydraulic Engineering, ASCE, 129(2): 120–128.

Wu W. (2001). CCHE2D-2.1, Sediment Transport model, Technical report no. NCCHE-TR-2001-3, National Center for Computational Hydroscience and Engineering, The University of Mississippi, Mississippi.

Yang, C.T. (1996). Sediment Transport: Theory and Practice. McGraw-Hill, USA.

Ye, J., and McCorquodale, J. A. (1997). Depth-averaged hydrodynamic model in curvilinear collocated grid. Journal of Hydraulic Engineering, ASCE, 123(5), 380–388.

Yen, C.L., Ho, S.Y. (1990). Bed evolution in channel bends. J. Hydraulic Engineering 116 (4), 544–562.

Yusuf, F.M (2001). Application of a Two-dimensional Hydrodynamic model to the Fraser River gravel reach. Unpublished M. A. Sc. thesis, University of British Columbia, 168p.

APPENDIX A: QUEENS BAR
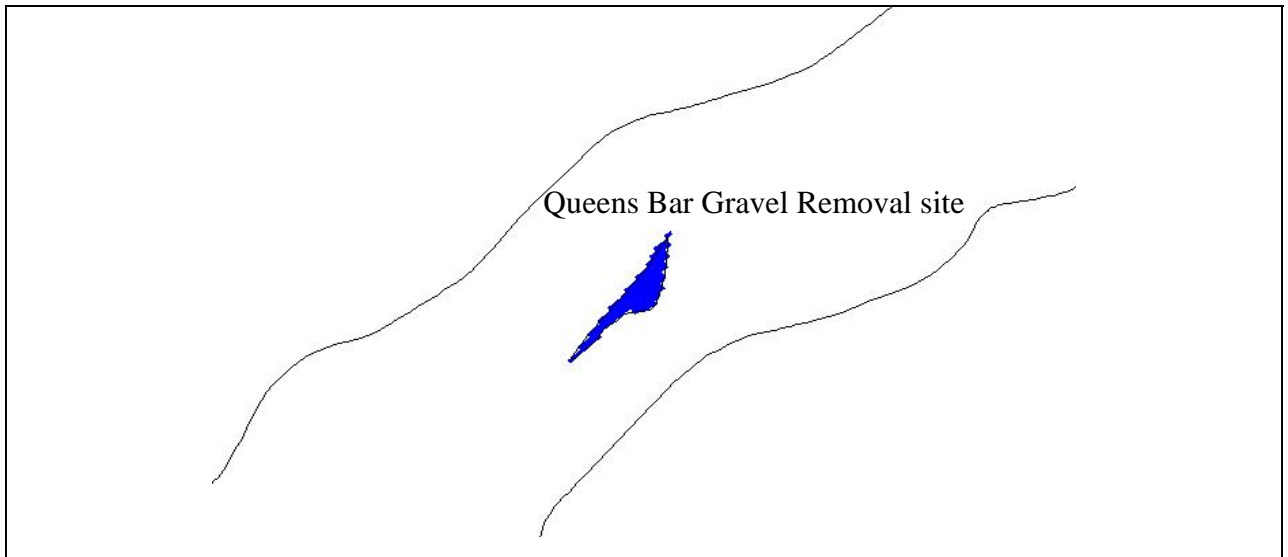
Figure A.1 Showing the Queens bar removal area in the model.
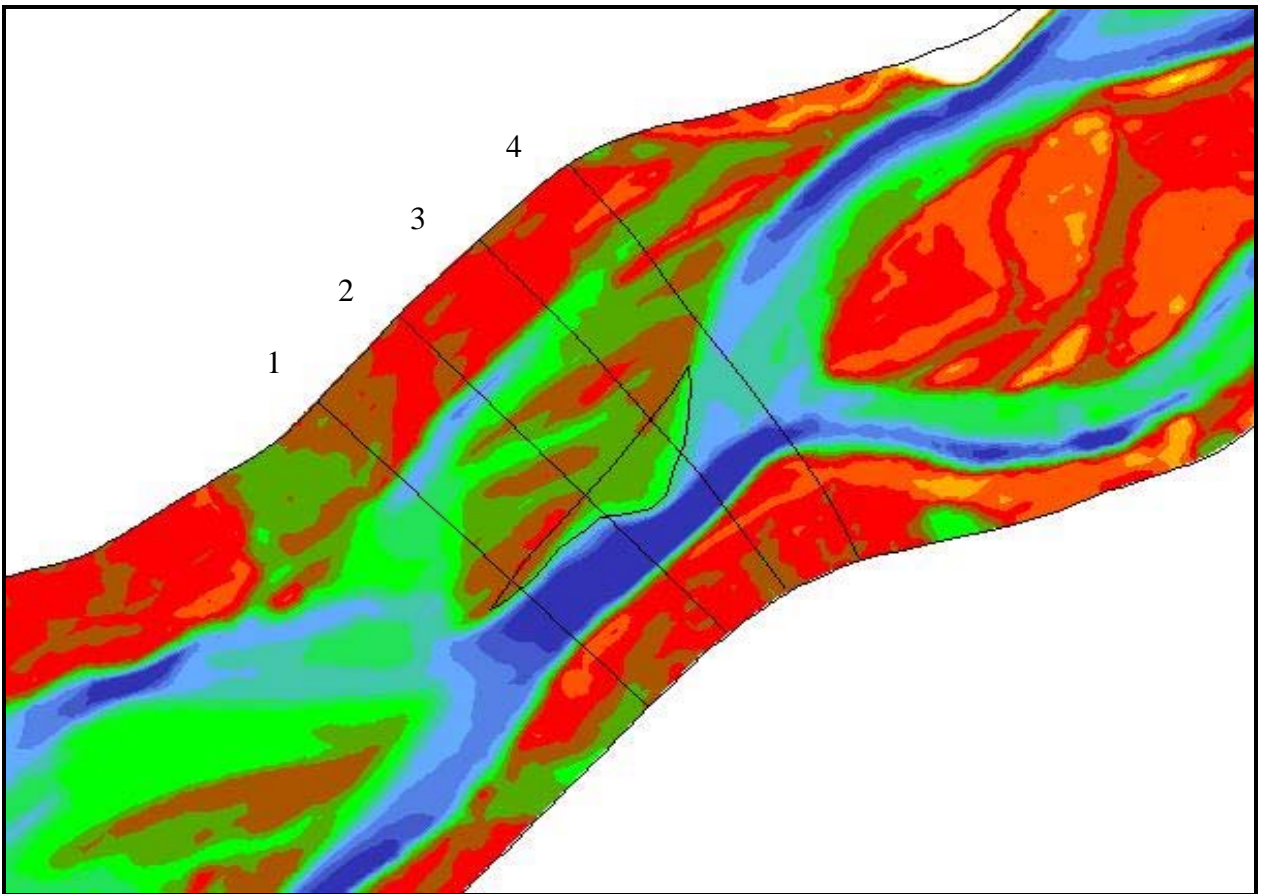
Figure A.2: Showing cross-Sections near Queens Bar gravel extraction site.
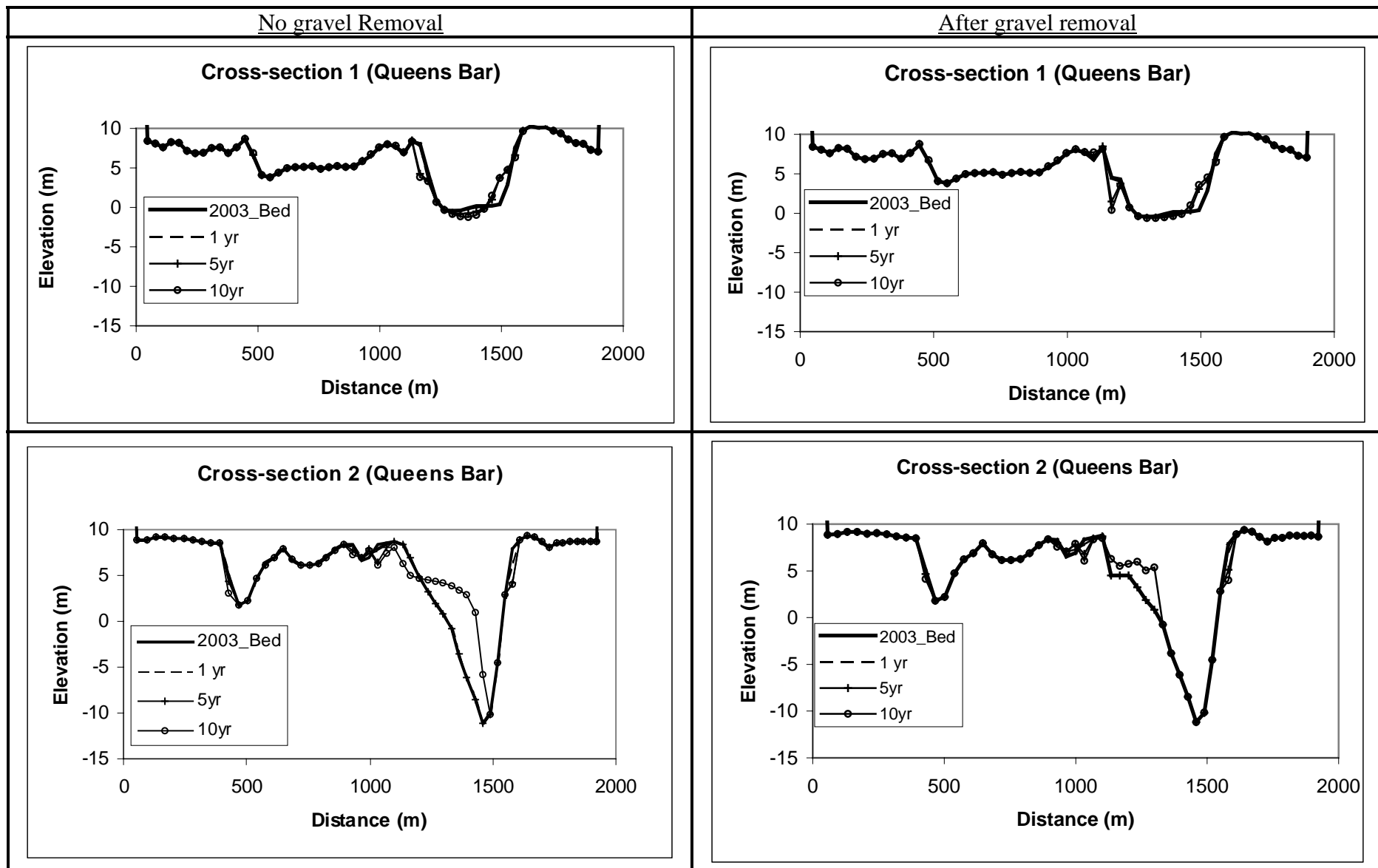
Figure A.3.1: Showing bed elevation without and with gravel removal near Queens bar gravel extraction site (cross-section 1 and 2).
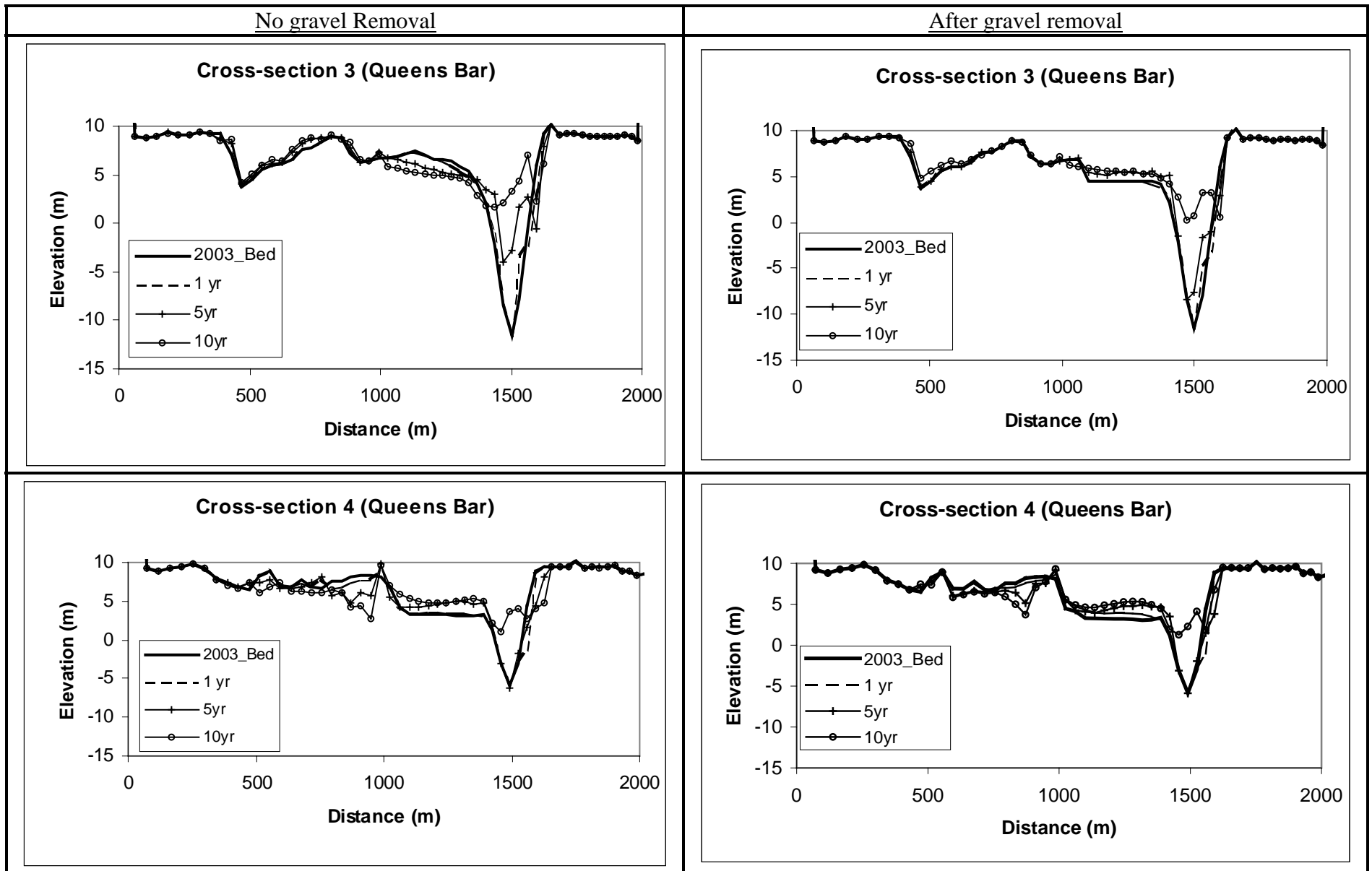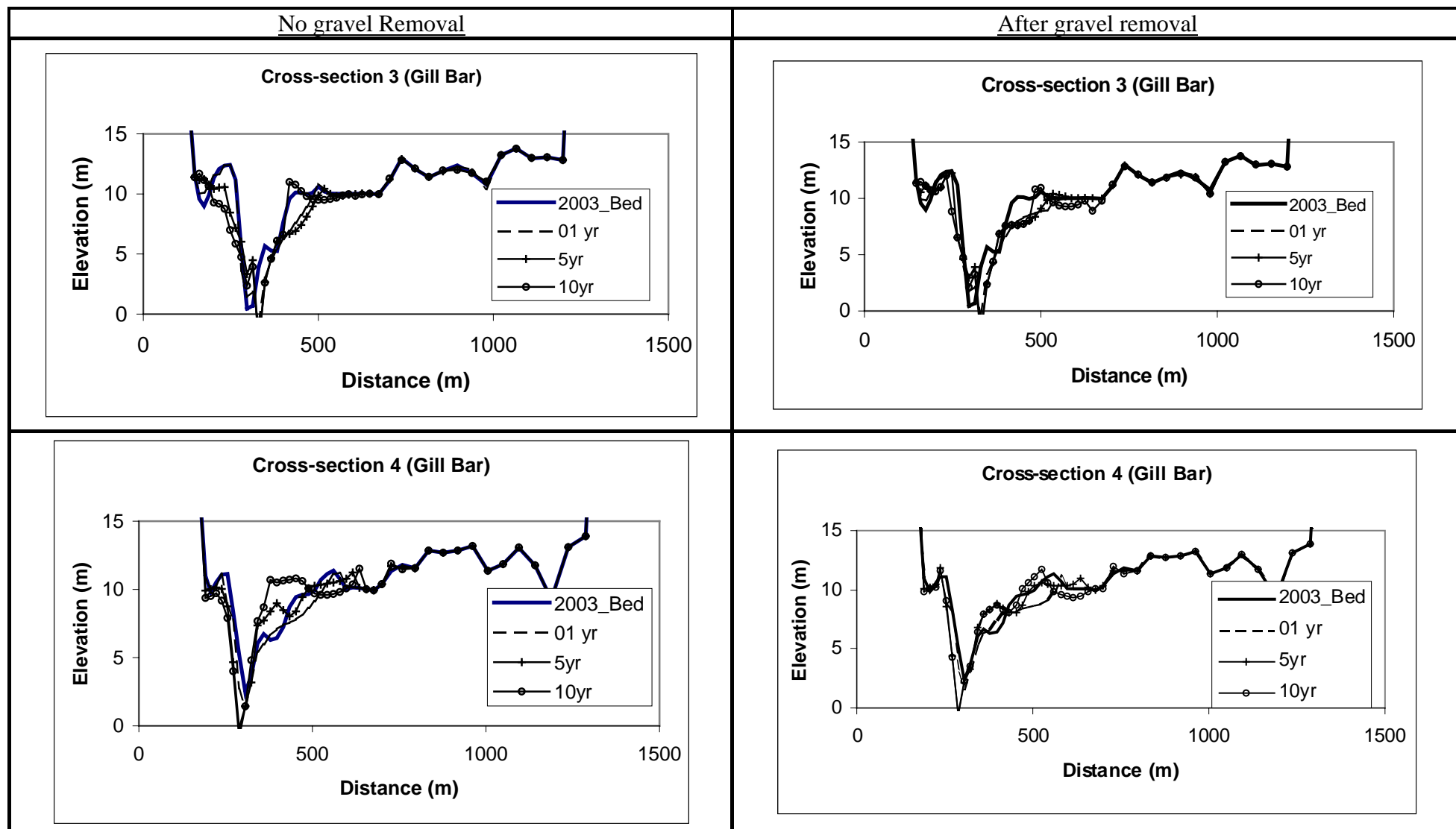
Figure A.3.2: Showing bed elevation without and with gravel removal near Queens bar gravel extraction site (cross-section 3 and 4).

APPENDIX-B: HARRISON BAR
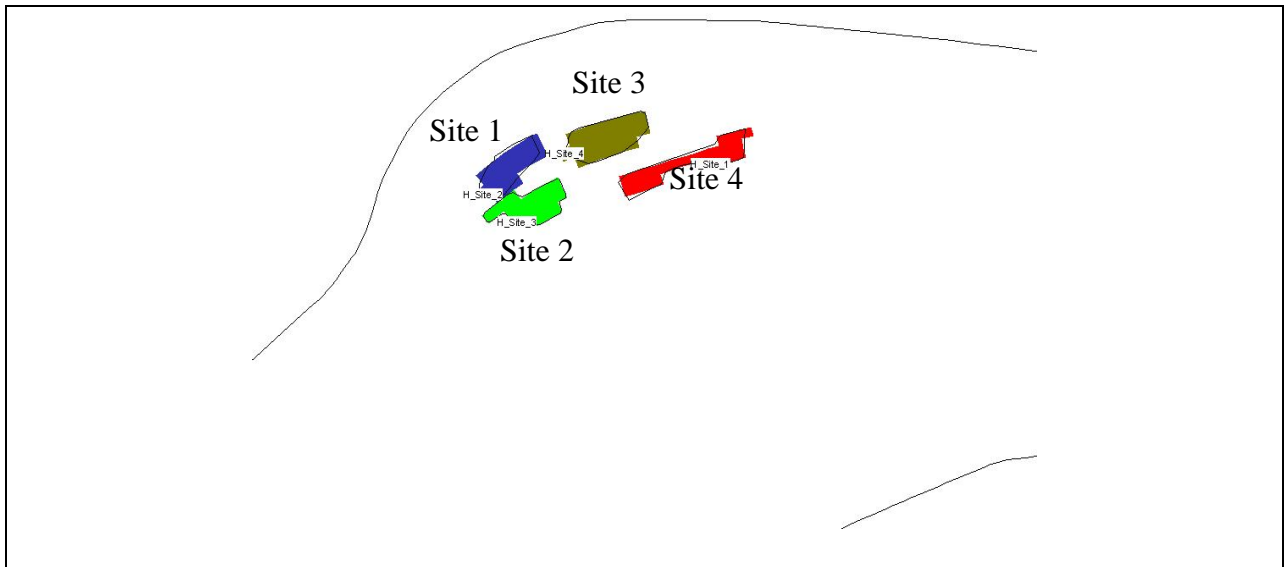
Figure B.1: Showing the 4 Harrison Bar removal areas in the model (B) Legends of the bed level changes for Figure B.1 (A) and Figure B.1 (.B).
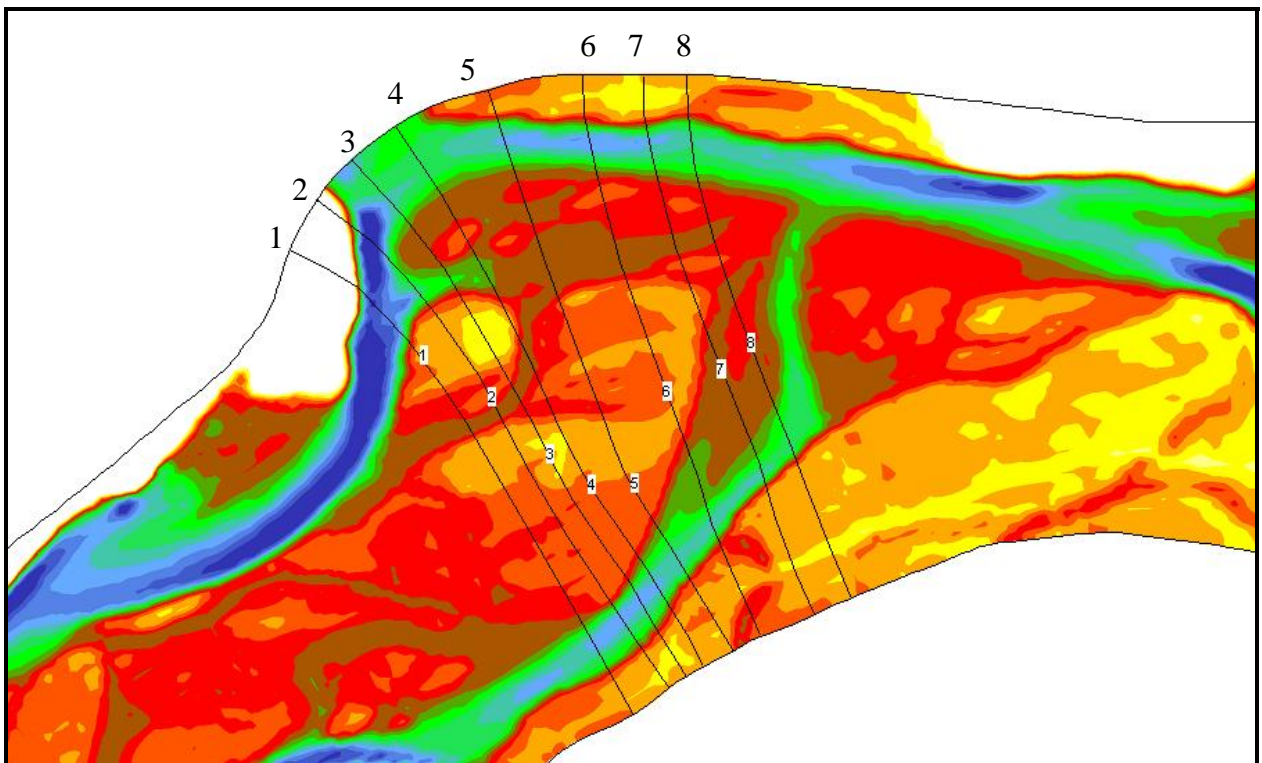
Figure B.2: Showing 8 cross-Sections near Harrison Bar gravel extraction sites for bed changes without and with removal.
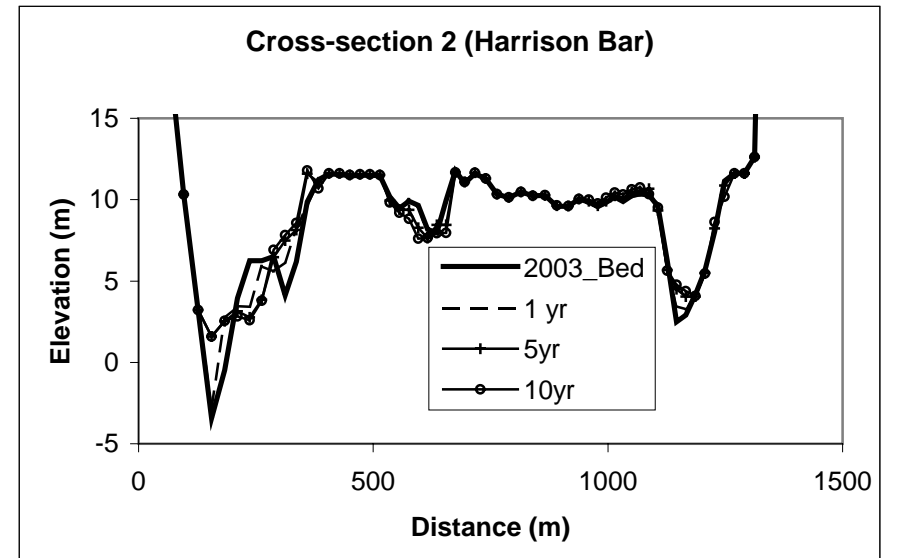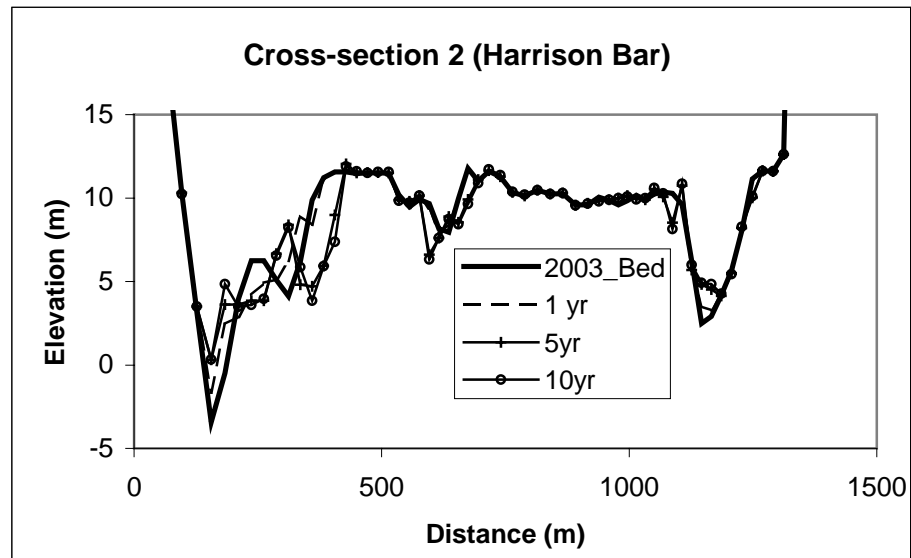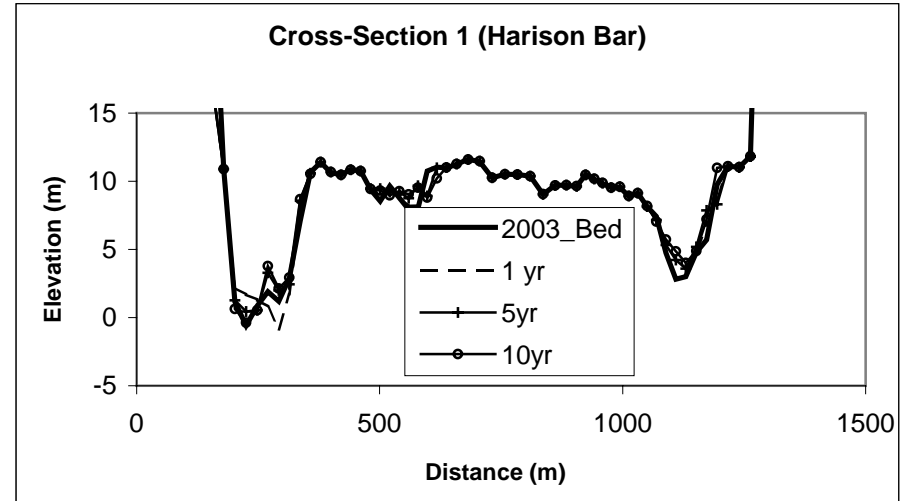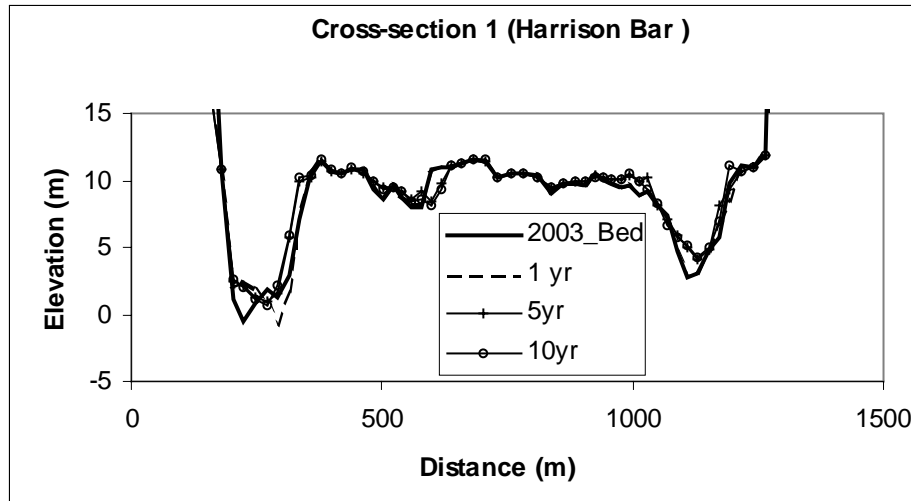
Figure B.3.1: Showing bed elevation without and with removal near Harrison Bar gravel extraction site (cross-section 1 and 2).

No gravel Removal   After gravel removal

Cross-section 3 (Harrison Bar)

Cross-section 3 (Harrison Bar)

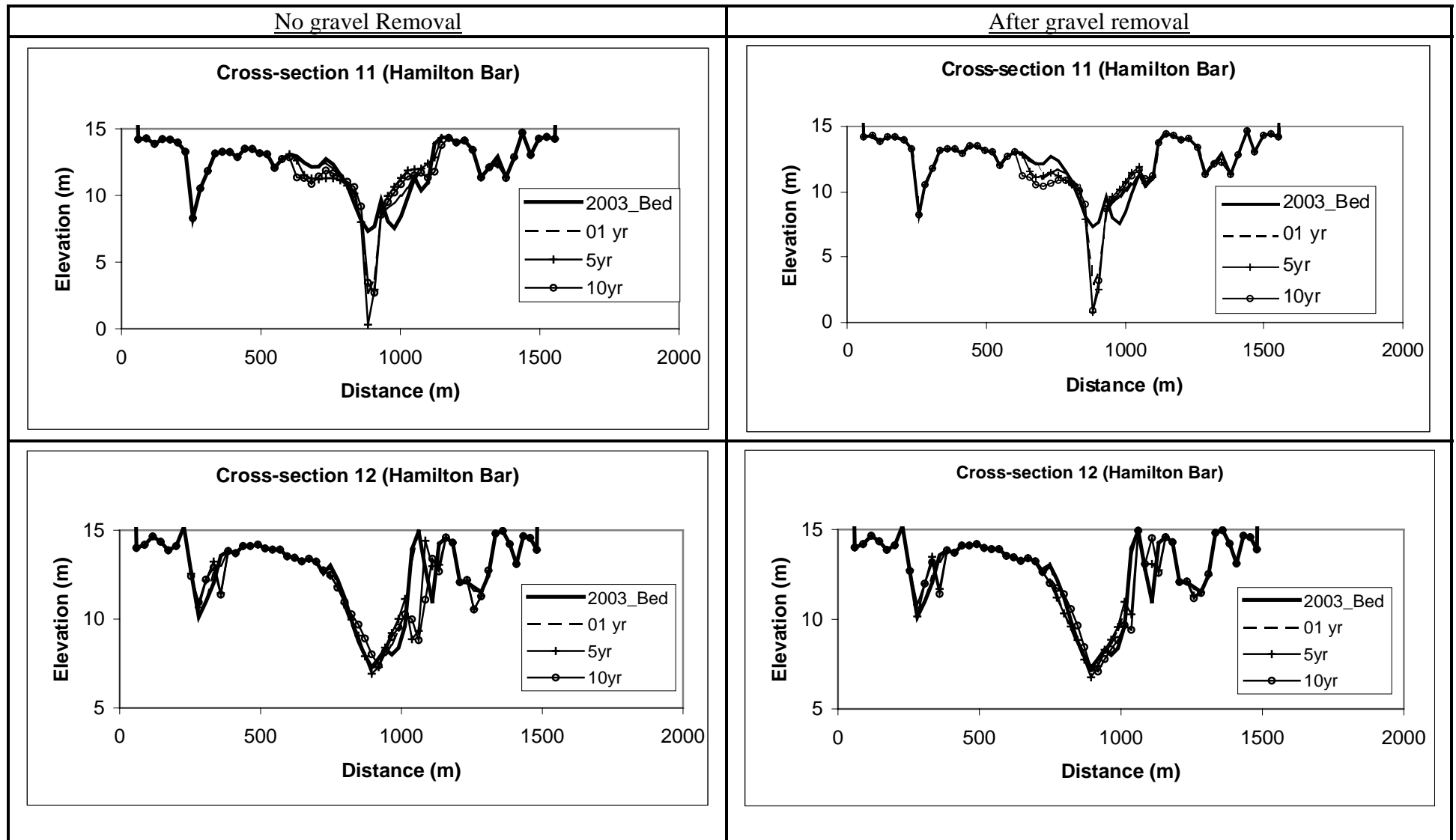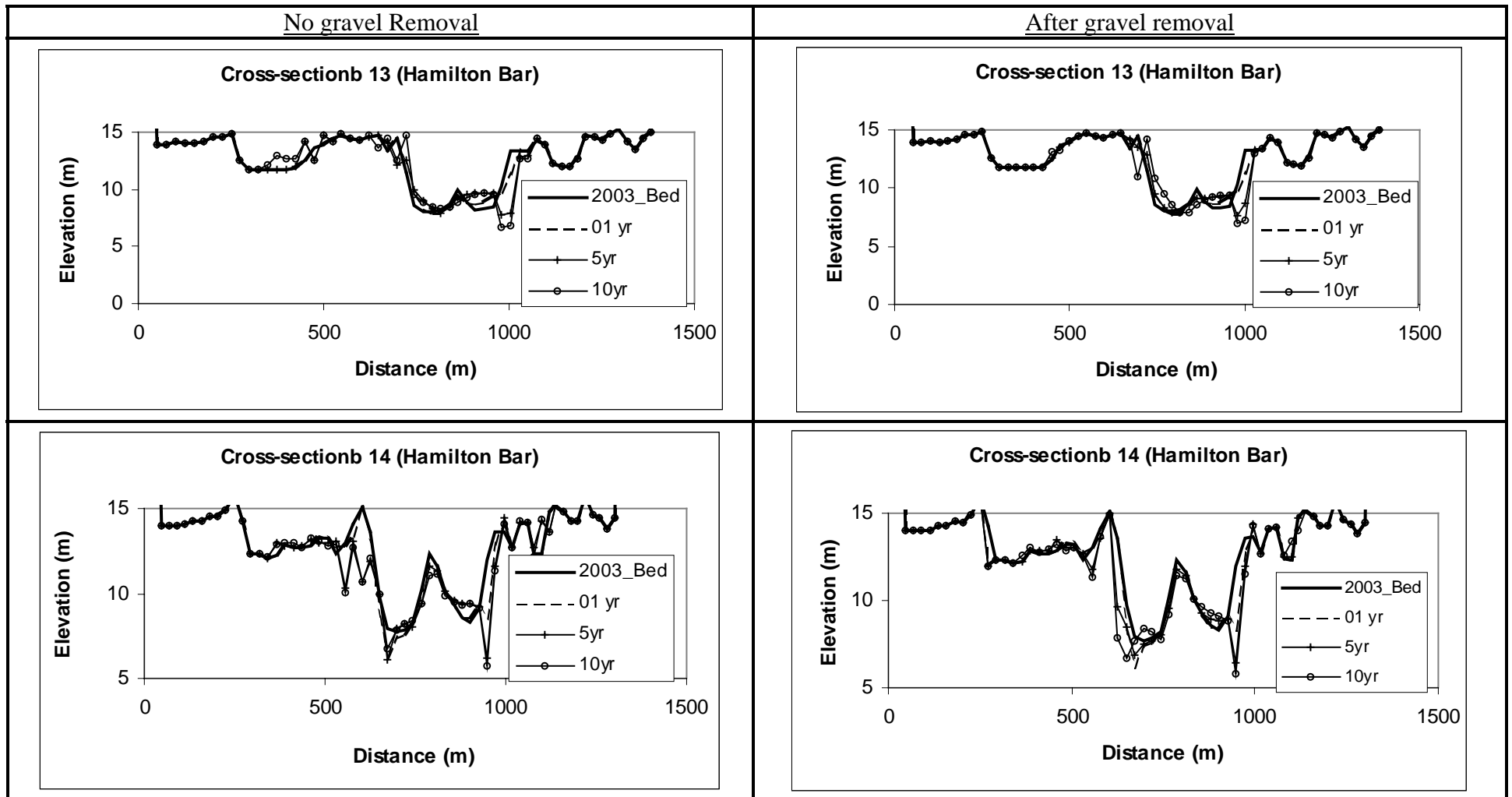**Cross-section 4 (Harrison Bar)**
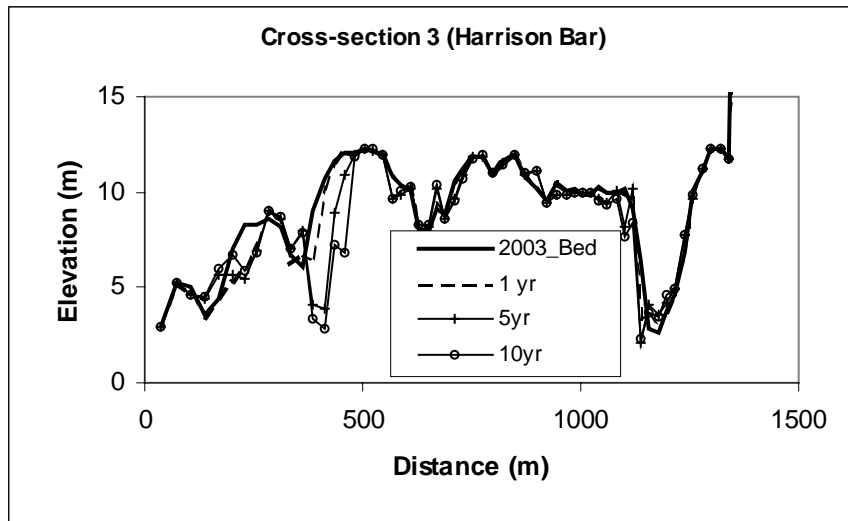
Cross-section 4 (Harrison Bar)
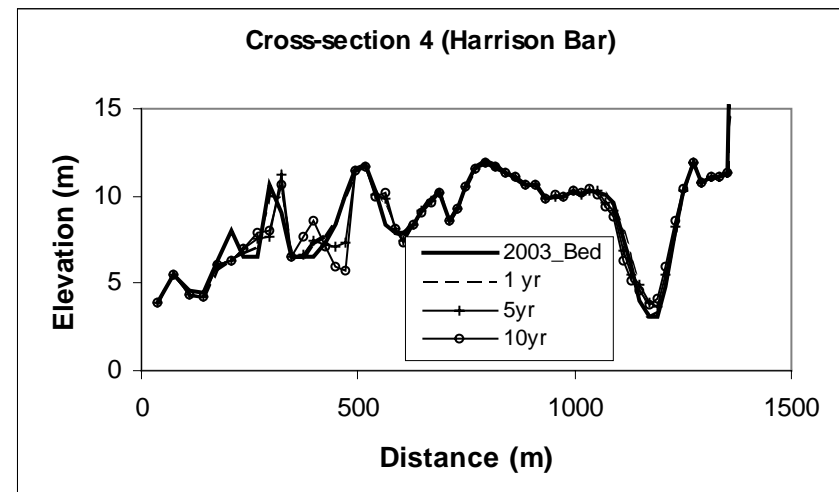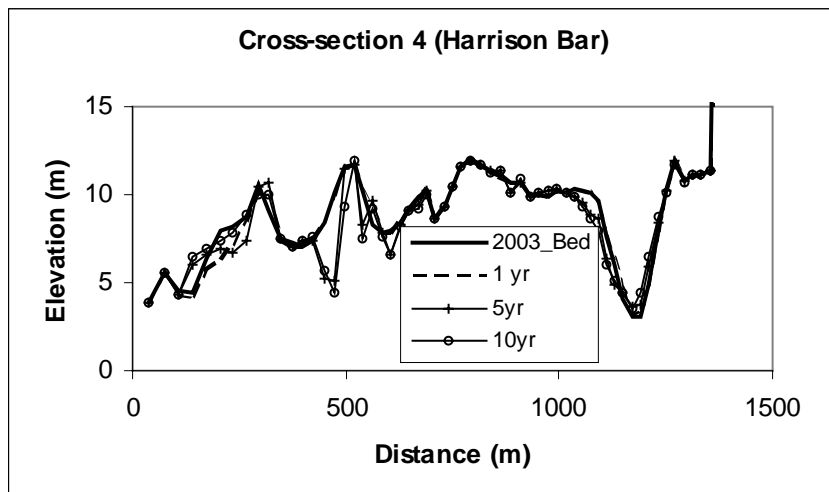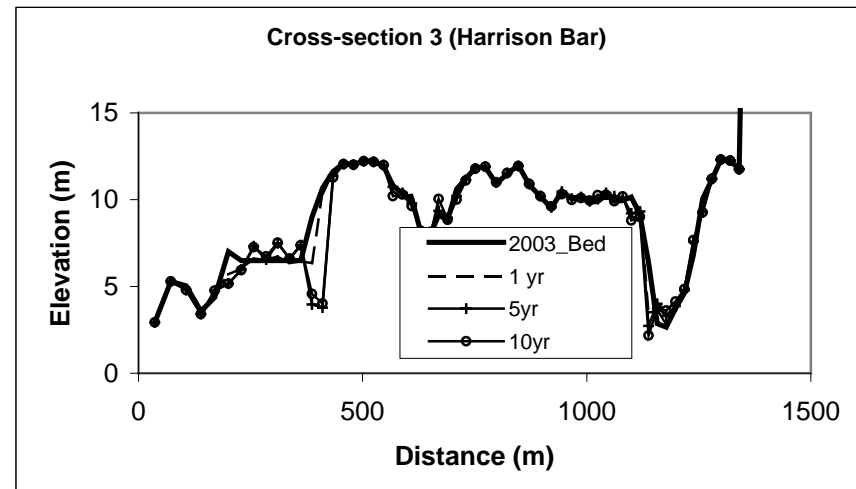
Figure B.3.2: Showing bed elevation without and with removal near Harrison Bar gravel extraction site (cross-section 3 and 4).
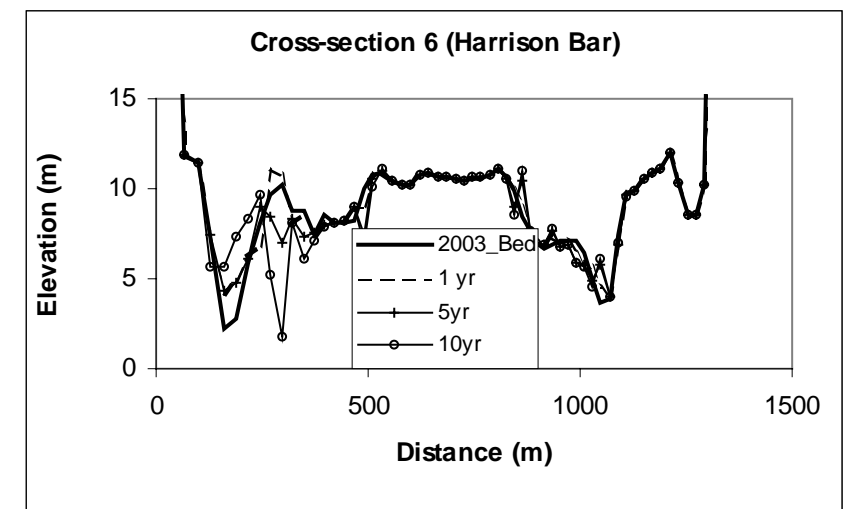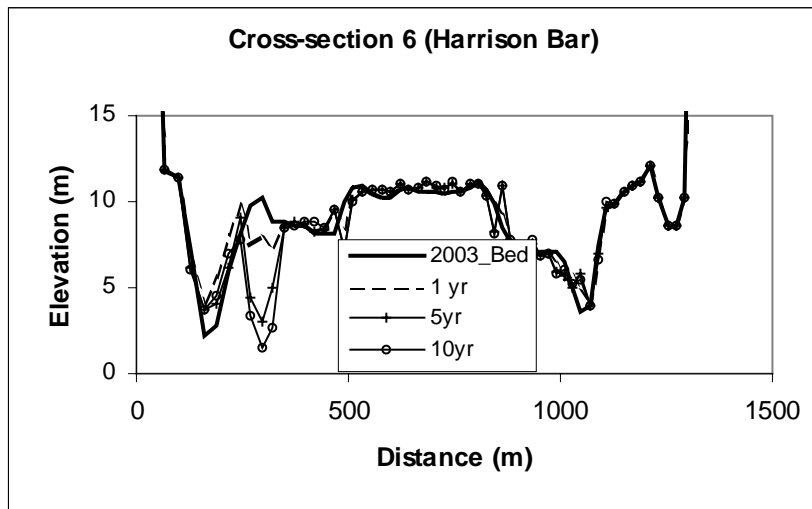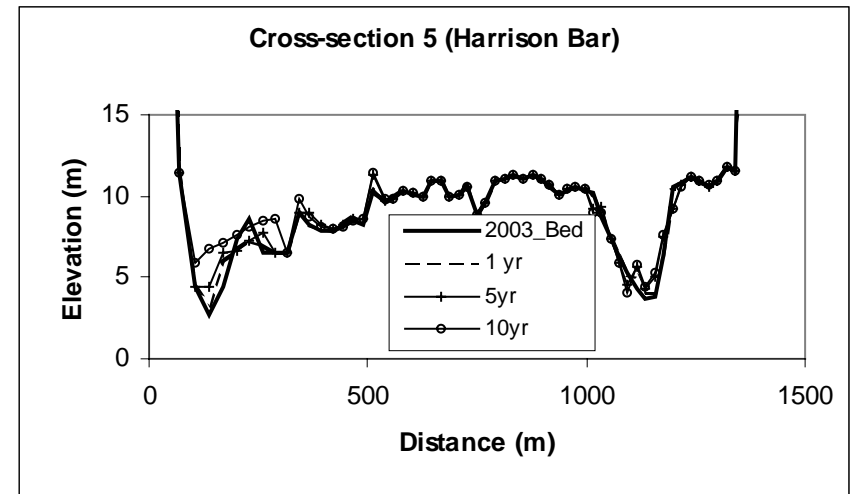
Figure B.3.3: Showing bed elevation without and with removal near Harrison Bar gravel extraction site (cross-section 5 and 6).
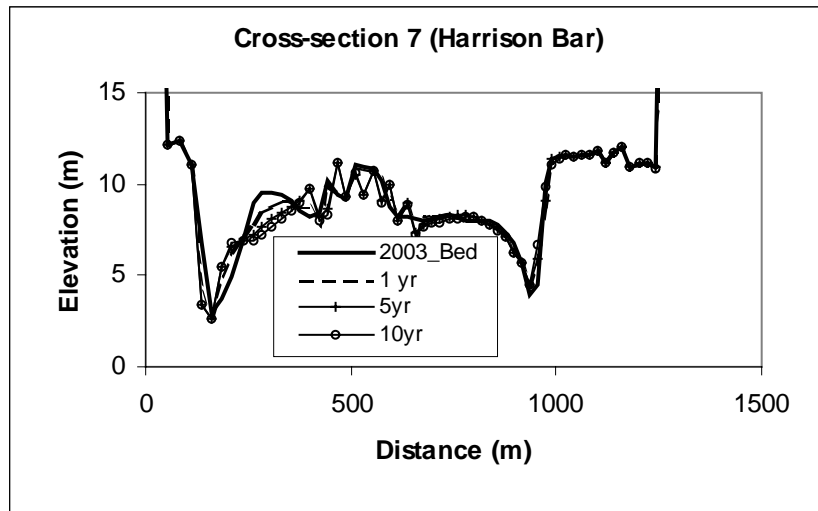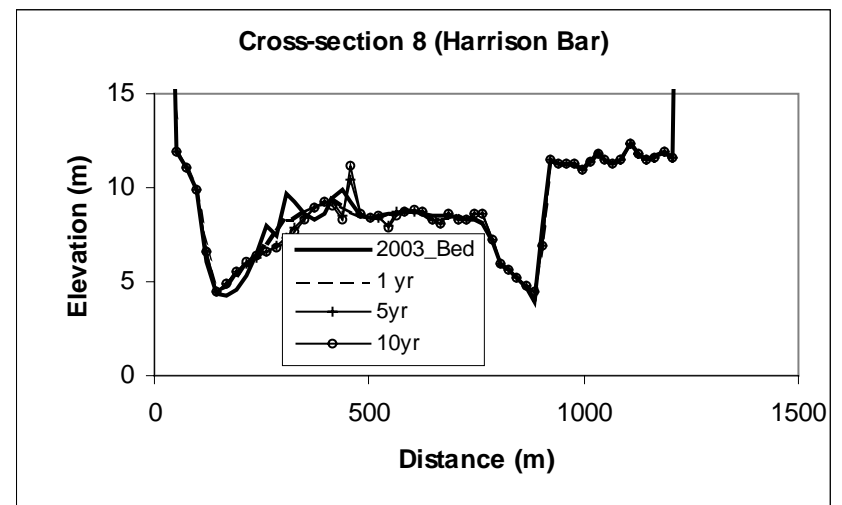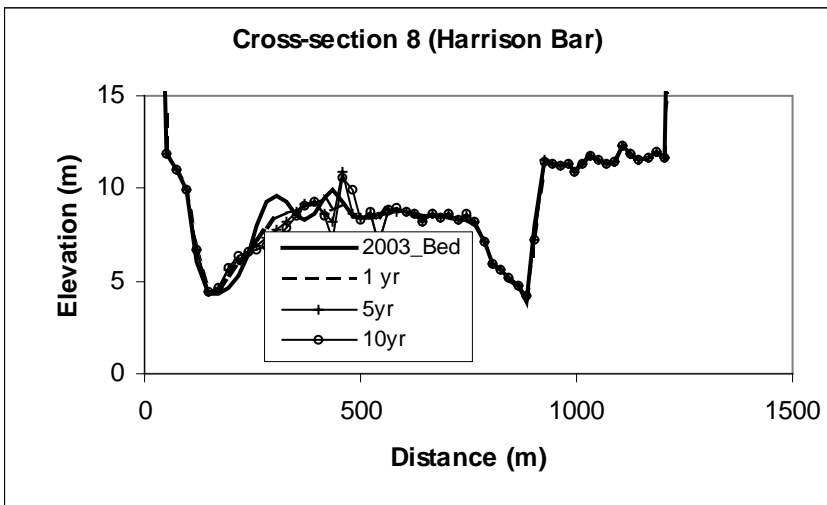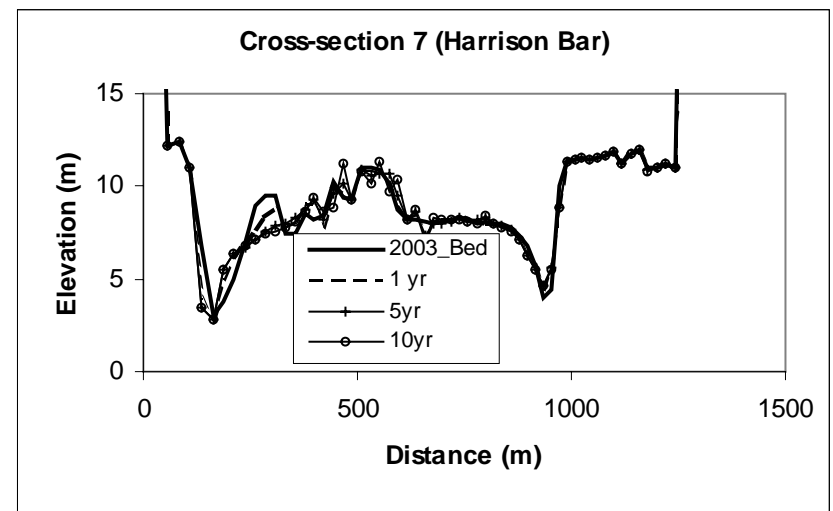
Figure B.3.4: Showing bed elevation without and with removal near Harrison Bar gravel extraction site (cross-section 7 and 8).

217
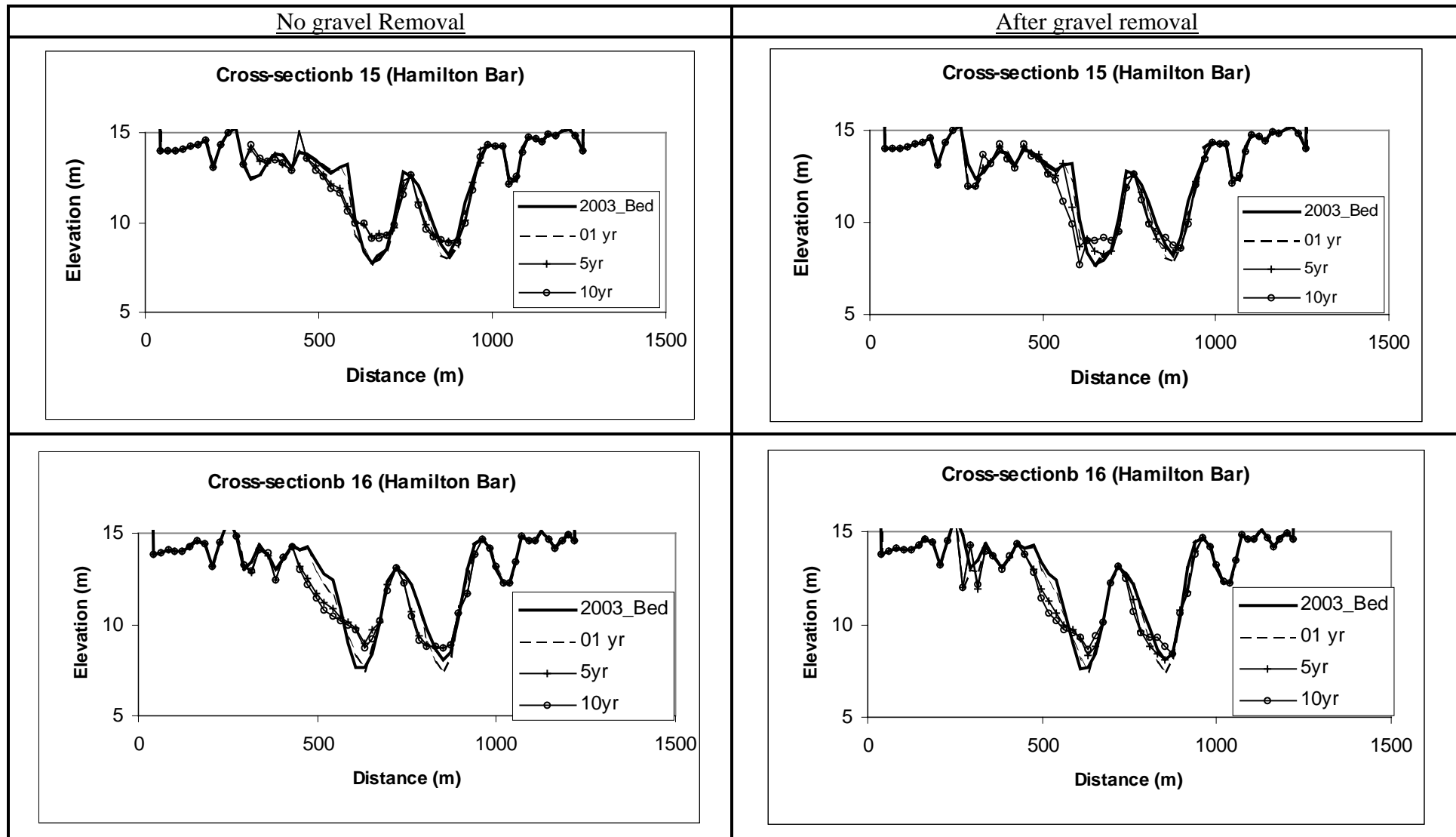
APPENDIX-C: GILL ISLAND AND HAMILTON ISLAND
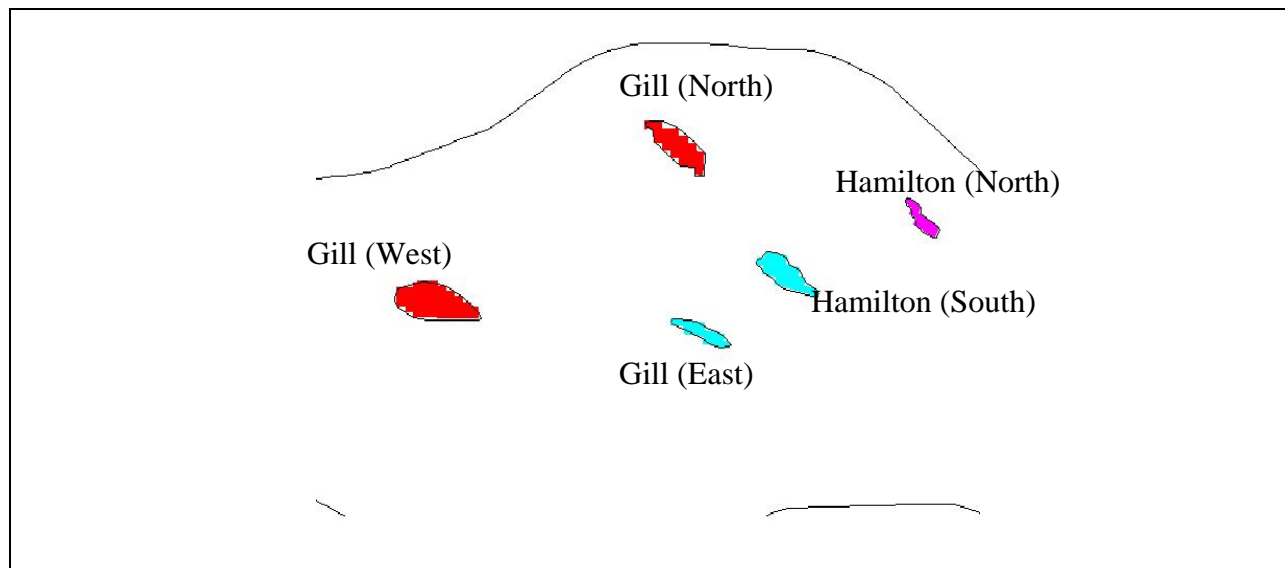
Figure C.1 Showing the 3 Gill Bar and 2 Hamilton Bar removal areas in the model.
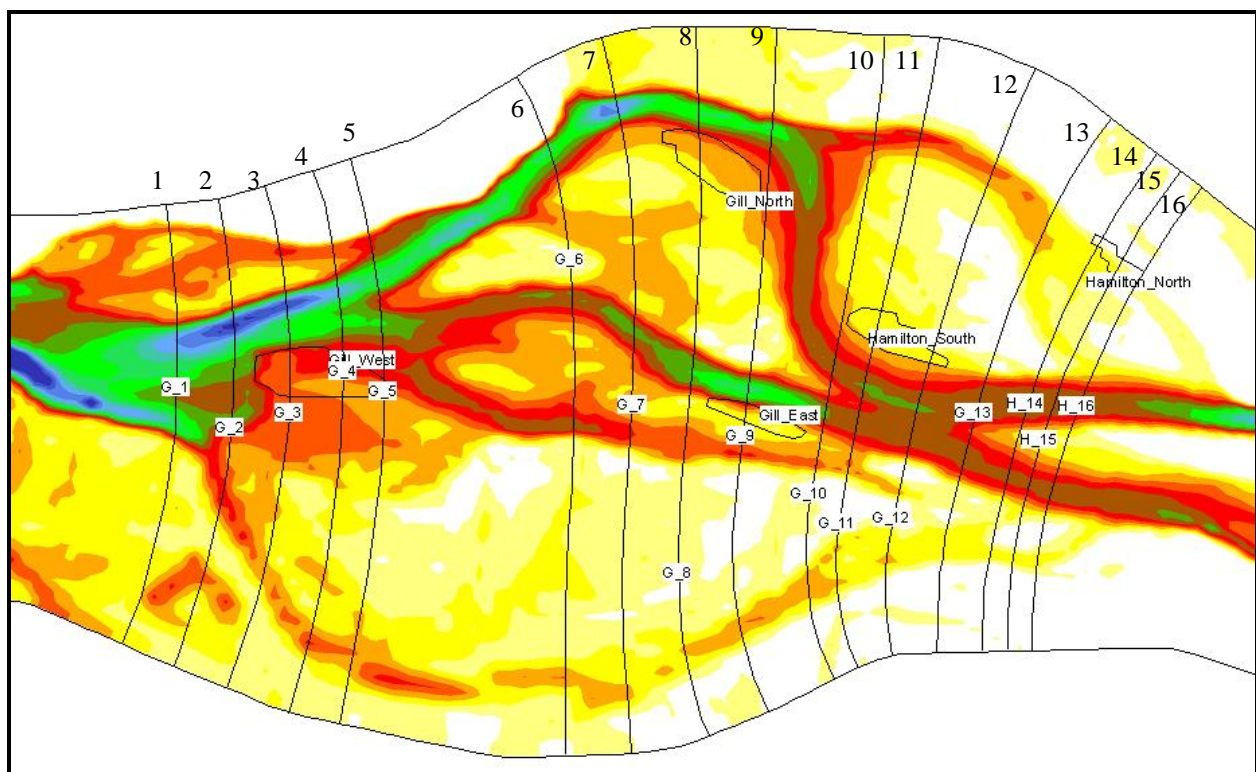
Figure C.2: Showing 16 cross-Sections near Gill Islands and Hamilton Islands gravel extraction sites.
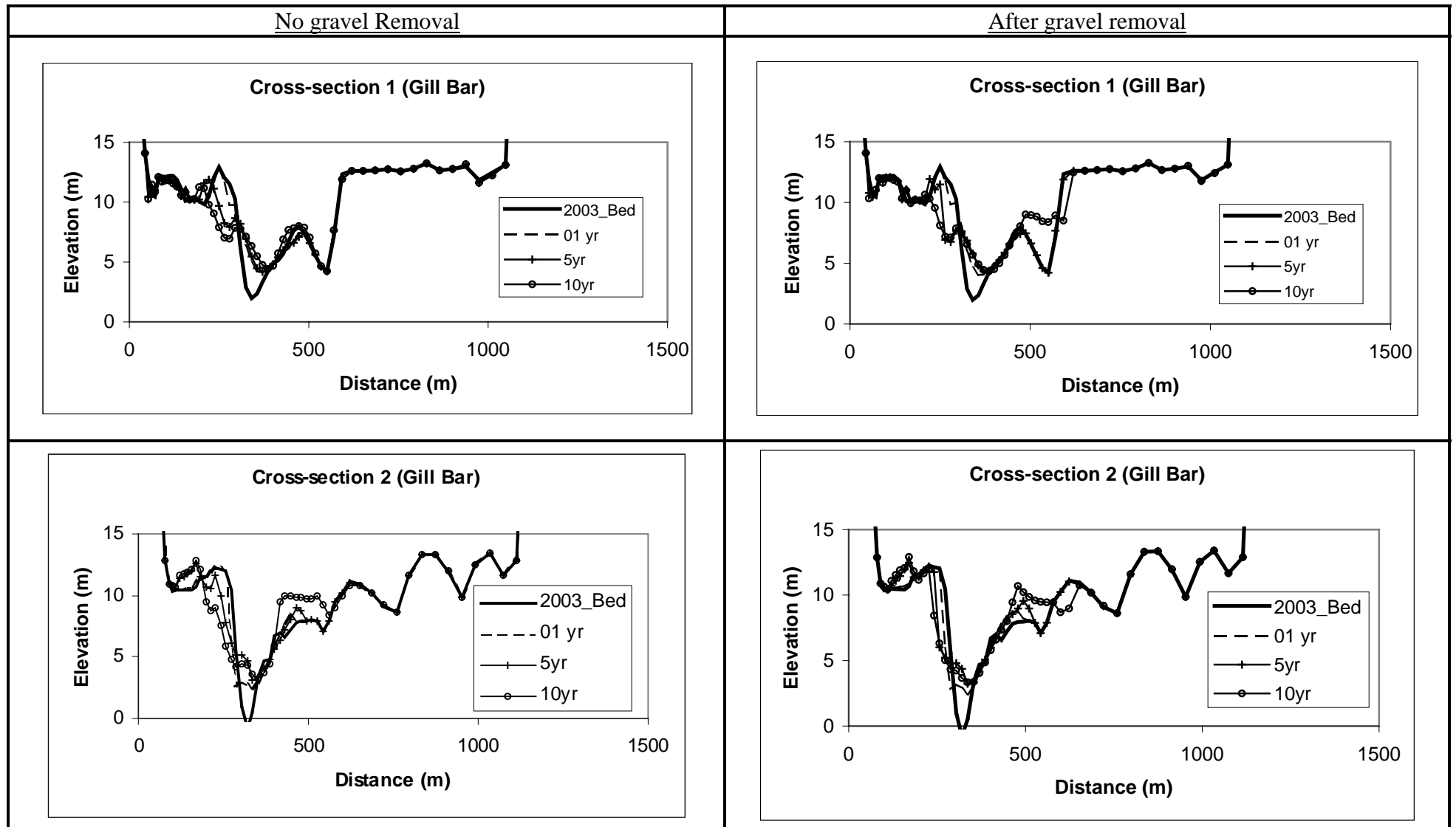
Figure C.3.1: Showing bed elevation without and with removal near Gill Bar gravel extraction site (cross-section 1 and 2).

Figure C.3.2: Showing bed elevation without and with removal near Gill Bar gravel extraction site (cross-section 3 and 4).
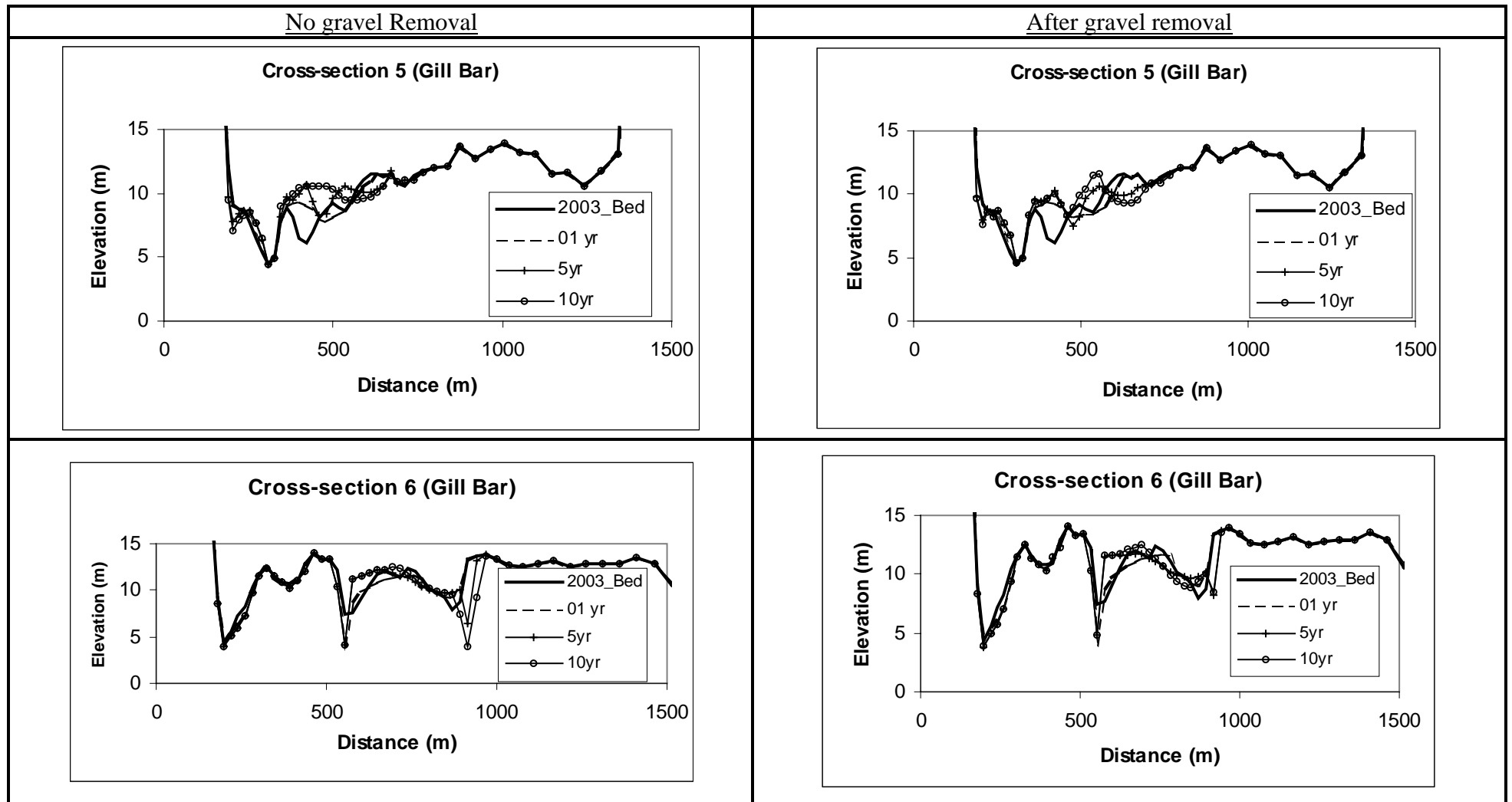
Figure C.3.3: Showing bed elevation without and with removal near Gill Bar gravel extraction site (cross-section 5 and 6).

Cross-section 7 (Gill Bar)

Cross-section 7 (Gill Bar)

Cross-section 8 (Gill Bar)

Cross-section 8 (Gill Bar)
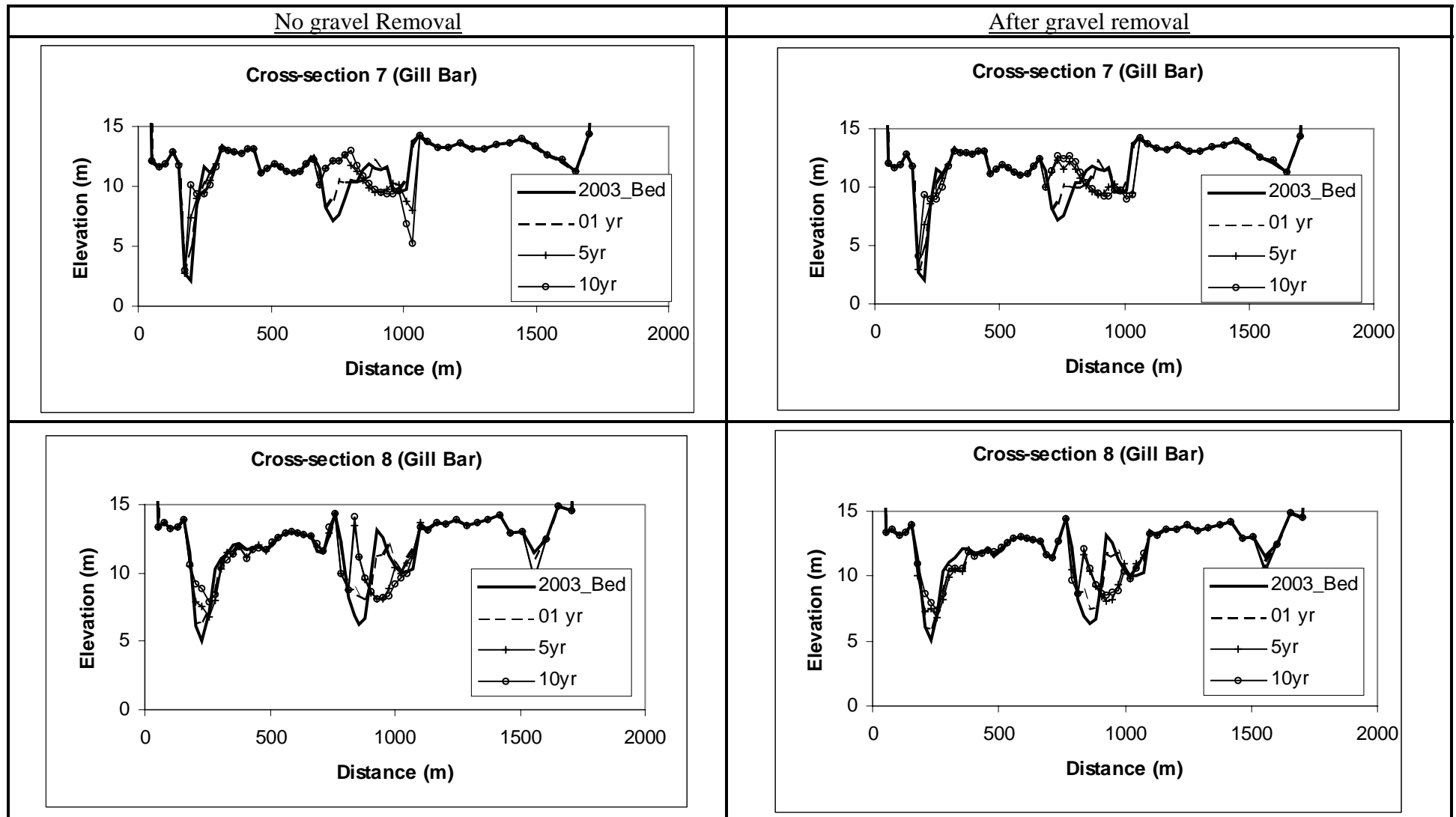
Figure C.3.4: Showing bed elevation without and with removal near Gill Bar gravel extraction site (cross-section 7 and 8).
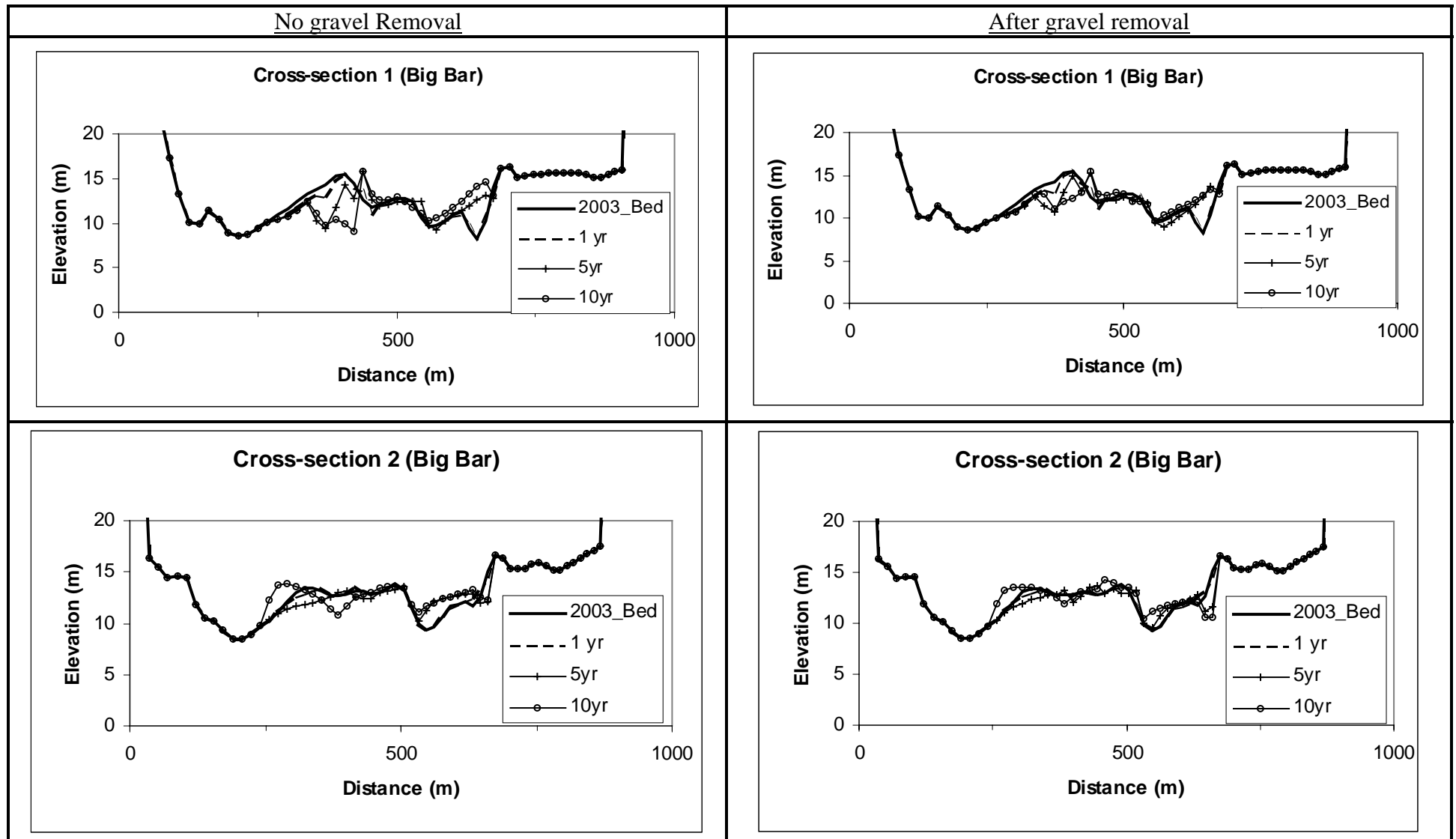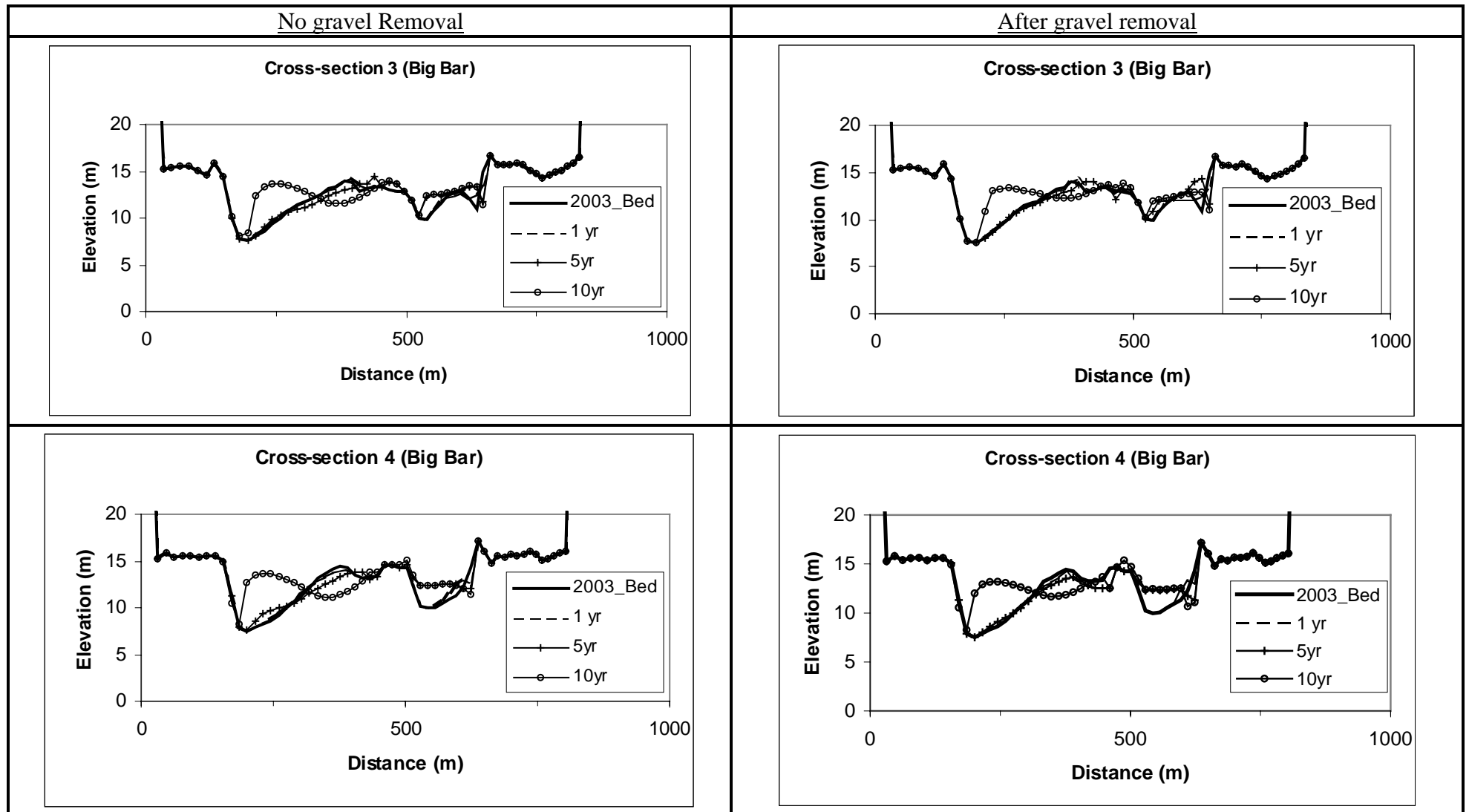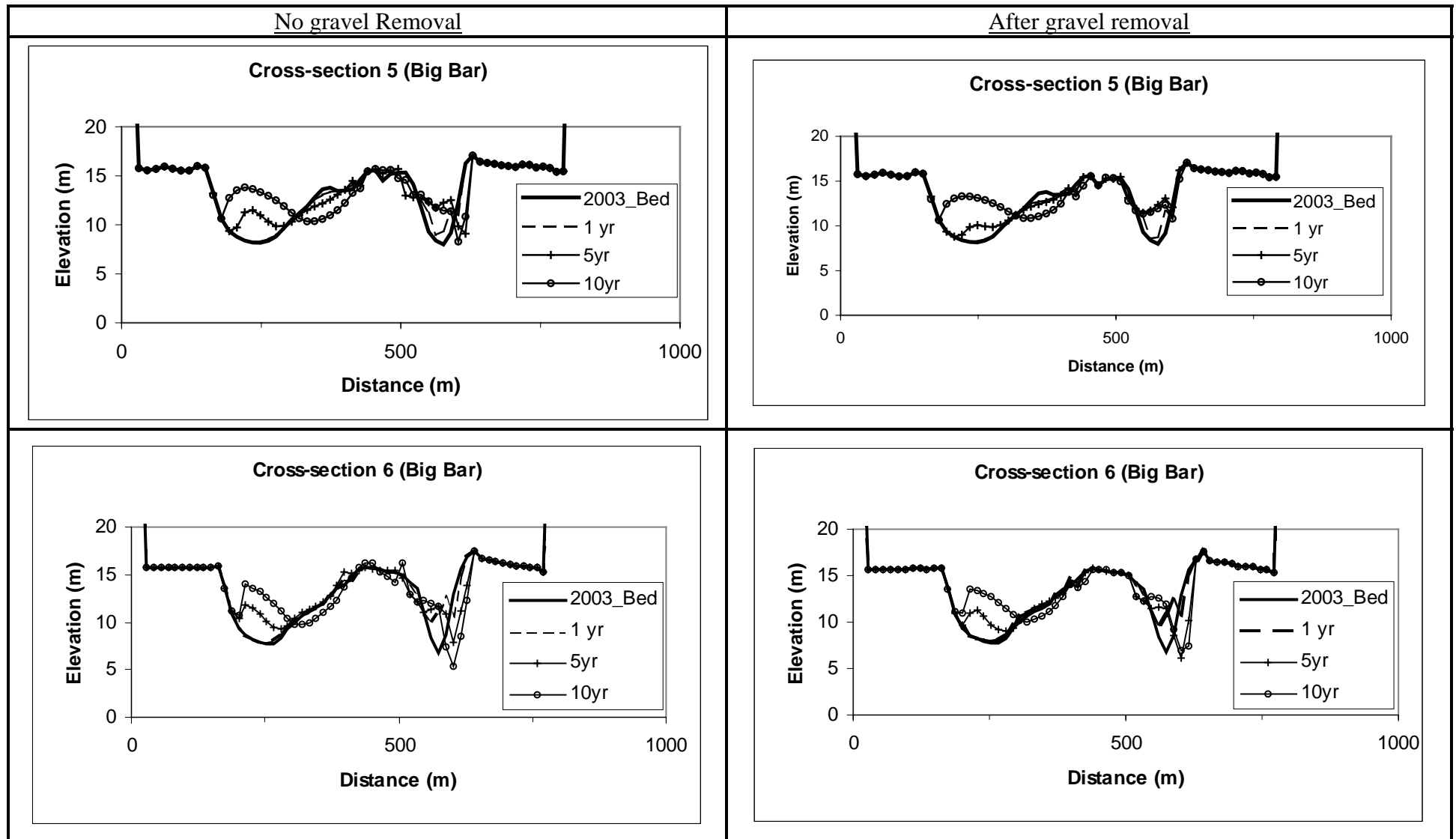
223
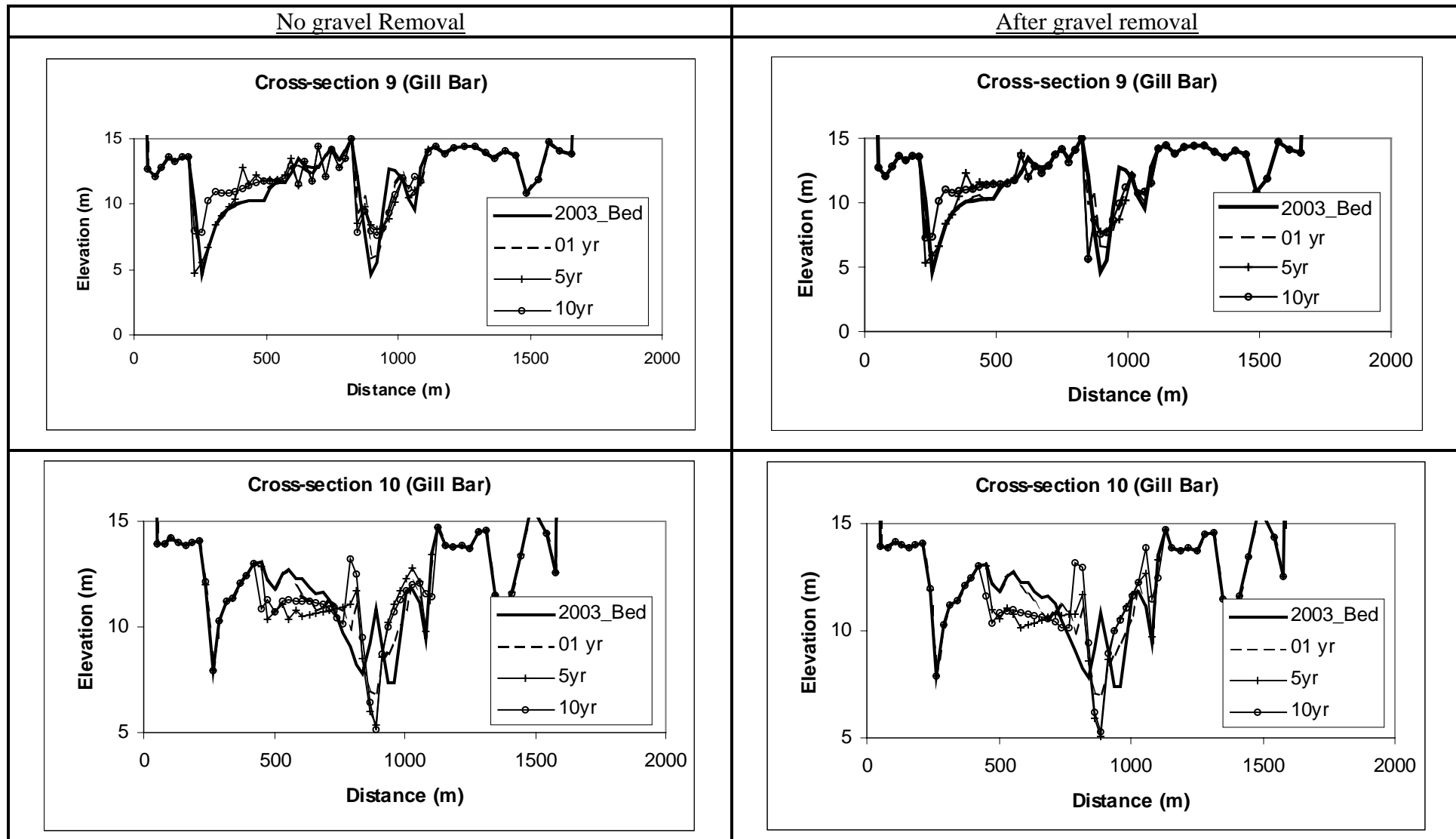
Figure C.3.5: Showing bed elevation without and with removal near Gill Bar gravel extraction site (cross-section 9 and 10).

Figure C.3.6: Showing bed elevation without and with removal near Hamilton Bar gravel extraction site (cross-section 11 and 12).

Figure C.3.7: Showing bed elevation without and with removal near Hamilton Bar gravel extraction site (cross-section 13 and 14).

No gravel Removal	After gravel removal

Cross-sectionb 15 (Hamilton Bar)

Cross-sectionb 15 (Hamilton Bar)

Cross-sectionb 16 (Hamilton Bar)

Cross-sectionb 16 (Hamilton Bar)

Figure C.3.8: Showing bed elevation without and with removal near Hamilton Bar gravel extraction site (cross-section 15 and 16).

APPENDIX-D: BIG BAR
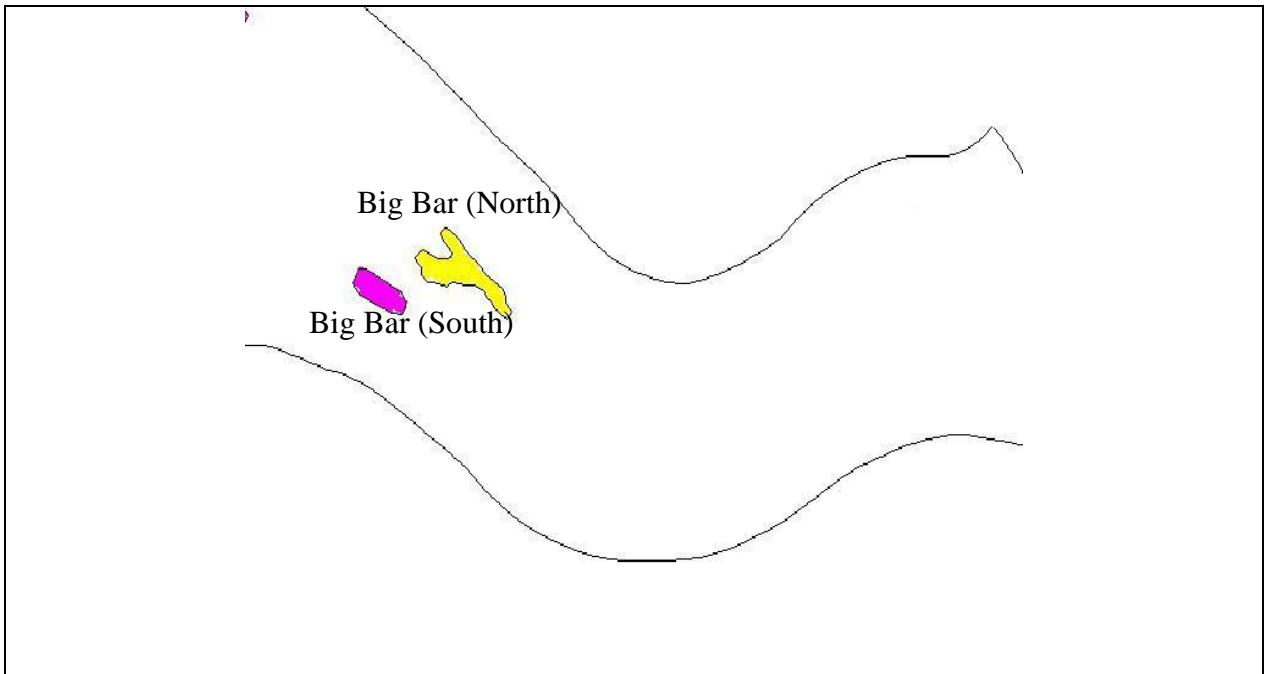
Figure D.1: Showing the Big Bar removal area in the model.
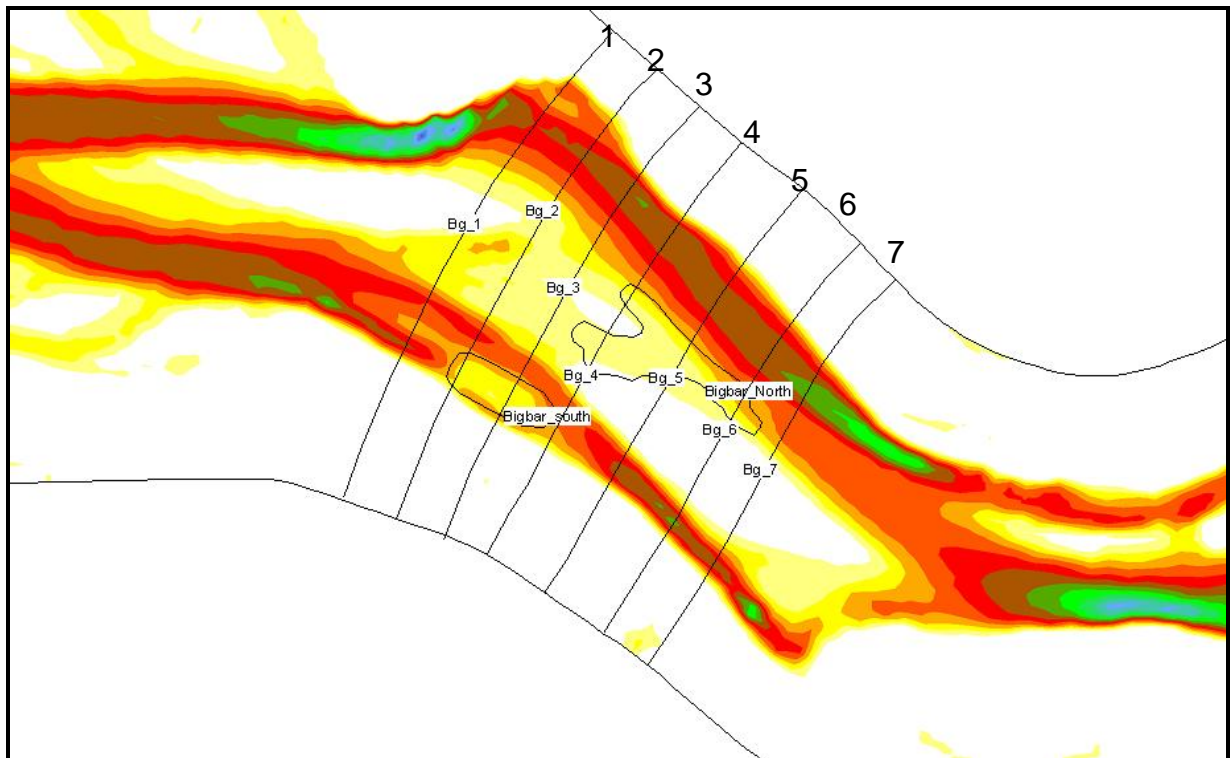
Figure D.2: Showing 7 cross-Sections near Big Bar gravel extraction sites.

Figure D.3.1: Showing bed elevation without and with removal near Big Bar gravel extraction site (cross-section 1 and 2).
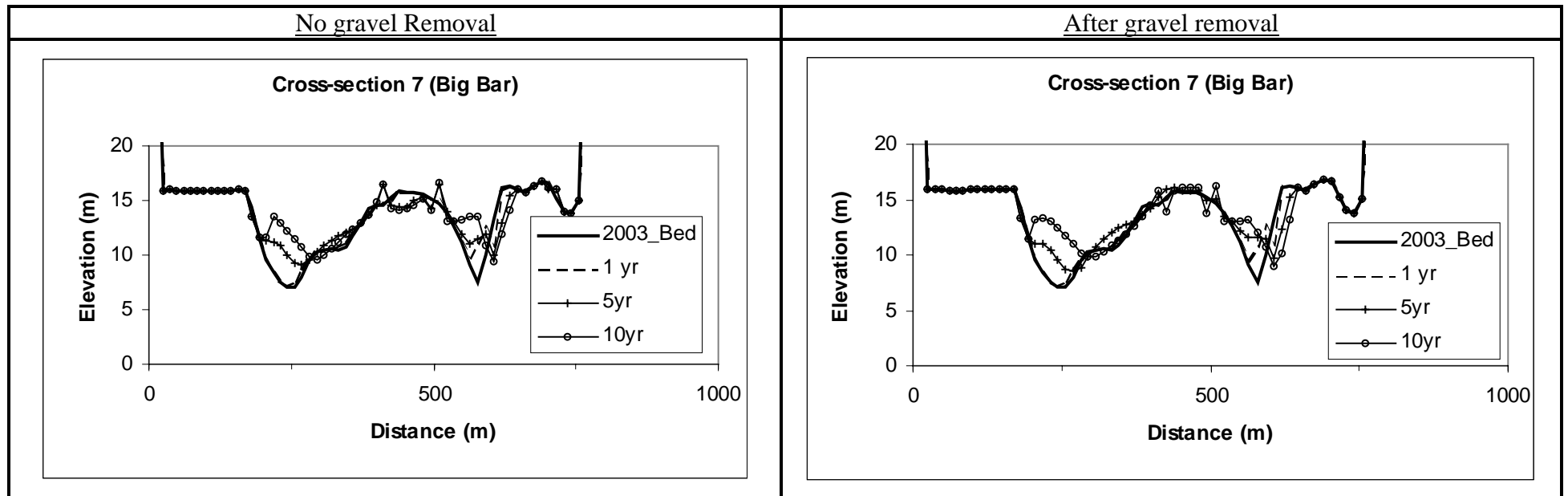
230

| No gravel Removal	After gravel removal

Cross-section 3 (Big Bar)

Cross-section 4 (Big Bar)

Figure D.3.2: Showing bed elevation without and with removal near Big Bar gravel extraction site (cross-section 3 and 4).

231

| No gravel Removal | After gravel removal |

Cross-section 5 (Big Bar)

Cross-section 6 (Big Bar)

Figure D.3.3: Showing bed elevation without and with removal near Big Bar gravel extraction site (cross-section 5 and 6).

232

No gravel Removal	After gravel removal

Cross-section 7 (Big Bar)

- 2003_Bed
- 1 yr
- 5yr
- 10yr

Elevation (m)

Distance (m)

Cross-section 7 (Big Bar)

- 2003_Bed
- 1 yr
- 5yr
- 10yr

Elevation (m)

Distance (m)

Figure D.3.4: Showing bed elevation without and with removal near Big Bar gravel extraction site (cross-section 7).

APPENDIX-E: MESH SIZES IN MODEL GRID
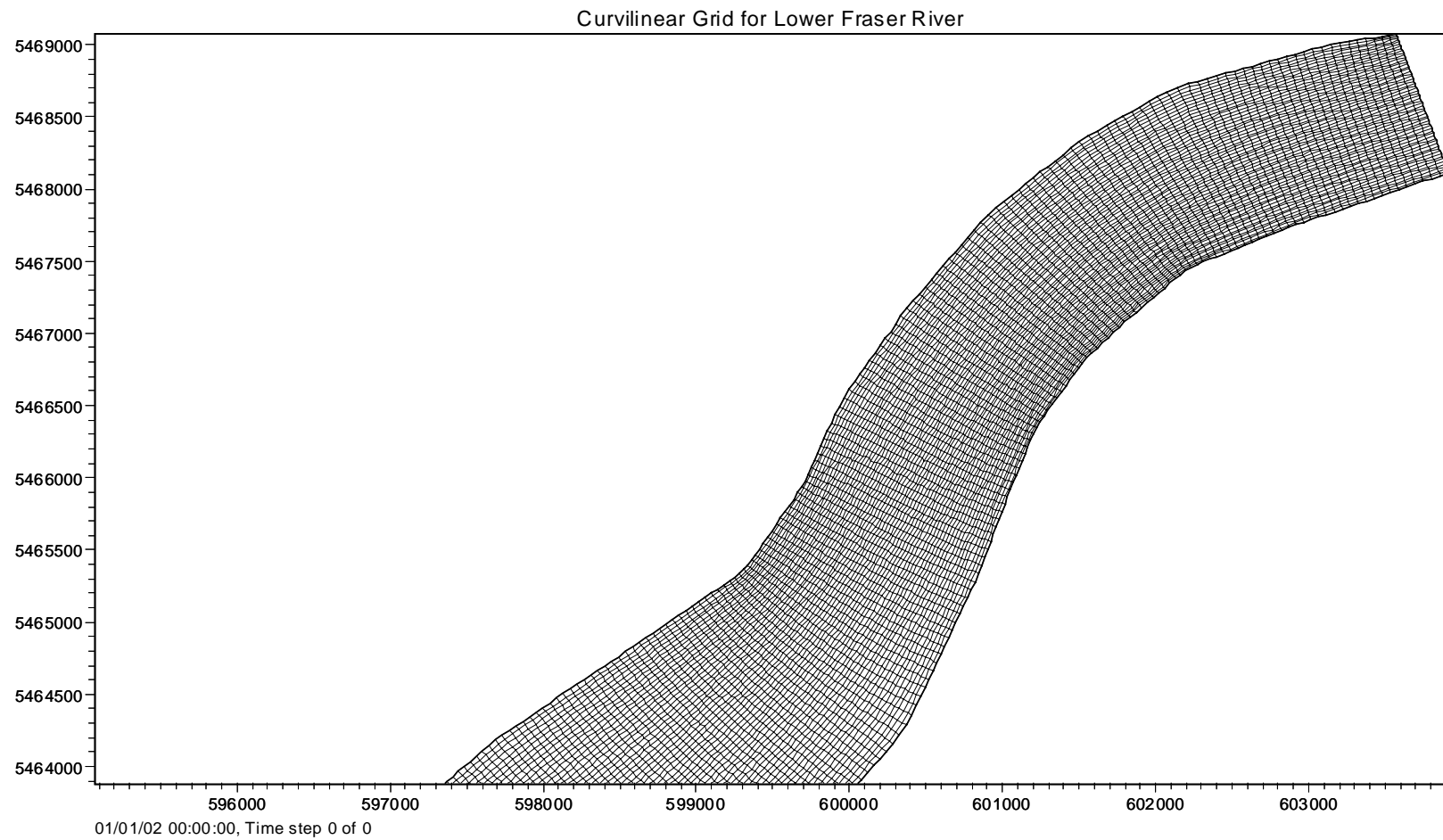
Figure E (A): Curvilinear grid size variation shown in detail for Frame A of Figure 4.6.
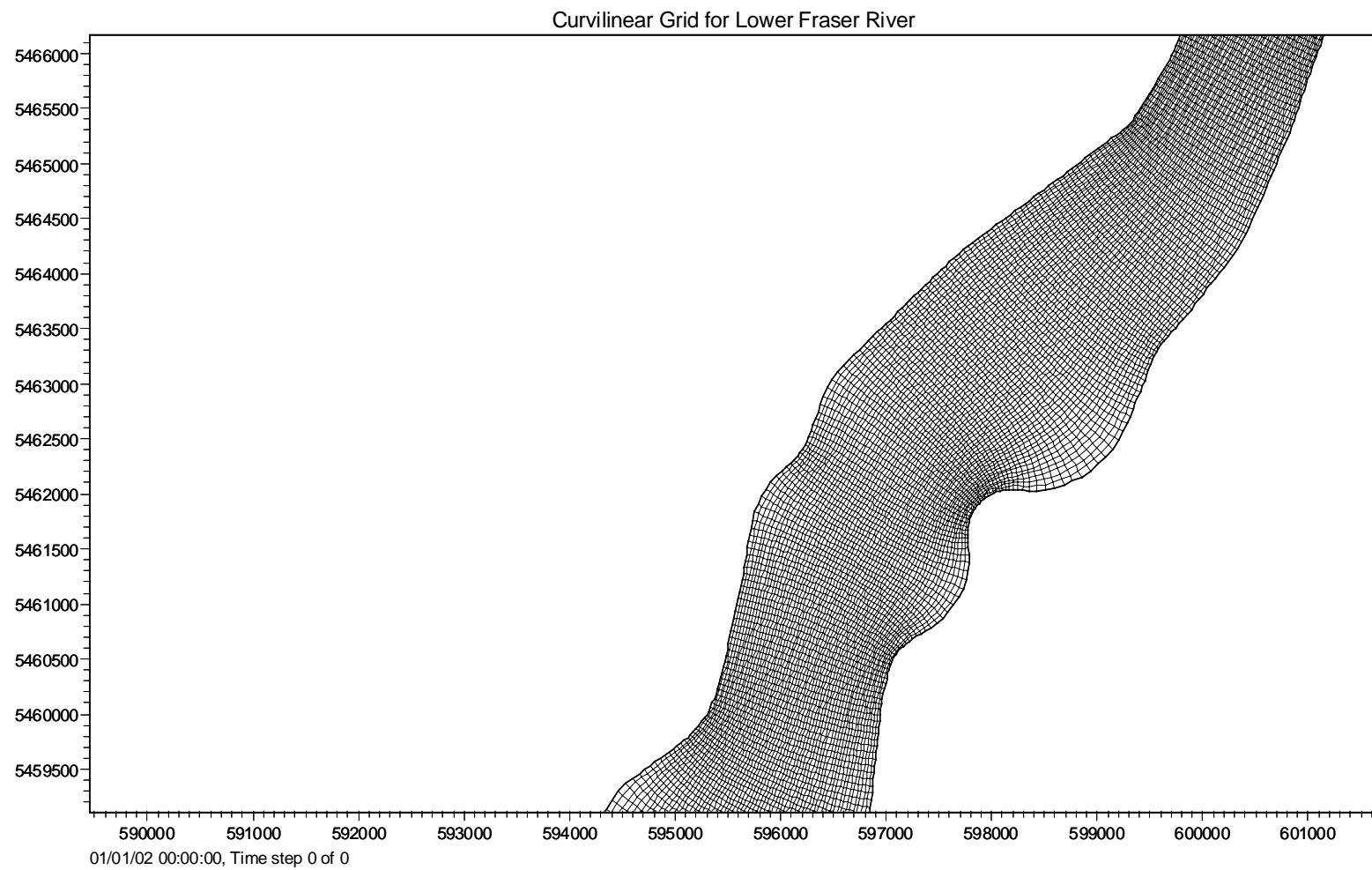
Figure E (B): Curvilinear grid size variation shown in detail for Frame B of Figure 4.6.
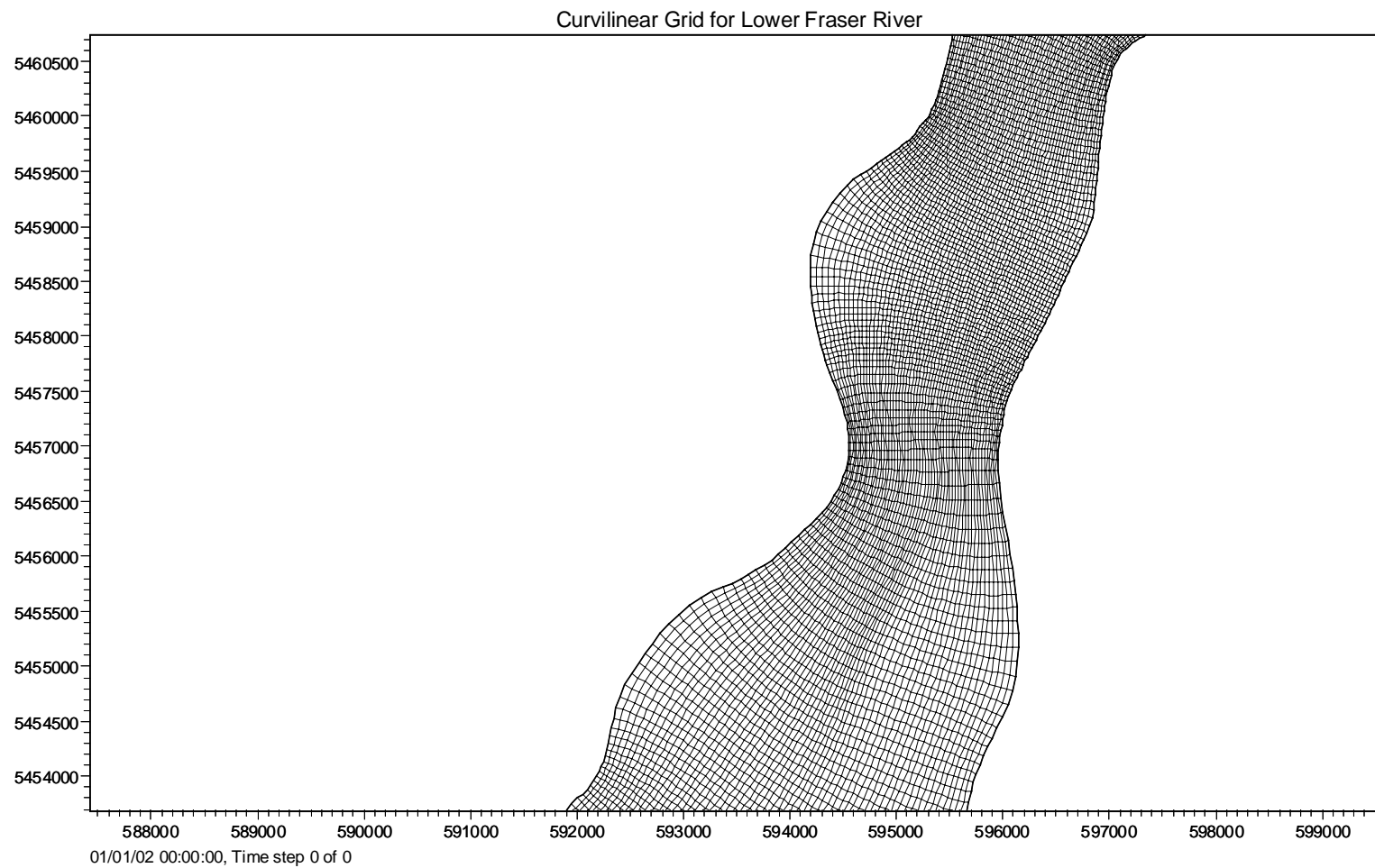
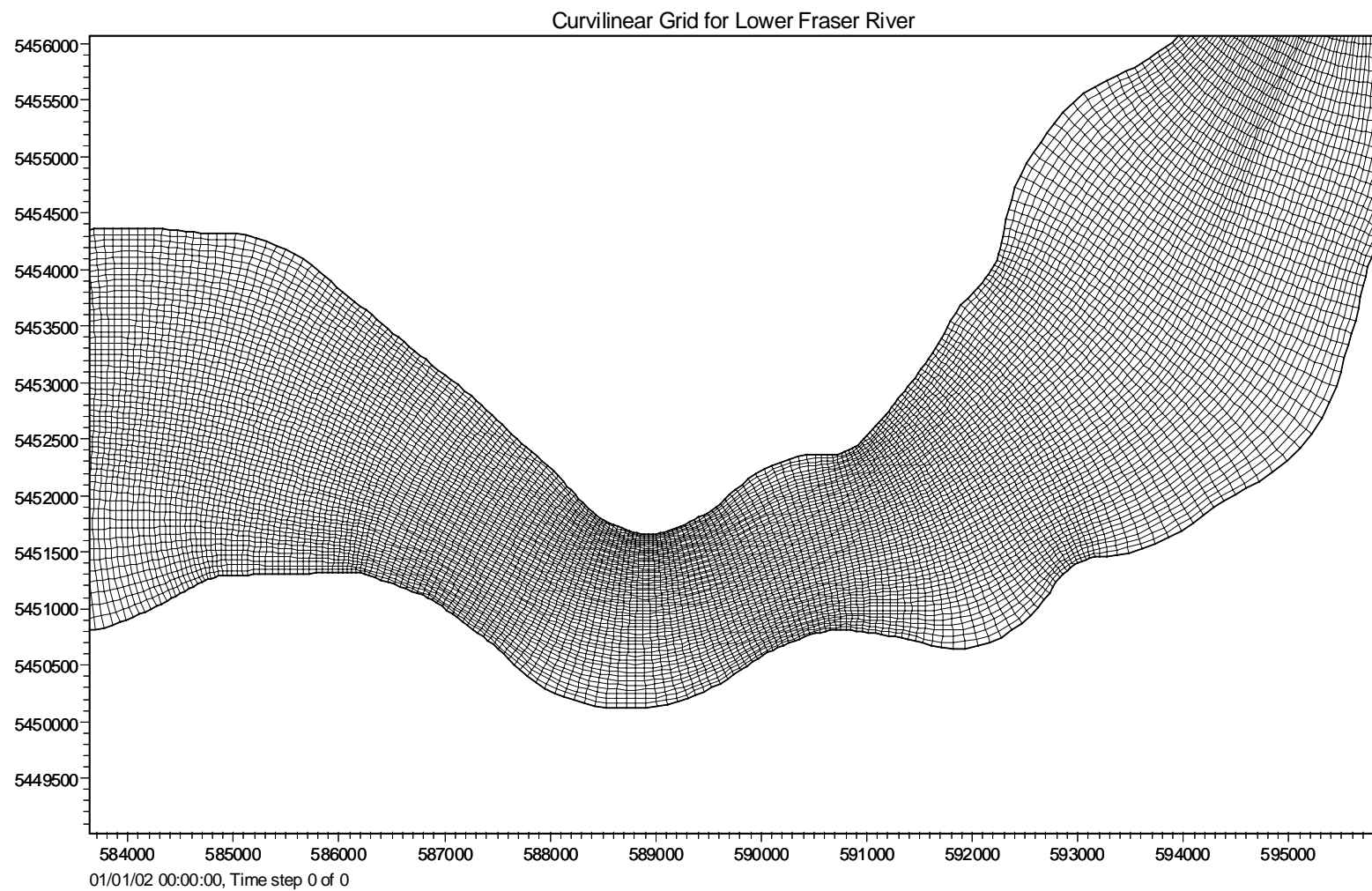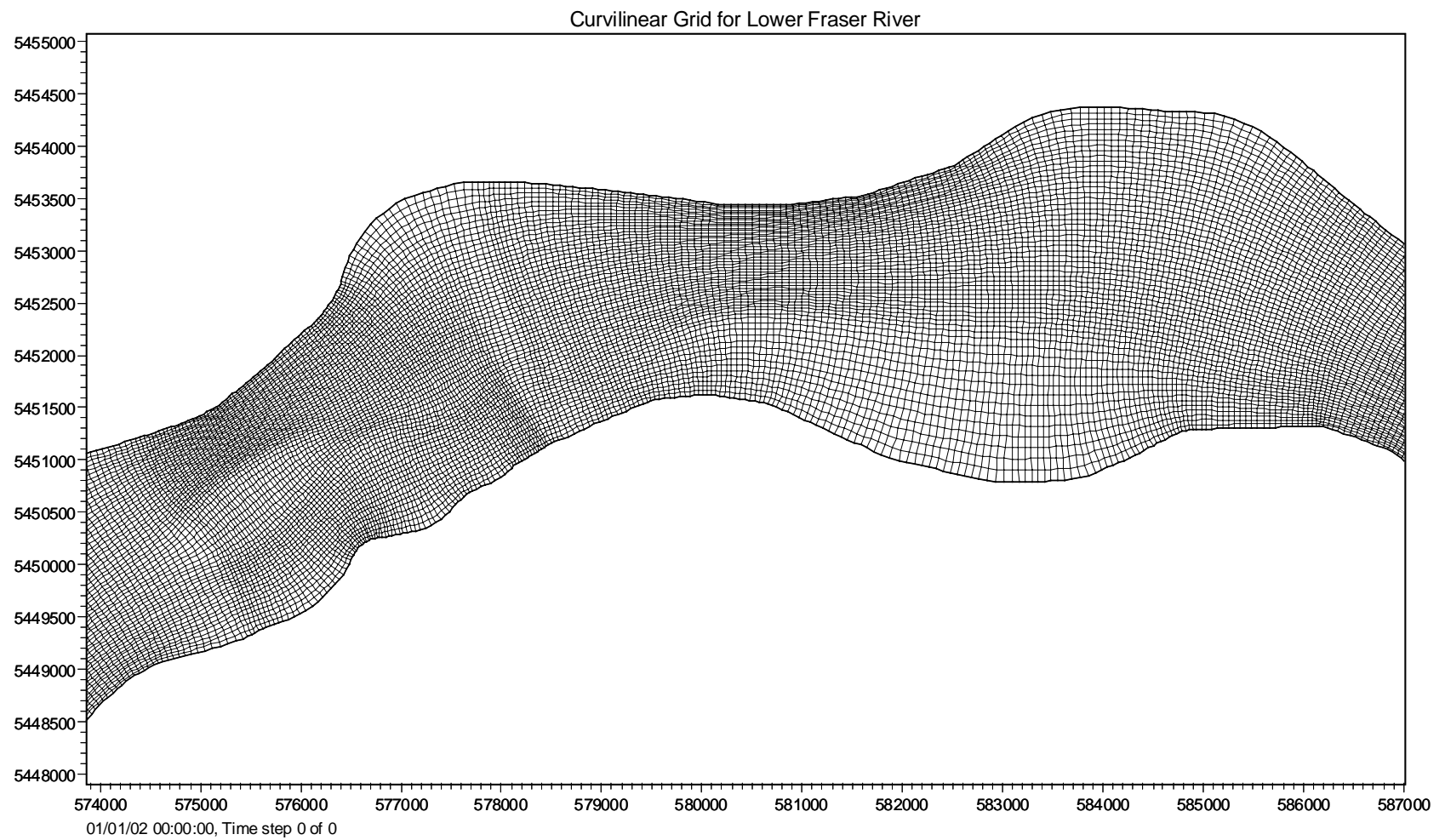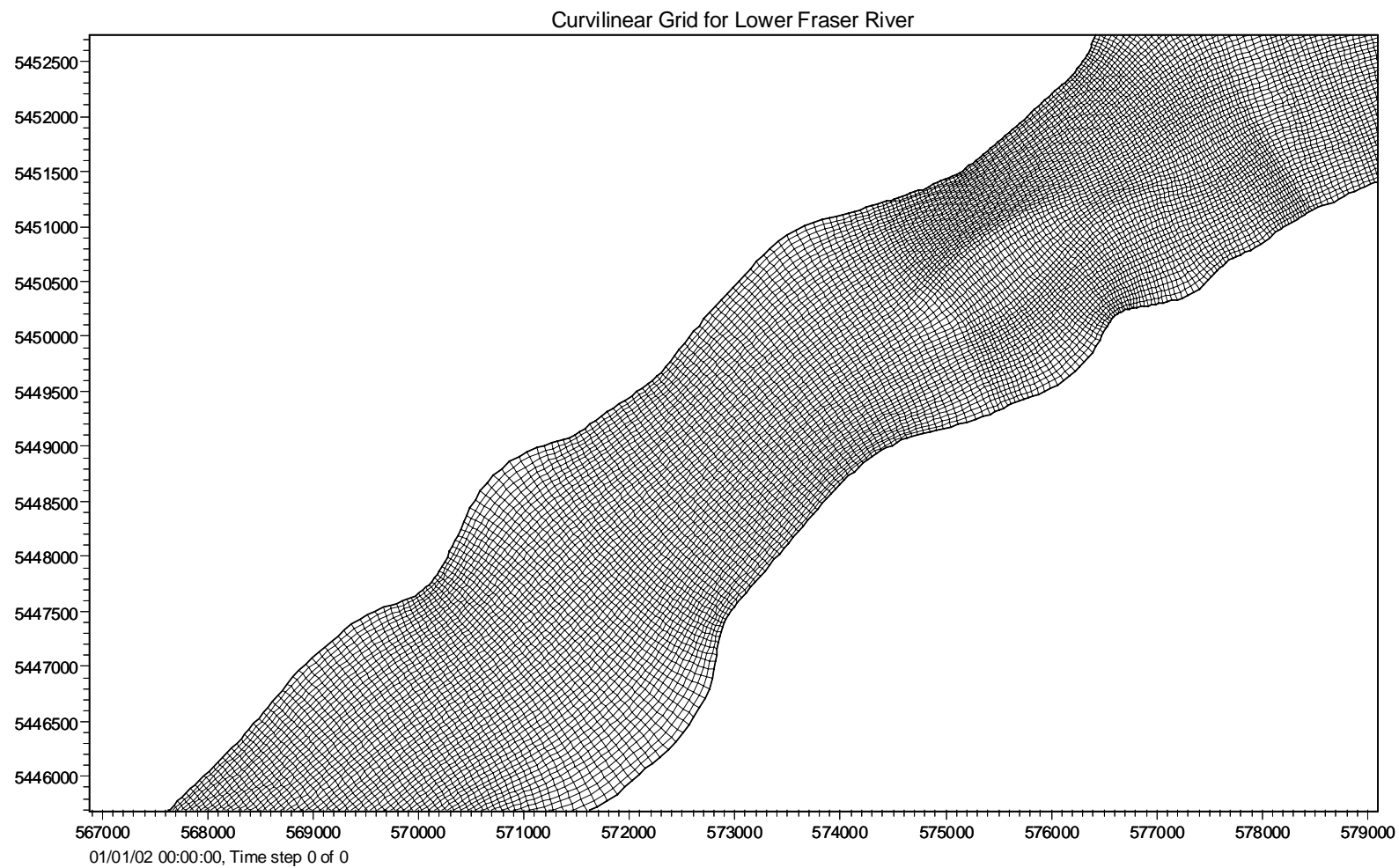Figure E (C): Curvilinear grid size variation shown in detail for Frame C of Figure 4.6.

Curvilinear Grid for Lower Fraser River

01/01/02 00:00:00, Time step 0 of 0

Figure E (D): Curvilinear grid size variation shown in detail for Frame D of Figure 4.6.

Curvilinear Grid for Lower Fraser River

01/01/02 00:00:00, Time step 0 of 0

Figure E (E): Curvilinear grid size variation shown in detail for Frame E of Figure 4.6.

239

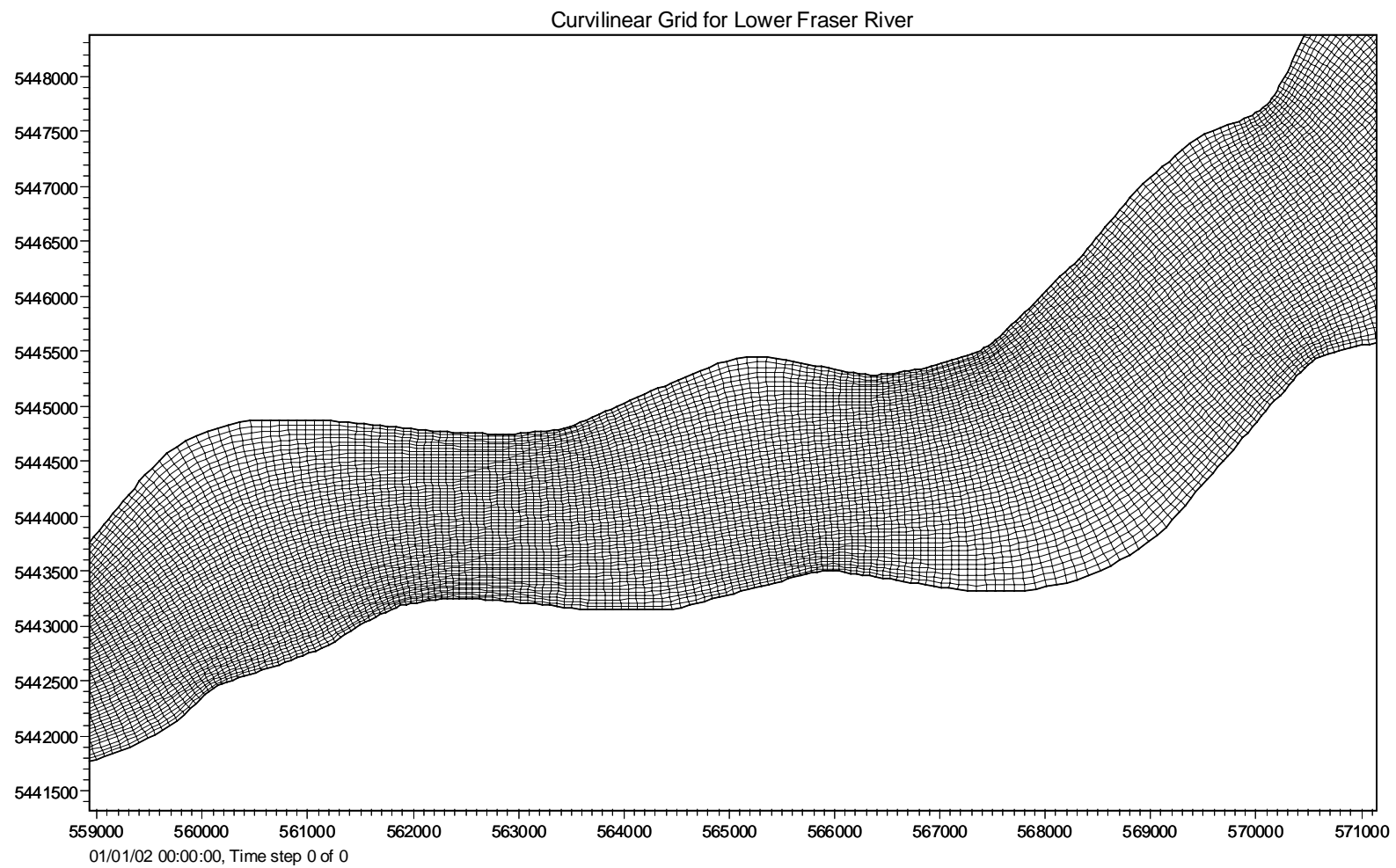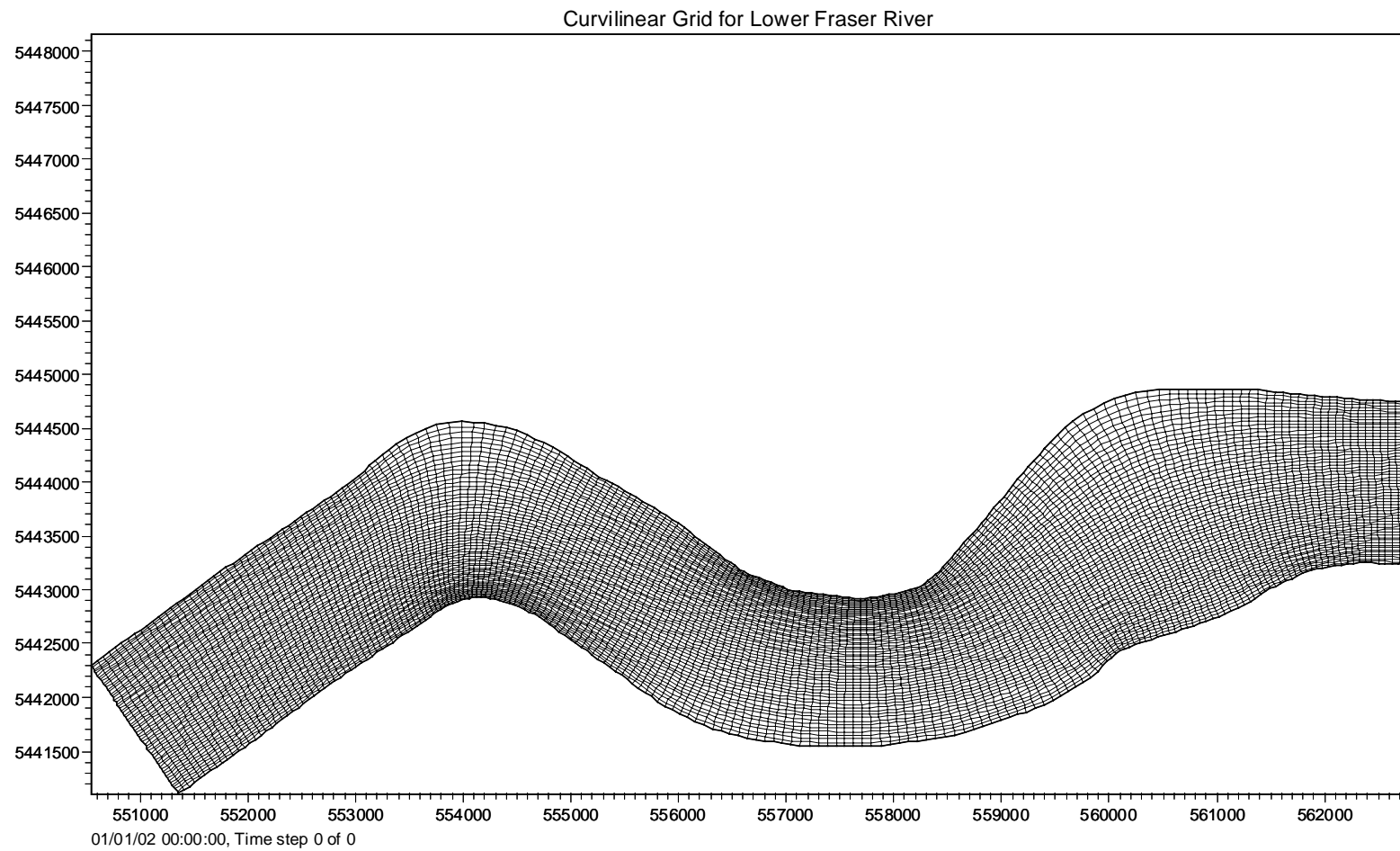Figure E (F): Curvilinear grid size variation shown in detail for Frame F of Figure 4.6.

Curvilinear Grid for Lower Fraser River

01/01/02 00:00:00, Time step 0 of 0

Figure E (G): Curvilinear grid size variation shown in detail for Frame G of Figure 4.6.

Curvilinear Grid for Lower Fraser River

01/01/02 00:00:00, Time step 0 of 0

Figure E (H): Curvilinear grid size variation shown in detail for Frame H of Figure 4.6.

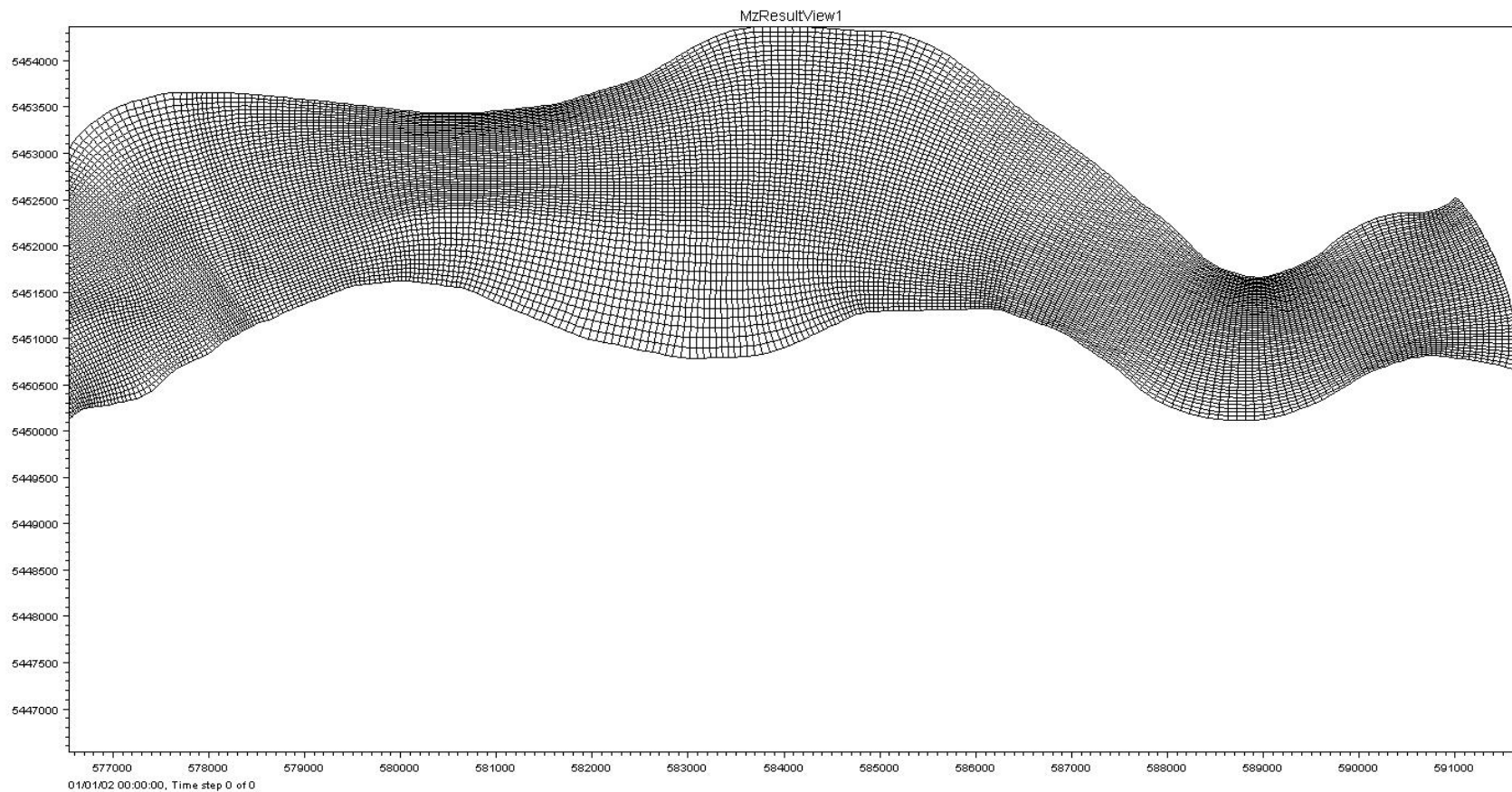**APPENDIX-F: MESH SIZES IN SEDIMENT TRANSPORT MODEL GRID**

Figure F (A): Sediment transport grid (Agassiz to Sumas Mountain) extracted from Hydrodynamic model grid (grid size variation in Frame A of Figure 4.13 shown in details).
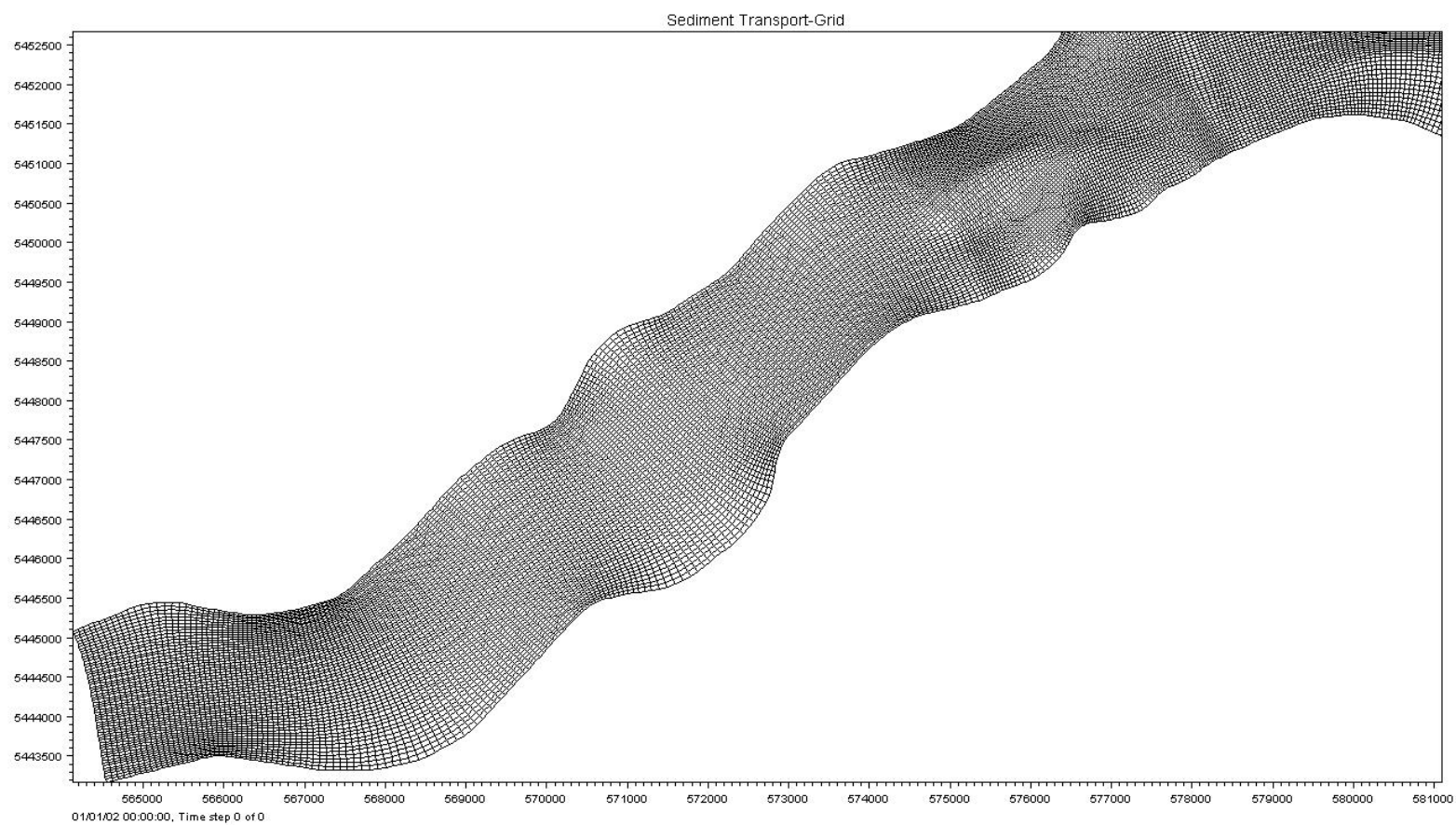
Figure F (B): Sediment transport grid (Agassiz to Sumas Mountain) extracted from Hydrodynamic model grid (grid size variation in Frame B of Figure 4.13 shown in details).